

Kristine Skogseide  
Fredrik Kleppe

# Stength analysis of prestressed reinforced bridge towers

Solution for a suspension bridge across Halsafjorden

Master's thesis in Bygg- og miljøteknikk  
Supervisor: Terje Kanstad  
June 2021



Illustration: Broer.no



Kristine Skogseide  
Fredrik Kleppe

# **Stength analysis of prestressed reinforced bridge towers**

Solution for a suspension bridge across Halsafjorden

Master's thesis in Bygg- og miljøteknikk  
Supervisor: Terje Kanstad  
June 2021

Norwegian University of Science and Technology  
Faculty of Engineering  
Department of Structural Engineering



**NTNU**

Kunnskap for en bedre verden





## MASTER THESIS 2021

SUBJECT AREA: Concrete structures	DATE: 10.06.2021	NO. OF PAGES: 131 + 35
--------------------------------------	---------------------	---------------------------

TITLE:

**Strength analysis of prestressed reinforced bridge towers; Solution for a suspension bridge across Halsafjorden**

Styrkeanalyse av spennarmerte brutårn: Løsning for hengebru over Halsafjorden

BY:

Fredrik Kleppe  
Kristine Skogseide



SUMMARY:

The thesis investigates the alternative of a suspension bridge across Halsafjorden in one span of 2050 meters. The focus will be directed towards a static analysis of the concrete towers, primarily using ordinary reinforcement. Henceforth, the thesis aims to investigate whether vertical prestressed reinforcement along the height of the towers is favourable or not.

The desired geometry is found by using scaling theory with Hardangerbrua as a template. However, a rectangular hollow cross-section with C90 concrete is used. Furthermore, the external loads that influence the bridge are the self-weight, the wind and traffic loads, controlled according to the ultimate limit state.

The finite element software Abaqus is used to perform a numerical analysis of the bridge. The free-standing towers and the complete model is analyzed with self-weight, traffic- and wind loads. An excel program based on the method of lamellae is used to perform capacity calculations. Moreover, the program is modified in the thesis to account for both ordinary and prestressed reinforcement in the cross-section.

Finally, the forces from the Abaqus model are extracted. The ordinary reinforcement in the towers is optimized regarding the utilization ratio and the bending stiffness. Shear, torsion and minimum reinforcement for the towers, including the transverse beams, are calculated according to Eurocode 2.1-1. To investigate the effect of prestressed reinforcement, some of the ordinary reinforcement is replaced by prestressed reinforcement.

RESPONSIBLE TEACHER: Terje Kanstad, NTNU

SUPERVISOR(S): Terje Kanstad, NTNU

CARRIED OUT AT: Department of Structural Engineering

## Abstract

Halsafjorden is one of the fjords along the road E39, where the ferry crossing are planned to be exchanged by a more efficient solution. The thesis investigates the alternative of a suspension bridge in one span with each tower on land. Hence, the span of the bridge will have a total length of 2050 meters, making it the world's longest. Initially, the focus will be directed towards a static analysis of the concrete towers, using ordinary reinforcement. Henceforth, the thesis aims to investigate whether vertical prestressed reinforcement along the height of the towers is favourable or not.

Hardangerbrua is currently the longest suspension bridge in Norway. Due to geological and geographical similarities, the design of Hardangerbrua forms the basis for the Halsafjorden bridge. However, the span of Halsafjorden is substantially longer, such that the scaling theory by Gimsing and Georgakis is implemented to find the desired geometry of the bridge components. In addition, the compressive strength of concrete is increased from 45 to 90 MPa. For this reason, the cross-section area of the tower columns is reduced from squared to rectangular. In addition, the wall thickness is reduced by 25%. The external loads that influence the bridge are the self-weight, the wind and traffic loads. According to Eurocode and the ultimate limit state, load combinations are implemented to find the critical forces acting on the structure.

The finite element software Abaqus is used to perform a numerical analysis of the bridge. Accordingly, both a free-standing tower and the complete bridge are modelled. During analysis, three load combinations are applied. The first load combination influences the free-standing towers, subject to both self-weight and wind forces towards the length of the bridge. Both the second and third load combinations affect the complete bridge. Thus, wind forces in respectively the longitudinal and the transverse direction, in addition to self-weight and traffic load. The program accounts for linear material behaviour and non-linear geometrical effects. An excel program based on the method of lamellae is used to account for non-linear material effects. It is modified in the thesis to account for the use of both ordinary and prestressed reinforcement.

Finally, the forces from the Abaqus model is extracted and used to determine the necessary reinforcement for the bridge. The towers are subject to a combination of axial forces and moments, which is accounted for by the lamellae program. The ordinary reinforcement in the towers is optimized regarding the utilization ratio and the bending stiffness. Shear, torsion and minimum reinforcement for the towers, including the transverse beams, are calculated according to Eurocode 2. To investigate the effect of prestressed reinforcement, initially, 50% of the ordinary reinforcement area is replaced with prestressed reinforcement. Henceforth, the prestressed reinforcement area is reduced by 50% for additional evaluation. Results show that prestressed reinforcement increases the moment capacity for the free-standing towers. However, the moment capacity of the complete bridge is reduced, mainly because of large compression forces. Based on this, vertical prestressed reinforcement is not recommended in the bridge towers but could be used for other tall, slim structures imposed by smaller axial forces.

## Sammendrag

Halsafjorden er en av fjordene langs E39, der den nåværende fergen skal byttes ut med en mer effektiv krysningsløsning. Denne masteroppgaven undersøker alternativet som tar for seg en hengebru i ett spenn der begge tårnene er plassert på land. Grunnet fjordens størrelse vil brua ha et hovedspenn på 2050 meter og bli verdens lengste hengebru. Fokuset med oppgaven vil være rettet mot å utføre en statisk analyse av tårnene ved bruk av slakkarmering. Videre er målet å undersøke om vertikal spennarmering i tårnene er gunstig eller ikke.

Hardagerbrua er i dag den lengste hengebrua i Norge. På grunn av geologiske og geografiske likheter danner Hardangerbrua grunnlaget for både geometri og beregninger i denne oppgaven. Med en økende lengde på spennet blir den ønskede geometrien funnet ved bruk av skaleringsteori av Gimsing og Georgakis. Videre blir betongfasthetsklassen økt fra B45 til B90. På bakgrunn av dette kan brutårnets tverrsnitt bli redusert fra en kvadratisk til rektangulær form og veggtykkelse kan reduseres med 25%. De ytre kreftene som påvirker brua er egenvekt, vind- og trafikklaster. I henhold til Eurokode 0 og bruddgrensetilstand blir lastkombinasjoner beregnet for å finne de kritiske lastene som virker på brua.

Elementmetodeprogrammet Abaqus blir brukt i denne masteroppgaven til numerisk analyse av tårnene. To modeller blir utviklet, et frittstående tårn og en global modell som inkluderer hele brua. Under analysen er det tre lastkombinasjoner som er relevante for oppgaven. Den første lastkombinasjonen påvirker det frittstående tårnet, utsatt for både egenvekt og vindlast i bruas lengderetning. Både den andre og den tredje lastkombinasjonen påvirker den globale modellen av brua med egenvekt, trafikklaster og vinslast som påvirker brua både på langs og på tvers. Videre tar programmet hensyn til en lineær elastisk materialoppførsel og geometriske ikke-lineære effekter. For å ta hensyn til ikke-lineære materialegenskaper benyttes et excel program. Programmet tar utgangspunkt i lamellemetoden for å beregne momentkapasitet til et tverrsnitt for ulike bøyestivheter. Dette er modifisert i denne masteroppgaven for å ta hensyn til en kombinasjon av slakk- og spennarmering i tverrsnittet.

Til slutt blir kreftene fra abaqusmodellen hentet ut og benyttet til å bestemme den nødvendige armeringsmengden i tårnene. Lamelleprogrammet tar hensyn til samtidig virkning av moment og aksialkraft. Mengden slakkarmering er optimalisert i forhold til utnyttelsesgrad og stivhet i tårnene. Skjær, torsjon og minimumsarmering for tårnene, inkludert riglene er beregnet i henhold til Eurokode 2. For å undersøke effekten av spennarmering blir først 50% av slakkarmeringen byttet ut med spennarmering. Deretter blir spennarmeringsarealet redusert med ytterligere 50% for videre evaluering. Resultatene viser at spennarmering øker momentkapasiteten i de frittstående tårnene. Derimot reduseres momentkapasiteten i den globale modellen av brua på grunn av store trykkrefter i tårnene. Basert på dette kan det konkluderes med at spennarmering ikke er gunstig i brutårnene, men at det kan bli brukt for høye slange søyler med mindre trykkrefter.

## **Preface**

This master thesis is written as the final part of our course of study at Bygg- og Miljøteknikk as a part of the structural engineering department. The thesis has 30 units of credits and is written towards the concrete group at NTNU.

We chose this theme because of our increased interest in statics and concrete throughout the course of study. This task challenged us and motivated us to learn more about concrete in general, prestressed reinforcement and nonlinear analysis. Equally important, we've been educated in modelling large structures using the finite element program Abaqus. In addition, it has been rewarding to take part in future-oriented research in regards to record-breaking bridge solutions.

Throughout the process of the thesis, several people have provided valuable information and guidance. First and foremost we want to thank our supervisor, Terje Kanstad from NTNU, for knowledge regarding the theme and guidance throughout the whole project. In addition, we want to thank Jørn Arve Hasselø from the Norwegian public roads administration for wind data from the bridge site and Aksel Fenerci from NTNU, regarding the understanding and calculation of the obtained wind measurement. Likewise, we want to thank Jelena Zivkovic from Equinor for information regarding the application of prestressed reinforcement on condeep oil platforms. Finally, we also want to thank Øyvind Wiig Petersen for help regarding the modelling of the bridge in Abaqus.

**Trondheim, June 2021**  
**Kristine Skogseide and Fredrik Kleppe**



# Symbols

## Large latin letters

$A$	Cross sectional area
$A_p$	Area of prestressing tendon or tendons
$A_s$	Cross sectional area of reinforcement
$E_c$	Modulus of elasticity of concrete
$E_p$	Modulus of elasticity of prestress
$G$	Shear modulus
$G_{k,j,inf}$	Lower characteristic value of permanent action j
$G_{k,j,sup}$	Upper characteristic value of permanent action j
$L$	Length
$M$	Moment
$M_{cr}$	Cracking moment
$M_y$	Yield moment
$P$	Relevant representative value of a prestressing action
$Q_{k,1}$	Characteristic value of leading variable action 1
$Q_{k,i}$	Characteristic value of the accompanying variable action i
$I$	Second moment of inertia of cross section

## Small greek letters

$\alpha_{cc}$	Coefficient taking account of long term and unfavorable effect
$\delta$	Deflection
$\epsilon_c$	Compressive strain in the concrete
$\epsilon_{c2}$	Compressive strain in the concrete at the peak stress
$\epsilon_{ck}$	Characteristic strain of reinforcement at maximum load
$\epsilon_{cu2}$	Ultimate compressive strain in the concrete
$\epsilon_{uk}$	Characteristic strain of prestressing steel at maximum load
$\gamma_c$	Partial factor for ultimate limit state of concrete
$\gamma_p$	Partial factor for prestressing actions

$\gamma_s$	Partial factor of ultimate limit state of reinforcement
$\gamma_{G,j,inf}$	Partial factor for permanent action j in calculating lower design values
$\gamma_{G,j,sup}$	Partial factor for permanent action j in calculating upper design values
$\gamma_{Q,i}$	Partial factor for variable action i
$\kappa$	Curvature at a particular section
$\nu$	Poisson's ratio
$\psi_0$	Factor for combination value of a variable action
$\rho_c$	Oven dry density of concrete
$\sigma_c$	Compressive stress in the concrete
$\xi$	Reduction factor
$E_s$	Modulus of elasticity of reinforcement

#### **Small latin letters**

$e$	Eccentricity
$f_{ck}$	Characteristic compressive cylinder strength of concrete at 28 days
$f_{pk}$	Characteristic tensile strength of prestressing steel
$f_{yk}$	Characteristic yield strength of reinforcement
$f_{p0.1k}$	Characteristic 0.1% proof-stress of prestressing steel
$k$	Von Karman constant
$n$	Exponent
$z$	Height above ground
$z_0$	Roughness length

# Contents

<b>Abstract</b>	<b>II</b>
<b>Sammendrag</b>	<b>III</b>
<b>Preface</b>	<b>IV</b>
<b>Symbols</b>	<b>VI</b>
<b>1 Introduction</b>	<b>1</b>
<b>2 Background</b>	<b>2</b>
2.1 Halsafjorden . . . . .	3
2.2 Suspension bridges in general . . . . .	4
2.3 Prestressed concrete in general . . . . .	7
<b>3 Materials, geometry and regulations</b>	<b>9</b>
3.1 Eurocode and regulations . . . . .	9
3.2 The bridge towers/pylons . . . . .	10
3.2.1 Material properties . . . . .	10
3.2.2 Scaling/geometry . . . . .	12
3.3 The main cables . . . . .	15
3.3.1 Material properties . . . . .	15
3.3.2 Scaling/geometry . . . . .	17
3.4 The vertical suspenders . . . . .	18
3.4.1 Material properties . . . . .	18
3.4.2 Scaling/geometry . . . . .	18
3.5 The stiffening girder/bridge deck . . . . .	18
<b>4 Loads</b>	<b>20</b>
4.1 Self-weight . . . . .	20
4.2 Traffic loads . . . . .	20
4.3 Wind loads . . . . .	21
4.3.1 Wind loads on the free-standing towers . . . . .	24
4.3.2 Wind loads on the complete bridge . . . . .	25
4.4 Load combinations . . . . .	25
<b>5 Modelling of the free-standing bridge towers</b>	<b>29</b>
5.1 Abaqus . . . . .	29
5.1.1 Element description . . . . .	30
5.2 Modelling the geometry . . . . .	31
5.3 Modelling the loads . . . . .	33

<b>6</b>	<b>Modelling of the complete bridge</b>	<b>35</b>
6.1	Modelling . . . . .	36
6.1.1	Bridge towers . . . . .	36
6.1.2	Main cables . . . . .	37
6.1.3	Anchor cables . . . . .	38
6.1.4	Vertical suspenders . . . . .	38
6.1.5	Stiffening girder . . . . .	39
6.1.6	Connection between the stiffening girder and the towers . . . . .	40
6.1.7	Boundary conditions . . . . .	41
6.2	Assembly . . . . .	43
6.3	Modelling the loads . . . . .	45
<b>7</b>	<b>Method of calculation</b>	<b>47</b>
7.1	Method of Lamellae . . . . .	47
7.1.1	The Lamellae . . . . .	47
7.1.2	Material Curves . . . . .	50
7.1.3	Excel Lamellae Program . . . . .	51
7.2	Verification of excel program . . . . .	54
7.2.1	Example 4.13 - Cross-section with ordinary reinforcement . . . . .	54
7.2.2	Example 4.13 - Cross-section with prestressing . . . . .	57
7.3	Link between Abaqus and the Lamellae program . . . . .	59
7.3.1	Moment-Curvature diagrams . . . . .	60
7.3.2	Deflection ( $\delta$ ) . . . . .	62
7.3.3	Effect of ordinary reinforcement . . . . .	64
7.3.4	Effect of prestressed reinforcement . . . . .	65
7.3.5	Effect of axial force . . . . .	66
7.4	Comparing cross section with ordinary and prestressed reinforcement . . . . .	68
7.4.1	M-N capacity curve comparison . . . . .	68
7.4.2	Moment-curvature curve comparison . . . . .	71
<b>8</b>	<b>Abaqus analysis</b>	<b>74</b>
8.1	Verification . . . . .	74
8.2	Abaqus analysis results . . . . .	77
8.3	Abaqus analysis of transverse beams . . . . .	82
<b>9</b>	<b>Design of the towers</b>	<b>85</b>
9.1	Design of the towers using ordinary reinforcement . . . . .	85
9.1.1	Free-standing towers . . . . .	85
9.1.2	Bending in the longitudinal direction of the complete bridge . . . . .	88
9.1.3	Bending in the transverse direction of the complete bridge . . . . .	89
9.2	Design of the towers using prestressing . . . . .	93
9.2.1	Free-standing towers . . . . .	93
9.2.2	Bending in the longitudinal direction of the complete bridge . . . . .	93
9.2.3	Bending in the transverse direction of the complete bridge . . . . .	94

9.3	Shear capacity . . . . .	96
9.4	Torsional capacity . . . . .	99
9.5	Transverse beams . . . . .	100
<b>10</b>	<b>Discussion</b>	<b>104</b>
10.1	Summary and comparison of the results . . . . .	104
10.2	Sources of errors . . . . .	109
<b>11</b>	<b>Conclusion</b>	<b>114</b>
<b>12</b>	<b>Future work</b>	<b>117</b>
<b>A</b>	<b>Calculations regarding scaling theory by Gimsing and Georgakis</b>	<b>123</b>
<b>B</b>	<b>Second moment of inertia of the main cables</b>	<b>128</b>
<b>C</b>	<b>Wind loads</b>	<b>130</b>
<b>D</b>	<b>User guide for the lamellae program</b>	<b>143</b>
<b>E</b>	<b>Calculations of a slim column</b>	<b>145</b>
<b>F</b>	<b>Abaqus analysis of the transverse beam</b>	<b>146</b>
<b>G</b>	<b>Calculations of shear reinforcement for the bottom transverse beam</b>	<b>150</b>

# 1 Introduction

Along the west coast of Norway, stretching from Kristiansand in the south to Trondheim further north, the European road E39 connects major cities like Stavanger, Bergen, Molde and Ålesund. Due to the challenging landscape along the coast, several ferry crossings characterises the road. As a result, travelling along the route has been time consuming and inefficient. Consequently, a major project is set in motion to exchange all ferry crossings with either subsea tunnels or bridges. Henceforth, connecting living- and business areas as well as reducing the travelling time [1].

One of the fjords along E39 is Halsafjorden, currently operated by ferry. The Norwegian public roads administration (Statens Vegvesen) has executed measurements at the bridge site to come up with the optimal crossing of the fjord. Results present that the fjord is approximately 2 km wide and 500 m deep with relatively calm wind conditions. Hence, four different options have been proposed, and the thesis will investigate the case that considers a suspension bridge in one span with both towers on land [2].

Norway has several suspension bridges throughout the country. Nevertheless, the currently longest bridge is crossing Hardangerfjorden, with a total span of 1310 meters [3]. Similarities in design for the two bridges make Hardangerbrua a solid foundation for the design and calculations in the thesis. Although the design is similar, the span of the bridge across Halsafjorden is substantially longer. Thus, scaling theory is used to find the suitable dimensions for the bridge.

The thesis aims to perform a capacity calculation of the towers according to the ultimate limit state. Along with the scaled geometry, the bridge will be subject to wind and traffic load, as well as self-weight. First, a capacity calculation of the bridge towers are found by the use of ordinary reinforcement to find a reference design. Then, the thesis will investigate whether it is favourable to use prestressed reinforcement along the height of the towers or not. Prestressed reinforcement is commonly used in beams and plates to enlarge the capacity and bending stiffness. In this case, prestressed reinforcement is added to increase transverse stability to withstand large horizontal forces imposed by the wind.

First, the thesis will address the background for the ferry free E39 project and the material properties of the components used in the bridge. Then, the scaling theory is presented and executed, and an Abaqus model of the bridge is developed. Along with the Abaqus model, an excel lamellae program will be modified to be valid for the respectable calculations to find the reinforcement design of the towers. In addition, the shear- and torsional capacity is investigated. Finally, the results will be evaluated in order to determine the effect of prestressed reinforcement.

## 2 Background

E39 is currently 1100 kilometres long, contains seven crossings by ferry and has a total travelling time of 21 hours. A major project is set in motion by the government to substitute all ferry crossings with bridges and subsea tunnels, improve existing infrastructure and dig new tunnels in order to shorten the route. The ultimate goal is to reduce total travelling time by half and increase the safety along the route [1].



Figure 2.1: Map of E39. Photo: Statens Vegvesen [1]

A project of this scale will be the most extensive and expensive infrastructure project ever built in Norway, with a current total cost of NOK 340 billion. Although the price tag is considerable, many people and industries along the coast will benefit from the project. The different regions will be linked together, leading to both industrial and economic growth. Calculations done by the Norwegian public roads administration shows that in addition to reduced travelling time, the transportation cost for both cars and heavy transportation lorries will half as soon as the tolls are entirely paid [4]

At the start of 2021, about 10 % of the project is completed. The construction of the southern crossing of E39, Boknafjorden, is assumed to be continued by the spring of 2021. Both the crossing of Bjørnafjorden and Nordfjorden are in a planning phase, while the propositions for Romsdalsfjorden and Julsundet are completed and awaiting economic aid from the government. For Sulafjorden and Halsafjorden, technical solutions are researched, and different proposals, including cost, are expected to be presented within 2022/23.

## 2.1 Halsafjorden

Halsafjorden is one of the crossings along E39, which is currently operated by ferry, running between Kanestraum and Hals. In addition to being wide and deep, the fjord is known to be exposed to rough weather. Therefore, record-breaking solutions are necessary to overcome the challenges a project of this scale will impose. Several years of research and mapping makes it possible to develop tailored solutions for a structure that could replace long ferry queues and slow average travelling speed.

In the latest article from the Norwegian public roads administration [2], preliminary project and cost estimation for four different solutions are to be completed within 2022. The various solutions are based on two main concepts, suspension bridge and pontoon bridge.

- Suspension bridge in one span
- Suspension bridge in one span with a tower positioned at Aakvikgrunnen
- Suspension bridge in two spans supported on a tension leg platform
- Pontoon/Floating bridge

The thesis considers the solution related to a suspension bridge in one span. Approximately two kilometres of water with depths of up to 500 meters need to be crossed. The suspension bridge will have a total span of 2050 meters and becomes the world's longest, exceeding the current leading Akashi-Kaikyo bridge (1991 meters) [5]. A bridge of this size will be a natural step towards even longer spans, which could solve challenges met in other fjord crossings.



Figure 2.2: Possible crossing site. Map: Norgeskart [6]



For such a project to become a reality, complex engineering challenges need to be solved. One of these challenges is strongly related to the concrete towers. The towers need to withstand significant local stresses at the top, where the forces from the main cables are transferred to the towers. At the same time, the towers need to withstand sizable transverse forces imposed by the wind.

Although the Akashi-Kayiko bridge is of similar length as Halsafjorden, it's not comparable. The geological, seismic differences and a greater demand for traffic capacity requires a more dense structure. Hardangerbrua, however, is a much slender bridge constructed in a similar environment as Halsafjorden. The main span is 1310 meters, and combined with the geometrical abilities, scaling theory will be used to obtain the desired geometry.

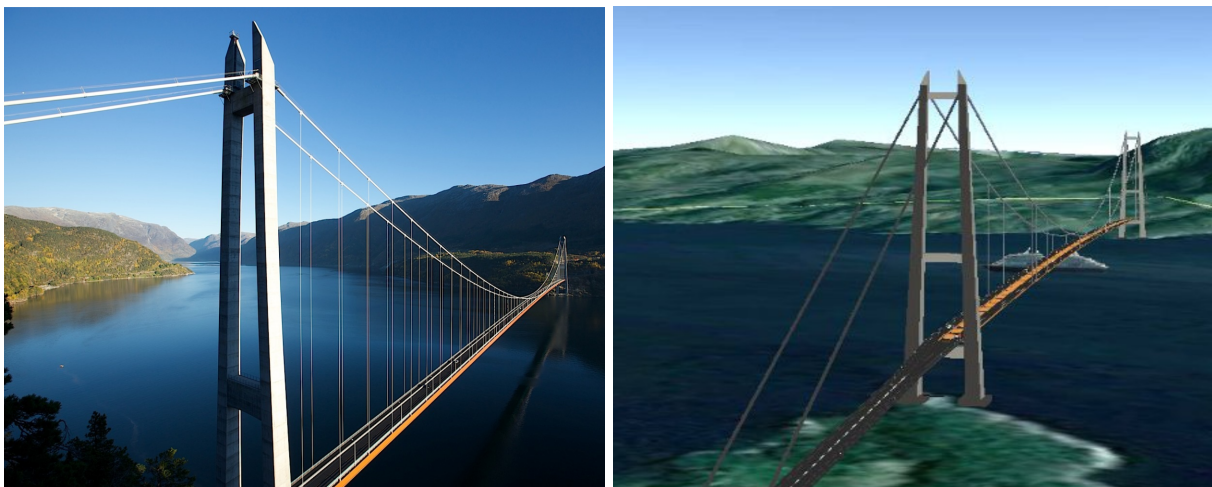


Figure 2.3: Hardangerbrua and Halsafjorden. Photo: Broer.no [7] and Statens Vegvesen [2]

## 2.2 Suspension bridges in general

As the name implies, a suspension bridge is a type of bridge in which the stiffening girder is hung below suspension cables. The main structural components of the bridge include vertical suspenders, main cables, anchorage for the cables, the towers and a stiffening girder. As figure 2.4 illustrates, the main cables are suspended between the towers and anchored at each end. Vertical suspenders connects the stiffening girder to the main cables, transferring the traffic load from the driveway to the towers [8].

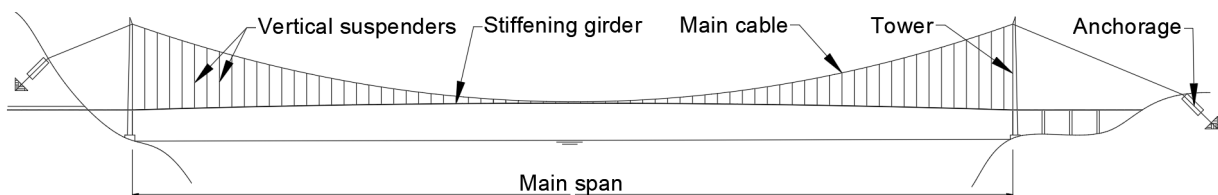


Figure 2.4: Main components of the suspension bridge

Suspension bridges are historically preferred for longer crossings along the coast of Norway [7]. The main advantages of the solution are closely related to the efficient use of materials. The main cable is made of high tension steel, and it's the main load-carrying component. Contributing to a reduced dead-weight which makes longer spans possible. Furthermore, the loads from the cables are transferred to the towers, creating compression forces that are favourable for concrete. Due to the geology of Norway, cables could be anchored in solid rock, which saves a lot of concrete compared to gravitational anchors. In addition, the esthetic appearance of suspension bridges is less intruded compared to a pontoon bridge.

### **The stiffening girder**

The stiffening girder also referred to as the deck, is a longitudinal stiffening system, which supports and distributes the vertical live load. Preferably for this project, the shape of the stiffening girder is an aerodynamic shallow box, which allows for low drag induced by wind. The girder could also be formed as a separate truss or plate, combined with lateral bracing systems, which is often preferred in areas of high traffic demand.



Figure 2.5: The stiffening girder of Hardangerbrua. Photo: Statens Vegvesen [3]

### **The suspenders**

The suspenders are usually designed either vertical or diagonal, in which vertical is most commonly used for suspension bridges. Hence, diagonal suspenders could increase damping and therefore improve the seismic performance of the bridge, suitable in areas prone to earthquakes.

### **The towers**

The towers are often classified dependent on how the main cables are attached. Hence, either flexible, rigid or locking. Flexible towers are the most commonly used option for long-span suspension bridges, which is the case for Hardangerbrua. Rigid towers are preferably utilised for multi-span suspensions bridges and locking towers are adapted for relatively short suspension bridges.

### The main cables

The main cables in modern suspension bridges are usually made of cold drawn galvanized steel wires bundled into a circular shape. Assembly of the cables is implemented by cable spinning, which enables an increased diameter of longer cables and therefore favourable for Halsafjorden. However, the method requires a lot of special equipment, and is dependent on the weather conditions [9]. Exemplified by Hardangerbrua, which got delayed by half a year during cable spinning due to harsh weather [10].

### The anchors

Anchorage are important components in the static system because the cables transfer most of the self-weight and additional loads to the anchorage system. Inside the anchors, the wires of the cables are spread evenly by the splay saddle to distribute the loads and prevent damage caused by the concentrated cable forces. The cables are first anchored to a force transition block and, from there, tread even further into the rock before it's finally anchored to a steel plate. Furthermore, the two most commonly used anchorages are either based on gravity or a tunnel. As for the gravity type, the weight of a vast concrete block resists the tension force induced by the main cables. The tunnel anchorages redirect the tension forces from the cables directly into the ground, requiring adequate geotechnical conditions, which is the case for both Hardangerbrua and Halsafjorden.

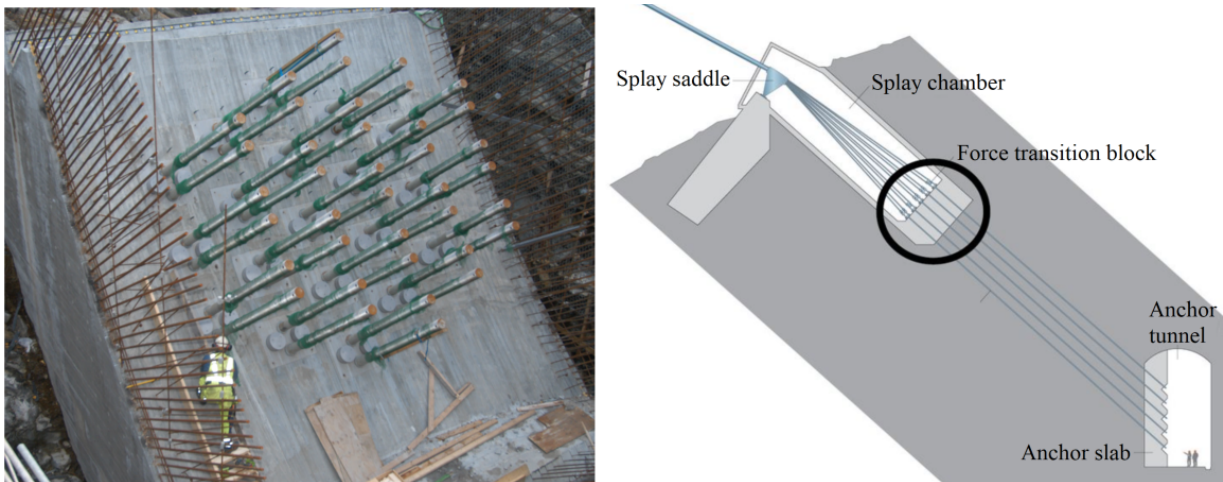


Figure 2.6: Main components of the anchors. Photo: Statens Vegvesen [3]

## 2.3 Prestressed concrete in general

Concrete is a material with great compressive strength and low tensile capacity. Thus, high tensile steel is added to strengthen the insufficient tensile abilities, either as ordinary or prestressed reinforcement. When the concrete is prestressed, tensile forces are applied to the steel, which transfers compressive stresses to the concrete. Hence, the tensile stresses imposed by external forces are managed. There are two methods in use for the implementation of prestressed concrete, either pre-tensioned or post-tensioned.

In pre-tensioned concrete, the steel tendons are stressed before the casting of concrete. While the concrete cures, the tendons bond to the concrete. When the desired strength is reached, the anchors are released, transferring compressive stresses to the concrete. The method is commonly used to prefabricate elements, mainly to increase efficiency on the construction site.

When the concrete is post-tensioned, the tendons are stretched after the concrete is cast. Indifferent from the pre-tensioning, the tendons are not placed in contact with the concrete but encapsulated within a duct or protective sleeve. In addition to protection, the duct makes room for motion during tensioning. A passive anchor is attached at one end, holding the cable steady, while an active anchor at the other end pulls the tendon through the anchorage by using a jack, creating tension. When the desired tension is reached, the jack is removed, and the tendon is fastened.

Commonly, only the transverse beams of suspension bridge towers are post-tensioned. However, in the thesis, the effects of using vertical post-tensioned reinforcement along the height of the towers are investigated. During construction, the towers are susceptible to horizontal wind forces when the concrete cast is finished and the cables not yet attached. Hence, the vertical tendons are meant to increase the horizontal strength of the free-standing towers.

The idea of vertically prestressing the concrete towers is inspired by the engineering of deep oil platforms. In regards to the oil platforms, the primary purpose of prestressing is related to the reduction of ordinary reinforcement, limit crack extent and widths, in addition to balancing the storage cells [11]. Prestressing also increases the capacity for deformation service in limit condition, specifically correlated to forces imposed by waves, colliding ships or icebergs. In regards to the extensive compressive forces, concrete with great compressive strength is used, in addition to solid shear reinforcement with T-heads. Practically, to enable the implementation of prestressing, the method of slip forming is used. In general, slip forming is based on constantly moving the concrete form upwards, while reinforcement and concrete are added. Thus, enabling the construction of up to 10 meters a day. Additionally, slip forming allows resizing the shape of the towers, demonstrated by the narrowing columns of the oil platform. The red lines in figure 2.7, illustrates the relevant placement of the post-tensioned tendons.

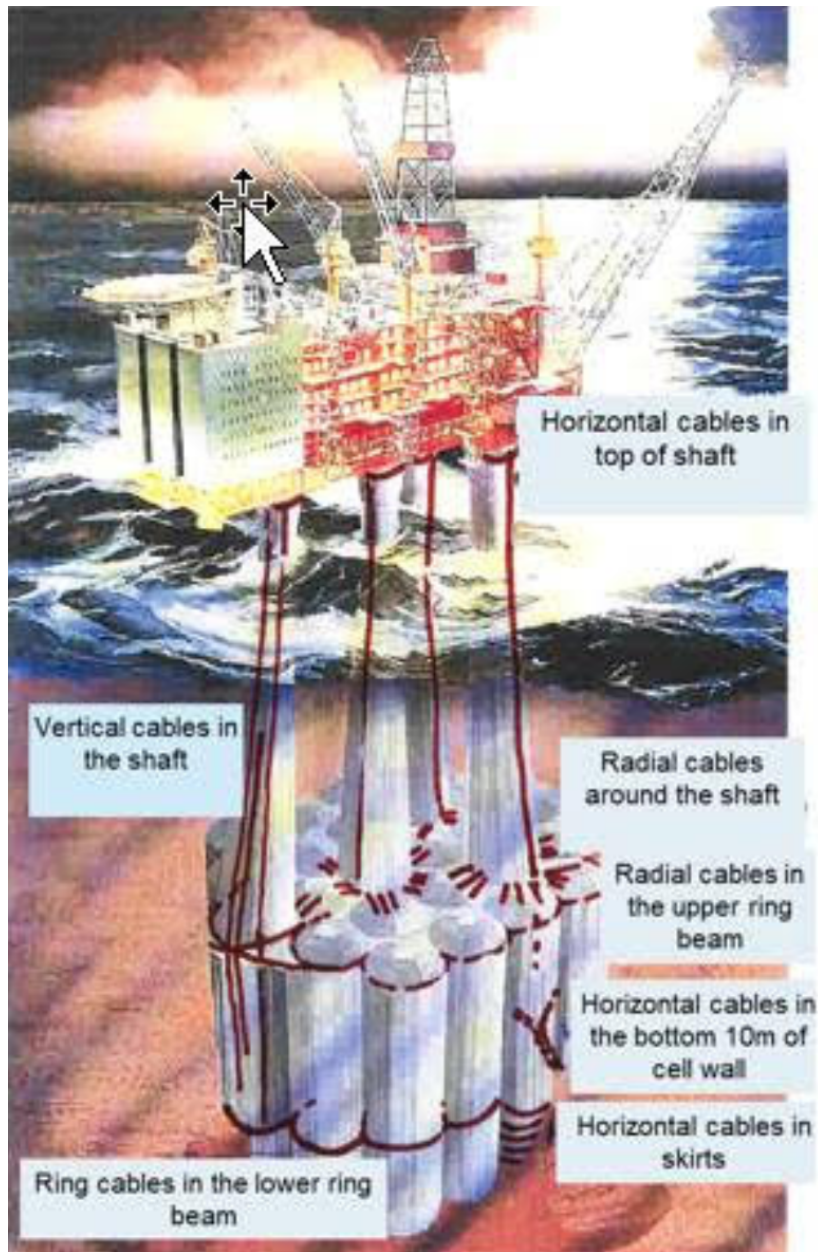


Figure 2.7: Condeep oil platforms with vertical prestressing. Photo: Equinor[11]

### 3 Materials, geometry and regulations

This section presents the relevant regulations and standards used for the design and capacity calculations of the bridge. Then, the material properties of each component of the bridge are listed. Henceforth, the material properties are found, and scaling theory will be presented and executed for the corresponding elements. The capacity of the towers is calculated in accordance to the ultimate limit state, hence assuring the safety of people and the structure.

#### 3.1 Eurocode and regulations

A set of rules and standards will be used as a guideline towards the design of the bridge across Halsafjorden. Inspired and based on the geometry, materials and construction of Hardangerbrua, the bridge is scaled and customized to cohere with the geological and geographical conditions in Halsafjorden. Report "12-2950 Hardangerbrua - Beregninger" [12], published by the Norwegian public roads administration (Statens Vegvesen), provides both material and geometrical properties of Hardangerbrua along with information regarding the external loads. Drawings of Hardangerbrua is used as an additional tool to simplify the design process of the towers [13].

The Eurocode is a set of European standards specifying how structural design should be conducted within the EU and connecting countries, such as Norway [14]. The regulations are used to document the structure's safety according to the requirements of the building regulations. Unique for each country is a national annexe of additional rules, attached to specify national requirements and customized to the politics and conditions of each country. The relevant standards used during the calculations of the bridge are listed below.

- NS-EN 1990:2002+A1:2005+NA:2016, Eurocode: Basis of structural design [15], further referred to as EC0.
- NS-EN 1991-1-1:2002+NA:2019, Eurocode 1: Actions on structures - Part 1-1: General actions - Densities, self-weight, imposed loads for building [16], EC1.1-1
- NS-EN 1991-1-4:2005+NA:2009 Eurocode 1: Actions on structures - Part 1-4: General actions - Wind actions [17], EC1.1-4
- NS-EN 1991-2:2003+NA:2010, Eurocode 1: Actions on structures - Part 2 - Traffic loads on bridges [18], EC1.2
- NS-EN 1992-1-1:2004+A1:2014+NA:2018, Eurocode 2: Design of concrete structures - Part 1-1: General rules and rules for buildings [19], EC2.1-1

Combined with the use of Eurocodes, the Norwegian public roads administration have developed a supplementary manual regarding the construction of bridges, named "Håndbok N400" [20]. The manual includes regulations towards all phases of the construction process, service life and maintenance, applicable for all Norwegian public roads. Hereafter, the referred to as N400.

Additionally, the Norwegian public roads administration has provided the report "Report 668 Beregningsveiledning for etteroppspente betongbruer" [21] as a guidance for the design of post-tensioned bridges. The report considers regulations, analysis and calculations following the Eurocode. Henceforth referred to as report 668.

During capacity calculations of the towers, the lamellae method briefly described in report "Norsk Betongforening Publikasjon nr. 38" is used [22]. However, the method is customized to accord with the use of ordinary and prestressed reinforcement. Further the report is referred to as NB 38.

## 3.2 The bridge towers/pylons

### 3.2.1 Material properties

The main component of the bridge towers is concrete. Even though C45 is used for Hardangerbrua, the preferred choice of concrete for Halsafjorden is C90, signifying a larger characteristic compressive strength. As a consequence, a slender cross-section could be used, compared to the one in Hardangerbrua. Thus, less concrete is needed for the towers, which is favourable for the environment. The material properties are extracted from table 3.1 in EC2.1-1 and presented in table 3.1. Based on a capacity calculation in ULS, the material factor is found in table 2.1N in EC2.1-1, assuming a "Persistent and Transistent" design situation.

Material Properties C90	Symbol	Value
Modulus of elasticity	$E_c$	44 000 MPa
Poisson's ratio	$\nu$	0.2
Shear modulus	G	18 333 MPa
Oven-dry density	$\rho_c$	2500 kg/m <sup>3</sup>
Characteristic compressive cylinder strength at 28 days	$f_{ck}$	90 MPa
Partial factor for ultimate limit state (ULS)	$\gamma_c$	1.5
Coefficient taking account of long term and unfavorable effects	$\alpha_{cc}$	0.85
Compressive strain at the peak stress	$\epsilon_{c2}$	$2.6 \cdot 10^{-3}$
Ultimate compressive strain	$\epsilon_{cu2}$	$2.6 \cdot 10^{-3}$
Exponent	$n$	1.4

Table 3.1: Material properties of C90 concrete

Despite the substantial compressive strength, concrete has an insignificant tensile capacity that needs to be considered. Reinforcement steel is commonly used in concrete to increase the tensile abilities extensively due to its considerable tensile strength. Each steel bar contains ribs/lugs contributing to a better bond between the steel and the concrete. Hence, appropriate transfer of forces between the materials is ensured. In Norway, the reinforcement bars are produced according to the regulations given in NS 3576-3, part 3 "Kamstenger klasse B500NC. Mål og egenskaper" [23]. The relevant material properties are listed in table 3.2 and found in section 7.2.2 in NS 3576 and section 3.2 in EC2.1-1.

Material properties B500NC	Symbol	Value
Modulus of elasticity	$E_s$	200 000 MPa
Characteristic yield strength	$f_{yk}$	500 MPa
Partial factor of ultimate limit state (ULS)	$\gamma_s$	1.15
Characteristic strain at maximum load	$\epsilon_{ck}$	$75 \cdot 10^{-3}$

Table 3.2: Material properties of B500NC reinforcement

The material properties of prestressed reinforcement are found in report nr. 668 "Beregningsveiledning for etteroppspente betongbruer" from the Norwegian public roads administration [21] and are listed in table 3.3. Usually, one cable consists of either 12, 15, 19 or 22 wires. Each wire has an area of either  $140 \text{ mm}^2$  or  $150 \text{ mm}^2$ . Thus, cables with 19 wires and an area per wire of  $150 \text{ mm}^2$  are chosen. For the consideration of concrete cover and minimum distance between bars, the outer diameter of the duct is 110 mm. The same prestressed reinforcement is chosen for the transverse beams and the tower due to simplicity.

Material properties prestressed reinforcement	Symbol	Value
Modulus of elasticity	$E_p$	195 000 MPa
Characteristic tensile strength	$f_{pk}$	1860 MPa
Characteristic 0.1% proof-stress	$f_{p0.1k}$	1670 MPa
Partial factor for ultimate limit state (ULS)	$\gamma_s$	1.15

Table 3.3: Material properties of prestressed reinforcement

In accordance with section 5.10.5 in EC2.1-1, loss of tensile stress is developed in the tendons over time. The losses are commonly divided into two categories, namely short- and long-time losses. Additionally, the maximum force applied to a tendon during jacking can't exceed 95 % of the characteristic proof stress ( $f_{p0.1k}$ ), according to 5.10.2.1 (2) in EC2.1-1. The short-time losses are losses that immediately affect the tendons' tension, often related to other materials or mechanical abilities. Three short time losses are accounted for by EC2.1-1, losses due to instant deformation of concrete, losses due to friction and losses due to the anchorage. Furthermore, long time losses are mainly related to creep, shrinkage and relaxation of steel under tension.

Deformation of concrete is mainly caused by systematical tensioning of tendons, one after the other. For each tensioning of a tendon, the nearby concrete is compressed. Hence, adding another tendon will affect the previous ones. Losses due to friction develop due to angular displacements. Mainly due to friction between the tendon and the duct caused by the profile of the cable. But also internal displacement caused by imperfections of the duct or untidy construction work. Anchorage losses occur due to small slippages when the tendon transitions from the jack to the anchor. The manufacturer usually provides information regarding the slippages. These short-time losses are calculated and accounted for during the capacity calculations, in accordance with chapter 5.10.5 in EC2.1-1.



Creep occurs when materials like concrete are deformed for a long period due to external loads. Time-dependent and compiled of a delayed elastic deformation and a viscous deformation. Shrinkage is a contraction of concrete caused by desiccation over time, independent of the load situation. Relaxation defines a stress reduction in the prestressed steel subjected to tension over time. A simplified method is used to calculate and account for these long-time losses during capacity calculations, in compliance with formula 5.46 in EC2.1-1.

There are three main reasons for implementing concrete cover between the surface of the embedded reinforcement and the outer surface of the concrete. Firstly, the steel reinforcement bars need protection from environmental effects to prevent corrosion. Secondly, the cover provides thermal insulation, protecting the reinforcement from fire. Thirdly, the reinforcement needs sufficient embedding to enable them to be stressed without slipping. The minimum concrete cover is decided with respect to either the bond strength or permanence, according to table NA.4.2 in EC2.1-1 and Table 7.2 in N400. In addition, the cover is increased by adding a deviation factor, provided by N400. Hence, the total concrete cover is calculated according to formula 3.1. The calculation process is equal for both reinforcement types, but the requirements are distinctive.

$$C_{nom} = C_{min} + \Delta C_{dev} \quad (3.1)$$

A minimum vertical and horizontal distance between the surface of each reinforcement bar is required to provide sufficient bond and compression to the concrete. The minimum distance accounts for both the aggregate size and sufficient space for vibrators to adequately compress the concrete, according to section 8.2 and figure 8.15 in EC2.1-1. Overall, the minimum concrete cover and the distances between the reinforcement bars are summarized in table 3.4.

<b>Reinforcement</b>	<b>Concrete cover</b>	<b>Horizontal distance between bar/tendon</b>	<b>Vertical distance between bar/tendon</b>
Ordinary reinforcement	75 mm	2.0 $\emptyset$	1.5 $\emptyset$
12-wire strands	110 mm	90 mm	90 mm
19-wire strands	130 mm	110 mm	110 mm

Table 3.4: Concrete cover and distances between reinforcement bars/tendons

### 3.2.2 Scaling/geometry

Initially mentioned, the geometry of the bridge is based on the geometry of Hardangerbrua. However, if all the bridge components are uniformly scaled to reach the desired length of 2050 meters, issues will occur. First of all, the cross-section area of the towers will be squared, which will increase the use of material, the self-weight and the cost. In addition, the large cross-section also increases the area of which the wind could strike. These issues will have unfavourable effects on the structure that need to be accounted for during calculations and design.

A possible solution could be found in "Cable Supported Bridges: Concept and Design", by Gimsing and Georgakis [24]. The book presents theories regarding the scaling of different components of a suspension bridge, including a formula that calculate the concrete quantity needed for suspension bridge towers. The formula includes the height of the towers, the density of steel, length of main and side span, cable sag and uniformly distributed dead and traffic load.

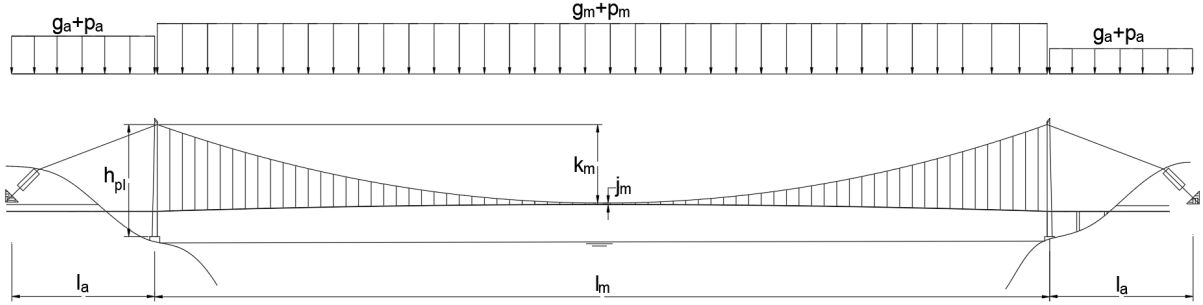


Figure 3.1: Illustration of the factors incorporated in equation 3.2

$$Q_{pl} = \frac{(g_m + p_m) \cdot l_m + Q_{cm}}{8} \cdot \left( \frac{k_m + 4k_a + b_a}{k_m} \cdot \frac{l_m}{l_a} + 4 \right) \cdot \left[ \exp \left( \frac{\gamma_{pl}}{f_{pld}} \cdot h_{pl} - 1 \right) \right] \quad (3.2)$$

Using formula 3.2, the amount of concrete needed for the tower of both Hardangerbrua and Halsafjorden are calculated in parallel. A scaling factor for the cross-section area can be found by dividing the quantities of the two bridges with the height of the towers as shown in formula 3.3. Correspondingly, the scaling factor equals 1.73. The complete calculations could be found in appendix A.

$$f_A = \frac{\frac{Q_{pl2050}}{h_{pl2050}}}{\frac{Q_{pl1310}}{h_{pl1310}}} \quad (3.3)$$

Based on the scaling ratio, the cross-section of the bridge can be designed. In general, the cross-section narrows by the height of the tower, which means every casting stage needs to be scaled individually. The method presupposes equivalent concrete compressive strength during application. However, Halsafjorden is designed by C90 and Hardangerbrua by C45 concrete. Using a greater compressive strength increases the corresponding capacity, implying an over-dimensioned cross-section area.

Even though the characteristic compressive strength of C90 concrete is twice the strength of C45 concrete, the cross-section can't be halved. The bending stiffness is reduced by a higher power than the area, and the available space for reinforcement would be too small. Additionally, the original cross-section of Hardangerbrua is nearly squared, mainly due to the esthetic appearance decided by the architect. From an engineering perspective, a more material-effective cross-section would be a rectangle. Generally, because the transverse beams provide transverse stability towards the short side of the rectangle.

Two modifications are implemented to reduce the area. Firstly, the wall thickness is reduced by 25%, from 600 mm to 450 mm. Secondly, the cross-section is reshaped, from squared to rectangular. The length is kept constant, while the width is reduced, illustrated by figure 3.2. By reducing the wall thickness by 25%, there is available space for three layers of  $\text{Ø}32$  reinforcement bars. The relevant cross-section properties could be found in appendix A.

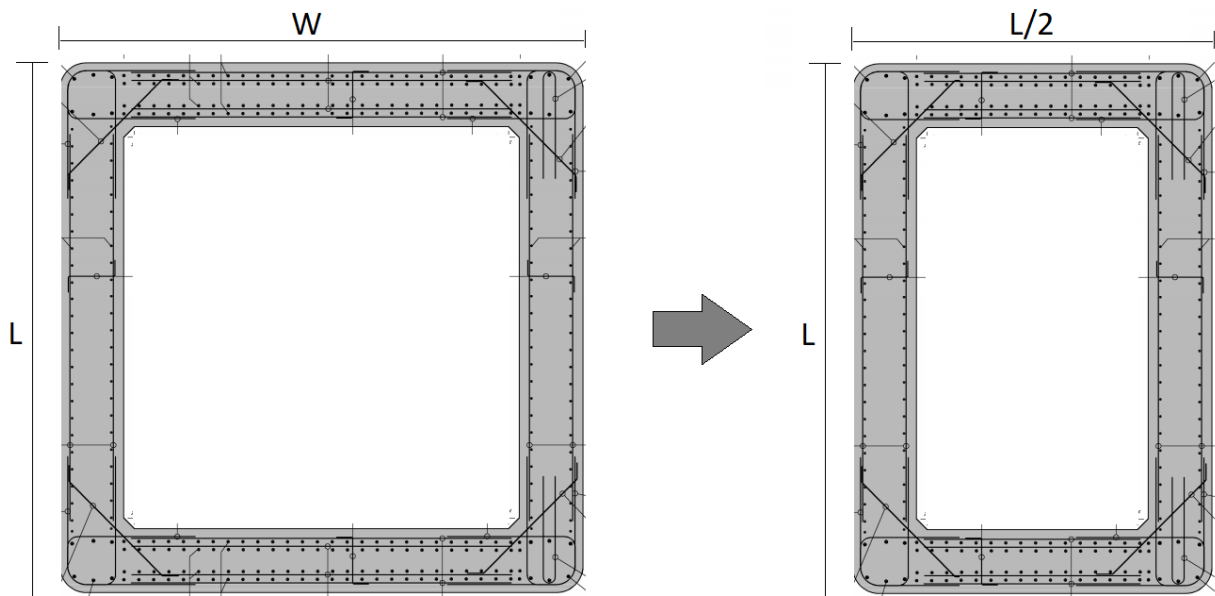


Figure 3.2: Reduction of the cross-section

Hardangerbrua is designed with a total of three transverse beams for each tower. Due to the increased height of the towers of the bridge across Halsafjorden, an extra beam is added. The beams are made of concrete with both ordinary and prestressed reinforcement, which continues into the pylons, creating fixed connections. In general, the additional beam improves the transverse stability and reduce the buckling length.

### 3.3 The main cables

#### 3.3.1 Material properties

The main cable of Hardangerbrua is constructed using a method called cable spinning. Similarly, the process will be used for the bridge across Halsafjorden, and the material properties are assumed to be equal. Hardangerbrua contains two main cables, each composed of 19 strands made out of 528 galvanised steel wires. Hence, the layout of the cross-section is made of semi-parallel wire strands. The tensile strength of each wire is 1570 MPa, and the modulus of elasticity is 200 000 MPa. After compaction, the diameter of the cable is 600 mm. However, the scaling theory increases the diameter of the main cable to 773 mm for the bridge across Halsafjorden. Figure 3.3 shows an illustration of the main cable in Hardangerbrua before compaction. Although the main cable in this paragraph accounts for the cable from anchor to anchor, the cables are divided by the towers for the rest of the thesis, named the "main cables" and the "anchor cables".

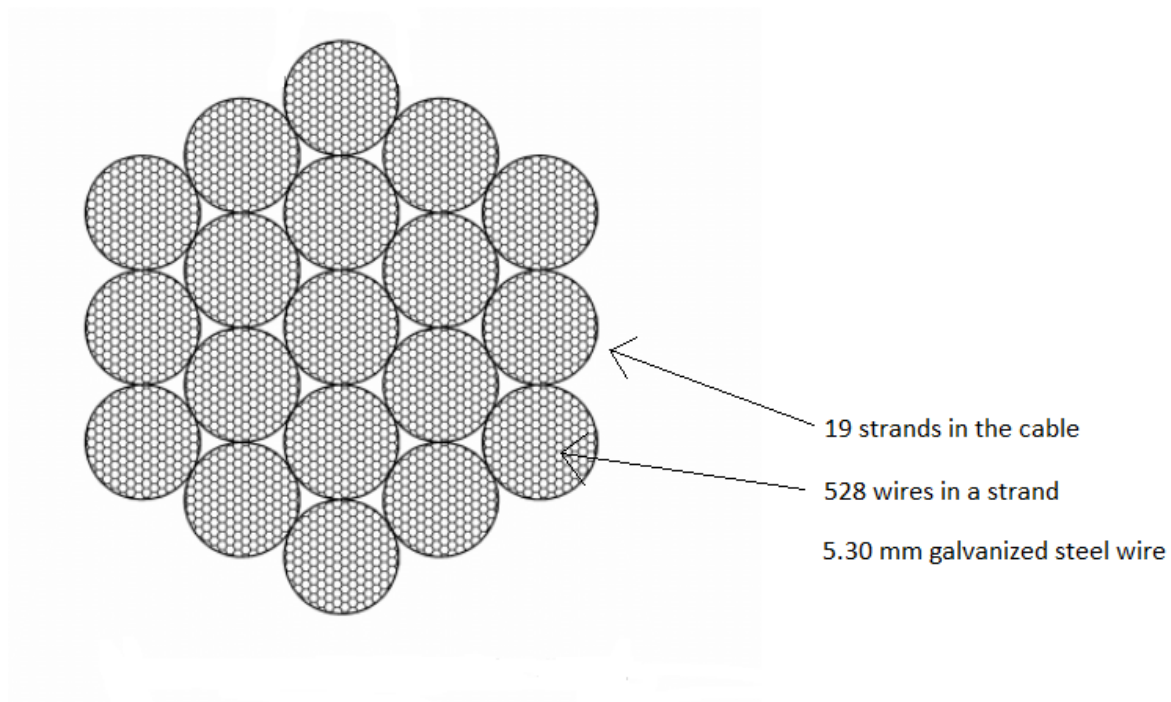


Figure 3.3: Main cable before compaction. Drawing 0701 [13]

Research states that critical errors may arise during the assembly of cable-supported bridges where the main cables are of significant length and size [25]. The modelling of Hardangerbrua considers the second moment of inertia equal to 0.1%-1% of the second moment of inertia of an equivalent compact cross-section. However, a method found in "Bending stiffness of parallel wire cables including interfacial slips among wires" [25] uses an analytical solution to calculate the moment of inertia. Hence, both methods are evaluated to examine the effect on the analysis of the towers.

The latter method idealises the cable as a laminated beam where the wires at the same plane form the basis for one layer. Between each layer, interfacial slips may arise depending on the slip rigidity. The article "Experimental research on bending performance of structural cables" [26] uses experimental trials to find an expression for the slip rigidity between the layers. Two limit states are assumed for the slip rigidity, either full slip between the layers or no slip. Furthermore, the article develops two solutions for the calculation of the bending stiffness. The first one considers an equally distributed load, while the second one uses a concentrated force. Due to complex empirical formulas, a Matlab script is developed to determine the bending stiffness of the cable. The script could be found in appendix B.

To evaluate how the second moment of inertia of the cable affect the towers, the different values of the moment of inertia are analysed for the complete bridge in Abaqus. The moment at the bottom of the tower is found and compared in table 3.5. Because the bending stiffness of the tower affects the moment capacity, two different modulus of elasticity are used. The analysis is performed with self-weight combined with traffic and wind load.

		<b>E = 12 000 MPa</b>	<b>E = 24 000 MPa</b>
<b>Initial condition</b>	<b>I [m<sup>4</sup>]</b>	<b>Moment [kNm]</b>	<b>Moment [kNm]</b>
[25] Concentrated force	0.01827	139000	181400
1% of compact cross-section	0.000175	134900	181600
0.1% of compact cross-section	0,0000175	dnf	dnf
[25] Equally distributed load	$7.7514 \cdot 10^{-8}$	dnf	dnf

Table 3.5: Abaqus analysis with different second moment of inertia and modulus of elasticity

Displayed by the result, it is shown that the moment at the bottom of the towers does not change significantly for different values of the second moment of inertia for the cable. Hence, for small values, numerical issues occur caused by a failure in the cable. Based on the results, it is decided to use the second moment of inertia equal to 1% of a compact cross-section,  $I = 0.000175 \text{ m}^4$  for further analysis of the bridge.

### 3.3.2 Scaling/geometry

Increasing the bridge span causes an increase in the height of the tower and the length of the cable. Correspondingly, the self-weight and external loads increase, imposing a more significant force throughout the cables. Managing the enlarged demand is naturally done by increasing the cross-section area of the cable. However, uniformly scaling is complex. For instance, the horizontal force in the cable is proportional to the length of the cable squared, and the vertical force is proportional to the length quadruple. In like manner as the bridge towers, the book by Gimsing and Georgakis provide theories regarding the scaling of both main cables and vertical suspenders. By taking the density, length, sag and cross-section area, in addition to the dead- and external loads into account, formula 3.4 by Gimsing and Georgakis could be used to calculate the quantity of steel needed for a cable. Following the same procedure as for the bridge towers, a scaling factor based on Hardangerbrua could be found and used on the bridge across Halsafjorden. The formulas return a scaling factor of 1.66, which implies a cross-section area for the main cable of Halsafjorden equal  $0.4686m^2$ . Calculations can be found in appendix A.

$$Q_{cm} = \frac{\gamma_{cb}}{f_{cdb}} (g_m + p_m) l_m^2 \frac{\sqrt{1 + 16 \left(\frac{k_m}{l_m}\right)^2}}{8 \frac{k_m}{l_m} - \frac{\gamma_{cb}}{f_{cdb}} l_m \sqrt{1 + 16 \left(\frac{k_m}{l_m}\right)^2}} \left[ 1 + \frac{8}{3} \left(\frac{k_m}{l_m}\right)^2 \right] \quad (3.4)$$



Figure 3.4: Assembly of the main cable. Photo: Statens Vegvesen [12]

## 3.4 The vertical suspenders

### 3.4.1 Material properties

Hardangerbrua contains 65 pairs of vertical suspenders connecting the stiffening girder to the main cables. Each suspender consists of a fastener in each end, coupled with a steel cable, as shown in figure 3.5. The fastener is designed to enable free rotation along the length of the bridge, while the other directions are fixed, contributing to some transverse stiffness. Equivalent to the material properties of Hardangerbrua, the tensile strength is 1570 MPa, and the modulus of elasticity equals 160 000 MPa. The cables between the fasteners are spirally woven and made out of galvanized steel, while the fasteners are produced using casting steel [13].



Figure 3.5: Vertical suspender cable. Drawing K709 [13]

### 3.4.2 Scaling/geometry

Due to the increased span of the bridge, the amount of vertical suspenders are increased from 65 to 81 pairs. In addition, the horizontal distance between each pair of suspenders is extended to 25 meters. Like the main cables, the forces on the suspenders are enlarged, requiring scaled dimensions to manage the new demands. The book by Gimsing and Georgakis includes a formula that calculates the quantity of steel in each vertical suspender. The quantity of both Hardangerbrua and the bridge across Halsafjorden is calculated and derived to find the scaled ratio. Furthermore, the scaling factor for the diameter is found by considering the average length and number of the suspenders. The scaling ratio is calculated to 1.4, implying a diameter of the suspender of Halsafjorden equal to 40.9 mm. Calculations are found in appendix A.

$$Q_{hm} = \frac{\gamma_{cb}}{f_{cdb}}(g_m + p_m) \left( j_m + \frac{k_m}{3} \right) l_m \quad (3.5)$$

## 3.5 The stiffening girder/bridge deck

Based on equal traffic load and road class for the two bridges, the stiffening girder used for Hardangerbrua could be used for the bridge across Halsafjorden. For this reason, the material properties are found in the calculation report of Hardangerbrua; "12-2950 Hardangerbrua - Beregninger" [12] and listed in table 3.6.

Material properties	Symbol	Value
Modulus of elasticity	$E$	210 000 MPa
Yield strength	$f_y$	355 MPa
Oven-dry density	$\rho_s$	7800 kg/m <sup>3</sup>

Table 3.6: Material properties of the stiffening girder - S355

In addition to the mechanical properties of the stiffening girder, the geometrical properties are found in the same report and listed in table 3.7. Furthermore, the stiffening girder is modelled by the implementation of shear flexible Timoshenko beam elements, thoroughly described in section 6.1.5. Hence, the elements require information regarding rotary inertia, found in "Modelling and dynamic analysis of long-span suspension bridges" [27], and added to the same table.

Geometrical properties	Symbol	Value
Area	$A$	0.5813 m <sup>2</sup>
Moment of inertia about the y-axis	$I_y$	0.974 m <sup>4</sup>
Moment of inertia about the z-axis	$I_z$	16.448 m <sup>4</sup>
Torsional constant	$I_T$	2.460 m <sup>4</sup>
Rotary inertia about the y-axis	$I_{yy}$	12515 kgm <sup>2</sup> /m
Rotary inertia about the z-axis	$I_{zz}$	217020 kgm <sup>2</sup> /m

Table 3.7: Geometric properties of the stiffening girder

The stiffening girder is a welded, closed steel box with pointed corners and aerodynamic abilities, mainly consisting of steel quality S355. Relevant geometrical details are illustrated by figure 3.6.

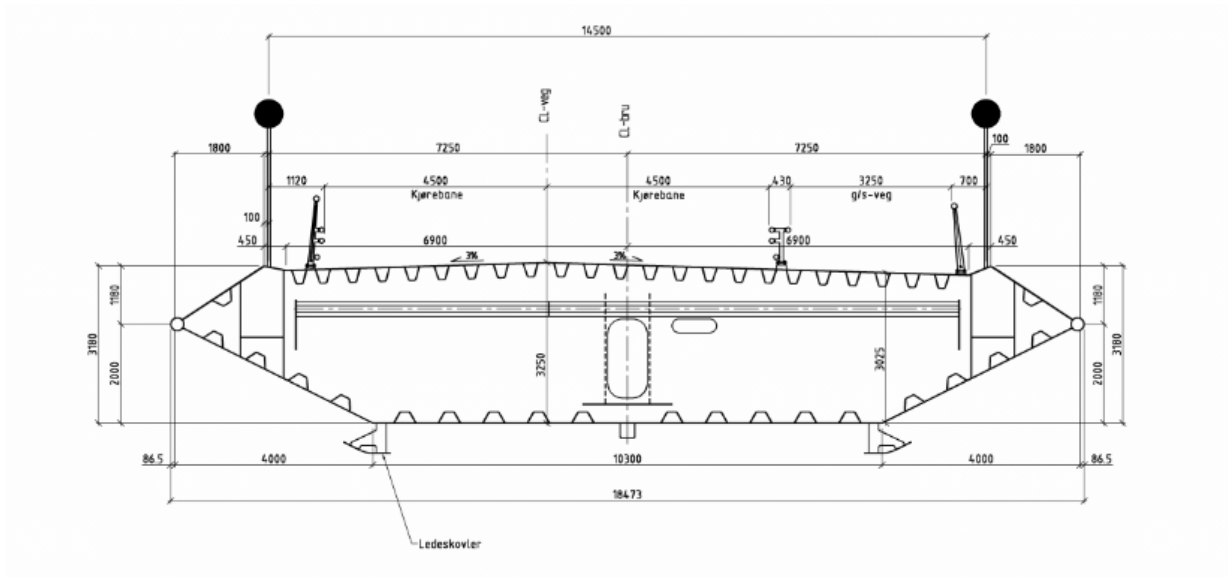


Figure 3.6: Stiffening girder. Drawing K803 [13]



## 4 Loads

The bridge is imposed by different loads, categorised according to their variation over time. N400 classifies three load categories; permanent loads, variable loads and accident impacts. Due to the extent of this project, only the most dominating loads are included during the analysis, hence the self-weight, traffic and wind load. The self-weight is classified as a permanent load, constant throughout the structure's lifetime and therefore compulsory during the analysis. Variable loads are characterised as loads that vary over time. Both traffic- and wind loads have a substantial impact on the structure and are therefore included. Other variable loads such as snow, avalanches, temperature and seismic forces from earthquakes are neglected. Furthermore, loads connected to the deformation of concrete caused by creep, shrinkage and relaxation are insignificant compared to the self-weight and the variable loads and is therefore neglected. Similarly, the loads caused by the accidental impact of cars and boats are consequently omitted.

### 4.1 Self-weight

The self-weight of Hardangerbrua found in "12-2950 Hardangerbrua - Beregninger - Kapittel 1: Grunnlag" will form the basis for the calculations of the bridge across Halsafjorden. The stiffening girder is equal in the two bridges, as previously mentioned, Thus, the self-weight includes all permanent equipment such as railing, electricity, lightning etc., including the attachment for the hangers. Both the hangers and the main cable are scaled. The results are found in table 4.1.

As for the towers, the case is slightly different. The self-weight is calculated by multiplying the area of each casting stage by the density of the concrete. The scaled geometry found in section 3 forms the basis for the calculations. Even though the self-weight could be calculated, Abaqus automatically finds the self-weight based on the model's material properties and geometry.

Self-weight	Hardangerbrua [kg/m]	Halsafjorden [kg/m]
Main Cable	1851	3073
Vertical suspenders	305	747
Stiffening girder	8825	8825

Table 4.1: Self-weight of bridge components

### 4.2 Traffic loads

Traffic loads are defined as horizontal and vertical loads caused by vehicles and pedestrians. EC1.2 states rules for the determination of traffic loads on bridges. However, the values in the national annexe are only valid for bridges with a total length of less than 200 m. "Forskrift for bruer, ferjekaier og andre bærende konstruksjoner i det offentlige vegnettet" [28] provides design rules for bridges with loaded lengths greater than 200 m. Hence, the requirements stated in this regulation are used as an additional tool to calculate the traffic load for Halsafjorden bridge.

Table 4.1 in EC1.2 divides the carriageway into notional lanes and a remaining area, in addition to the walkway. The width of the carriageway is 9 m, as shown in figure 3.6. For this reason, the carriageway is divided into three notional lanes, each of width 3 m and no remaining area. The width of the walkway is 3.25 m. Furthermore, the lanes are numbered and loaded independently to create the most adverse load situation.

Section 4.3 in EC1.2 defines four load models relevant to determine the traffic effects on the bridge. Due to the scope of the thesis, only load model 1 will be taken into account. Load model 1 represents a normal traffic situation with double axle concentrated loads and uniformly distributed loads. Each notional lane can only include one system of concentrated loads. Due to the span of the bridge, the concentrated loads will influence the towers in a small matter compared to the uniformly distributed load. Thus, only the latter will be considered in the calculations, and these are listed in table 4.2 with the adjustment factors included. The traffic loads in the transverse direction are relevant to consider if focusing on the construction of the deck but will not be included in the thesis.

Lane	Distributed load [ $kN/m^2$ ]
Notional Lane 1	4.5
Notional Lane 2	2.5
Notional Lane 3	2.5
Walkway	0.625

Table 4.2: Traffic loads

Each distributed load is multiplied by the width of the associated lane, giving a total load of 30.50  $kN/m$ . The distributed load is considered as a line load along the total length of the stiffening girder.

### 4.3 Wind loads

For the ferry free E39 project, the Norwegian public roads administration, in cooperation with Kjeller Vindteknikk, Fugro Oceanor and meteorologisk Institutt, are carrying out measurements of the wind speed at the bridge site for the fjords Halsafjorden, Sulafjorden and Vartdalsfjorden [29]. The data are measured by anemometers, an apparatus that measures the horizontal and vertical wind speed in addition to the wind direction for three different altitudes. Furthermore, the data is collected in monthly files for each year. Due to the scope of the thesis, only the horizontal wind speed and the direction are considered. For Halsafjorden, the relevant anemometers are named Halsaneset and Aakvik, which have measurements from respectively February 2014 and March 2015. Halsaneset anemometer is located at the bridge site near Kanestraum, and Aakvik is situated at the bridge site near Halså.

The towers will be designed to withstand the forces caused by the external loads that influence the bridge. For the static wind load, three different load cases are considered. The first load case considers wind in the longitudinal direction of the bridge influencing the towers after construction before the attachment of the cables and the stiffening girder. Secondly, the same wind load is considered for the bridge after completion. Wind in the longitudinal direction of the bridge is considered for both the construction phase and the complete bridge because the wind on the free-standing towers could form a dimensioning design situation. The last load case includes the wind that influences the bridge in the transverse direction.

Requirements in section 5.4.3.3 in N400 should be considered when controlling the bridge design in the ULS. Thus, the wind speed with a return period of 50 years is used during the design of the towers. Because the measured data only cover a few years, an extreme value analysis using Gumbel distribution [30] is performed to find the respectable wind speed. As the name implies, the annual maximal wind speed needs to be determined. The annual wind speed is found during one storm season, defined from summer one year until summer the following year. The duration correlates with large storms during fall, winter and early spring. Furthermore, the analysis considers several factors, such as the location and scale parameters. These are dependent on the mean annual maximal and the standard deviation. These parameters along with the return period form the basis for determining the wind speed.

The dataset contains 5-6 years of measurements with twelve files for each year. Hence, the large amount of files makes Matlab a handy tool to sort the data. First, the storm season is chosen from June one year until May the next year. Then the wind direction that corresponds to wind in the longitudinal direction of the bridge and the transverse direction of the bridge has to be determined before the analysis could start. Wind forces in the longitudinal direction of the bridge correspond to measured data between  $0^\circ - 145^\circ$  and  $185^\circ - 310^\circ$ . Furthermore,  $145^\circ - 185^\circ$  and  $310^\circ - 360^\circ$  are relevant for the wind blowing in the transverse direction of the bridge. The result from the Gumbel extreme value distribution are presented in table 4.3 for Halsaneset and 4.4 for Aakvik. In addition, the Matlab script for the wind blowing in the longitudinal direction of the bridge for Halsaneset anemometer is found in appendix C.

<b>Halsaneset</b>		
<b>Altitude [m]</b>	<b>Windspeed along the bridge (<math>v_{b,0}</math>) [m/s]</b>	<b>Windspeed across the bridge (<math>v_{b,0}</math>) [m/s]</b>
50.2994	26.25	22.95
31.9004	25.53	21.35
12.7002	25.58	21.39

Table 4.3: 50 year wind speed Halsaneset

Aakvik		
Altitude [m]	Windspeed along the bridge ( $v_{b,0}$ ) [m/s]	Windspeed across the bridge ( $v_{b,0}$ ) [m/s]
48.2998	25.67	25.26
31.9004	24.81	22.00
17.0000	18.96	19.21

Table 4.4: 50 year wind speed Aakvik

Moreover, the logarithmic law [31] presented in equation 4.1 is used to find the distribution of the wind along the height of the towers, hence the basic wind velocity ( $v_{b,0}(z)$ ).  $k$  is the von Karman constant equal to 0.4.  $z_0$  is a factor representing the terrain surrounding the bridge and is determined in accordance with table 4.1 in EC1.1-4. It is assumed a terrain category 0 for the wind blowing across the bridge and terrain category 2 for the wind blowing along the bridge, giving  $z_{0,0} = 0.003\text{m}$  and  $z_{0,2}=0.05\text{m}$ .  $u_*$  is determined based on the 50-year wind speed and used to calculate of the wind distribution along the height.

$$\frac{U(z)}{u_*} = \frac{1}{k} \cdot \ln\left(\frac{z}{z_0}\right) \quad (4.1)$$

By plotting the distribution of the wind, a suitable function could be found by the curve fitting tool in Matlab. The wind profiles are shown in figure 4.1 and 4.2 for Halsaneset and figure 4.3 and 4.4 for Aakvik. Based on the results, the wind speed at Halsaneset is generally larger than the wind speed at Aakvik. Conservatively, the wind profile for Halsaneset both along and across the bridge will be used in the calculations.

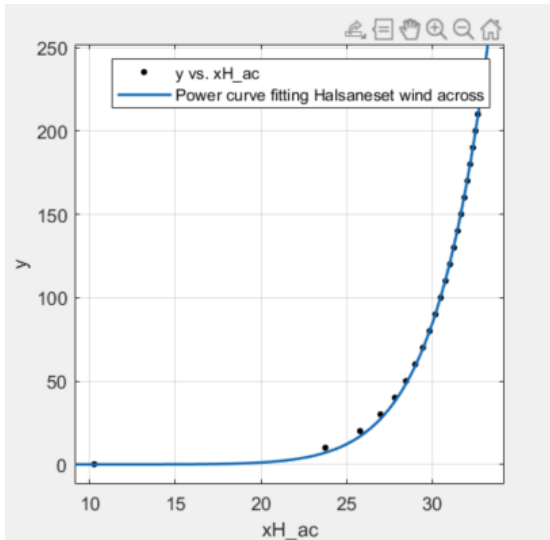


Figure 4.1: Wind profile Halsaneset across

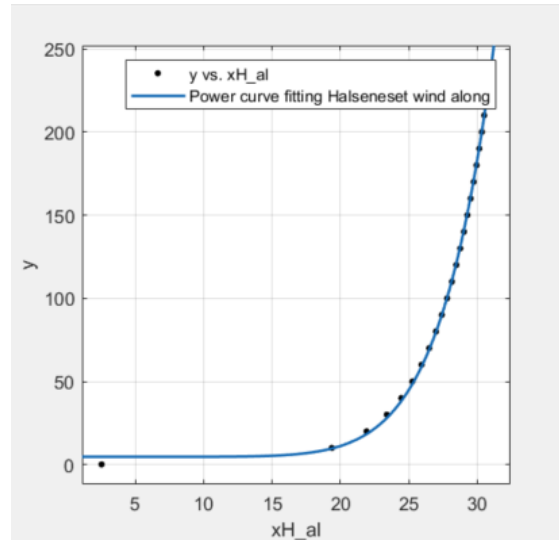


Figure 4.2: Wind profile Halsaneset along

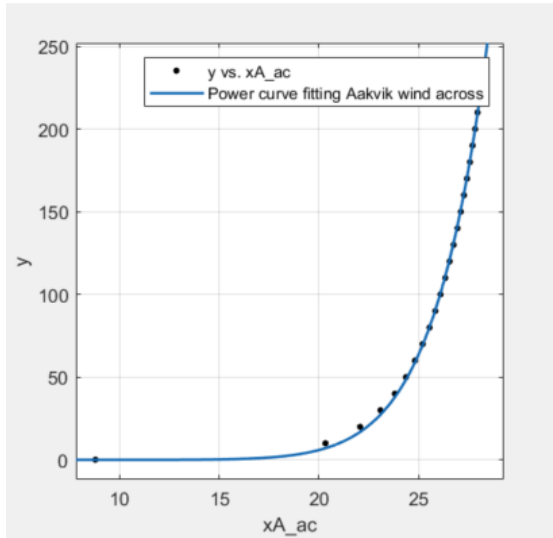


Figure 4.3: Wind profile Aakvik across

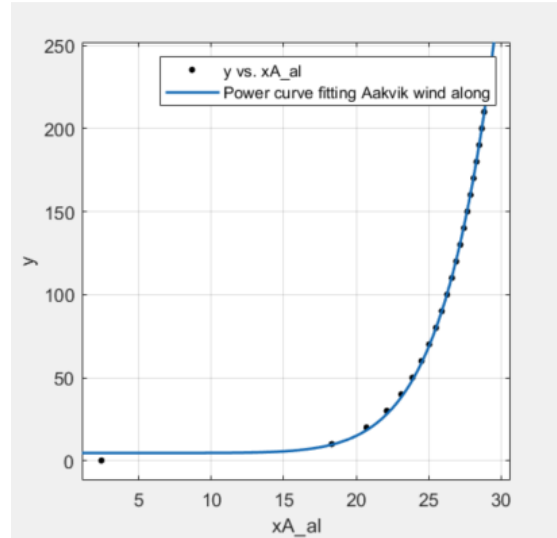


Figure 4.4: Wind profile Aakvik along

Based on the reference wind speed at the bridge site, the top value for the gust speed pressure is calculated based on formulas in "12-2950 Hardangerbrua - Beregninger" and EC1-1.4 section 4. The maximum gust speed pressure is used to calculate the static wind load acting on the structure, described more thoroughly in the sections below. The force coefficients included in calculating the static wind pressure are calculated based on formulas in EC1-1.4 section 7.6.

#### 4.3.1 Wind loads on the free-standing towers

The towers are at their most vulnerable when the casting is finished, and the cables and stiffening girder are not yet attached. At this stage, the tower statically works as a large vertical cantilever exposed to horizontal winds. Hence, the towers are responsive to significant displacements imposing large moments at the bottom of the towers.

During construction, additional equipment such as the crane, the construction elevator and the form-work is still a part of the structure. The area influenced by the wind is enlarged, hence increasing the forces along the height of the towers. The elevator and the crane is taken into account as an additional width up to 240 m. Thus, the wind influencing the last part of the crane will be considered a point load at the top of the towers. Furthermore, the form-work will be added as an additional width of 1.5 m at the tower top.

The static wind load is calculated for each casting stage and considered an evenly distributed load along the centre line of the tower. In addition, the longitudinal wind is of considerable matter influencing the transverse beams. Consequently, added as an evenly distributed load along the width of the beams. Thorough calculations are found in appendix C. A large part of the vertical reinforcement and the foundation could be decided based on these forces. Analysing the free-standing towers is a special case during the global analysis which need extra attention.

### 4.3.2 Wind loads on the complete bridge

There are two load cases relevant for the complete bridge, wind pressure along the length of the bridge and across the bridge. In these load cases, the crane, construction elevator and form-work are removed, hence not increasing the area affected by the wind. Along the length of the bridge, the wind will affect the towers and the transverse beams. In this case, the tower top is restrained, implying a stiffer structure than the free-standing tower and smaller displacements.

Across the bridge, wind pressure on the main cable, stiffening girder, and vertical suspender has to be taken into account. The wind pressure on these components is calculated and assumed transferred to the tower top. Displacements in the transverse direction of the bridge are relatively small due to the transverse beams, which contribute to the horizontal stiffening of the towers. However, transverse wind could force each tower column in different directions, moving one column upwards and the other downwards, creating transverse stresses which should be investigated. The wind pressure will similarly be calculated for each casting stage and added as an evenly distributed line load at the center-line of the towers and the transverse beams. The complete calculations are found in appendix C.

## 4.4 Load combinations

Load combinations are used to determine the design value of the external loads affecting a structure. The relevant design value should be determined according to the rules and guidelines given in EC0, hence by combining the loads that could occur simultaneously. The eurocode states principles and requirements for the safety, serviceability and durability of structures and addresses the two limit states relevant for the design of a structure.

Design according to the ultimate limit state should secure the safety of people and the structure and is often used for larger structures and for global analysis. The serviceability limit state considers the function of the structure, well-being of the people and the appearance after construction. However, this limit state often focuses more on the details, such as joints and displacements. As a result, calculations according to the ultimate limit state form the basis for the design of the bridge across Halsafjorden.

The ultimate limit state is defined as the capacity of the structure at risk of fracture, large inelastic displacement or strains. EC0 defines four different ultimate limit state conditions EQU, STR, GEO and FAT. EQU represents the loss of static equilibrium. STR and GEO define failure or excessive deformations of respectively the structure and the ground. In contrast, FAT takes into account the fatigue failure of the structure. The thesis will address the STR ultimate limit state because it accounts for external loads and internal resistance for the structure. Thus, section 6.4.3.2 in EC0 present two equations for the combination of rules according to STR, equations 6.10a (equation 4.2) and 6.10b (equation 4.3). The most adverse of the two will form the basis for the design value of the relevant load case.

$$\sum_{j \geq 1} \gamma_{G,j} G_{k,j} + \gamma_P P + \gamma_{Q,1} \psi_{0,1} Q_{k,1} + \sum_{i > 1} \gamma_{Q,i} \psi_{0,i} Q_{k,i} \quad (4.2)$$

$$\sum_{j \geq 1} \xi_j \gamma_{G,j} G_{k,j} + \gamma_P P + \gamma_{Q,1} Q_{k,1} + \sum_{i > 1} \gamma_{Q,i} \psi_{0,i} Q_{k,i} \quad (4.3)$$

The relevant load cases for the towers are listed below and based on the three external loads applicable in the thesis. Furthermore, the combinations follow the rules listed in table NA.A2.4(B) in EC0, shown in table 4.5. Moreover, the related factors are found in table A2.1 and NA.A2.4(B).

1. Wind load along the length of the bridge on the free standing pylons in addition to self-weight.
2. Wind load along the length of the bridge after completion in addition to self-weight and traffic load.
3. Wind load across the length of the bridge after constriction in addition to self-weight.

Persistent and transient design situation	Permanent actions		Prestress	Dominating variable action	Other variable actions
	Unfavorable	Favorable			
Equation 6.10a	$\gamma_{G,j,sup} G_{k,j,sup}$	$\gamma_{G,j,inf} G_{k,j,inf}$	$\gamma_p P$	$\gamma_{Q,1} \psi_{0,1} Q_{k,1}$	$\gamma_{Q,i} \psi_{0,i} Q_{k,i}$
Equation 6.10b	$\xi \gamma_{G,j,sup} G_{k,j,sup}$	$\gamma_{G,j,inf} G_{k,j,inf}$	$\gamma_p P$	$\gamma_{Q,1} Q_{k,1}$	$\gamma_{Q,i} \psi_{0,i} Q_{k,i}$

Table 4.5: Load combination in the ultimate limit state

#### Load combination one

During load combination one, only self-weight and wind load are affecting the free-standing towers. The wind load initiates to bending in the longitudinal direction of the bridge and is therefore unfavourable. Furthermore, the self-weight generates additional bending due to second-order moments, which is considered as unfavourable. The wind load contributes to the bending of the tower to a much greater extent than the self-weight. Thus, it is relevant to use equation 6.10b with the wind as the dominating force. The distribution of the forces is shown in figure 4.5.

$$\text{Equation 6.10b} : 1.20 \cdot Q_g + 1.60 \cdot Q_w \quad (4.4)$$

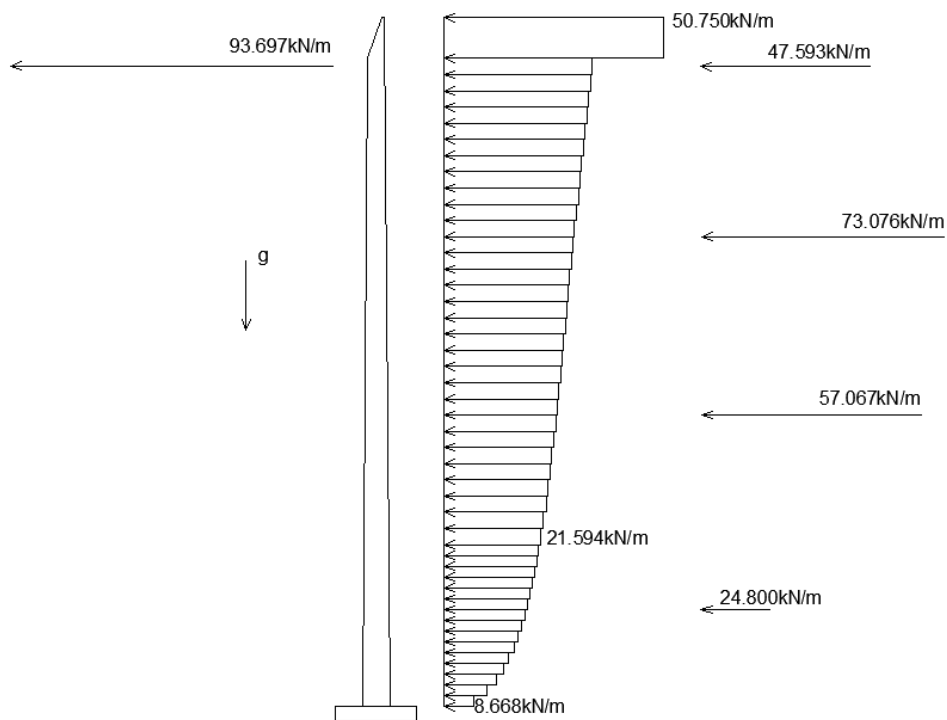


Figure 4.5: Forces imposed by load combination one

#### Load combination two

For the second load combination, the self-weight, traffic load and wind load will all be considered. The self-weight will influence the structure to a greater extent than the wind and traffic load; thus, equation 6.10a is relevant. In addition, the traffic load is unfavourable for bending in the longitudinal direction of the bridge and is therefore included in load combination two. Thus, the traffic load is characterized as the dominating variable force, hence including traffic load without changing the influence of the wind load. The distribution of the forces is shown in figure 4.7 and globally in figure 4.6.

$$\text{Equation 6.10a} : 1.35 \cdot Q_g + 1.12 \cdot Q_W + 0.945 \cdot Q_T \quad (4.5)$$

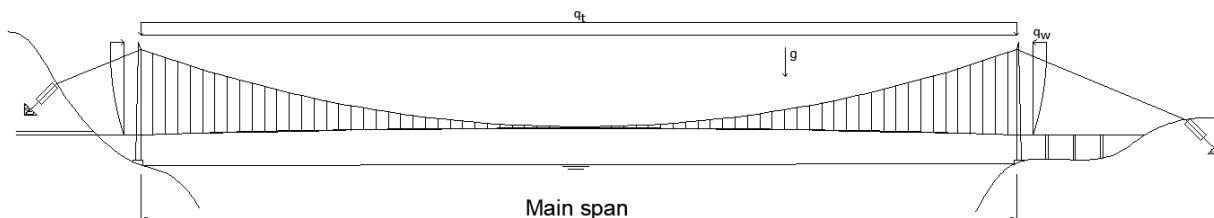


Figure 4.6: Forces imposed by load combination two - global perspective



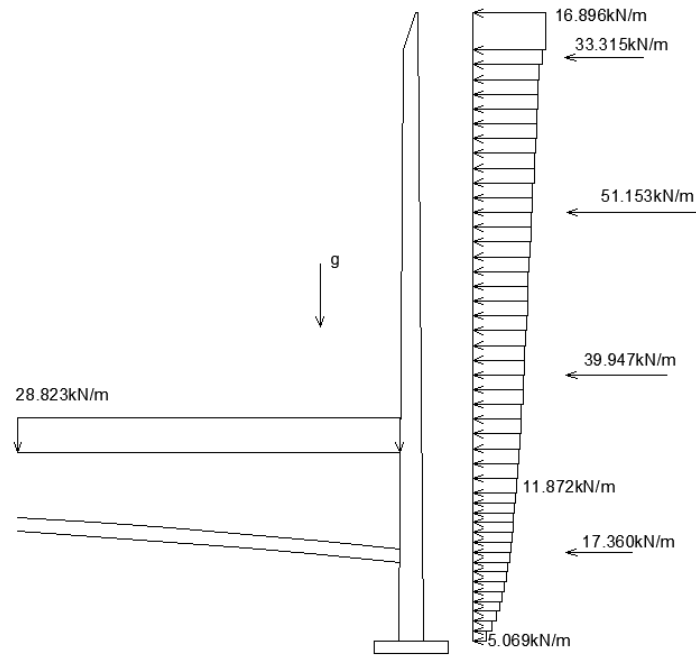


Figure 4.7: Forces imposed by load combination two

Load combination three

For the third load combination, the wind load acting on the structure will be dominating. Thus, table A2.1 notice 3) in EC0 states that the reduction factor for the traffic load should be equal to zero. Hence, only the self-weight and the wind load will be included. Similar to load combination one, the self-weight contributes to second-order effects on the structure. Based on this, equation 6.10b is used.

$$\text{Equation 6.10b} : 1.20 \cdot Q_g + 1.60 \cdot Q_W \quad (4.6)$$

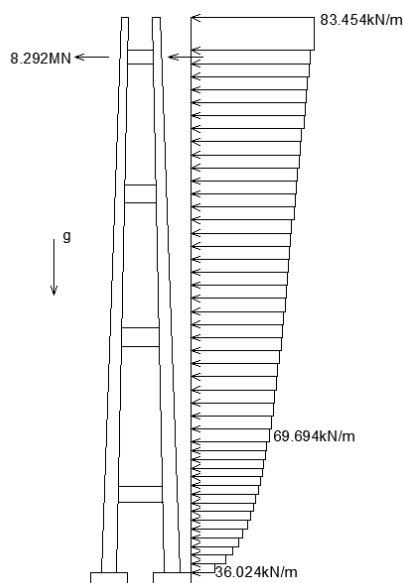


Figure 4.8: Forces imposed by load combination three

## 5 Modelling of the free-standing bridge towers

The purpose of running an analysis is to find the largest forces acting on the structure in order to determine the reinforcement. The finite element method software Abaqus is a convenient program that could perform the desired analysis. A 3-dimensional analysis is necessary to include all stresses and forces. By comparison, a 2-dimensional analysis would only provide the stresses and forces of a single plane. Each component is modelled by one-dimensional elements and given dimensional data such as e-modulus, cross-section area, density and moment of inertia. The method is preferred when the elements have a large extent in one direction, compared to the other directions, suitable for this model.



Figure 5.1: Southern bridge tower of Hardangerbrua. Photo: Roth T. [32]

### 5.1 Abaqus

Abaqus is a powerful finite element analysis software that offers complete solutions. Both for routine and sophisticated engineering problems covering a vast spectrum of industrial applications [33]. Especially suitable for non-linear analysis, which is convenient to obtain the desired geometrical effects during the analysis of the towers. The finite element software solves systems of equations numerically to obtain solutions. Compared to an analytical solution that provides the exact answer, the numerical solution will only approximate the answer. Often used for engineering problems which is difficult to solve analytically. In detail, the software divides the model into different elements, connected by nodes. Depending on the element, each node is provided with degrees of freedom and corresponding equations. Increasing the number of elements usually improve the accuracy of the solution, but also the computational cost.

During the analysis, some elements will be exposed to large deformations, which will be accounted for by implying non-linear geometrical effects. The software considers the effect by continuously updating the stiffness matrix during the analysis. Furthermore, linear material behaviour is used during the analysis, leaving out second-order effects such as cracking of concrete. These non-linear material effects, in addition to yielding of reinforcement, are accounted for during capacity calculations.

Abaqus offers two relevant element types, either beam-elements or truss-elements. The beam elements include both translational and rotational degrees of freedom, which enables the element to extract both axial and shear forces in two directions, in addition to moment in all three directions. On the other hand, the truss element only include translational degrees of freedom, enabling the extraction of axial forces. By using truss elements, it's assumed that there are no transverse forces acting on the elements and pinned connections in both ends.

For the beam elements, the software offers different alternatives. Suitable for the analysis of the bridge, B31 and B32 elements could be used [34]. Both elements are based on the Timoshenko beam theory, which includes shear deformations, enabling modelling of both thick and thin beams. Assuming linear elastic transverse shear behaviour of the beams with a fixed modulus. The shear deformations are usually small compared to the bending deformations of long, slender beams. However, the inclusion of shear deformations will provide a more accurate answer.

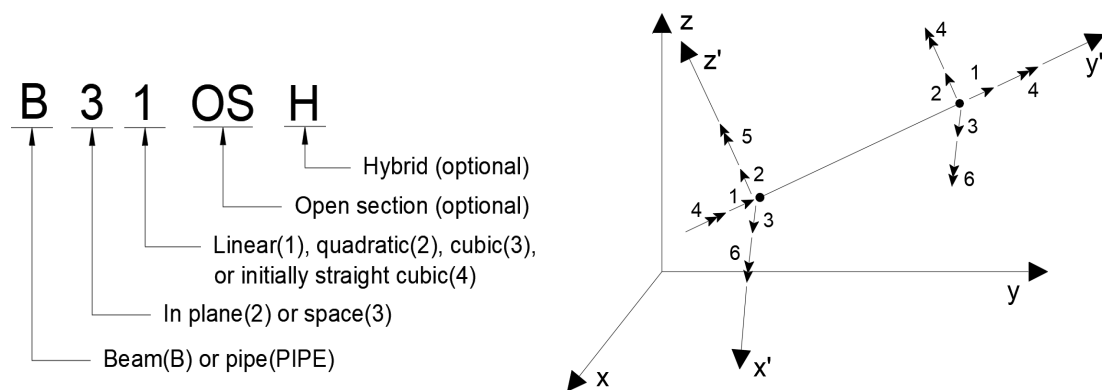


Figure 5.2: Explanation of beam element

### 5.1.1 Element description

The B31 element is a linear beam element in three dimensions, with one node at each end. Each node contains six degrees of freedom, illustrated by figure 5.2. Forces, stresses and boundary conditions at the nodes describe the deformation pattern of the beam. Compared to the alternative elements, B31 is computational cost-effective, making it especially suitable for modelling large structures without line loads and complicated deformation patterns.

The B32 element is a quadratic beam element with three nodes, one at each end and one in the centre. The extra node in the centre of the beam is assigned with boundary conditions, which allows for a more precise deformation pattern. The B32 elements are therefore preferred when the elements are exposed to distributed loads. However, the elements require a higher computational cost.

Hybrid elements are favourable when it is numerically challenging to compute axial and shear forces in the beam by the usual finite element displacement method. The problem often arises in geometrically non-linear analysis when the beam undergoes large rotations combined with a very rigid axial and shear deformation. However, the problem could be solved by simplifying the general problem such that the axial and transverse shear forces in the elements are included, along with nodal displacement and rotations as primary variables [34]. These elements usually converge faster, making them more efficient, even though the initial computational cost is higher.

Truss elements are used to model slender two and three dimensional, line-like structures, only exposed to loads along the centre line of the element. The T3D2 element is a 3-dimensional, 2-node truss element, which uses linear interpolation for position and displacement over constant stress. A hybrid version of the element treats the axial force as an additional unknown, making the elements useful when the truss represents a very rigid link whose stiffness is much larger than the overall structural model.

## 5.2 Modelling the geometry

The global axis system is defined with a horizontal x-axis parallel to the length of the bridge. The height of the towers is modelled along the global z-axis with a positive vertical direction pointing up towards the tower top. The y-axis defines the depth of the structure with a positive direction perpendicular to the length of the bridge.

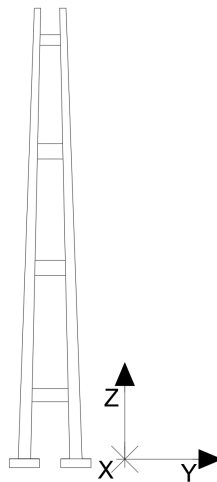


Figure 5.3: Axis system

As described in the previous section, one-dimensional elements are used to model the towers. The elements are positioned along the central line of the towers before cross-section, and material properties are specified. Since the towers are exposed to both self-weight and distributed wind loads along the height, B32 are the most suitable elements for the model. Along the height of the towers, the cross-section area, moment of inertia and torsion constant vary. For this reason, the geometrical properties are calculated and added individually for each casting stage. The towers are divided into 45 casting stages, where the first 15 stages are 4 meters tall, and the last 30 are 6 meters, making it a total of 240 meters. In addition, an equivalent tower top like the one used for Hardangerbrua is added, extending the towers to 257.5 meters. Furthermore, the towers at each side of the bridge are assumed to have an identical geometry, along with equivalent geological and weather conditions. Therefore, calculating one tower is applicable for both.

Four transverse beams connect the two columns of each tower, creating a solid link that prevents transverse motion in the global y-direction. The first beam is positioned at 36 meters above ground, supporting the stiffening girder in addition to creating transverse stability. The second and third transverse beams are positioned at respectively 108 and 174 meters, while the top beam is positioned slightly below the cable connection point, at 237 meters. Each beam is modelled with five B32 beam elements with a total of 11 nodes. Accordingly, node 1 and 11 is shared with the tower.



Figure 5.4: Abaqus model of the free-standing tower

Boundary conditions are essential for the model to work appropriately. Since the towers are built along the fjords, the ground conditions are primarily solid rock, which is favourable for a strong foundation. Small rotations and translations could have catastrophic consequences for the bridge, both during construction and when finished. For this reason, it is reasonable to apply fixed boundary conditions at the bottom of each pylon.

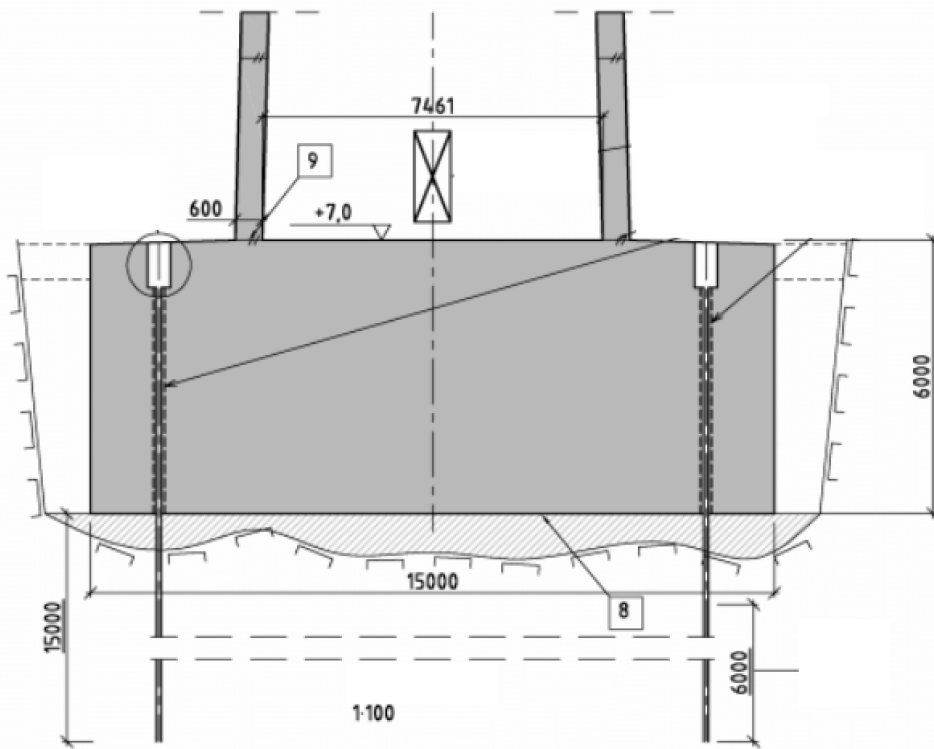


Figure 5.5: Foundation used on Hardangerbrua. Drawing K405 [13]

### 5.3 Modelling the loads

The free-standing towers are subject to load combination one, hence self-weight and static wind pressure. The self-weight is modelled by adding the gravitational constant, the density and a cross-section area to each element. By implying a function contained by the software, the self-weight is calculated and added as a force vector. The vector is added at the mass centre of each element. During the analysis, second-order moments occur when the tower bends due to wind loads, illustrated by figure 5.6. While the gravitational centre moves away from its original position, a moment arm is created, increasing the second-order moment. These non-linear geometrical effects are taken into account by continuously updating the force balance with respect to the deformed geometry. Correspondingly, the first-order moments develops from the external loads imposed horizontally along the height of the tower. Henceforth, the analysis from Abaqus returns the summarized value of the first and second-order moment.

Initially, the wind pressure for each casting stage, transverse beams and additional equipment such as the crane and casting form is calculated as described in section 4.3. The cross-section area of each component is taken into account during the calculations to enable the unit of measurement  $[N/m]$  to match the use of one-dimensional elements. A line load is added based on the intensity and direction of the force. The additional forces caused by the crane top is conservatively modelled as a point load at the highest connecting point in between the crane and the tower.

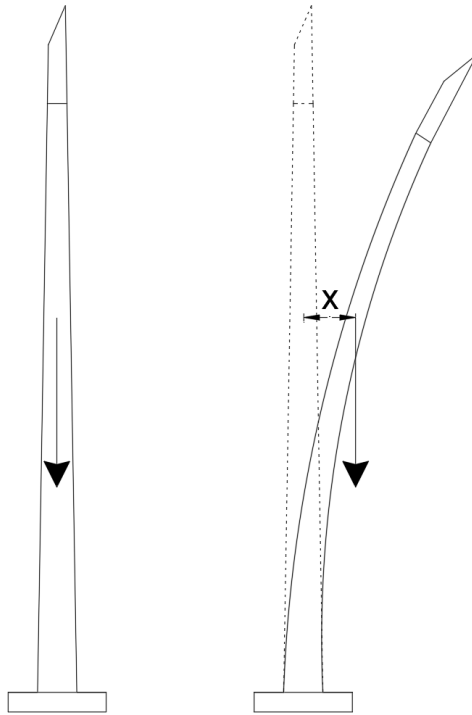


Figure 5.6: Development of second-order moment

The towers are affected by multiple loads at the same time. In order to find the most adverse load situation, load combinations are used, more thoroughly explained in section 4.4. Regarding the modelling of wind load, a combination factor is multiplied by the magnitude of the wind force. For the gravity, the simplest way of application is through the gravitational constant. By multiplying the gravitational constant with a load combination factor, the dead-weight is increased to its desired magnitude.

To ensure that the loads are imposed in the right order, the application is divided into two steps. In the first step, the gravitational force, including the load combination factor is added to each element. By default, the software increases the magnitude of the load linearly throughout the step. Implying full magnitude first by the end of each step. Practically, the dead-weight is therefore completely applied by the start of the second step. Throughout step two, the wind load is added, with full effect by the end of the step.

## 6 Modelling of the complete bridge

A global analysis of the complete bridge will provide a broader view regarding the distribution of forces throughout the static system of the structure. Because the most significant compressive forces occur after completion, a global analysis of the whole bridge is necessary. In addition to the self-weight, the bridge is affected by distributed traffic and wind loads, generating large compressive forces in the towers.



Figure 6.1: Assembly of the stiffening girder. Photo: Norconsult [35]

In opposite to the free-standing tower, the bridge towers for the global model are connected to the stiffening girder, the main cables and anchor cables. These new attachments change the static system of the bridge, and hence the critical load combinations. On the positive side, the stability of the towers along the longitudinal direction is substantially increased. On the negative side, the enlarged compressive forces increase the chances of crushing and buckling. The attachment of the cables and stiffening girder also contributes to increased transverse stability. Due to significant crosswinds and compressive forces, transverse moments needs to be taken into account.

For the same reason as described in section 5, a 3-dimensional analysis will be the preferred analysis type for the complete bridge. Accordingly, the finite element method software Abaqus is used. Even though the global model contains complicated components such as the stiffening girder, it's preferred to model every part as one-dimensional elements during a global analysis. In particular, beam or truss elements with material properties and geometrical abilities added to each element group, as described in section 5.1.1.



## 6.1 Modelling

The process of modelling the complete bridge is similar to the modelling of the bridge towers described in section 5. At first, the global axis system is defined. The horizontal x-axis stretches along the length of the bridge. The y-axis represents the depth. Finally, the z-axis is defined as positive in the direction towards the height of the bridge. Each bridge component is separately modelled before it's assembled into a complete bridge.

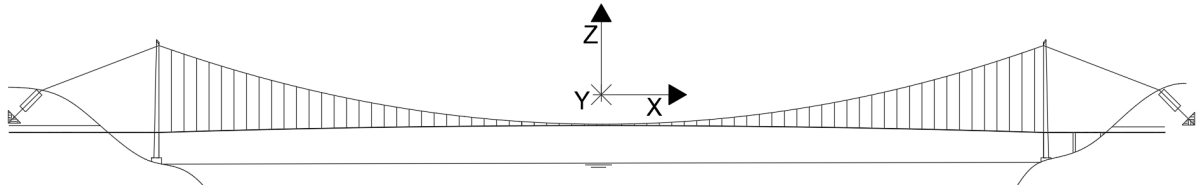


Figure 6.2: Axis system

As described in section 3, scaling theory by Gimsing and Georgakis is used to find the geometric properties of the different components of the bridge, illustrated by figure 6.3.

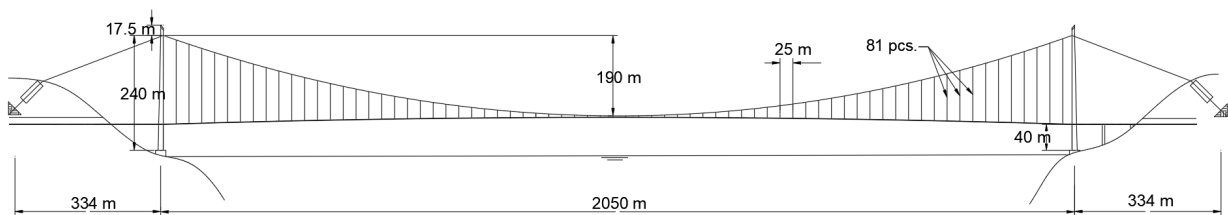


Figure 6.3: Bridge parameters

### 6.1.1 Bridge towers

The bridge towers for the global analysis are modelled in the same way as the towers used for the local analysis described in section 5. The elements are positioned along the centre line of the cross-section and provided with geometrical and material properties. Geometrical abilities such as area, the moment of inertia about the major and minor axis and torsional constant are added individually for each casting stage. In addition, equivalent material properties such as the density, e-modulus and shear modulus are added for all tower elements. Since the towers are exposed to large compressive forces from the main cables and self-weight, in addition to horizontal wind loads, B32 beam elements are the preferred element type.

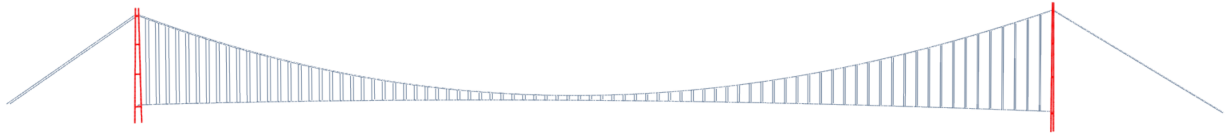


Figure 6.4: Bridge towers

### 6.1.2 Main cables

The main cables are initially divided into two parts, separated by the towers, to simplify the modelling. The first part, named the main cables, is addressed in this section. While the second part, called the anchor cables, is described in section 6.1.3.

The main cables are curved like a quadratic function, implying efficient material use of the high tension steel cables. Based on the height of the towers and the sag of the cable, the quadratic function could be found. Furthermore, the main cables are affected by the self-weight, vertical forces transferred from the suspenders in each connection point and evenly distributed wind pressure, more thoroughly described in section 6.3. Preferably for the specified loads and abilities of the cables, B32 beam elements are used. The three-node beam element enables a quadratic representation of the deformation, increasing the accuracy, but at the same time also the computational cost.

Based on flexible towers, the cables can rotate freely without transferring any moments to the towers. In reality, the cables could slide along the saddle, best described by a roller. For modelling purposes, the connection point is modelled as pinned by implementing releases to the relevant connecting elements.

The purpose of modelling the cables with beam elements instead of truss elements is mainly due to the different geometric abilities of each element. In general, when the large compact cables are highly tensioned, geometric properties such as the moment of inertia and torsional constant needs to be taken into account. Beams enable adding of the moment of inertia and torsional constant during modelling, unlike the truss elements.

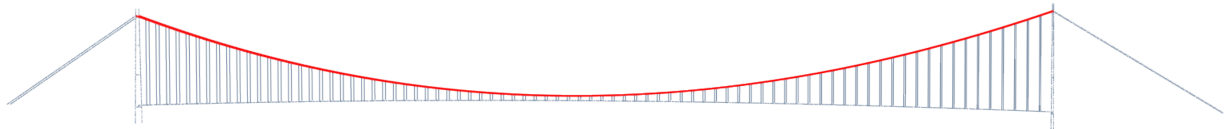


Figure 6.5: Main cables

### 6.1.3 Anchor cables

The primary function of the anchor cables is to transfer horizontal forces from the main cables to the ground, keeping the bridge towers in place. By modelling the cables linearly, the large tensile forces are efficiently distributed. The anchorage cables are subject to both self-weight and static wind pressure. Furthermore, the wind forces are summarized and added as a point load at the tower top for simplicity and numerical stability. As a result, only self-weight affect the linear cables, making B31 elements favourable. Alike the main cables, the connection points between the anchor cables and the towers are pinned, enabling transition of axial forces, but not moments. The material and geometrical properties of the anchor cables are the same as for the main cable, including the same cross-section, geometrical stiffness and torsional constant.

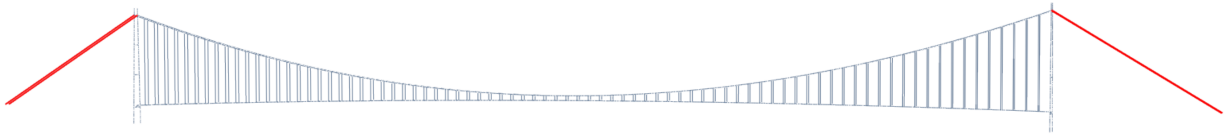


Figure 6.6: Anchor cables

### 6.1.4 Vertical suspenders

The main task of the vertical suspenders is to distribute forces from the stiffening girder to the main cables. In addition, the suspenders are subjected to self weight and wind forces. Like the main cables, the wind forces are summarised into a point load and applied at the tower top. The suspenders are subjected to large tensile axial forces for the relevant load cases and contribute to minor geometrical stiffness. Hence, truss elements are favourable because of their ability to transfer axial forces and low computational cost. As described in section 3.4.1, the fastening joint between the suspenders and the main cables rotate freely about the y-axis but is kept fixed about the x- and z-axis. However, the truss elements are pinned at the ends, implying free rotation in all directions. The simplification is assumed to have insignificant effects on the results.

Considering that each suspender is subjected to only self-weight and forces at the connection points, each suspender could be modelled by the use of one element. In other words, efficient use of elements, saving computational cost and reduces the chances for numerical difficulties. The preferred truss element is T3D2, a 3-dimensional 2-node truss element more thoroughly described in section 5.1.1. Unlike the beam elements, truss elements don't have any initial stiffness. Notably, no geometrical stiffness or torsional constant needs to be added. Figure 6.7 marks the vertical suspenders in the global system of the suspension bridge.

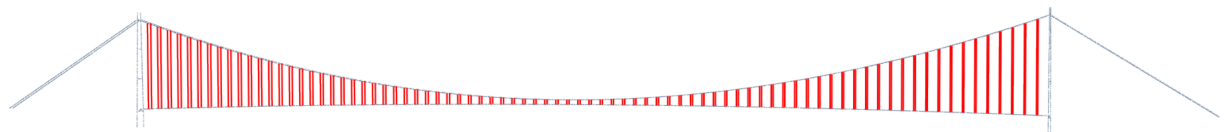


Figure 6.7: Vertical suspenders

### 6.1.5 Stiffening girder

The stiffening girder is a hollow steel box with aerodynamic abilities, wide enough to include two driving and one pedestrian lane, as described in section 3.5. With a complicated shape and connections to several other components, the girder's modelling needs special attention to obtain the desired effects during a global analysis.

At first, the quadratic function describing the curvature of the complete stiffening girder needs to be decided. The reference height equals the height of the asphalt driveway. Based on this, the traffic loads could be applied at the correct height later during the analysis. However, the reference height moves the mass centre of the stiffening girder above its original position, moving the force vector of each element upwards. Hence, during a static analysis, the moved mass centre will affect the results insignificantly and are not considered.

At each end of the span, the stiffening girder is positioned 4 meters above the bottom transverse beam to ensure space for the extended parts of each component. Due to the use of one-dimensional elements, a connecting element is needed to fill the 4-meter gap, more thoroughly described in section 6.1.6. In the middle of the span, the concave quadratic function is positioned 3.2 m below the main cable sag. Over the distance of 2050 meters, the difference in height between the start and centre point is only 8.3 meters and could therefore be simplified into a straight line. However, such simplification would decrease the length and therefore also the total self-weight and traffic load. As a result, the quadratic form is kept constant.

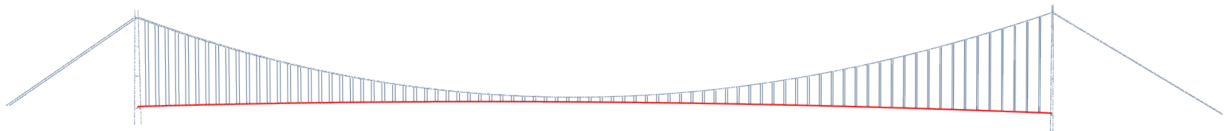


Figure 6.8: Stiffening girder

The stiffening girder is mainly affected by self-weight, traffic loads and wind loads. B32 beam elements are favourable to attain the affection of the girder's distributed traffic loads and curved shape. The additional centre node improves the deformation and distribution of forces throughout the static system but increases the computational cost. Furthermore, geometrical and material properties are added to each beam element according to the properties calculated in section 3.5. Values for mass and rotary inertia per unit length needs to be added, generally, these values are implemented by adding a beam added inertia with the desired properties from table 3.7. By adding mass and rotary inertia, the software automatically defines the mass proportional damping, enabling dynamic analysis of the bridge.

Initially mentioned, the stiffening girder has a transverse extent such that the vertical suspenders can be attached to the girder directly. However, by using one-dimensional elements along the centre line of the bridge, a horizontal gap appears between the stiffening girder and the bottom of each vertical suspender. Beam elements are used to account for the gap. The main function of the connecting elements is to transfer forces from the stiffening girder to the suspenders without affecting the deformation of the static system. B31H, hybrid beam elements with an enlarged stiffness, is used to obtain the desired effect. The large stiffness is acquired by adding large material properties to the elements, such as  $A = I = J = 1000$ . In comparison, the stiffening girder itself has an area of  $0.58m^2$ ,  $A = 0.58$  and  $I_y = 16.448$ . Hybrid elements are used to prevent numerical issues related to high stiffness elements combined with the usual elements. The connections between the stiffening girder and the stiff beam connectors are modelled as fixed to ensure for free distribution of forces.

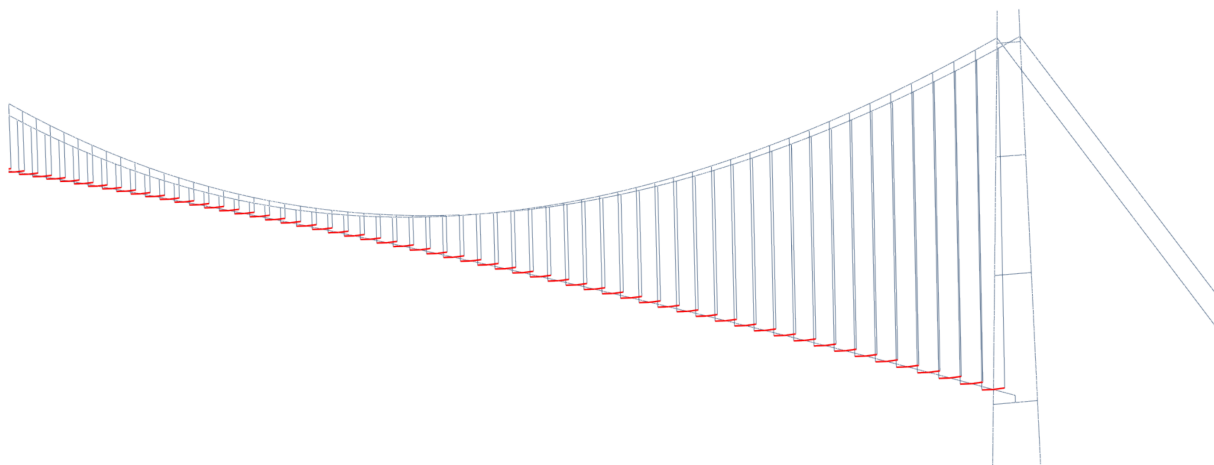


Figure 6.9: Connecting beam elements with high stiffness

### 6.1.6 Connection between the stiffening girder and the towers

The stiffening girder and the bottom transverse beam are modelled with one dimensional beam elements in which the material properties are added afterwards. Even though material properties such as the area is added, the elements still don't have any extent, leaving a gap between the components. A connecting element is needed to connect the stiffening girder to the tower. Correspondingly, the forces between the elements need to be transferred realistically, without interfering with the static system.

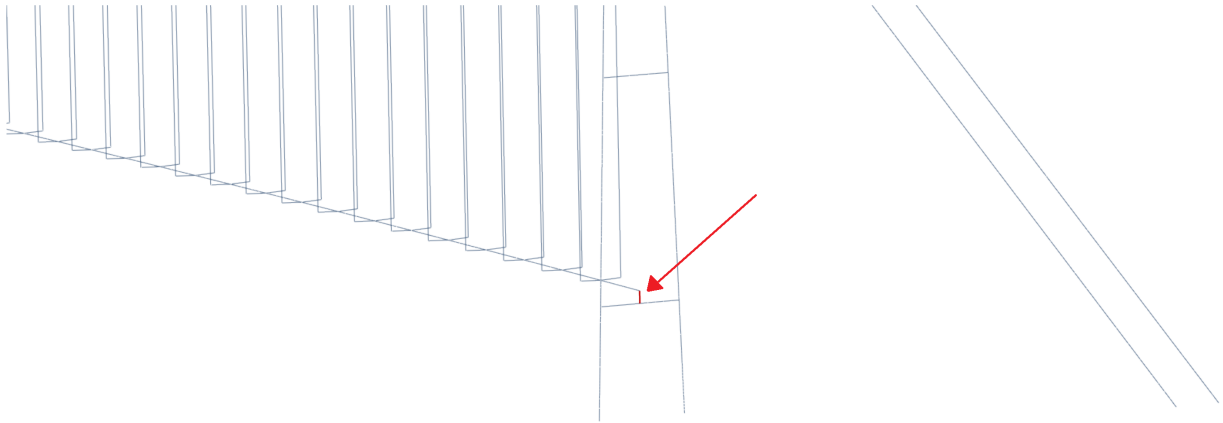


Figure 6.10: Connecting element between the stiffening girder and the transverse beam

As figure 6.13 shows, the connection is simply supported with a horizontal roller and a damper in the longitudinal direction. Additionally, a couple of pendulum bearings distributes some vertical forces but mainly function as stabilizers. A truss element combined with boundary conditions at the connection point is used to ensure the transition of axial forces only and not shear forces and moments. The most suitable element, in this case, is a 2-node, hybrid truss element with enlarged stiffness, named T3D2H. By increasing the stiffness, the distribution of forces is imposed without interfering with the static system and prevent failure due to buckling. Like the connecting elements at the stiffening girder, hybrid elements are used to account for the increased stiffness compared to the connecting elements. Furthermore, the truss elements are pinned at each end, enabling the transfer of only axial forces. Combined with the boundary conditions explained in section 6.1.7, the transition is almost equivalent to reality and valid for the desired analysis of the tower.

### 6.1.7 Boundary conditions

Boundary conditions are added to recreate transitions. It can be used between either the model and the ground or between different components of the model. The correct application of boundary conditions contributes to obtaining the desired behaviour. Boundaries could also be added to remove undesirable effects which contribute to unfavourable behaviour or numerical issues. Illustrated by figure 6.11, the translational boundaries are represented by the orange cones, while the blue cones represent the rotational boundaries.

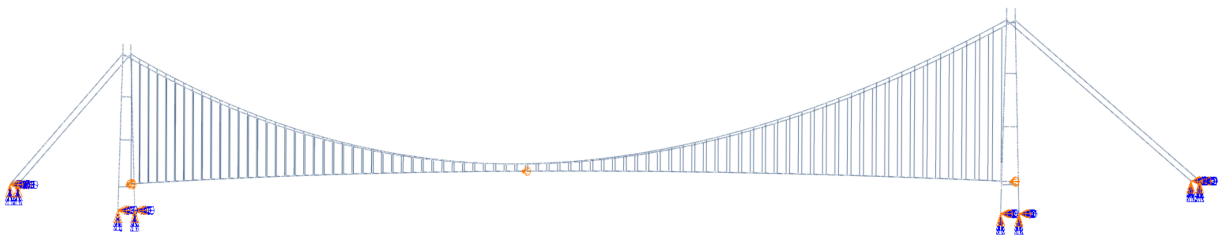


Figure 6.11: Boundary conditions

A boundary condition is added to the stiffening girder at the middle of the span to prevent translational motion along the  $y$ -axis. The connecting joints between the suspenders and both the stiffening girder and the main cables are automatically modelled as pinned when using T3D2 elements for the vertical suspenders. Therefore, the static system is not very resistant to transverse motion, and numerical complications could occur, also without any transverse loads. In reality, the connecting joints to the stiffening girders are constrained about the  $y$ -axis, contributing to transverse stiffness. In addition, the stiffening girder itself incorporates some stiffness in the transverse direction.

Initially described in section 5, the foundation is cast in a solid rock which creates a strong base without translational or rotational movement. Therefore, it is reasonable to model the bottom node of each tower as fixed.

The anchor system used for both Hardangerbrua and the bridge across Halsafjorden is based on the method of tunnel anchorage. Inside the anchor system, the cables are spread and tread further into the mountain before the forces are distributed onto the solid rock. The cables are fastened in all directions, which prevents both translational and rotational movement. Accordingly, the connections are modelled as fixed.

Boundaries need to be added to complete the transition between the stiffening girder and the transverse beam. Illustrated by figure 6.12, there is a horizontal roller, a damper in the longitudinal  $x$ -direction and a couple of pendulum bearings. The damper allows for small displacements. However, from a global perspective, the displacements are insignificant. Thus the displacements along the  $x$ -axis are constrained. There is little movement allowed in the transverse direction of the roller, and in combination with the pendulum bearings, the joint obtain some stiffness along the depth/ $y$ -direction. To obtain the desired behaviour and the correct distribution of forces in the joint, translational motion in the  $y$ -direction is constrained. By implementing these constraints combined with the use of T3D2H truss elements, as described in section 6.1.6, only axial forces along the vertical/ $z$ -axis are transferred in the joint. Furthermore, rotational stability is obtained by the pendulum bearers. However, due to the pinned connection and distribution of axial forces from the truss elements, it's not necessary to implement additional constraints.

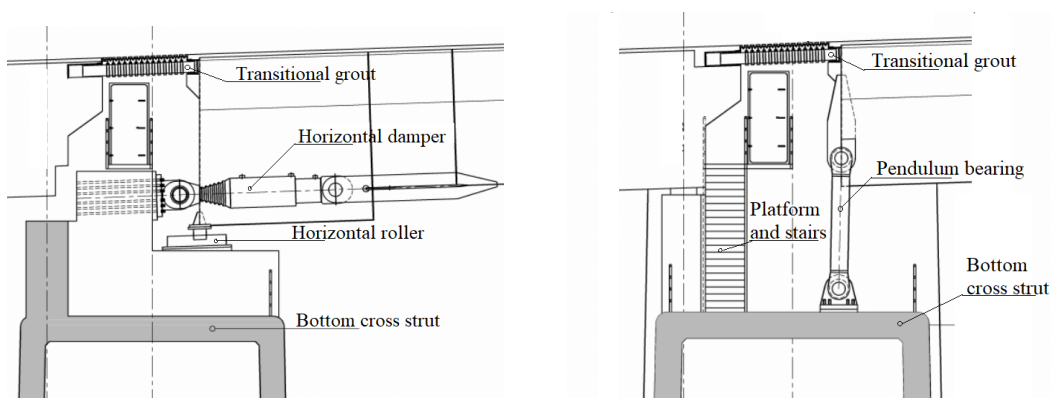


Figure 6.12: Perpendicular view of the connection. Drawing: K807 [13]

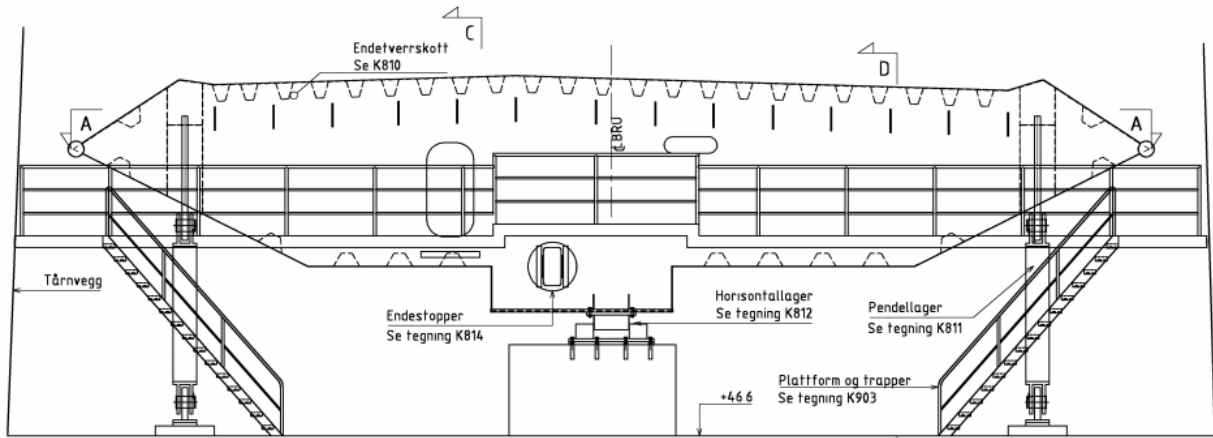


Figure 6.13: Connection between the stiffening girders and the transverse beam. Drawing: K807 [13]

## 6.2 Assembly

In general, the construction of suspension bridges is a complicated process that requires good planning and intelligent solutions to complex problems. Usually, the process is divided into three major steps, each responsible for the assembly of different bridge components [36].

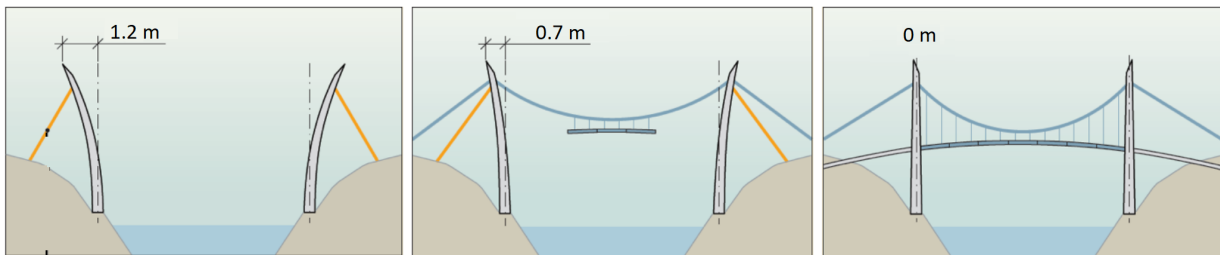


Figure 6.14: Assembly of a suspension bridge. Technical brochure of Hardangerbrua: [36]

### First step - Contraction of the towers

In the first step, the towers are constructed. When the cast is finished, a retraction cable is attached to the tower top. The cable is used to pull the top of the towers out of position, back towards the shore. As shown in figure 6.14, the towers are initially pulled between 1.2-2 meters, depending on the bending stiffness of the tower. Implementation of the pull-back effect in Abaqus could be done in different ways. For instance, a temperature contraction could be implemented by applying an initial temperature to the system and then decreasing the temperature in the anchor cable. If a temperature coefficient is provided, the cable will contract and thereby pull the towers backwards. However, the implementation of temperature contractions could result in numerical difficulties, and another option is therefore used. By simply adding a concentrated point load at the saddle joint in the desired direction, the preferred pull back motion of the towers could be obtained. The magnitude of the load is adjusted to obtain the correct pull back length.



### Second step - Assembly of the main cables

During the second step, the main cable, including the anchor cable, is attached. Due to the pullback of the towers, the main cables are initially tensioned while the anchor cables are not. The force from the main cable is larger than the anchorage cable throughout the step because of greater length, hence also a larger self-weight. Correspondingly, pulling the towers in the opposite direction, towards a neutral position. In reality, the cables are spun, increasing the diameter and therefore also the self-weight linearly, making the step function in Abaqus particularly suitable. At the end of the step, the weight of the main cables moves the towers partially towards a neutral position.

### Third step - Assembly of the stiffening girder and hangers

In the third step, the vertical suspenders and the stiffening girder is attached, increasing the tension in the main cable. Thus, by the end of the third step, the point load applied during the first step is scaled to match the combined weight of the cable, vertical suspenders and stiffening girder. Therefore, the towers are moved back to the original position, vertically straight, illustrated by figure 6.14. In this position, the towers are only subjected to compressive axial forces and the corresponding moments are about zero, as illustrated by figure 6.15 and 6.16. The figures show how the desired force distribution is obtained throughout the steps.

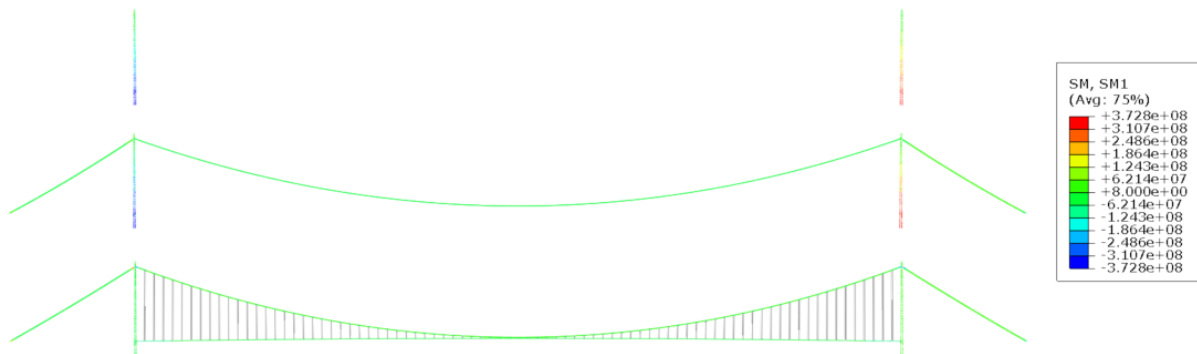


Figure 6.15: Distribution of moment stresses during assembly.

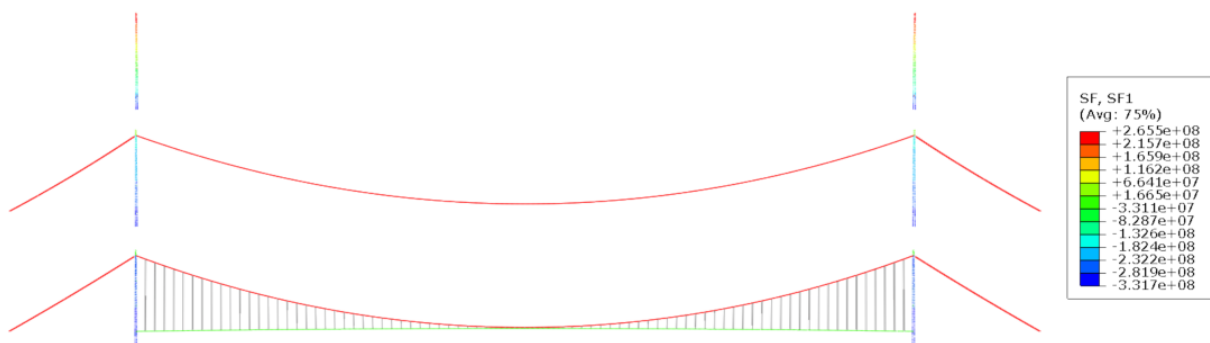


Figure 6.16: Distribution of axial forces during assembly.

In general, materials with tensile abilities will extend while exposed to large tensile forces. Hence, the main cable extends when imposed by self weight as well as the weight of the vertical suspenders and the bridge deck. The nodes of the main cable are initially modelled up to 15 meters above the desired position to account for the increased tension in the cable, thus making the curve less convex. At the end of the third step, the sag is increased by 15 meters, moving the cable to its desired height. Correspondingly, the nodes of the stiffening girder are initially modelled up to 8.1 meters above the final height, making the function more concave. Due to self-weight, the stiffening girder will return to the desired position by the end of step three. By implying the modified functions, the gravitation will move the static system to its desired position by the end of the third step. When the balanced, moment-free static state is achieved, external loads such as traffic and wind could be applied.

### 6.3 Modelling the loads

The complete bridge is subject to load combination two and three. Thus, self-weight, wind and traffic load in the longitudinal direction of the bridge and self-weight and wind load in the transverse direction.

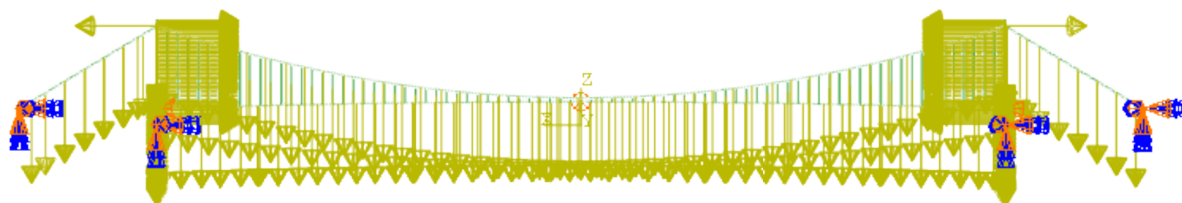


Figure 6.17: Loads and boundary conditions at step four (LC2)

The self-weight is implemented by adding the gravitational constant, density and a cross-section area to each element. A built-in function in Abaqus calculates the contribution of the self-weight for each element and applies a corresponding force vector. As explained in section 5.3, geometrical non-linear second-order effects due to bending are accounted for by Abaqus.

The wind loads are initially calculated as described in section 4.3. To enable the unit of measurement  $[N/m]$  to match the use of one-dimensional elements, the surface area of each casting stage is taken into account during the calculations. Furthermore, loads are implemented by adding a line-load to each element, combined with a direction and a magnitude. In addition to wind forces on the towers, other elements such as the stiffening girder, the vertical suspenders and the main cables are affected by wind. The wind loads affecting these elements are summed up and modelled as a point load in each tower top for simplicity. In reality, some of the forces are transferred directly from the stiffening girder to the tower. Thus the simplicity is conservative.

Another dominating force that needs to be accounted for is the traffic load. In accordance with the requirements stated by the traffic standard, the magnitude and application area is calculated as described in section 4.2. Like the wind load, the traffic load is modelled by adding a line load. The traffic line load is added to each element of the stiffening girder, with a direction and a constant intensity.

As described in section 4.4, load combinations are used to determine the dimensioning forces. Like the free standing towers, the load factors are implemented by multiplying each load with its respected factor. The multiplication is conducted directly for the wind and traffic loads, while for the self-weight, the gravitational constant is changed according to the respectable combination factor.

Furthermore, the loads are applied in different steps to ensure the correct behaviour of the static system during the analysis. Thoroughly described by section 6.2, the three first steps addresses the application of self-weight, in addition to a point load that enables the neutral position of the towers. During the fourth step, external loads such as wind and traffic loads are applied. The loads are applied linearly, enabling full effect at the end of each step. Thus, the full force and stress situation are available by the end of step four.

## 7 Method of calculation

### 7.1 Method of Lamellae

The method of lamellae is a general method frequently used in many applications, briefly explained in *"NB Publikasjon nr. 38"* [22]. For this project, the method is formatted in a modified version of an excel program, officially developed for fibre concrete. The master thesis *"Styrkebergening av brutårn: Løsning for rekordlang hengebru tilknyttet "Ferjefri E39"* [37] modified the method such that it was valid for an ordinary reinforced cross section. However, additional modifications are performed in the thesis to make the method valid for a cross-section using both ordinary and prestressed reinforcement. During analysis, the method is used as an additional tool to include non-linear material behaviour, which is not accounted for by the Abaqus analysis. Examples of non-linear effects are yielding of reinforcement, cracking of concrete in tension and crushing of concrete in compression. The application of the method is based on certain preconditions. Notably, the validity of the hypothesis of Navier Bernoullis and the negligible tensile capacity of concrete.

The bending stiffness of a cross-section only exposed to bending moment is constant. However, when the cross-section is imposed by axial force and moment simultaneously, the bending stiffness changes by the moment's size. Furthermore, the relationship between the moment and bending stiffness is given by the curvature, illustrated by formula 7.1. Therefore, the ultimate aim of the analysis is to find the moment capacity and the corresponding bending stiffness of a given cross-section.

$$\kappa = \frac{M}{EI} \quad (7.1)$$

#### 7.1.1 The Lamellae

As the name implies, the method is based upon dividing the cross-section area into different sections or lamellae. By default, the initial geometry of the program is set to a solid rectangle with 20 lamellae. However, both the geometry and amount of lamellae could easily be adjusted, making the program suitable for multiple geometries like the ones illustrated by figure 7.1. The cross section area is given a strain distribution during an analysis, implying an individual strain to each lamella according to the distribution.

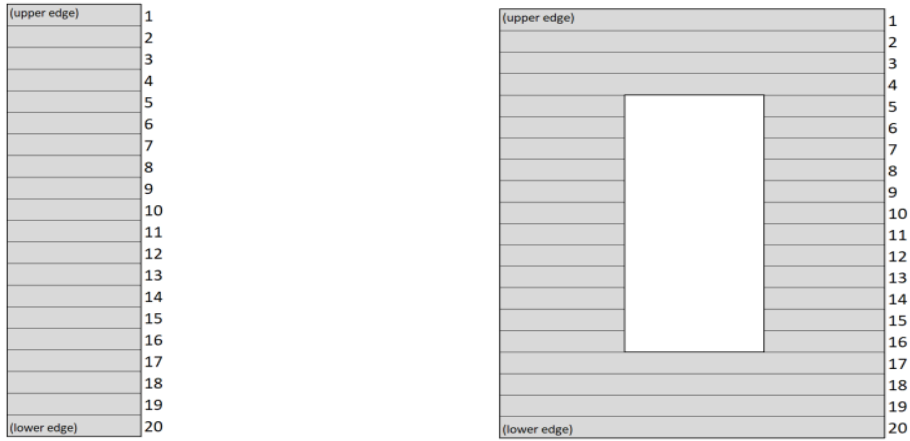


Figure 7.1: Cross-sections divided into lamellae

The strain condition which gives the desired curvature is unknown at the start of the analysis, enabling the power of excel to become handy. At first, the strain at the lower edge is given a value and fed into the program. Accordingly, an excel function called "solver" is used to find the strain at the upper edge, which corresponds to a specific force distribution, more thoroughly explained in a section 7.1.3. Furthermore, the relation between the curvature, strain and height of the cross-section is given by equation 7.2, illustrated by figure 7.2.

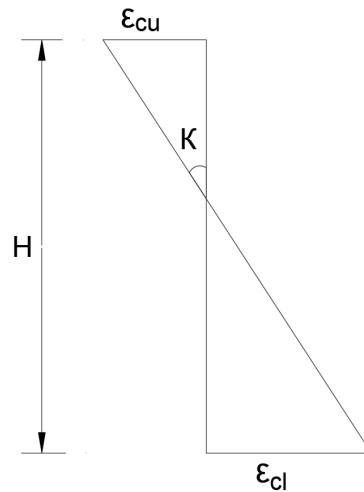


Figure 7.2: Illustration of the relationship between strain and curvature

$$\kappa = \frac{1}{R} = \frac{\epsilon_{cu} + \epsilon_{cl}}{H} \quad (7.2)$$

Following the strain distribution along the height of the cross-section, each section or lamella is given a strain, illustrated by figure 7.3. The use of the material curves finds the corresponding stress, thoroughly described in section 7.1.2. By multiplying the stress component of each lamella with its respectable area, an axial force is calculated. Likewise, the same procedure is implied to find the strain, stress and axial force for the ordinary and prestressed reinforcement.

The axial force from each lamella and the reinforcement contributes to the internal moment of the cross-section. By multiplying the axial force with the corresponding distance between the force vector and the mass centre of the cross-section, the moment is found, illustrated in figure 7.3. Summation of forces are performed according to formula 7.3 and 7.4.

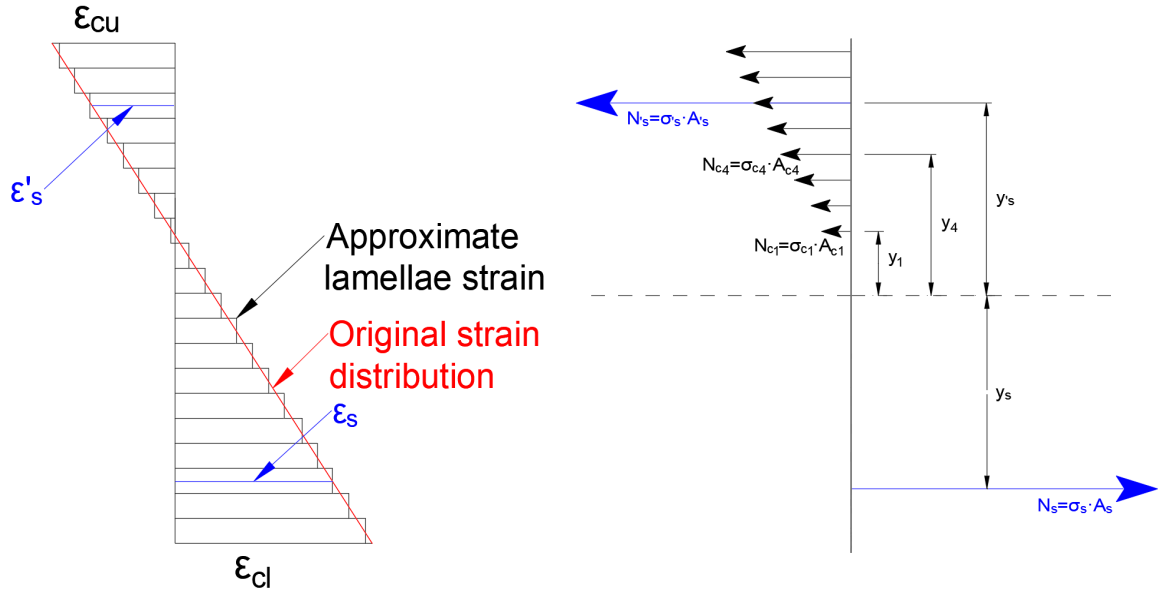


Figure 7.3: Force distribution

$$N = \sum_{i=1}^n \sigma_i \cdot A_i \quad (7.3)$$

$$M = \sum_{i=1}^n y_i \cdot \sigma_i \cdot A_i \quad (7.4)$$

When these calculations are executed in total for the predetermined strain at the lower edge and the assumed strain at the upper edge, one point on the moment-curvature curve is found in addition to one strain distribution. Furthermore, the strain at the lower edge changes with predetermined step size and the method in total is performed with the new strains. The analysis continues until the strain at the lower edge reaches its predetermined maximum value. This method is thoroughly explained in section 7.1.3.

### 7.1.2 Material Curves

To be able to calculate the stresses for each lamella as described in section 7.1.1, material curves for both concrete, reinforcement and prestressed reinforcement is essential. These curves describe the relationship between stress and strain for the different materials. The analysis is conducted according to the ultimate limit state. Equation 3.17 and 3.18 in EC2.1-1 provide the stress-strain relation for concrete, including non-linear effects, represented by equation 7.5.  $f_{cd}$  is the design compressive strength,  $\epsilon_{c2}$  is the strain at the maximum strength and  $\epsilon_{cu2}$  is the ultimate strain.

$$\sigma_c = f_{cd} \cdot \left[ 1 - \left( 1 - \frac{\epsilon_c}{\epsilon_{c2}} \right)^n \right] \quad \text{for } 0 \leq \epsilon_c \leq \epsilon_{c2} \quad (7.5)$$

$$\sigma_c = f_{cd} \quad \text{for } \epsilon_{c2} \leq \epsilon_c \leq \epsilon_{cu2}$$

By implying the formula for the stress-strain relation of concrete, the compressive material behaviour is shaped like a parabola-rectangle, illustrated by figure 7.4. The compressive capacity is reduced from the compressive strength ( $f_{ck}$ ) to the design compressive strength ( $f_{cd}$ ) by both a partial safety factor ( $\gamma_c$ ) and a coefficient ( $\alpha_{cc}$ ) which takes the long term and unfavorable effects into account. Accordingly, the non-linear material effect of cracking is taken into account. In accordance with the preconditions, the capacity of concrete in strain is assumed to be zero.

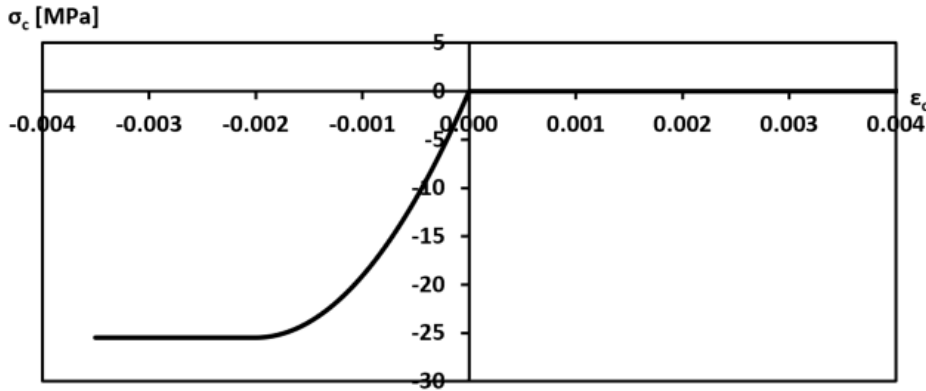


Figure 7.4: Stress-strain diagram for C45 concrete

Section 3.2.7 in EC2.1-1 provide guidelines regarding the material behaviour of reinforced steel. A bilinear stress-strain curve is used to represent the abilities of the material during the ultimate limit state, illustrated by figure 7.5. The characteristic of a bilinear curve is that it assumes an elastic, perfectly plastic model with a yielding plateau. On the contrary, an engineering curve is familiarized with a linearly increasing capacity after the design yield strength is reached due to strain hardening. It's also worth emphasizing that the capacity of the steel is reduced from the yield strength ( $f_{yk}$ ) to the design yield strength ( $f_{yd}$ ) by material factor ( $\gamma_s$ ). Due to a bilinear representation, the strain limits are extended towards 0.075 to allow large yield strains.

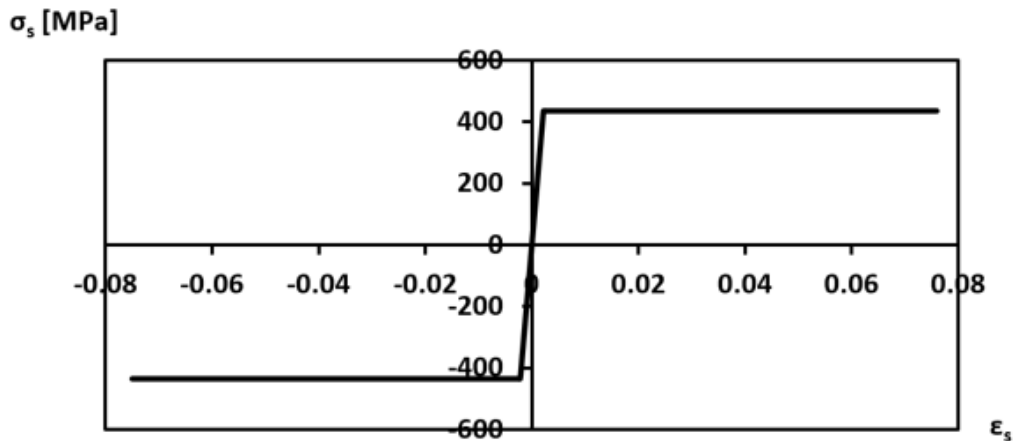


Figure 7.5: Stress-strain diagram for B500NC reinforcement

Alike concrete and reinforcement, EC2.1-1 also provide instructions towards the material behaviour of prestressing steel. Described by section 3.3.6 in EC2.1-1, the stress-strain relation for prestressing steel is represented by a bilinear curve which assumes an elastic, perfectly plastic model behaviour, illustrated by figure 7.6. The capacity is reduced from the characteristic 0.1% proof-stress ( $f_{p0.1k}$ ) to the design stress ( $f_{pd}$ ) by the material factor of steel ( $\gamma_s$ ).

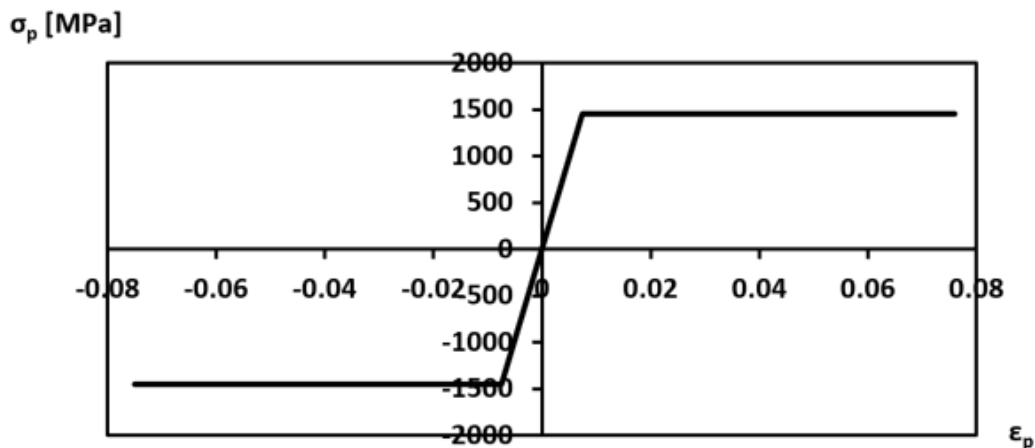


Figure 7.6: Stress-strain diagram for prestressing

### 7.1.3 Excel Lamellae Program

With section 7.1.1 and 7.1.2 in mind, this section accounts for the functionality of the excel program. Excel is a broadly used cell based program with a wide range of functions and it's expected that the reader knows basic functions like "if", "sum" and diagram tools. However, functions like "solver" and "macros" might be unfamiliar and therefore more thoroughly explained.



The *"solver"* function in excel is a tool that enables iterative search for a specific solution based on several unknowns [38]. One or several marked cells are allowed to change within predetermined limits. While these cells change, a target cell, connected to the marked cells, is given a target value. The solver's objective is to change the marked cells for the target cell to reach its desired value. The target value could be a maximum, minimum or a specific value.

The *"macros"* function generates an algorithm based on all actions the user implies within a recording [39]. To create a macro, push the record button in the development toolbar. While the recorder is on, implement the actions to be automatized, then stop the recorder. The macros automatically generate an algorithm that could be placed in the excel program as a button. Each time the user hits the button, the algorithm runs, and the actions are repeated.

Four important components need to be fed into the program, marked in appendix D.

- The initial strain at the lower edge
- The maximum strain at the lower edge
- The strain step size at the lower edge
- The axial force target

Since the ultimate compressive strain of concrete is -3.5‰ for strength classes  $\leq C50$ , it's reasonable to imply a less negative initial strain at the lower edge. Typically, it's interesting to see how the cross-section corresponds to a wide range of strains. Therefore, the maximum strain at the lower edge could be set to a larger positive value, for instance, 5.0‰. The difference between the initial strain and the maximum strain marks the range of which the analysis will run. Based on the range, the step size decides how many increments/steps the analysis will perform. These values are determined within the macros algorithm and possible to change for each analysis.

For each step, the strain at the upper edge is determined as the marked cell by the solver. The value of the marked cell is allowed to change within certain boundaries. While the strain at the upper edge change, the strain distribution along with the height of the cross-section also change, in accordance with formula 7.2. Furthermore, since each lamella's strain and force component depends on the strain distribution, modifying the strain will affect the axial force balance. By selecting the internal axial force balance as the target cell, the different components of the solver are linked. Correspondingly, the internal axial force from the target cell is set equal to the exterior axial force. With all the pieces tied together, the program is ready to perform a cross-section analysis.

During the analysis, the solver will always try to find the best possible solution which satisfies the objective and print the results. For each successful step, the strain distribution, curvature, axial force, and moments are printed and linked to moment-curvature and strain distribution diagrams. After a successful step, the strain at the lower edge changes according to the step size and the analysis is repeated, continually creating new points and lines in the diagrams, illustrated by figure 7.7 and 7.8. The analysis ends when all steps are completed, which means that the maximum strain at the lower edge is reached, or the strain at the upper edge exceeds the ultimate compressive strain of concrete.

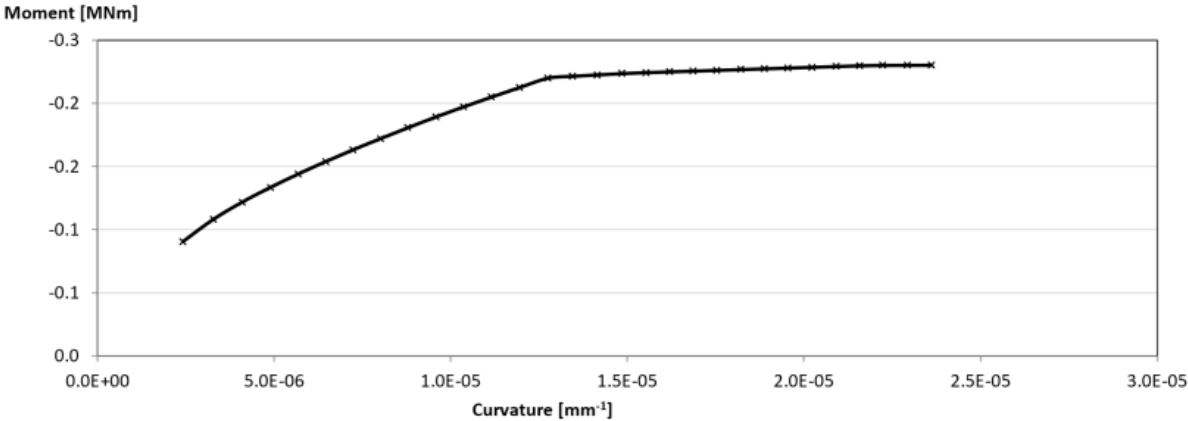


Figure 7.7: Moment-curvature diagram

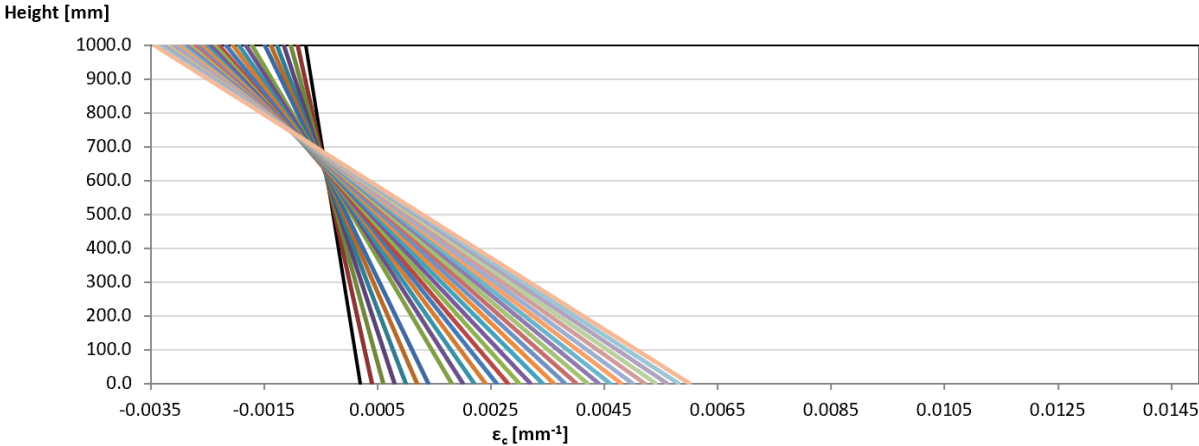


Figure 7.8: Strain distribution along the height of the cross section

## 7.2 Verification of excel program

The excel program is verified before it is used for capacity calculations of the towers. Given that the towers will be designed using both ordinary and prestressed reinforcement, the method must be verified accordingly. Due to the scope of the thesis, the method will be verified in relation to the ultimate limit state.

Example 4.13 in "*S. I. Sørensen*" [40] will form the basis for the verification of an ordinary reinforced cross-section. The same example is calculated with prestressed reinforcement replacing the ordinary reinforcement. Thus, the results will be compared to the solution obtained by the excel lamellae program to investigate whether the program computes valid results.

### 7.2.1 Example 4.13 - Cross-section with ordinary reinforcement

First, example 4.13 from "*S. I. Sørensen*" [40] with ordinary reinforcement will be verified. The example takes into account a column influenced by a combination of both moment and axial force. The column has a rectangular cross-section with an equal amount of tensile and compressive reinforcement shown in figure 7.9. A capacity curve for the combination of moment and axial force is calculated based upon five different strain conditions, listed below and shown in figure 7.10. The determination of strain conditions is based on the fracture and yield criteria for respectively the concrete and the reinforcement. C30 concrete and B500C reinforcement are used in the analysis.

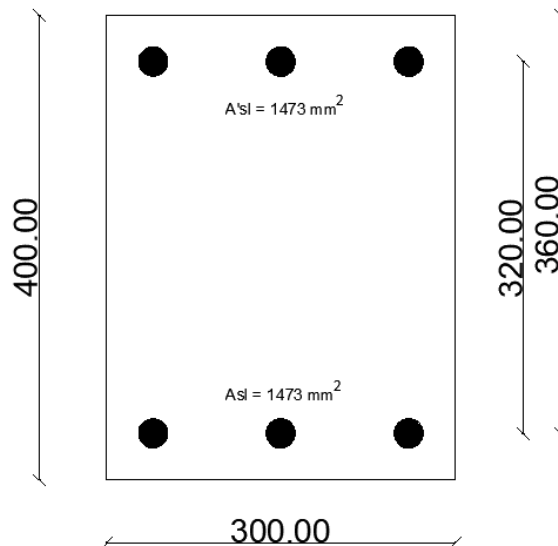


Figure 7.9: Cross-section in example 4.13

1. The entire cross-section in compression.
2. Ultimate compressive strain in the concrete at the upper edge and no strain at the lower edge.
3. Ultimate compressive strain in the concrete at the upper edge and yield strain in the reinforcement at the lower edge.
4. Ultimate compressive strain in the concrete at the upper edge and double yield strain in the reinforcement at the lower edge.
5. Ultimate compressive strain in the concrete at the upper edge and a large strain in the reinforcement at the lower edge.

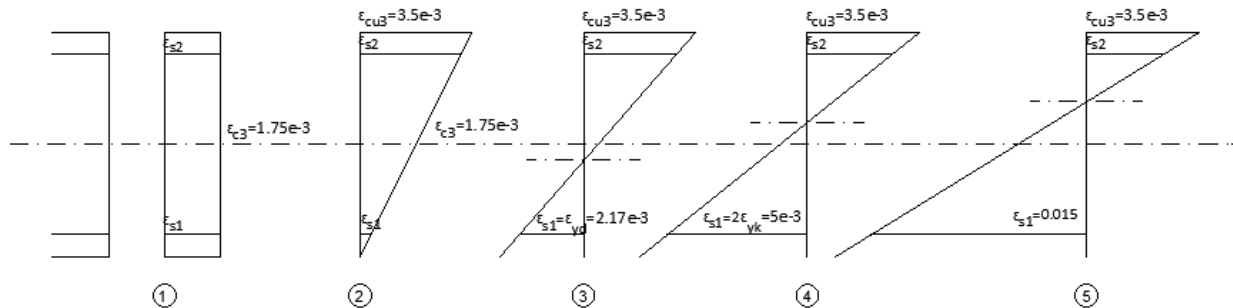


Figure 7.10: Strain conditions using ordinary reinforcement

A comparison of the results from the lamellae program and the solutions from "S. I. Sørensen" is performed and presented in table 7.1. The corresponding M-N diagram for both solutions are found in figure 7.11.

Strain condition	M-N Method		Method of lamellae	
	Axial force [kN]	Moment [kNm]	Axial force [kN]	Moment [kNm]
1	3071	0	3071	0.1
2	2374	151	2374	144
3	906	305	906	303
4	605	290	605	290
5	63	218	63	218

Table 7.1: Verification of the lamellae program for an ordinary reinforced cross-section

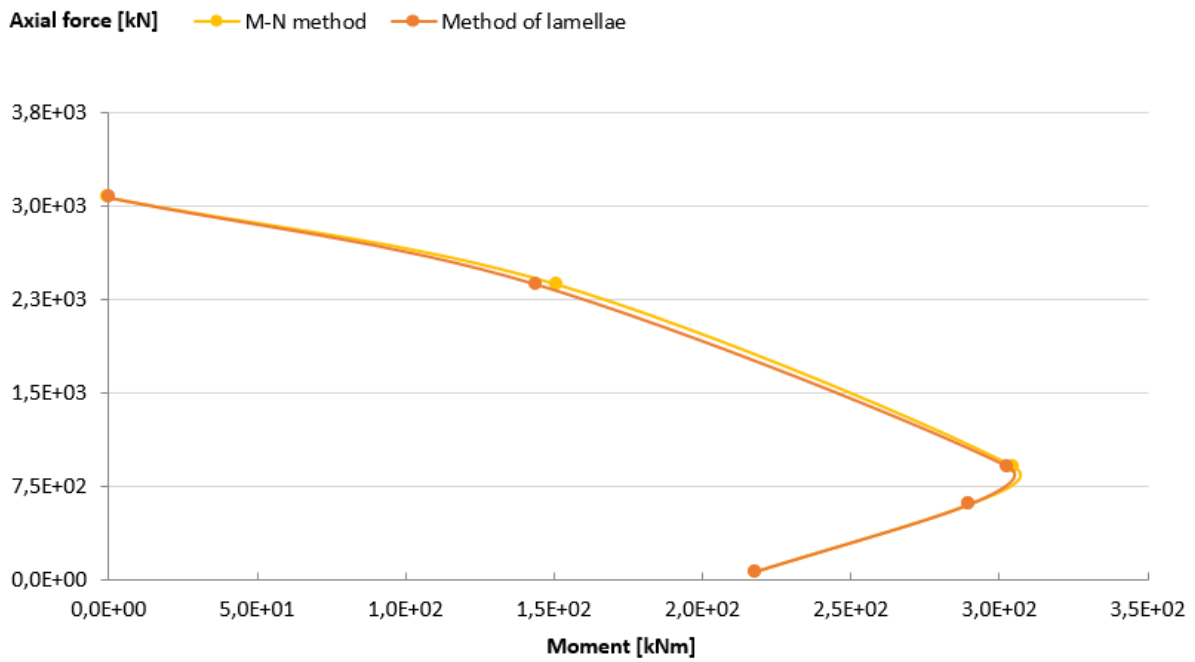


Figure 7.11: Comparison of M-N diagrams for an ordinary reinforced cross-section

The results of the analysis for the third strain condition is presented in figure 7.12 and 7.13. Representations of respectively the moment-curvature relationship and the strain distribution along the height of the cross-section are displayed. Moreover, this strain condition allows for the cross-sections highest moment capacity, and it differentiates compression and tensile fracture of the cross-section.

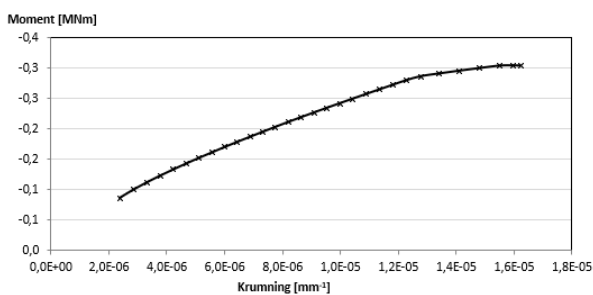


Figure 7.12: Moment-curvature diagram

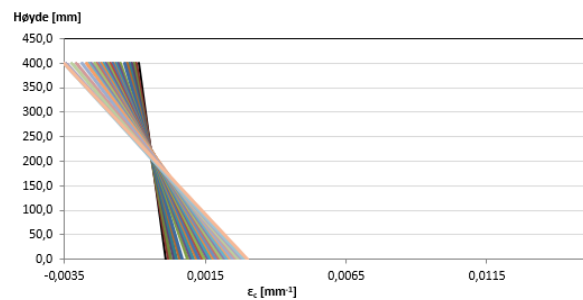


Figure 7.13: Strain distribution

Table 7.1 and figure 7.11 displays that the lamellae program computes moments that are close or equal to the values obtained in "S. I. Sørensen". The deviations can possibly be explained due to differences in the initial conditions of the material curves for the concrete. A non-linear stress-strain relationship is used in the lamellae program, while in the example in Sørensen, a bilinear stress-strain relationship is used. However, the method of lamellae computes a conservative M-N curve, and the deviations are so small that the method is assumed to be valid for further calculations containing ordinary reinforcement.

**7.2.2 Example 4.13 - Cross-section with prestressing**

In this example, the same cross-section is selected, but the ordinary reinforcement is replaced by prestressed reinforcement, illustrated in figure 7.14. Thus, the excel lamellae program could be verified for the use of prestressing in the towers. The amount of reinforcement is determined by equation 7.6, providing an equal force balance from the two types of reinforcement. Finally, the results could be compared to investigate the advantages and disadvantages of using ordinary and prestressed reinforcement, thoroughly discussed in the next section.

$$A_p = A_s \cdot \frac{f_{yd}}{f_{pd}} \tag{7.6}$$

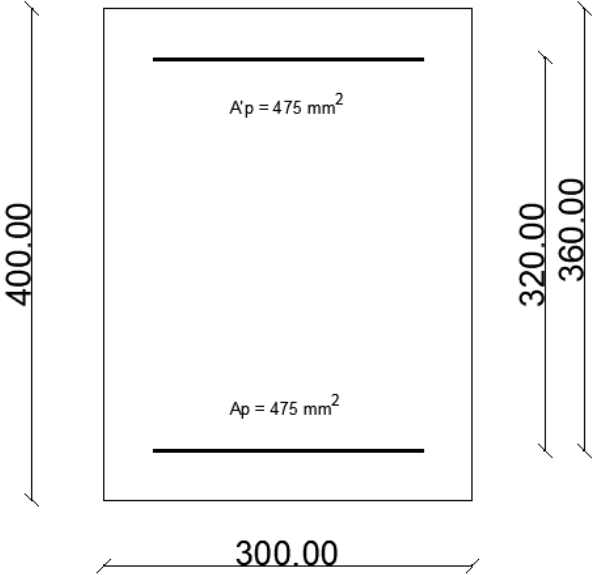


Figure 7.14: Cross-section with prestressing

Equivalently to the previous example, a capacity curve for the combination of axial force and moment will be studied. C30 concrete is used along with the material properties for prestressing given in table 3.3. Furthermore, the prestressed reinforcement is given an initial strain equal to 5‰. Four different strain conditions are chosen and analysed based upon the fracture and yield criteria of respectively concrete and prestressing. These are listed below and shown in figure 7.15.

1. The entire cross-section in compression.
2. Ultimate compressive strain in the concrete at the upper edge and no strain at the lower edge.
3. Ultimate compressive strain in the concrete at the upper edge and yield strain in the reinforcement at the lower edge.
4. Ultimate compressive strain in the concrete at the upper edge and double yield strain in the reinforcement at the lower edge.

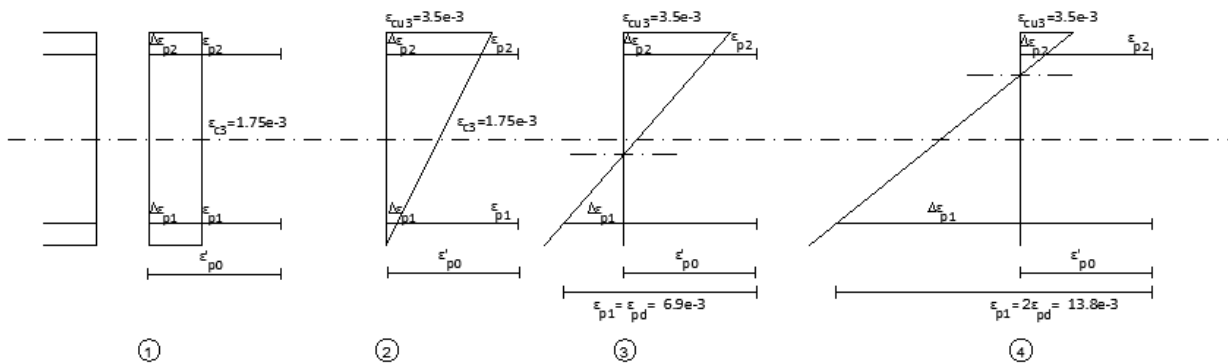


Figure 7.15: Strain conditions using prestressed reinforcement

First, the capacity curve is calculated by hand. Then, the same analysis is executed by the use of the lamellae program. Lastly, the two solutions are compared in table 7.2 and shown in figure 7.16.

Strain condition	M-N Method		Method of lamellae	
	Axial force [kN]	Moment [kNm]	Axial force [kN]	Moment [kNm]
1	1437	0	1437	0
2	1029	107	1029	97
3	118	173	118	170
4	-488	126	-488	126

Table 7.2: Verification of the lamelle program for a prestressed reinforced cross section

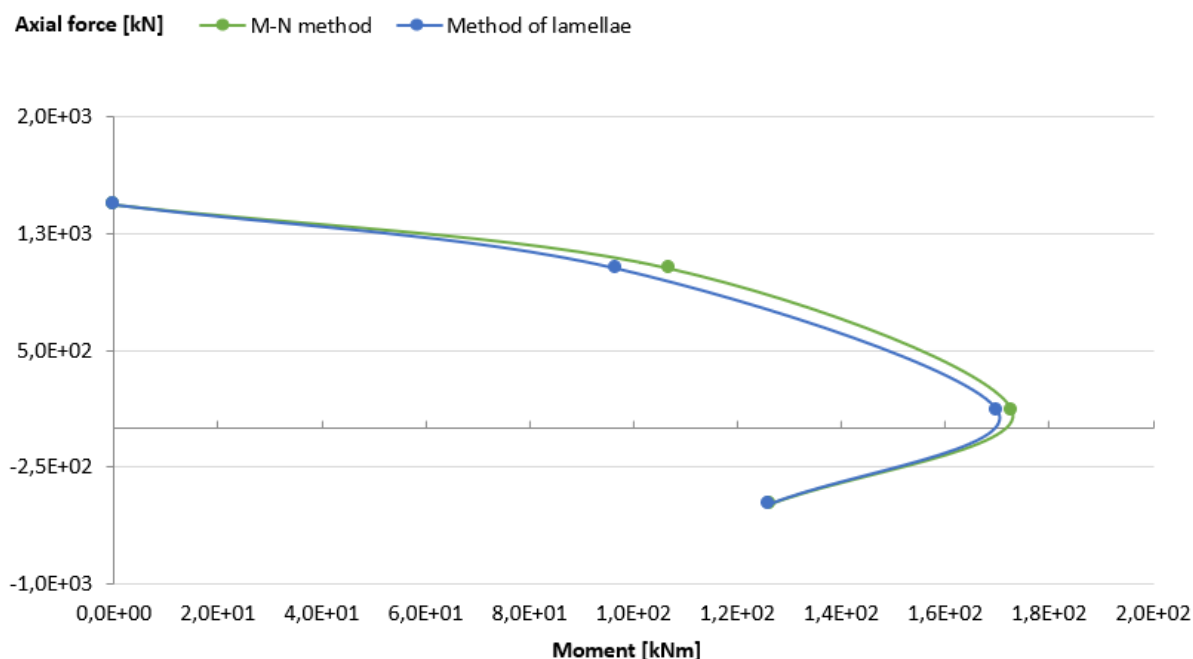


Figure 7.16: Comparison of M-N diagrams for a prestressed reinforced cross-section

Displayed by figure 7.16, it is observed that the lamellae program computes values that are close or equal to the solutions found by hand calculations. Supplementary, the solution in the lamellae program calculates conservative values. As previously mentioned, the calculations in "S. I. Sørensen" presupposes a bilinear stress-strain curve for the concrete while the lamellae program uses a non-linear curve. The minor deviations are therefore closely related to the use of different material curves. Hence, it could be concluded that the program is valid for capacity calculations of a cross-section using prestressed reinforcement.

### 7.3 Link between Abaqus and the Lamellae program

Due to the complexity of the bridge towers, a simplified column is calculated to exemplify the design process implied by Abaqus and the excel-based lamellae program. The column illustrated by figure 7.17 is designed according to chapter 6.2 in "S. I. Sørensen" and thereby just within the accepted limits of a slender column. Thorough calculations regarding the slenderness criteria can be found in appendix E. Since the thesis aims to illustrate the differences between ordinary and prestressed reinforcement, calculations for both reinforcement types are conducted separately and compared by the use of moment-curvature diagrams. The material properties for ordinary and prestressed reinforcement are listed in section 3.2.1, while the characteristic strength of concrete corresponds to the material properties of C45, listed in table 3.1 in EC2.1-1.



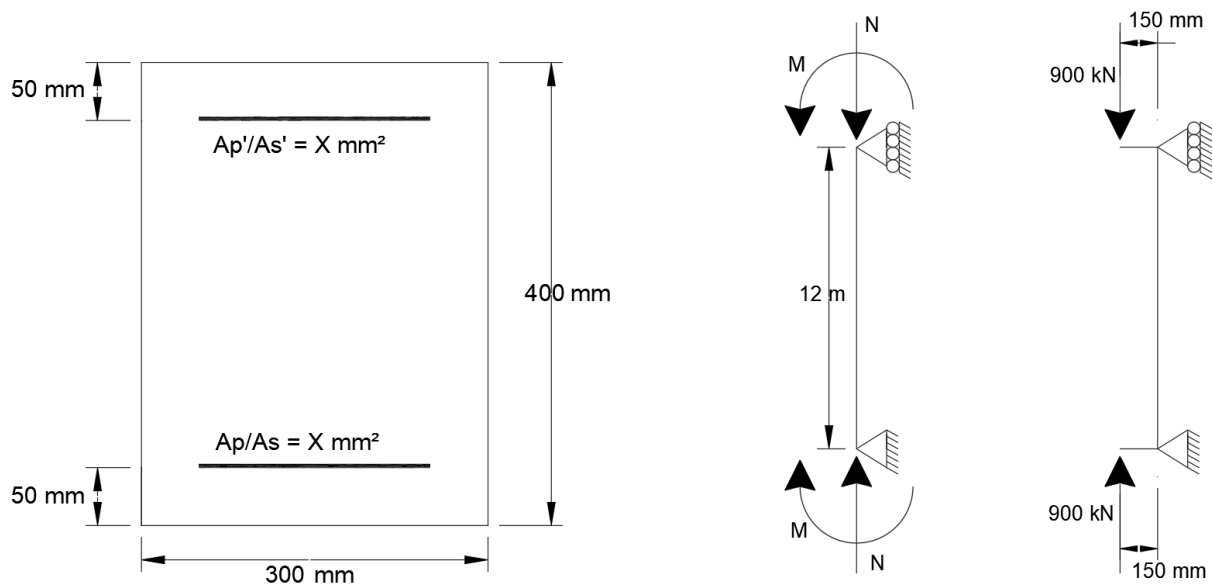


Figure 7.17: Exemplified column

### 7.3.1 Moment-Curvature diagrams

Moment-curvature curves are the key factor for the presentation and analysis of the results, linking the values from Abaqus and the lamellae program. A basic understanding of the diagram is therefore essential for further explanations of the method. A moment-curvature curve is calculated by the excel program to exemplify the results, illustrated by the blue line in figure 7.18. At the same time, a calculation is conducted in Abaqus for an identical column and presented by the red line in the same diagram. The red line is determined by performing the analysis with different bending stiffness for the column, each providing a point along the line. By changing the modulus of elasticity of concrete, the bending stiffness could be manipulated to obtain the desired effect. Because the analysis in Abaqus includes both first and second-order moments, a grey parallel line is computed from origo, marking the amount of total moments corresponding to second-order moments. Which will be proportional to the curvature in the critical section.

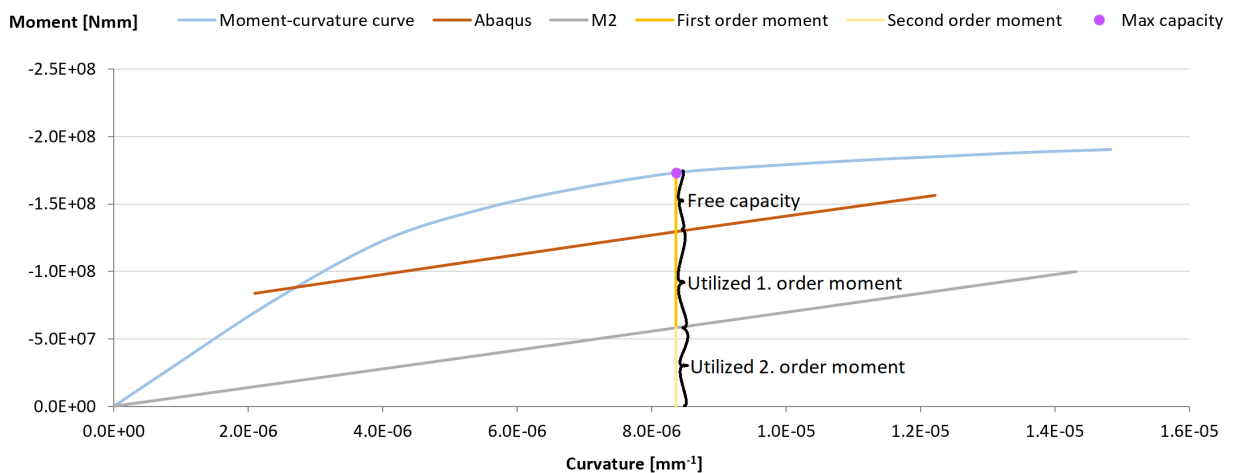


Figure 7.18: Explanation of moment-curvature curve

The red and grey line are parallel because the gradient of both lines depends on the second-order moment. Furthermore, the second-order moment depends on the curvature, so the moment increases proportional with the curvature, creating a linear inclination. In reality, due to material abilities such as cracking, the second-order moment doesn't increase linearly. Hence, the linearity originates from the linear elastic material specified in the Abaqus analysis. The gap between the red and grey line corresponds to the constant first-order moment, inflicted by the external load. The contribution of first and second-order moments are illustrated by figure 7.19.

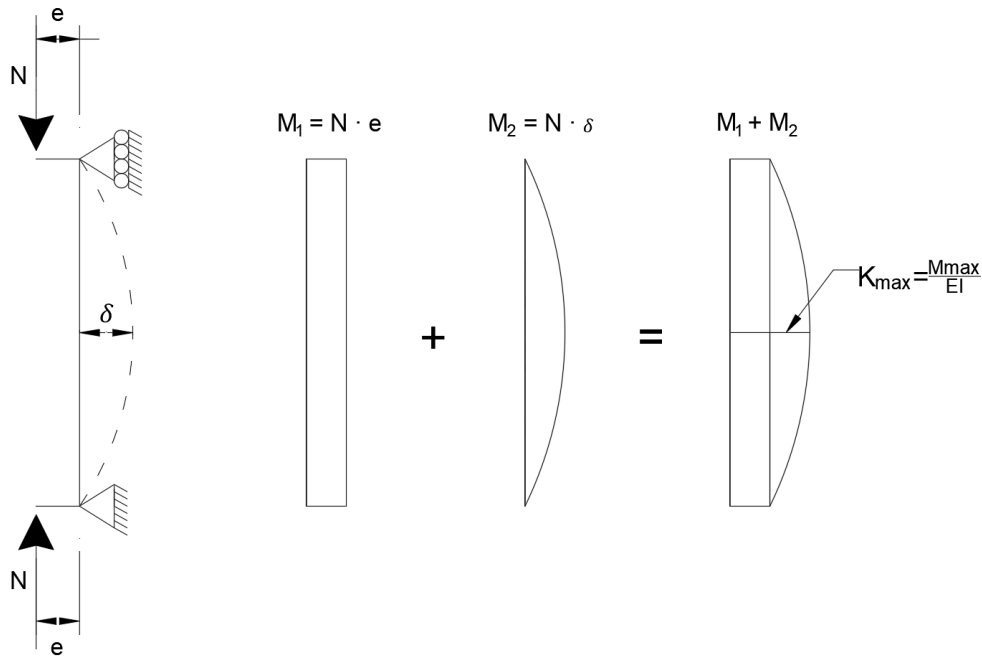


Figure 7.19: Contribution of first and second-order moments

At the tangential point (purple dot), the gradient of the blue line equals the gradient of the red and grey, marking the maximum capacity of the first-order moment. Since first-order moments are proportional to the external loads, an increasing moment capacity implies a larger capacity of external loads. The tangential point is therefore decisive during a capacity control.

The light yellow line illustrates the portion of the total moment corresponding to the second-order moment while the yellow line indicates the capacity of the first-order moment for the cross-section. The amount below the red line is utilized, while the amount above is free, marked in the figure. Therefore, the column's capacity is not entirely exploited, and more load could be applied before the material properties of concrete are surpassed and failure occurs.

The moments of different sizes are analysed in Abaqus and compared in figure 7.20 to illustrate how the magnitude of the moment affect the column in figure 7.17. Practically implemented by increasing the eccentricity of the axial force while keeping the magnitude constant. The tangential line indicates a situation where the cross-section is 100 % exploited. At this point, the line is equivalent to the tangent of the maximum capacity point (purple dot). At the light red line, failure will occur, while at the darker red line, more capacity is at hand.

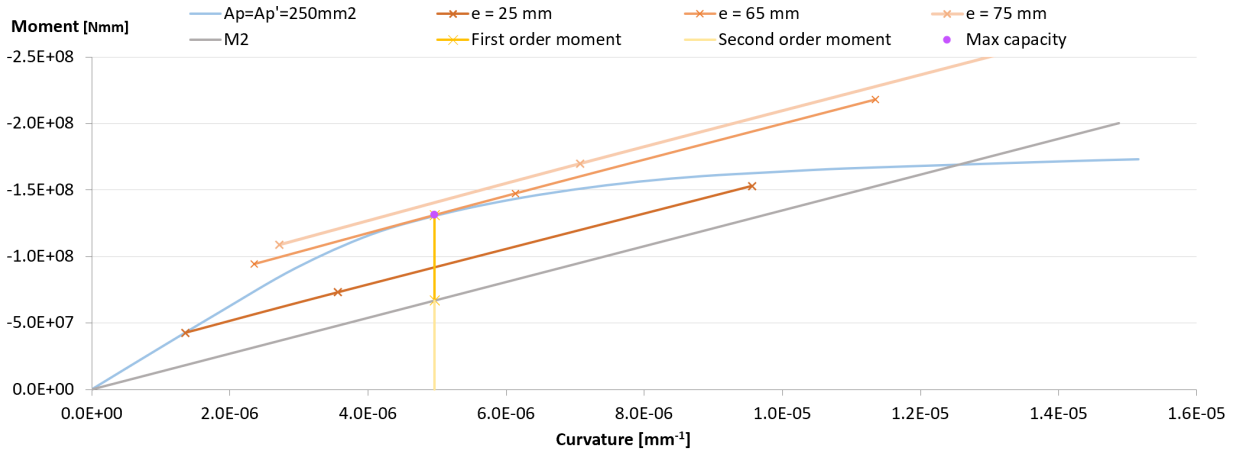


Figure 7.20: Effect of increased external moment

### 7.3.2 Deflection ( $\delta$ )

Illustrated by figure 7.19, the second-order moment depends on the axial force and the maximum deflection ( $\delta$ ) at mid-span. Increasing the deflection causes the curvature to increase, as well as the second-order moment.

Known from mechanics, the method of virtual work is a handy tool for calculations regarding the deflection of columns exposed to both axial forces and moments. The method is based on the simple equation where external work equals internal work, illustrated by equation 7.7. A virtual load is applied externally to the system at the point where the deflection will be calculated. Combined with the use of table 3.6 in *"Stålkonstruksjoner - Profiler og formler"* [41], a fast-integration scheme could be implemented to find the deflection.

$$\tilde{W}_e = \tilde{W}_i \quad (7.7)$$

Therefore, the method of virtual work may be used to verify the deflection calculated by combining the stiffness from the excel lamellae program and Abaqus. Based on a 100 % exploited cross-section, the curvature could be retrieved from the excel program and fed into formulas based on the method of virtual work. An equivalent analysis is conducted in Abaqus for deflections and compared to verify the results.

By implementing the method of virtual work, the shape of the moment diagrams is decisive for deflection calculations. Based on the example in figure 7.19, the form of the total moment diagram for the column is shaped by a combined rectangle and parabola. The table used for fast integration doesn't provide any equivalent moment diagram. However, by conducting calculations based on a smaller and a larger moment diagram, the expected deflections should be somewhere in between, illustrated by figure 7.21. Which is where the deflection from the analysis in Abaqus is expected to be positioned.

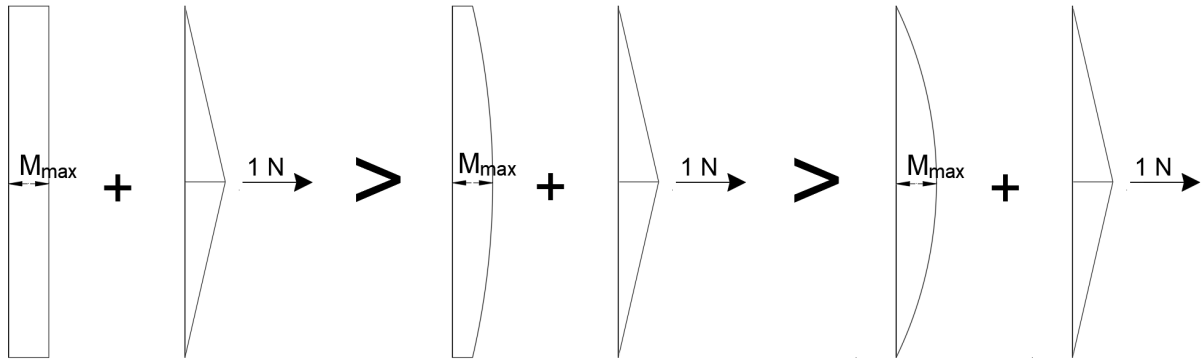


Figure 7.21: Method of virtual work: Square, Abaqus and Parabola

The upper limit of the deflections are represented by a squared moment diagram (formula 7.8), while the lower limit is based on a parabola (formula 7.9). Since the moment area of a square is larger than the parabola shaped ones, the magnitude of the force is larger, and therefore also the deflections.

$$\delta = \kappa_{max} \cdot \frac{L}{4} \cdot \frac{1}{2} \cdot L = \kappa_{max} \frac{L^2}{8} \quad (7.8)$$

$$\delta = \kappa_{max} \cdot \frac{L}{4} \cdot \frac{5}{12} \cdot L = \kappa_{max} \frac{L^2}{9.6} \quad (7.9)$$

The deflections are verified based on the tangential point in figure 7.20 for both the excel program and Abaqus. By use of the method of virtual work, the deflections are found and compared to the results from Abaqus in table 7.3. As expected, the deflection calculated by Abaqus lies between the two examples based on the method of virtual work, confirming the results from the excel lamellae program and Abaqus.

Calculation method	Deflection ( $\delta$ )
Square	89.4 mm
Abaqus	80.5 mm
Parabola	74.5 mm

Table 7.3: Verification of deflection

### 7.3.3 Effect of ordinary reinforcement

Exemplifying how ordinary reinforcement affect the moment capacity, the column in figure 7.17 are analysed by the lamellae program with different amount of reinforcement. Although ordinary reinforcement doesn't affect the axial force, prestressed reinforcement will. Comparing the results subsequently, the axial force in figure 7.17 is halved, from 900 kN to 450 kN during this example. For the ordinary reinforcement, the results from each analysis are printed and compared in the same diagram, illustrated by figure 7.23. An equivalent analysis is conducted in Abaqus and drawn as a red line in the same diagram. Parallel to the red line, the grey line marks the second-order moment.

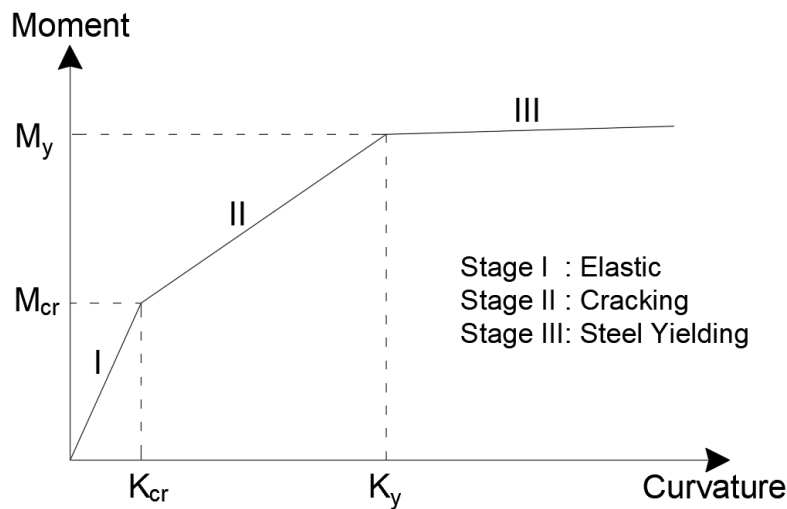


Figure 7.22: Ordinary reinforced concrete

Presented by figure 7.22, the shape of each capacity curve is quite similar, consisting of three sections, divided by two distinct bends. A number characterizes each section; stage I, II and III. The first stage marks the elastic zone, and the second one represents the zone of which cracking occur, while in the third zone, the steel yields. Transitioning in between different stages require a certain amount of energy, creating bends in the diagram when fulfilled. These portions of energy are characterized as the cracking moment ( $M_{cr}$ ) and the yield moment ( $M_y$ ), more thoroughly explained by the end of section 7.3.5. Due to non-linear effects, stage II isn't linear when axial forces are applied. However, due to minor deviations, it appears linear, as illustrated by the results from the analysis. Another interesting observation is based on the position of the yield moment. By increasing the reinforcement, the yield moment transition both up and to the right, increasing the capacity. Hence, making the bend more distinct, requiring a more significant portion of energy to transition.

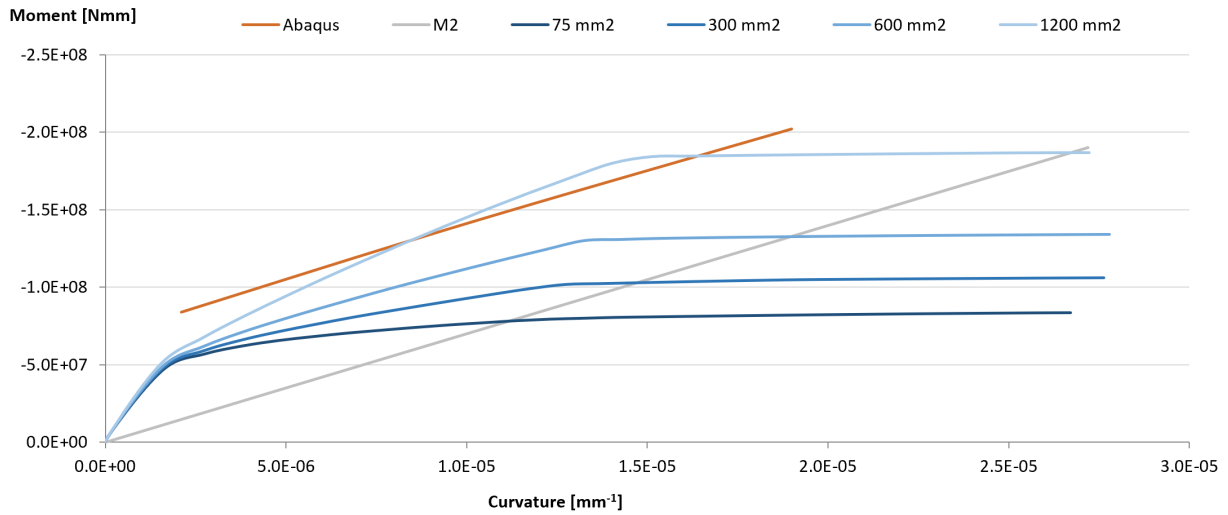


Figure 7.23: Effect of increasing the ordinary reinforcement

The moment capacity of the first three analysis ( $75 \text{ mm}^2$  to  $600 \text{ mm}^2$  reinforcement) are determined by the cracking moment, thereby below the moments from the Abaqus analyses. Indicating that the material abilities of concrete are exceeded, causing crushing. However, the moment capacity of the light blue line ( $1200 \text{ mm}^2$ ) is marked by the yield moment, surpassing the equivalent forces from Abaqus. In this case, the moment capacity is within the moments forces from the analysis conducted in Abaqus.

### 7.3.4 Effect of prestressed reinforcement

Based on the same column (figure 7.17), the effects of the prestressed reinforcement is found by replacing the ordinary reinforcement with prestressed reinforcement. Correspondingly, the axial force is halved from 900 kN to 450 kN. Illustrated by figure 7.25, analyses are conducted by the lamellae program for different amount of reinforcement and presented in the diagram. An equivalent column is analysed in Abaqus, represented by the red line in the same diagram. The grey line marks the amount of moment corresponding to the second-order moment.

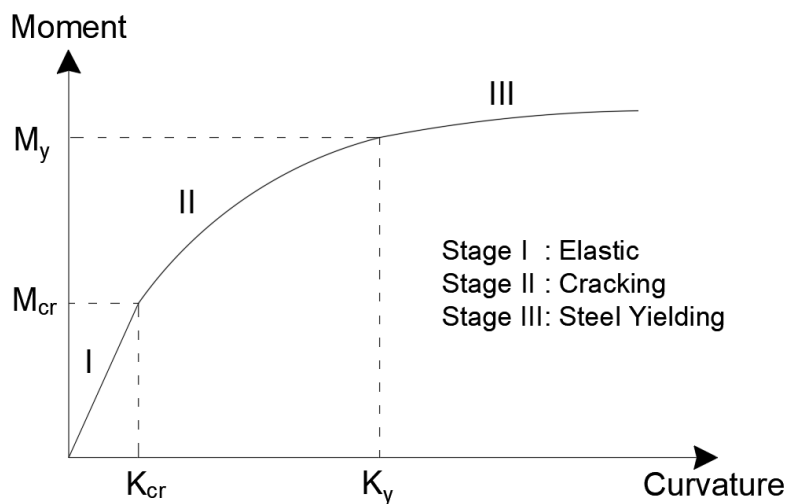


Figure 7.24: Prestressed reinforced concrete

Alike the ordinary reinforcement, the moment-curvature curves describing the capacity of the prestressed cross sections are represented by three stages. By comparison, the shape of stage II is more curved, making the transitions in between each stage less distinct and therefore harder to locate. Mainly because the prestressed reinforcement initially is stressed, increasing the axial force balance, requiring less energy to transition in between different stages (section 7.3.5). Illustrated by figure 7.24, the cracking moment ( $M_{cr}$ ) marks the transition between stage I and II, while the yield moment ( $M_y$ ) marks the transition from stage II to III.

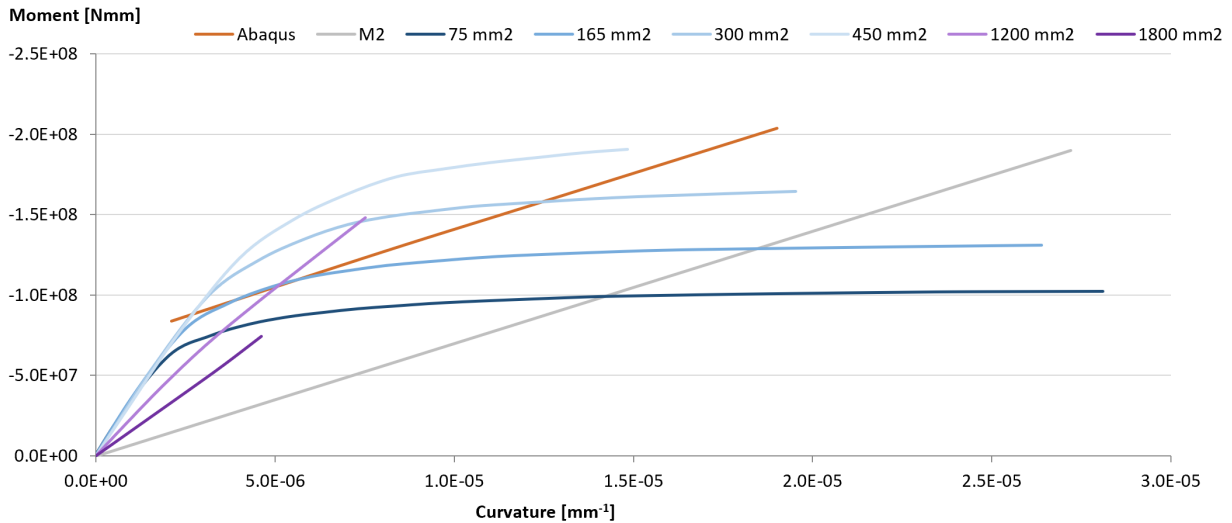


Figure 7.25: Effect of increasing the prestressed reinforcement

By examining figure 7.25, the moment capacity increases by adding more reinforcement. Comparing the capacity curves with the solution from Abaqus, both the light blue lines ( $450 \text{ mm}^2$  and  $300 \text{ mm}^2$ ) contains extra capacity, while the capacity of the dark blue lines ( $150 \text{ mm}^2$  and blue  $75 \text{ mm}^2$ ) is exceeded. However, the  $165 \text{ mm}^2$  reinforced capacity curve is tangential to the red Abaqus line, illustrating 100 % exploitation of the cross-section. Furthermore, by increasing the prestressed reinforcement additionally, the capacity decreases, illustrated by the purple lines. Enlarging the reinforcement also increases the compressive forces, which leads the cross-section to failure during stage I, before the cracking moment is reached.

### 7.3.5 Effect of axial force

To compare the impact of ordinary and prestressed reinforcement, the differences between the reinforcement methods are enlightened. The key factors in understanding the behaviour of the moment-curvature curves are mainly connected to the axial force. Figure 7.26 represents the behaviour of the column exposed to three different axial forces. In the first case, the column is only affected by moment and no axial forces. Until the cracking moment is reached ( $M_{cr1}$ ), concrete on the tension side will be bonded, contributing to the force balance. Transferring from stage I til II requires all the energy represented by the grey area under  $M_{cr1}$  in figure 7.26, creating a distant bend in the moment-curvature diagram. Further, the moment capacity is instantly reduced before continuing linearly until failure.

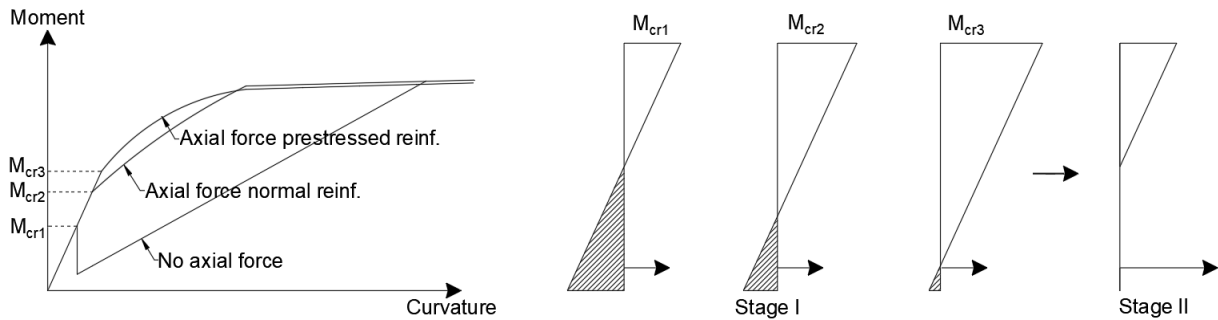


Figure 7.26: Effect of axial force on the moment-curvature diagram

In the second case, an axial force is applied to the ordinary reinforced column. The axial force compresses the concrete, enabling the concrete on the tension side to be bonded for a longer period. Due to the compressive forces, the cracking moment ( $M_{cr2}$ ) is moved higher up in the moment-curvature diagram, and at the same time, the grey area is reduced. Therefore, the energy needed to transfer between stage I and II is reduced, making the bend less distinct. Dependent on the magnitude of the axial force, the curve is slightly curved throughout stage II before the yield moment is reached. Transferring from stage II to III require enough energy for the reinforcement to yield, creating another bend in the curve.

In the third case, both the axial force and the prestressing contribute to compressive forces. The extra compression increases the cracking moment ( $M_{cr3}$ ), reducing the concrete area of tension additionally. Less energy is needed to transfer from stage I to II, making the bend indistinct. The same account for the transition between stage II and III. In accordance with the increased axial load, the shape of stage II is more curved in the last example.

While the cases above are mainly directed towards different reinforcement types, the non-reinforced Abaqus model is also affected by the axial force. By applying a larger axial force, the second-order moment increases, and therefore also the gradient of the 1. and 2. order moment. Correspondingly, by decreasing the axial force, the 1. and 2. order moment lines would flatten out, illustrated by figure 7.27. Although the prestressing compresses the concrete, it is important to mention it would not affect the 1. and 2. order moment mainly because the forces imposed by the prestressing is internal and not external. For this reason, the compression of concrete is equivalent to the tension of the reinforcement. However, increasing the amount of reinforcement affects the bending stiffness of the structure, which is taken into account by changing the e-modulus of concrete in Abaqus. For this reason, the Abaqus solution line is linear.



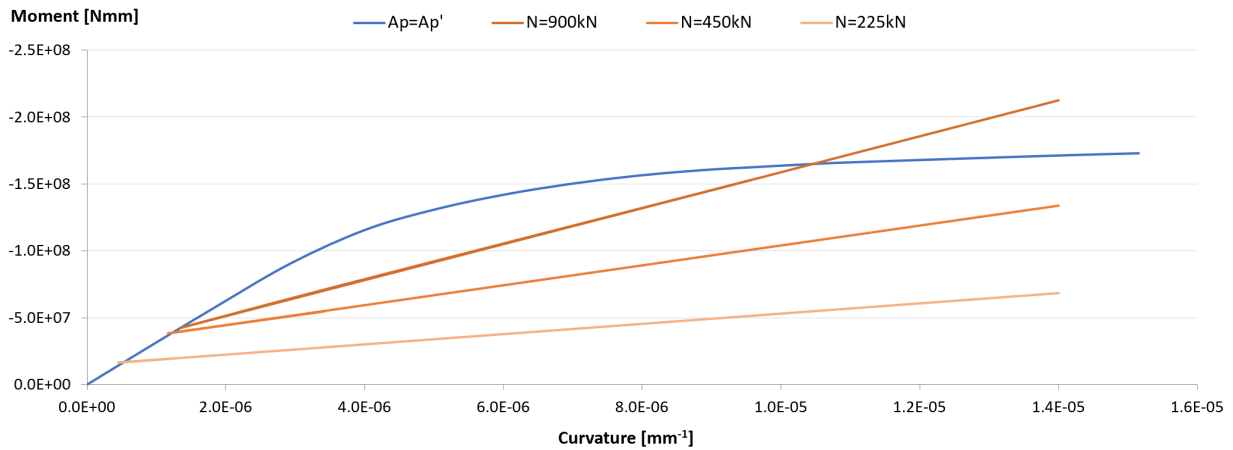


Figure 7.27: Effect of axial force on the Abaqus analysis

## 7.4 Comparing cross section with ordinary and prestressed reinforcement

The thesis aims to investigate whether it is favourable to use prestressing instead of ordinary reinforcement along the height of the towers. Moreover, the comparison will be performed regarding both M-N capacity curves as well as moment-curvature diagrams. The M-N capacity curves highlight the effects at yield and fracture criteria for both concrete and reinforcement, while the moment-curvature curves investigate the capacity with respect to first and second-order moments. Both comparisons will be based on the analysis executed in the previous sections with the relevant cross-sections and examples.

### 7.4.1 M-N capacity curve comparison

A comparison of the solutions found in the previous sections is performed and shown in figure 7.28. The orange line represents the ordinary reinforced cross-section, while the blue line represents the prestressed reinforced cross section. The results illustrate that the combined M-N capacity is reduced when prestress is used, both regarding axial force and moment. A possible explanation for the reduction is related to the initial strain in the prestressing.

By the start of the analysis, the entire cross-section is in compression. At this instance, the strain in the column is smaller than the initial strain of the prestressing. Consequently, the prestressing imposes a tension force to the column, resulting in a decreased axial force. On the contrary, when ordinary reinforcement is used, the reinforcement contributes with a compression force, resulting in a higher axial force.

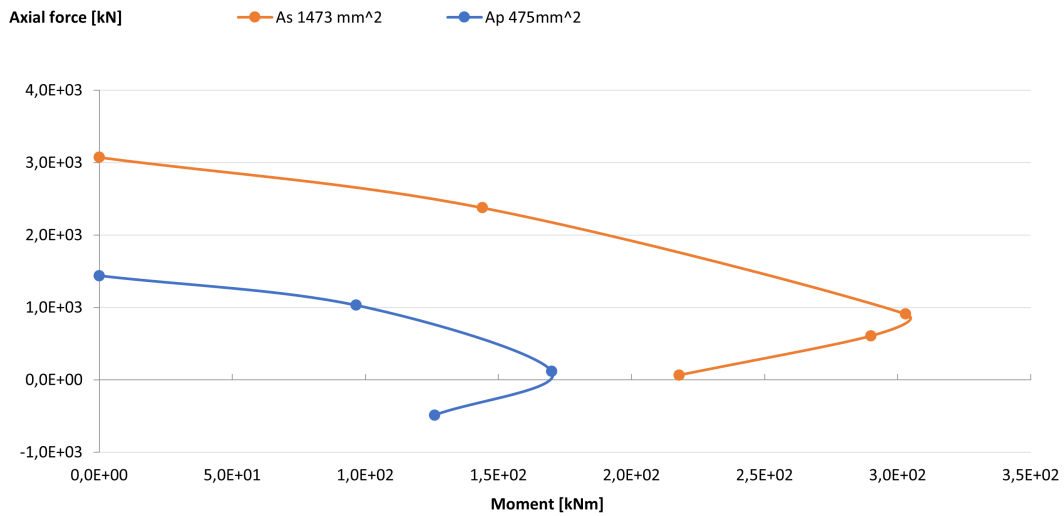


Figure 7.28: M-N diagram for comparison of ordinary and prestressed reinforced

Throughout the analysis, the column is exposed to both axial force and moment. In the third strain condition, the ultimate compressive strength of the concrete is reached, and yielding has occurred in the reinforcement. At this point, the strain of the prestressing at the upper edge is smaller than the initial strain. As a result, the compressive prestressing will impose a small tensile force to the column. Meanwhile, the strain in the tensile prestressing has increased beyond the initial strain, resulting in a larger tensile force acting on the column. Contrarily, the ordinary reinforcement contributes with force represented by the strain condition of the cross-section. The reinforcement generates a compressive force for the cross-section in compression and a tensile force for the cross-section in tension. Thus, the small tensile force from the compressive prestressing and a larger yielding strain decreases the axial force and the moment capacity of the column.

In order to evaluate whether the use of prestressing is favourable or not, it is relevant to look into the capacity of the column with different reinforcement areas for both ordinary and prestressed reinforcement. An example for both increased and decreased amount of reinforcement is calculated, and the results are shown in figure 7.29. Hence, the figure shows that the change of reinforcement area does not change the capacity, such that it is favourable to use prestressed reinforcement instead of ordinary reinforcement.

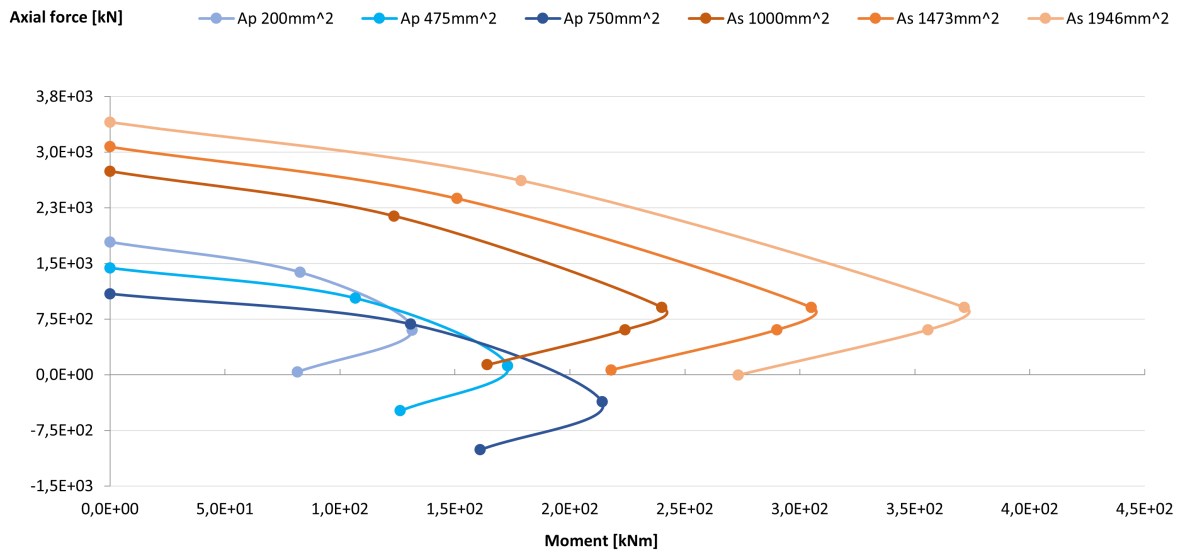


Figure 7.29: M-N diagram for comparison of different reinforcement area

Additionally, the column is calculated with prestressed and ordinary reinforcement on both the compression and tensile sides of the cross-section. The smallest reinforcement areas are selected, and the result is shown in figure 7.30. Illustrated by the results, the column with combined reinforcement has a larger capacity than the column, including only prestressing. Whereas for the column with only ordinary reinforcement, the capacity is slightly smaller regarding the axial forces, but the moment capacity is increased.

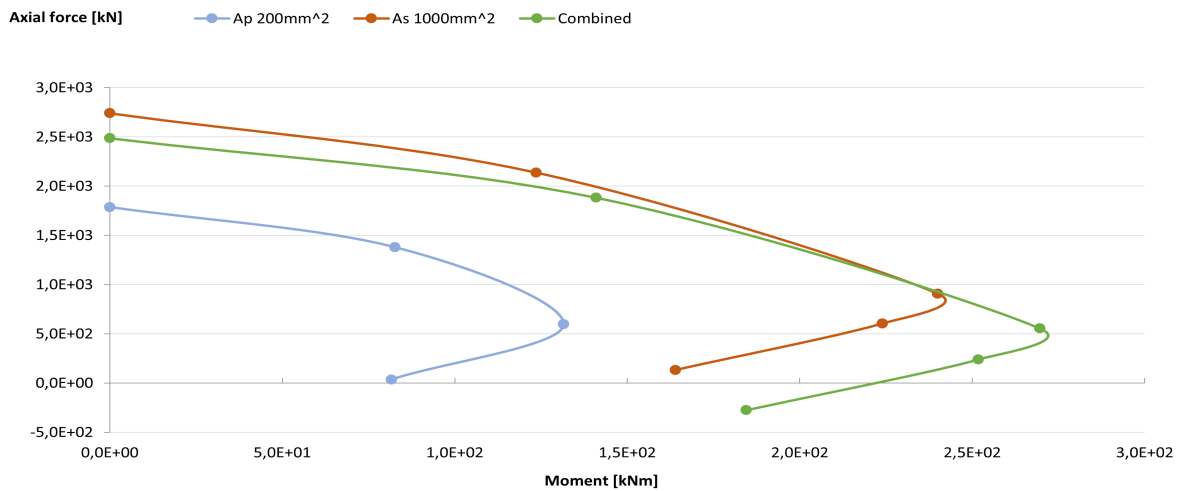


Figure 7.30: M-N diagram for combined prestressing and ordinary reinforcement

### 7.4.2 Moment-curvature curve comparison

Comparisons are made in moment-curvature diagrams for the moment capacities of the different reinforcement types with respect to first and second order moments. In the first example,  $150 \text{ mm}^2$  ordinary and prestressed reinforcement are analysed and presented in figure 7.31. The yellow lines indicate the maximum first-order moment capacities. The example is based on figure 7.17, with an axial force equal to 450 kN.

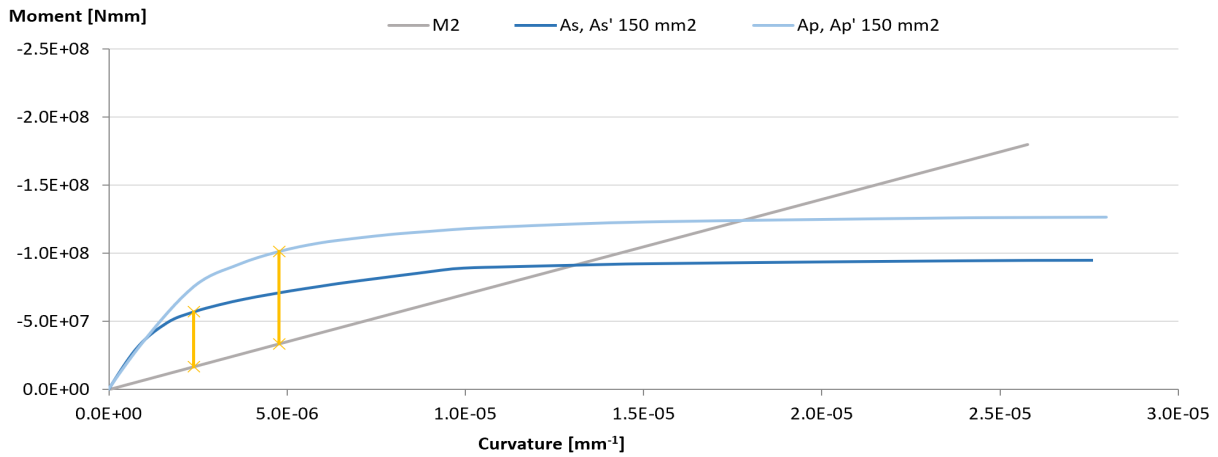


Figure 7.31: Comparison of  $150 \text{ mm}^2$  ordinary and prestressed reinforcement

In addition, the same procedure based on  $450 \text{ mm}^2$  reinforcement is implemented and presented by figure 7.32.

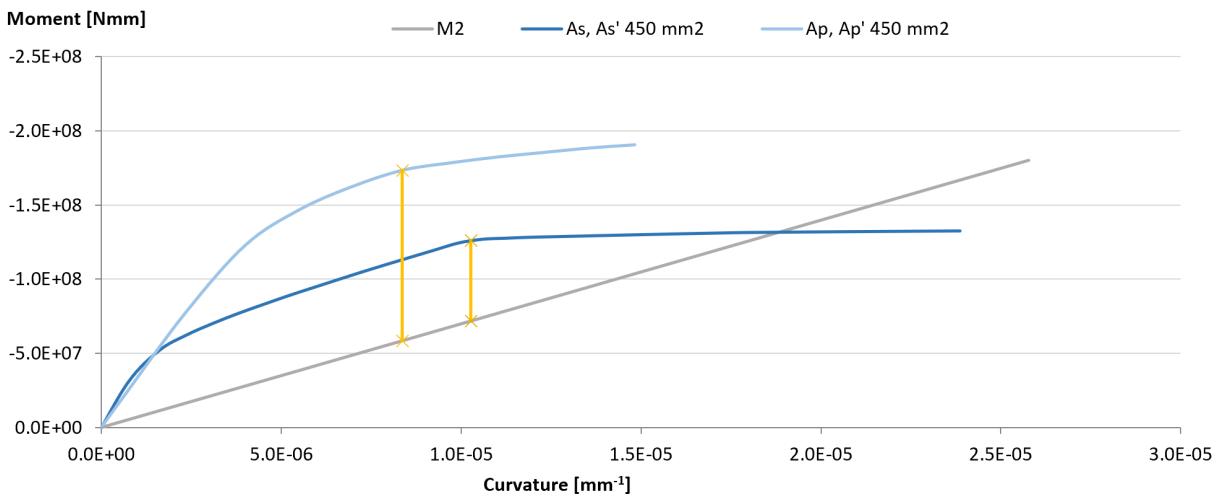


Figure 7.32: Comparison  $450 \text{ mm}^2$  ordinary and prestressed reinforcement

In accordance with the figures, the moment capacity of the prestressed reinforcement is relatively larger than the moment capacity of the ordinary reinforcement. The main reason for the differences relates to the fact that the characteristic strength of the prestressed reinforcement is larger than the characteristic strength of ordinary reinforcement. In addition, the prestressed reinforcement is initially stressed, which enables an earlier and, therefore, a larger contribution to the moment and axial equilibrium. Furthermore, the cracking moment is increased, and stage II are more curved. Additionally, the compressive capacity of the cross-section is responsive to additional compressive forces imposed by the prestressing.

A third situation is also analysed, and the results are printed in figure 7.33. In this situation, the design stress of both ordinary and prestressed reinforcement is taken into account, creating an equal force situation by reducing the prestressed reinforcement according to formula 7.10. Identical to the previous examples, the column in figure 7.17 is analysed, with an axial force equal to 450 kN.

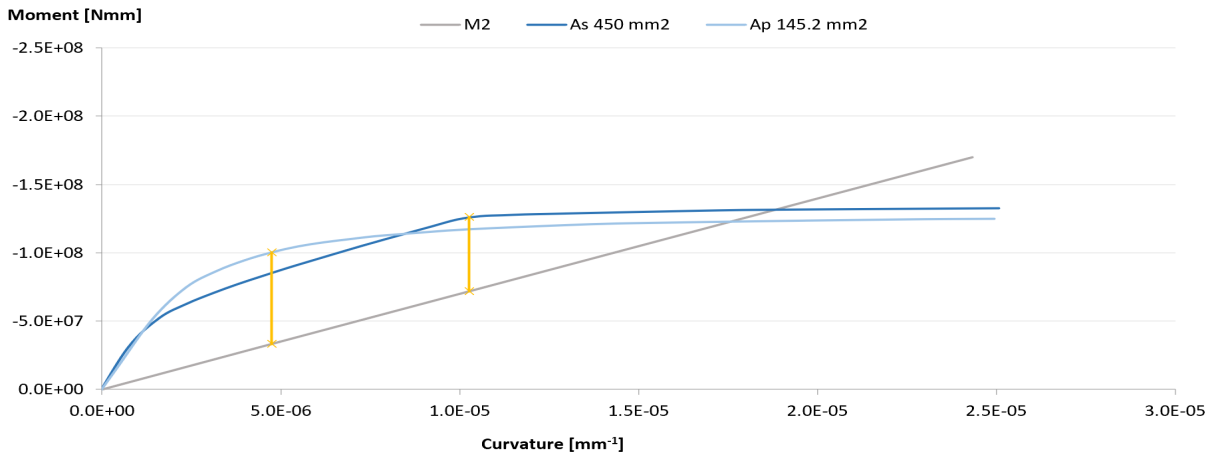


Figure 7.33: Equivalent amount of ordinary and prestressed reinforcement

$$A_p = A_s \cdot \frac{f_{yd}}{f_{pd}} \quad (7.10)$$

The different first-order moment capacities are listed in table 7.4 and compared by ratio. In all cases, the capacity of the prestressed reinforcement is larger. Especially for the selected example of  $450 \text{ mm}^2$ , the capacity of the prestressing is more than two times the capacity of ordinary reinforcement. The advantage acquired by the prestressing is specifically convenient if there is a lack of area in the cross-section, typically for a long slender hollow column like the bridge towers. However, symmetrically prestressing could be unfortunate, illustrated by the decreased moment capacity in stage III in figure 7.33. Based on the combined evaluation of the columns and the towers, all the effects are thoroughly explained in the discussion, chapter 10.

Amount of reinforcement	First order moment capacity		Ratio
	As	Ap	
$150 \text{ mm}^2$	4.03E+07 Nmm	6.79E+07 Nmm	1.69
$450 \text{ mm}^2$	5.44E+07 Nmm	1.15E+08 Nmm	2.11
$A_s \cdot f_{yd} = A_p \cdot f_{pd}$	5.44E+07 Nmm	6.70E+07 Nmm	1.23

Table 7.4: Summary of the comparisons

## 8 Abaqus analysis

During the analysis of the towers, two models are created for the bridge; one model of the free-standing towers and one global model of the complete bridge. The first model is subject to load combination one, while the second model is affected by load combination two and three. Hence, the dimensioning forces are extracted from each analysis and used during capacity calculations, presented in section 8.2. Verification is conducted by convergence control and control of the global equilibrium to ensure that the forces obtained from the analysis are accurate.

### 8.1 Verification

Initially mentioned in section 5.1, Abaqus divides the model into different elements, connected by nodes. Depending on the element, each node has degrees of freedom and corresponding equations. Increasing the number of elements enhance the accuracy of the solution but increases the computational cost. Additionally, the type of elements will affect the precision of the solution and the computational cost. For example, the B32 beam element contains three nodes, improving the performance compared to the two-node B31 element. However, it increases the computational cost. In general, the user is responsible for choosing the correct elements for a specific problem. A convergence analysis is performed to examine the effect of the different elements.

A specific result is chosen during a convergence analysis and examined with different types and numbers of elements. Usually, the most relevant data for the analysis or particularly large side effects are investigated. The process starts by analysing the model with few and simple elements, expecting a less accurate answer. Further, the analysis is repeated with a larger amount or more complex elements, expecting an increased precision. The process continues by repeating the analysis and continuously modifying the elements until the margin of error between the last and present result is within predetermined limits. Based on the scale of the project, the margin of error is equal 1 ‰.

While running an analysis, numerous control parameters are associated with the convergence and integration accuracy algorithms within the software. These parameters are assigned default values chosen to optimize the accuracy and efficiency of the solution of non-linear problems. In general, it implies that the solution provided by Abaqus already has converged. However, to exemplify how the different element types and the number of elements affect the results, multiple comparisons are conducted for the different load combinations.

In load combination one, the largest displacement and moment are analysed. The greatest displacement occur at the top of the tower, whereas the largest moment develop at the bottom for the free-standing tower. At least one element is required to model one casting stage, such that the lowest amount of elements possible is 45. Therefore, the first analysis is conducted with one B31 element per casting-stage. In the following analysis, each casting stage is modelled with two B31 elements. In addition, the towers are analysed with one, two and four B32 elements per casting stage. The e-modulus used during the verification equals 12 000 MPa. By choosing a small e-modulus, the effect on the displacements is enhanced due to a low bending stiffness.

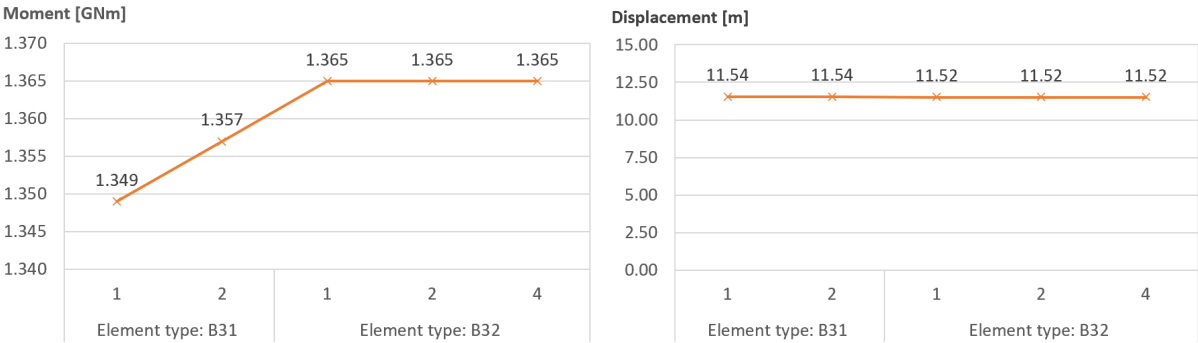


Figure 8.1: Convergence control of load combination one

Figure 8.1 presents the largest moment and displacement obtained from the convergence analysis of load combination one. Based on the results, it is reasonable to conclude that the solution has converged for the B32 beam elements. Thus, the differences between B31 and B32 elements are quite small, and thus it is debatable whether one element type is preferred ahead of the other.

The displacement at the top and the moment at the bottom of the tower are used for the convergence analysis when considering load combination two. Like load combination one, the largest moment occur at the bottom of the tower. However, the largest displacement develop vertically at the middle of the span. Thus, the displacement at the top of the towers is relevant according to the capacity calculations and is therefore prioritised during the convergence control.

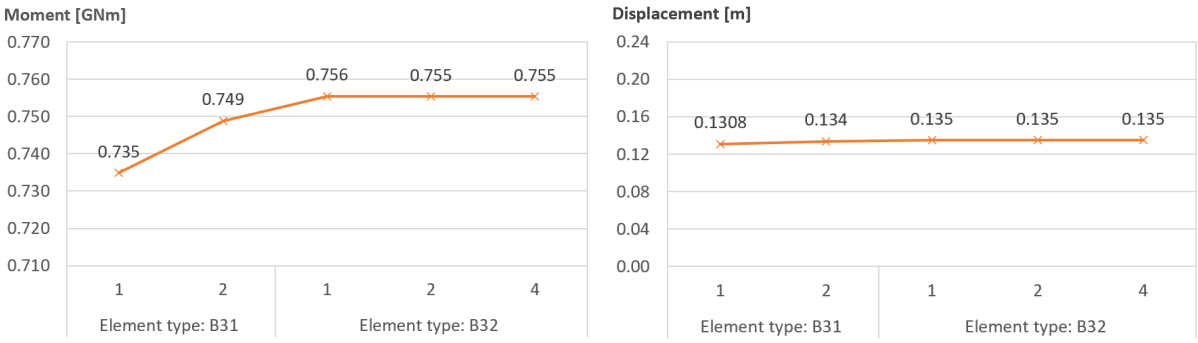


Figure 8.2: Convergence control of load combination two



Figure 8.2 shows the results obtained from the different element types and sizes for load combination two. Illustrated by the figure, the analysis have converged for the B32 beam elements.

During load combination three, the global model is highly affected by transverse winds. For that reason, the largest moment is developed perpendicular to the length of the bridge. Hence, in the sections close to the stabilizing transverse beams. The transverse beams transfer large moments between the columns of each tower, creating critical sections around the transitions. In addition to the moment, large transverse displacements occurs at the tower top, which needs extra attention. Correspondingly, moment and displacement are investigated for convergence.

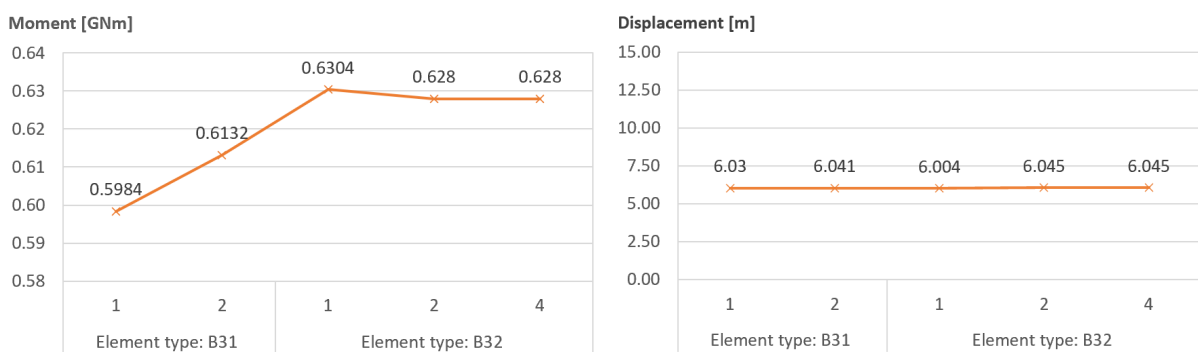


Figure 8.3: Convergence control of load combination three

Figure 8.3 illustrates the solutions obtained from load combination three. Unlike load combination one and two, load combination three requires a minimum of two B32 elements per casting stage to obtain the converged solution. For this reason, beam-type B32 with two elements per casting stage is used for further analysis of the towers.

Another important verification of the Abaqus model is the global equilibrium. By comparing the loads applied to the structure by the reaction forces at each boundary condition, the global equilibrium could be controlled. Hence, the application of the correct material densities, type of loads and boundary conditions could be verified. Table 8.1 presents the vertical forces for the free-standing towers and the global model, mainly subjected to self-weight, as well as traffic load for the global model during load combination two. Table 8.2 shows the horizontal equilibrium for the free-standing towers during load combination one and the global model during load combination three. During load combination two, the wind force at each tower is applied in the opposite direction, globally cancelling each other. Henceforth, the values presented in the tables are without load combination factors.

Model	Load		Abaqus		Difference
	Self weight	Traffic load	Tower	Anchor	
Free standing tower	-169.5 MN	-	-169.1 MN	-	0.236%
Global model [LC2]	-777.1 MN	-62.5 MN	-1433.2 MN	595.8 MN	0.617%

Table 8.1: Vertical equilibrium

Model	Load Wind	Abaqus			Difference
		Tower	Anchor	Boundaries	
Free standing tower	10.796 MN	10.800 MN	-	-	0.037%
Global model [LC3]	65.107 MN	58.135 MN	5.115 MN	2.017 MN	0.245%

Table 8.2: Horizontal equilibrium

As shown by the tables, the difference between the applied loads and the reaction forces are insignificant. Therefore, its reasonable to conclude that the model is working properly and ready for further analysis.

## 8.2 Abaqus analysis results

The resulting forces obtained from the two Abaqus models will be presented and compared. In order to obtain a better understanding of the results, load combination one, two and three will be presented and displayed in the same diagram for respectively axial force, moment, shear force and torsional moment. In consideration of analysing the towers, an e-modulus equal to 12 000 MPa is used for the free-standing tower. For the global model, a larger e-modulus is necessary to account for the increased bending stiffness obtained by the attachment of the main cable and the bridge deck. Hence an e-modulus of 25 000 MPa and 27 000 MPa are considered for respectively load combination two and three. During capacity calculations, the optimal e-modulus will be determined. Furthermore, the forces are extracted from the lowermost node in each casting stage, which is a conservative assumption. The results are used for the capacity calculations of the towers in section 9.

The blue lines coincide with load combination one, whilst the orange lines represent the result from the analysis of load combination two. Load combination three is more complex. During this load combination, the wind forces push one column upwards while the other column is pushed downwards, mainly due to the static system of the tower. For this reason, the resulting forces will be different in each column. Even though both columns are in compression, one of the columns will have greater compressive forces and be referred to as the "compressive" column, represented by the yellow lines. The second column is represented by the grey lines and referred to as the "tensile" column.

Figure 8.4 presents the axial forces in the tower obtained from the analysis. It is shown that the axial forces are small in the free-standing towers compared to the global model. Furthermore, the significant increase in axial force at approximately 240 meters is caused by the self-wight imposed thru the main cable. The irregularities of the curves correlate to the position of transverse beams. In load combination one and two, the influence of the transverse beams is small but present. The small deviations could be explained by the fact that the wind affects a larger area at the height of the transverse beams. In load combination three, the effect from the transverse beams is more significant, mainly due to the distribution of forces between the "compressive" and "tensile" column.

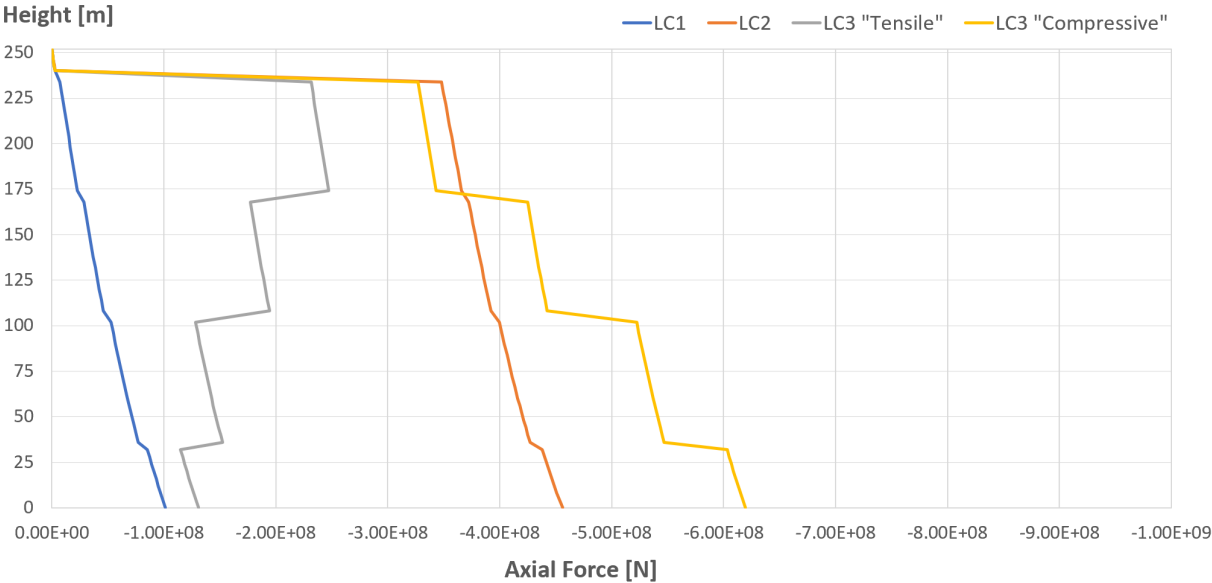


Figure 8.4: Axial forces

The shear forces in the global x-direction are shown in figure 8.5 and are caused by wind in the longitudinal direction of the bridge. Correspondingly, large shear forces are obtained from the analysis of load combination one and two, while the forces are small for load combination three. The transverse beams similarly cause unevenness in the curves. Moreover, the main cable is the reason for the distinct bend at the height of approximately 240 meters for load combination three.

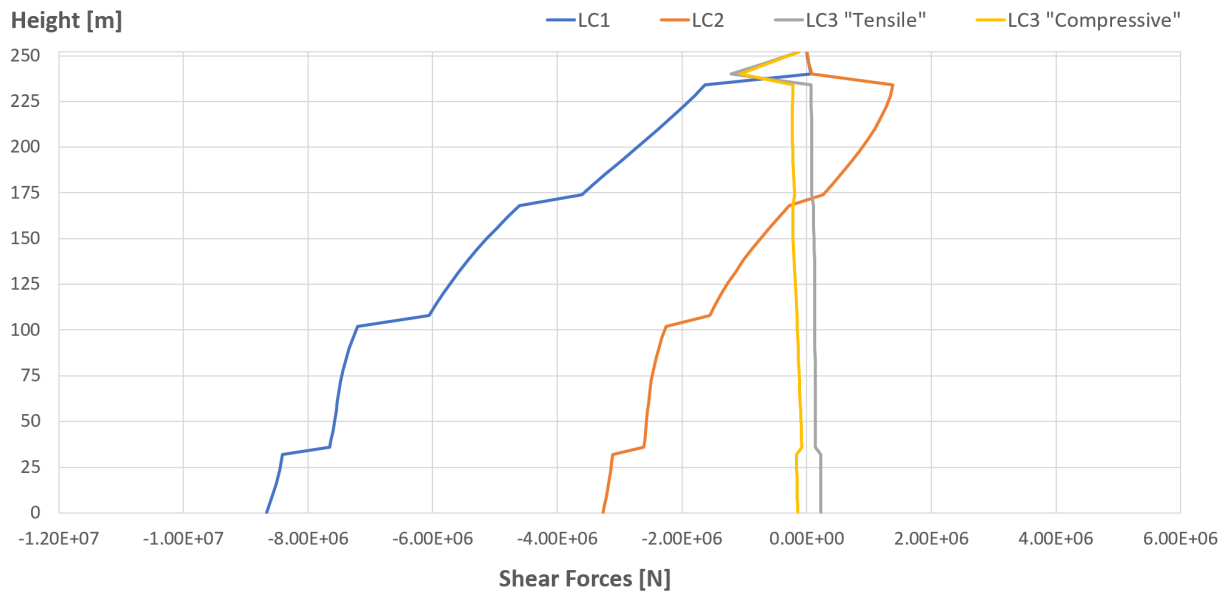


Figure 8.5: Shear forces in the x-direction

Wind in the transverse direction of the bridge causes the shear forces presented in figure 8.6. In this case, the shear forces are remarkable for load combination three. In contrast, they are small for load combination one and two. Furthermore, the unevenness is caused by the transverse beams. The figure clearly shows that the transverse beams cause reduced shear forces for load combination three. Additionally, the adjustment around 240 meters relates to the wind forces at the main cable, transferred to the tower top.

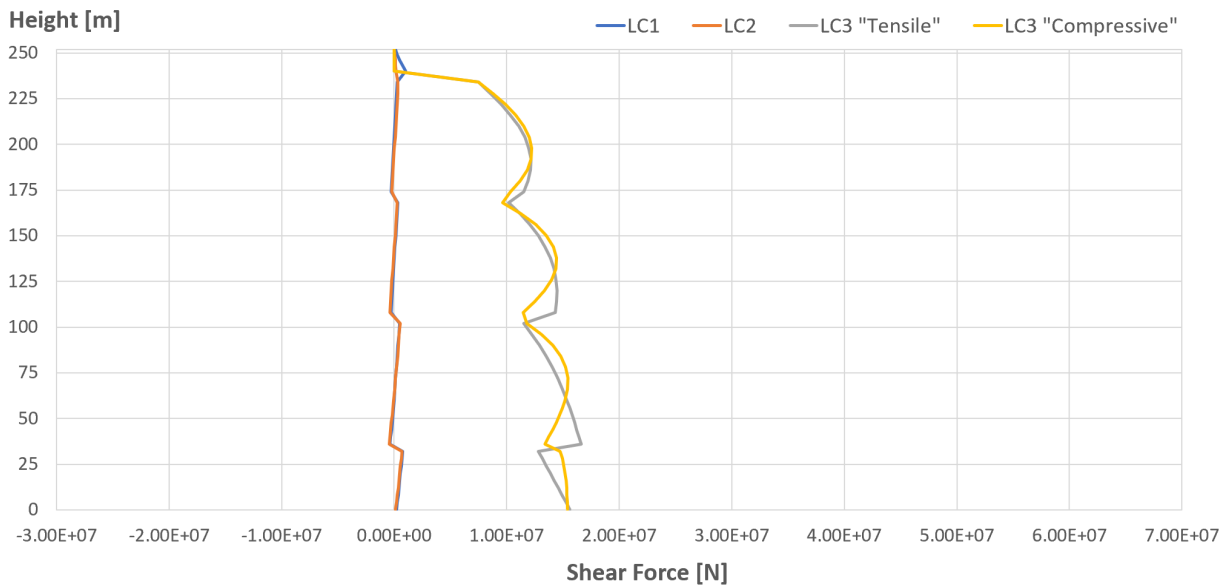


Figure 8.6: Shear forces in the y-direction

Figure 8.7 presents the moment about the global y-axis. These moments are caused by the wind that affects the towers in the longitudinal direction of the bridge. For this reason, the values for load combination one and two are significant, while the values for load combination three are small. Smooth curves represent the moments in the towers for load combination one and two, which means that the transverse beams do not significantly affect the result. The moment at the bottom of the towers is higher for the free-standing towers than for the global model, mainly because the static system is different. The free-standing towers are unrestrained at the top, causing the tower to work as a cantilever beam responsive to great displacement that induce large moments. For this reason, the analysis of the free-standing towers forms a dimensioning load case for determining the reinforcement in the flange. The attachment of the main cables and the stiffening girder stiffens the system. For this reason, the tensile and compressive side of the cross-section changes throughout the height.

The shear forces and the moments caused by wind in the longitudinal direction is comparable. For load combination one, the shear force and the moments are negative throughout the total height of the towers. A different situation occurs for load combination two. The moment and shear forces change from negative to positive throughout the height because of the constrained tower top. Additionally, when the shear forces are zero, the greatest positive moment is obtained, whereas when the moment is zero, the highest negative shear force is obtained.

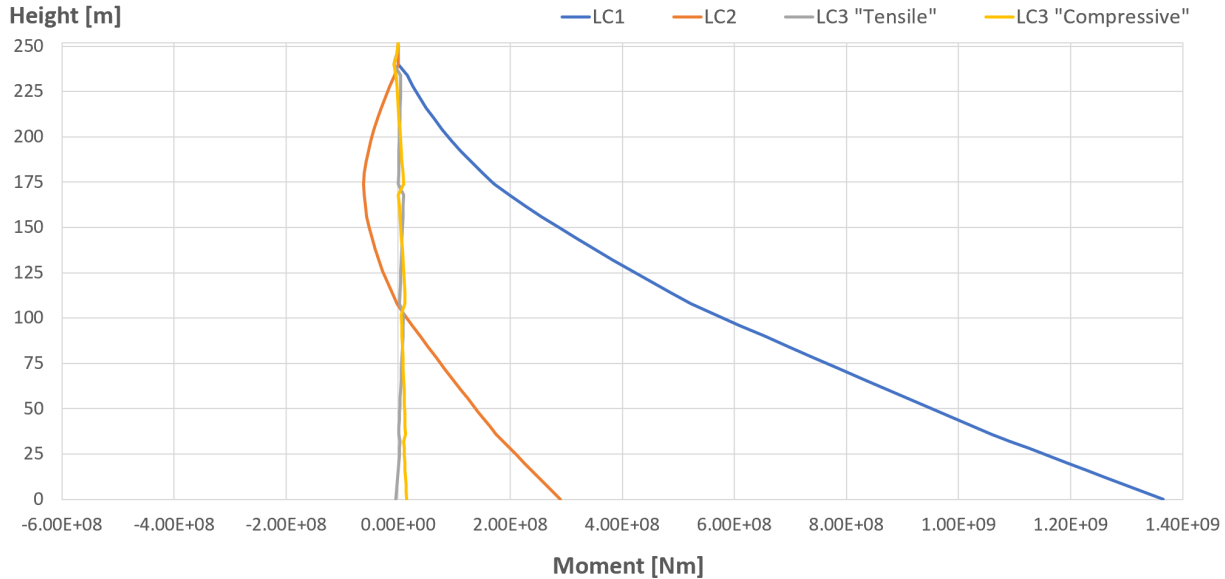


Figure 8.7: Moments about the y-axis

Moments about the global x-axis is vastly affected by the transverse beams, as shown in figure 8.8. The transverse beams stiffen the system and cause the strain distribution to change multiple times throughout the height during load combination three. Regarding load combination one and two, the moments are in comparison negligible.

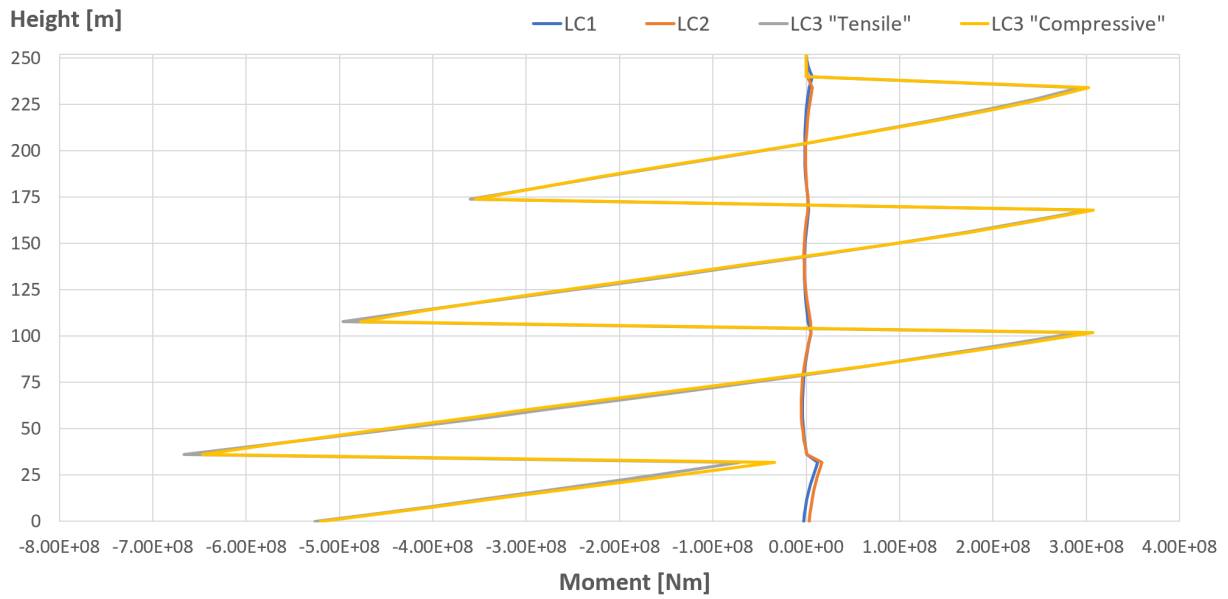


Figure 8.8: Moments about the x-axis

Finally, the torsional moment, represented by the last degree of freedom in the node, is presented in figure 8.9. The free-standing towers obtain a large torsional moment at the bottom of the tower. On the contrary, the global model subjected to load combination three has larger torsional moments at the top of the tower. While the torsional moment is significant for load combination one and three, these are remarkably smaller for load combination two. The distinct bends correlate to the transverse beams and the attachment of the main cable. When the towers are unrestrained at the top, the towers rotate freely, while the restraining of the system reduces the rotations. However, for load combination three, the transverse forces from the main cables generate additional rotation, illustrated by the large adjustment around 240 meters. The transverse beams is stiffening the structural system reducing the torsional moments.

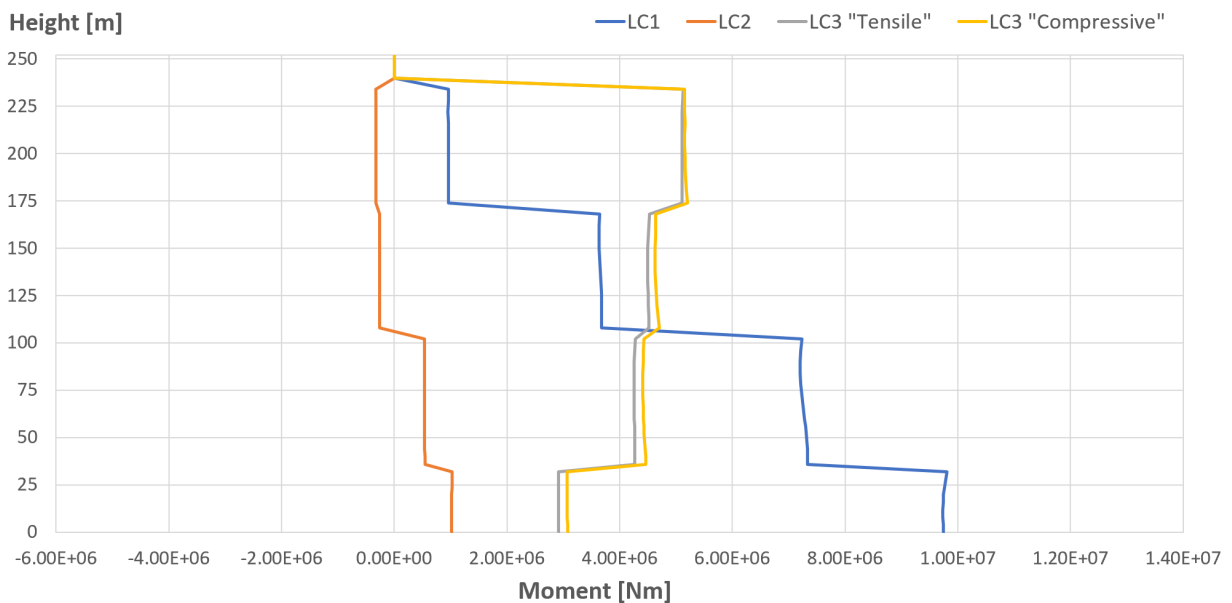


Figure 8.9: Torsional moments about the z-axis

### 8.3 Abaqus analysis of transverse beams

Due to the different load combinations, large forces occur in the transverse beams. The complete result of the analysis, including curves of the force distribution along the length of the transverse beams, could be found in appendix F. Since the dimensioning forces depend on the bending stiffness of the tower, the analysis is performed with different modulus of elasticity. Accordingly, the different load combinations are analysed with an e-modulus equal to 17 000 MPa and 25 000 MPa. The dimensioning forces in each transverse beams are presented in the tables below and used in the capacity calculations in section 9.5. The global axis system is kept unchanged, as illustrated by figure 8.10.

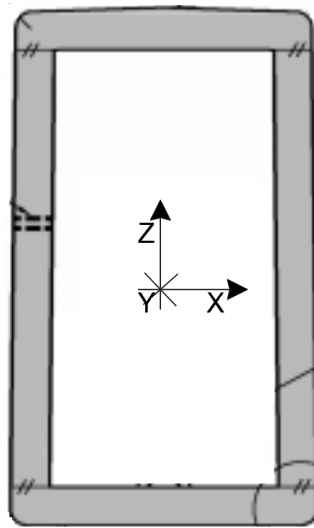


Figure 8.10: Axis system of transverse beam

In general, the largest bending moments develop about the x-axis during load combination three. Closely related to the large forces transferred by/to the transverse beams during this load combination, illustrated by figure 8.8. Correspondingly, the beam is shaped like a rectangle to increase the bending stiffness about the x-axis.

Transverse beam	Load combination	Dimensioning moment	Corresponding axial force
Bottom	LC3	529 MNm	3.04 MN
Lower middle	LC3	597 MNm	0.58 MN
Upper middle	LC3	676 MNm	1.77 MN
Top	LC3	266 MNm	8.85 MN

Table 8.3: Bending moments about the x-axis

The bending moments about the z-axis are significantly smaller than the moment about the x-axis. Based on this, less stiffness is required, and correspondingly less moments occur. In detail, the moment about the z-axis in the beams develop due to torsion in the columns of the tower, illustrated by the distinct bends in figure 8.9. For this reason, load combination one is critical for the three bottom beams, while load combination three is critical for the top beam. Additionally, the evenly distributed wind force along the beams during load combination three will contribute to the moments. But the forces are small compared to the forces transferred from the columns of the towers.

Transverse beam	Load combination	Bending moment	Corresponding axial force
Bottom	LC1	7.23 MNm	1.36 MN
Lower middle	LC1	5.59 MNm	0.74 MN
Upper middle	LC1	8.82 MNm	0.98 MN
Top	LC3	4.74 MNm	8.85 MN

Table 8.4: Bending moments about the z-axis

During load combination three, the towers are affected by transverse winds and self-weight pulling the tower diagonally. For this reason, torsional moments occur, which needs to be accounted for, presented by table 8.5.

Transverse beam	Load combination	Torsional moment	Corresponding axial force
Bottom	LC3	5.18 MNm	4.10 MN
Lower middle	LC3	11.4 MNm	6.86 MN
Upper middle	LC3	10.8 MNm	1.77 MN
Top	LC3	7.70 MNm	8.85 MN

Table 8.5: Torsional moments about the y-axis



Correspondingly to the moments, the shear forces are substantially larger along the z-axis than in the transverse direction (x-axis). Accordingly, the forces occur during load combination three, when the tower columns are pushed in the opposite direction. The dimensioning shear forces are presented in table 8.6.

Transverse beam	Load combination	Dimensioning shear force	Corresponding axial force
Bottom	LC3	52.8 MN	3.10 MN
Lower middle	LC3	84.1 MN	0.58 MN
Upper middle	LC3	78.3 MN	1.77 MN
Top	LC3	52.5 MN	8.85 MN

Table 8.6: Shear forces in the z-direction

Like the transverse moment, the transverse shear forces are closely related to the torsional moment of the columns. Therefore, the largest forces occur during the same load combinations as stated above. The dimensioning shear forces are presented in table 8.7.

Transverse beam	Load combination	Dimensioning shear force	Corresponding axial force
Bottom	LC1	567 kN	1.36 MN
Lower middle	LC1	563 kN	0.74 MN
Upper middle	LC1	785 kN	0.97 MN
Top	LC3	798 kN	8.85 MN

Table 8.7: Shear forces in the x-direction

## 9 Design of the towers

The towers will be designed based on the results from Abaqus and by application of the excel lamellae program. As previously stated, the excel lamellae program is used to determine the required reinforcement to withstand the combined axial forces and moments. The reinforcement design should be determined for each casting stage to obtain the complete design of the towers. In the thesis, simplifications are made such that every fifth casting stage will be investigated. Each load combination in Abaqus is analysed for three different bending stiffnesses to create a sufficient basis for calculation, as described in section 7.3.1.

A total of three reinforcement specifications are calculated first by using ordinary reinforcement to create a reference design. After that, 50% of the ordinary reinforcement is replaced by prestressed reinforcement. Lastly, the prestressed reinforcement is reduced to a total of 25%. Accordingly, the moment capacity and the corresponding reinforcement specifications will be presented. The result will form the basis for determining whether the use of prestressed reinforcement are favourable along the height of the towers or not. Finally, the shear- and torsional capacity is calculated in accordance with EC2.1-1 to specify the reinforcement design. Alike the towers, the required reinforcement for the transverse beams are determined to withstand the bending moments, shear forces and torsional moments that occur.

Manual N400 [20] states that the reinforcement diameter should be chosen greater than 12 mm in bridge design. The longitudinal reinforcement bars used in the towers of Hardangebrua is  $\text{Ø}32$ ; hence this will form the basis for the towers of Halsafjorden bridge. Due to the slenderness of the towers and large external forces, bundled reinforcement bars are often used. Consequently, the reinforcement amount can be increased as well as the capacity without increasing the concrete area which is favourable. Furthermore, the transverse beams are designed using  $\text{Ø}25$  in the flange and  $\text{Ø}20$  in the web. The centre-centre distance is determined according to table 3.4. As for the shear reinforcement,  $\text{Ø}16$  is used in the flange and  $\text{Ø}20$  in the web of the towers. For the transverse beams,  $\text{Ø}25$  is used in the flange and  $\text{Ø}16$  is used in the web. The reinforcement is symmetrical, meaning that the reinforcement in both flanges are equal and the amount in both webs are equal.

### 9.1 Design of the towers using ordinary reinforcement

#### 9.1.1 Free-standing towers

The reinforcement relevant to withstand the forces obtained by load combination one is placed in the flange of the cross-section. Systematically it is chosen to find the reinforcement amount such that the cross-section in each casting stage is 100% utilised. The methodology is explained in section 7.3, hence by the use of moment-curvature diagrams. The light orange line presents the result in figure 9.1.

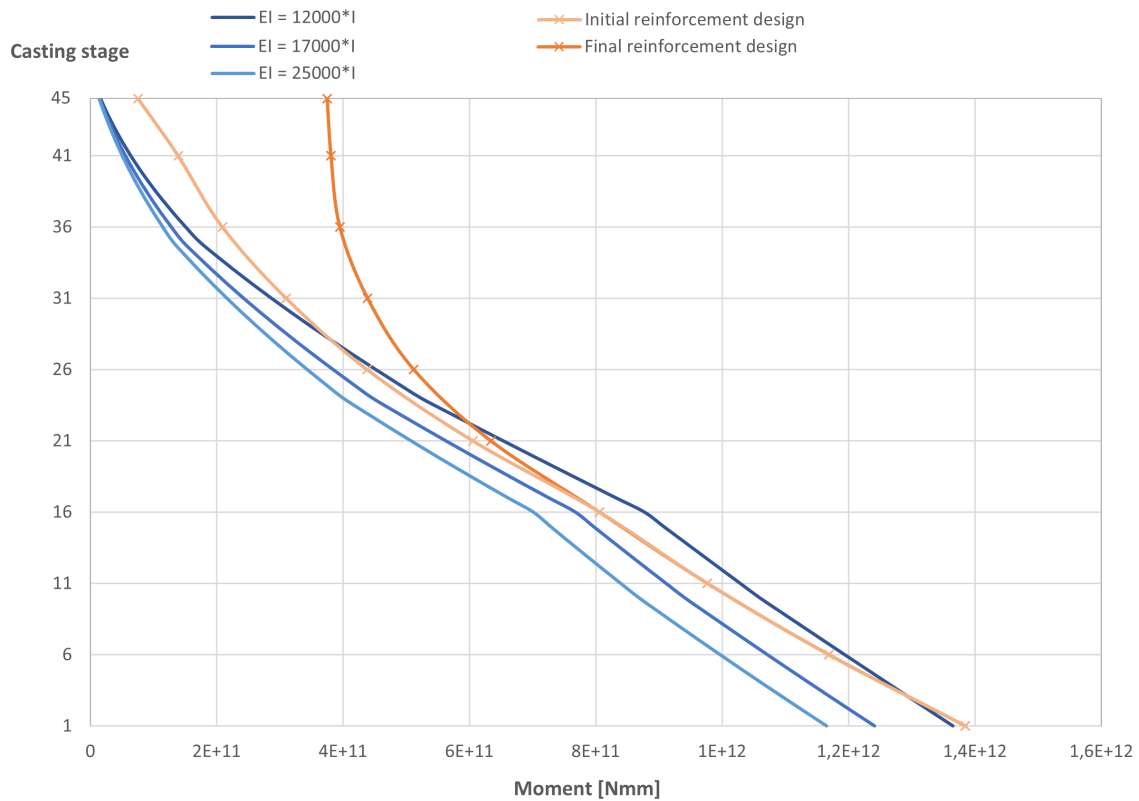


Figure 9.1: Moment capacity for the free standing towers using ordinary reinforcement

Furthermore, the corresponding modulus of elasticity is determined, presented by the light orange line in figure 9.2. Due to the second-order moments, the corresponding e-modulus has to be equal or increased along the height. If the e-modulus decreases throughout the height, the bending stiffness is too low. Consequently, the forces obtained from the analysis in Abaqus is invalid. For this reason, the bending stiffness of casting stage 17 to 45 is increased by increasing the reinforcement amount. Thus, reducing the utilization ratio below 100% for these casting stages. The updated moment capacity is presented by the orange line in figure 9.1, along with the modulus of elasticity and the corresponding bending stiffness in figure 9.2 and 9.3.

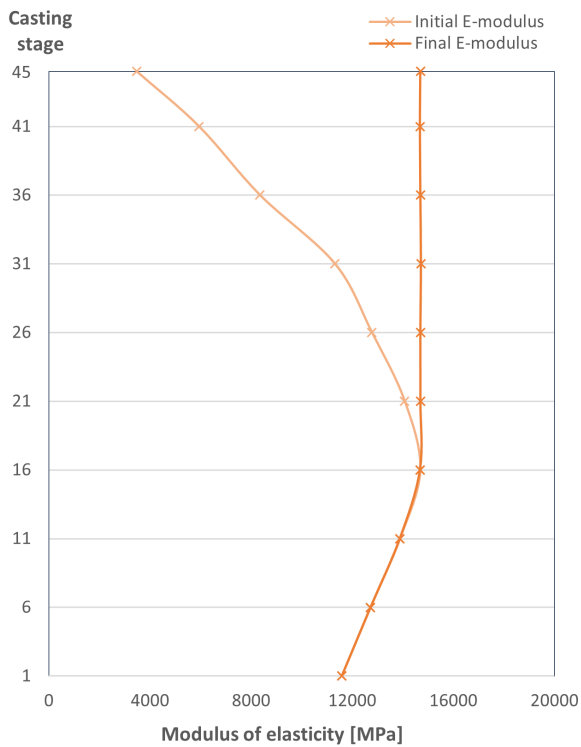


Figure 9.2: Modulus of elasticity LC1

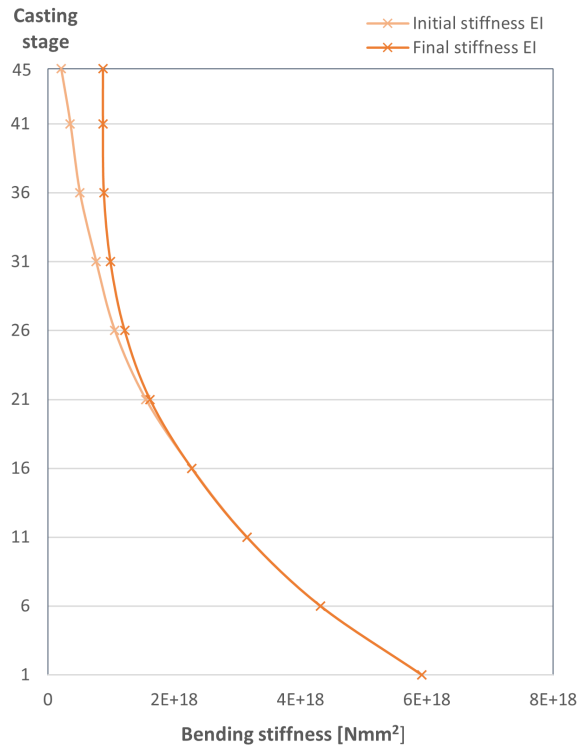


Figure 9.3: Bending stiffness LC1

The number of Ø32 bars corresponding to the moment capacity shown in figure 9.1 is given in table 9.1, and bundled reinforcement is not necessary before casting stage 16. In addition to the reinforcement, the decreased utilization ratio is shown in the same table. The fourth column in table 9.1 displays the total amount of Ø32 bars that could be placed in each flange. The calculations take into account the requirements regarding concrete cover and minimum distance between the reinforcement bars from table 3.4. Hence, non of the casting stages are fully reinforced.



Figure 9.4: Placement of reinforcement in the flange

### 9.1.2 Bending in the longitudinal direction of the complete bridge

Based on the reinforcement determined in the previous paragraph and table 9.1, the moment capacity for load combination two is calculated. Figure 9.5 present the result of the analysis in the lamellae program. Based on this, it can be determined that the reinforcement amount listed in table 9.1 is sufficient to withstand the moments caused by load combination two. The utilization ratio is given in table 9.1.

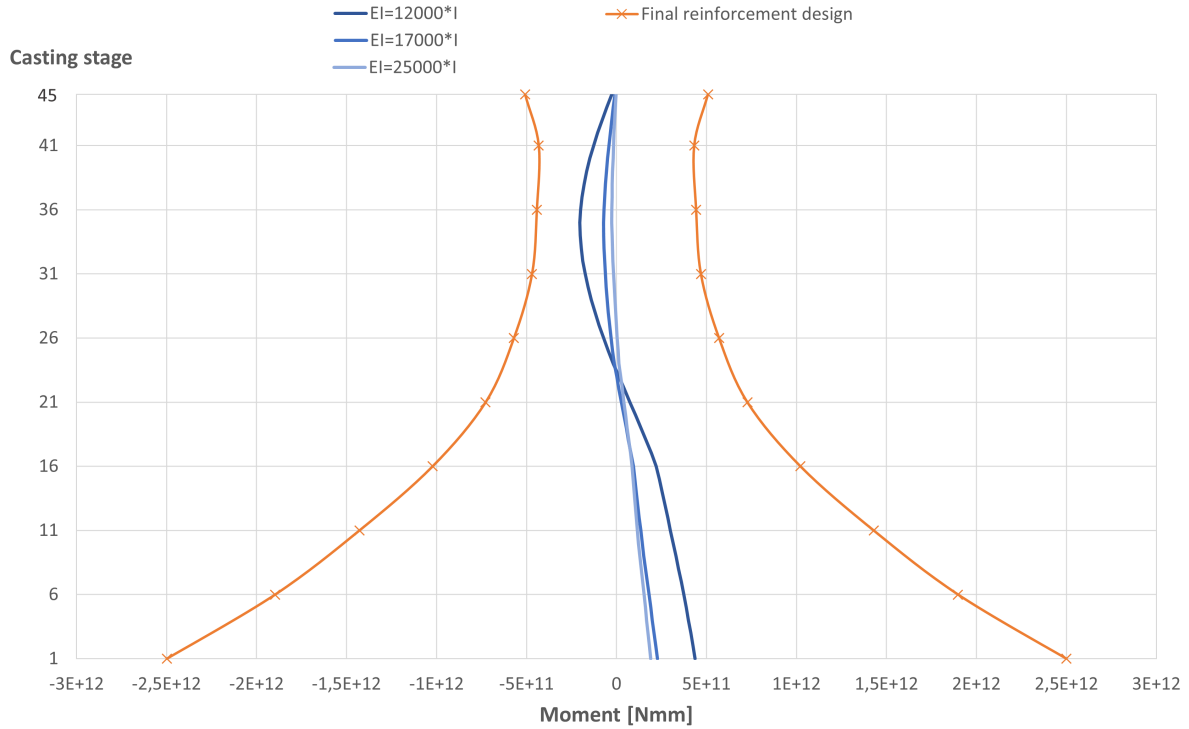


Figure 9.5: Moment capacity during load combination two using ordinary reinforcement

Casting stage	Number of Ø32 (each side flange)	Utilization ratio LC1	Utilization ratio LC2	Maximum Ø32 (each side flange)
45	150	23 %	41 %	216
41	144	39 %	39 %	216
36	139	55 %	40 %	216
31	135	72 %	43 %	228
26	140	86 %	49 %	240
21	146	95 %	33 %	264
16	162	100 %	40 %	300
11	168	100 %	41 %	336
6	160	100 %	45 %	384
1	154	100 %	48 %	438

Table 9.1: Reinforcement specifications in the flange

### 9.1.3 Bending in the transverse direction of the complete bridge

By adding reinforcement in the web of each tower column, the moment capacity is increased in order to withstand the transverse wind forces imposed during load combination three. Due to the transverse beams, large forces are transferred between the column of the towers, enhancing the transverse stability. Based on this, the capacity calculations are performed for some extra casting stages, especially around the transitions between the tower and transverse beams.

Unique for load combination three, each column of the towers are subjected to different axial forces and moments, more thoroughly described in section 8.2. For this reason, the capacity calculations regarding bending in the transverse direction require extra attention. Firstly, the reinforcement specification is calculated individually for the "compressive" and the "tensile" column. Secondly, the specifications are compared and the largest requirements selected for both columns. Thirdly, the modulus of elasticity is verified, and additional reinforcement added to both columns if necessary. The light orange line illustrates the individually calculated reinforcement specification, and the darker orange line draws the final reinforcement design. Even though the same reinforcement is used for both columns, the bending stiffness is different due to the axial force. For this reason, the moment capacity in the diagram is distinctive.

Based on the individual calculations, the "tensile" column determines the reinforcement specification for casting-stage 1-11, while the "compressive" column decides the reinforcement for casting-stage 12-45. The verification is performed for the "compressive" column, indicating insufficient bending stiffness for casting-stage 31-45, thoroughly described later in this section.

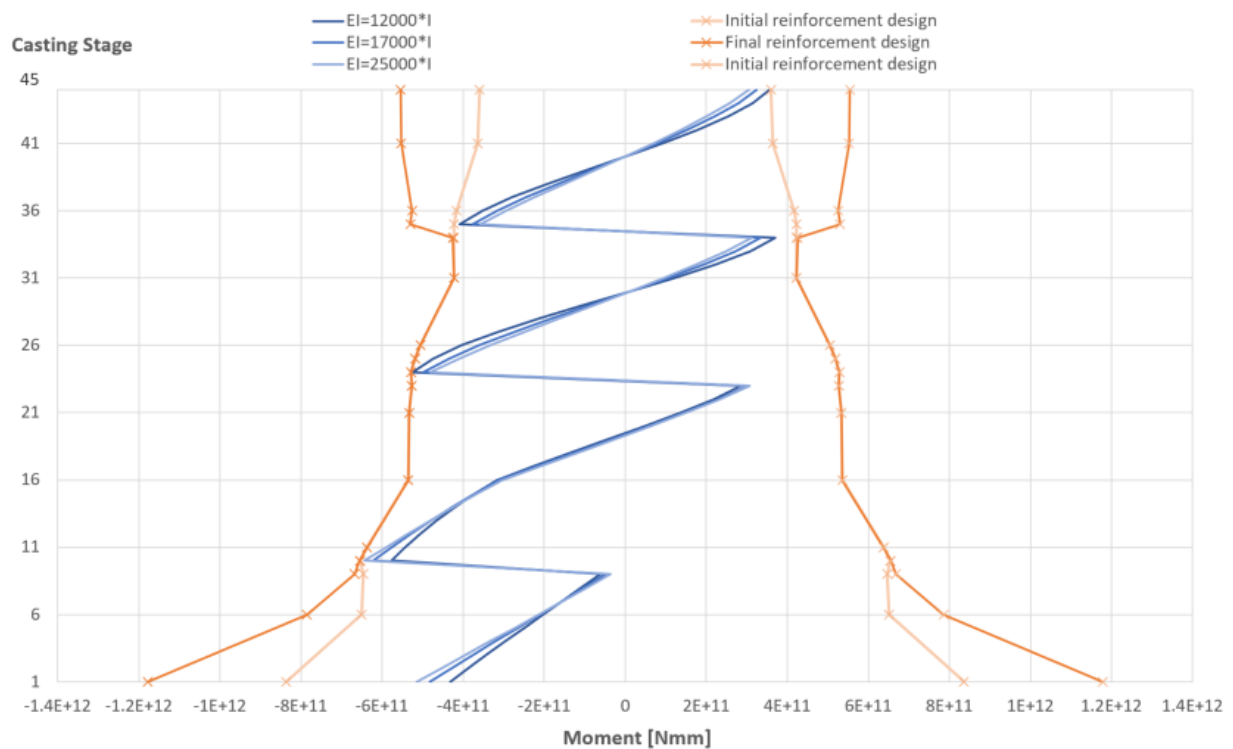


Figure 9.6: Moment capacity during load combination three. "Compressive" column

The moment capacity for the "compressive" column is illustrated by figure 9.6. As previously described, the reinforcement for casting stage 1-11 needs to be increased, shown by the enlarged capacity of the darker orange line in the diagram. In order to obtain substantial stiffness at the top, the reinforcement is increased for casting stage 31-45, shown by the diagram. The highest utilized casting stages are casting stage 10 and 11, with a utilization ratio of respectively 94% and 98%. However, both the cross-section areas have additional space for reinforcement, which means the utilization ratio could be decreased.

The moment capacity of the "tensile" column is presented by figure 9.7. Alike the "compressive" column, the "tensile" column is analysed individually before comparisons are made, illustrated by the light orange line in figure 9.7. The "tension" column decides the reinforcement required for casting stage 1-11, shown by the overlapping orange lines in the diagram. From casting-stage 12-45, the reinforcement is decided by the "compressive" column, including the stiffness verification between casting-stage 31-45. The darker orange curve illustrates the final reinforcement design. Henceforth, the most critical casting stage is stage number 10, with a utilisation ratio of 98 %.

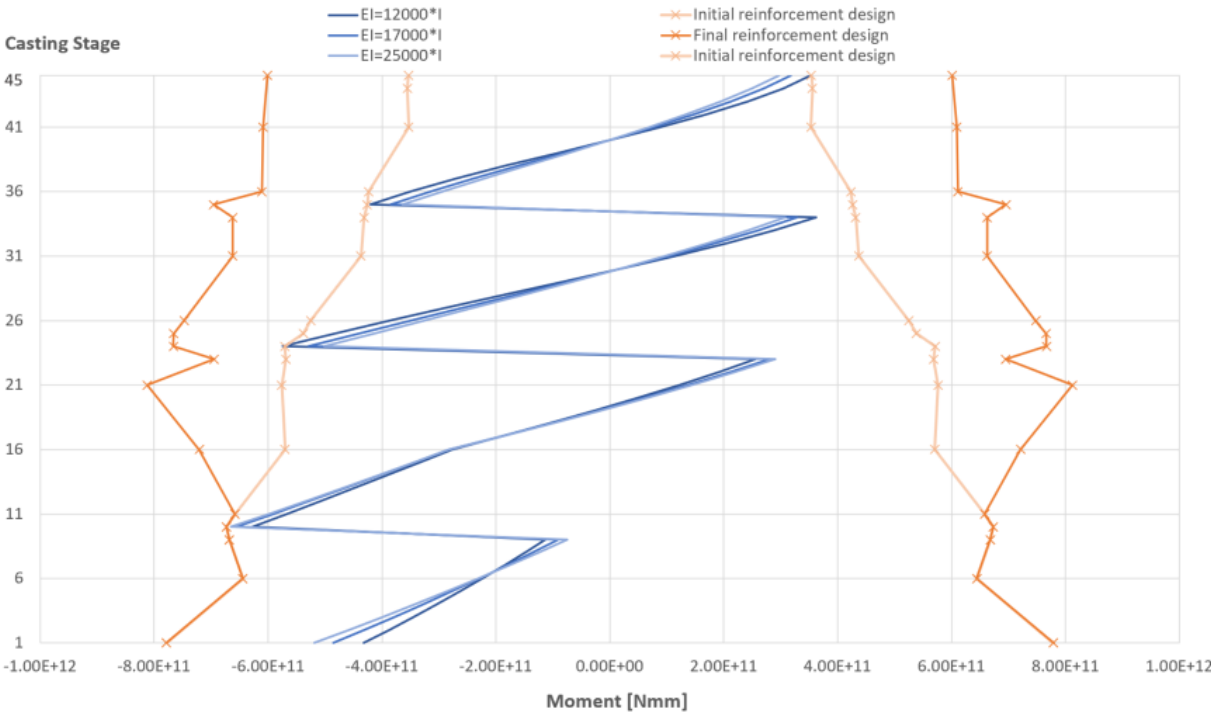


Figure 9.7: Moment capacity during load combination three. "Tensile" column

As described in section 9.1.1, the bending stiffness is controlled to verify the results. The verification is conducted for the "compressive" column mainly because the column determines the reinforcement specification of the upper casting stages. Illustrated by figure 9.8, the modulus of elasticity decreases past stage 31. As mentioned above, the reinforcement is therefore increased to retain sufficient bending stiffness towards the top of the tower.

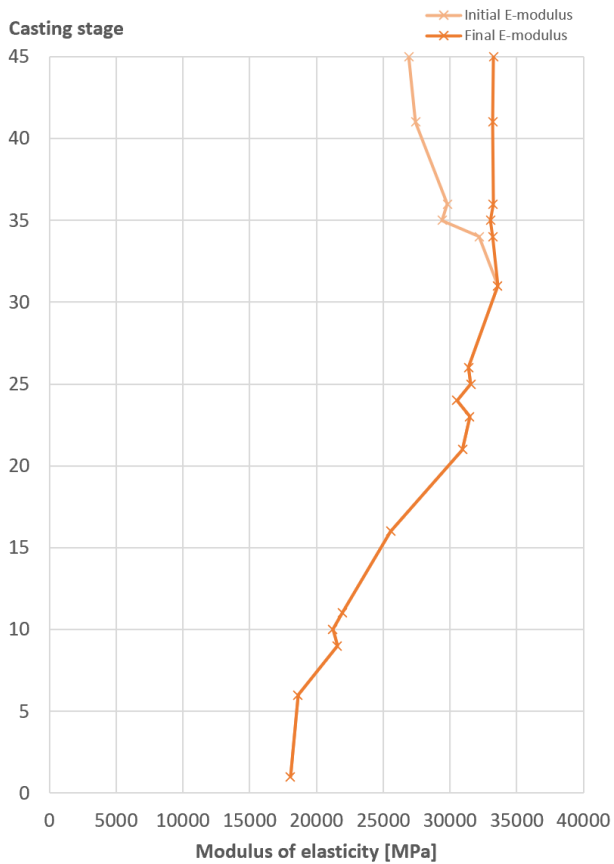


Figure 9.8: Modulus of elasticity LC3

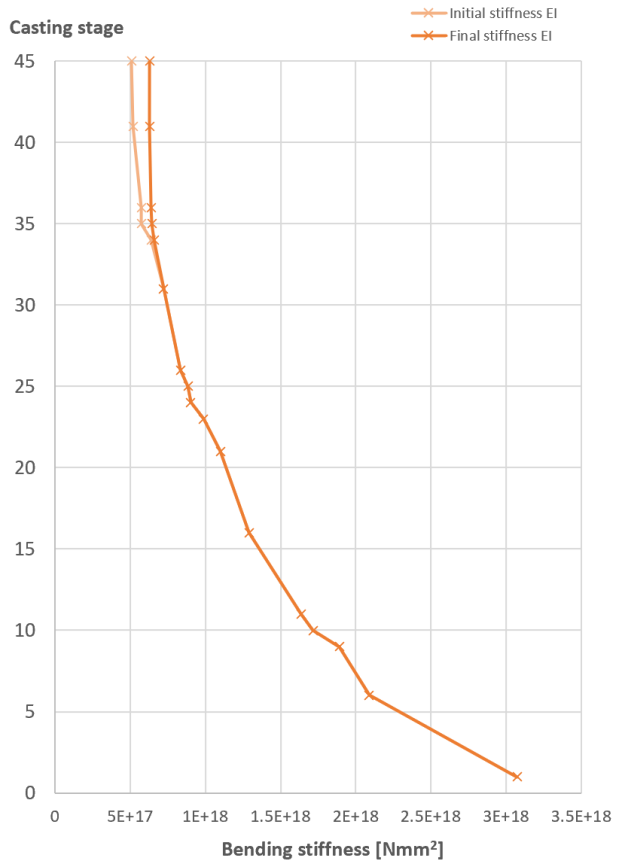


Figure 9.9: Bending stiffness LC3

Based on the results above, the final reinforcement specifications for the web is obtained, presented by the table 9.1.3. Furthermore, the utilization ratio is calculated to enlighten the critical stages. Illustrated by the last column in the table, each cross-section has extra space such that additional reinforcement could be included to increase the capacity and reduce the utilization ratio.





Figure 9.10: Placement of reinforcement in the web

Casting stage	Number of Ø32 (each side web)	Utilization ratio "tensile"	Utilization ratio "compressive"	Maximum Ø32 (each side web)
45	410	58%	53%	444
41	410	27%	25%	444
36	390	58%	53%	450
35	390	68%	57%	450
34	380	74%	52%	456
31	355	34%	26%	462
26	370	70%	50%	498
25	370	79%	59%	504
24	355	90%	68%	516
23	370	58%	28%	522
21	410	50%	50%	546
16	280	58%	57%	606
11	180	94%	91%	684
10	165	98%	98%	702
9	200	23%	58%	726
6	150	25%	36%	780
1	150	42%	60%	894

Table 9.2: Reinforcement specification in the web

## 9.2 Design of the towers using prestressing

### 9.2.1 Free-standing towers

Figure 9.11 presents the result of the analysis using a combination of ordinary and prestressed reinforcement. The dark red line represents the moment capacity when 50% of the ordinary reinforcement is replaced by prestressed reinforcement. Based on this, the moment capacity is increased substantially compared to the ordinary reinforced cross-section. Furthermore, the dark orange line represents the moment capacity when the prestressed reinforcement area is reduced by 50%. Thus, the moment capacity is reduced, obtaining a slightly higher moment capacity than if ordinary reinforcement is used, represented by the orange line.

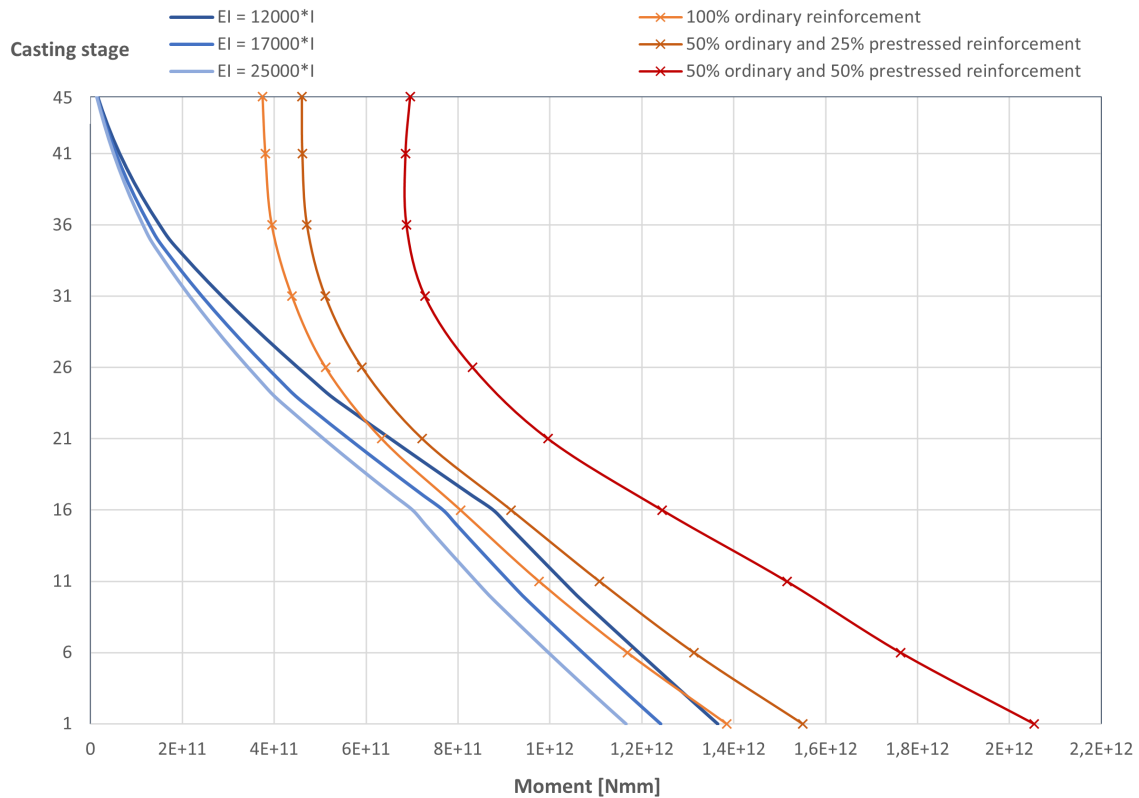


Figure 9.11: Moment capacity for the free standing towers using prestressed reinforcement

### 9.2.2 Bending in the longitudinal direction of the complete bridge

The same methodology follows for the complete bridge imposed by load combination two. The orange line represents a cross-section with 100% ordinary reinforcement. Moreover, the dark red line represents 50% ordinary and 50% prestressed reinforcement, and for the dark orange line, the prestressed reinforcement area is reduced by 50%, shown in figure 9.12. Unlike the free-standing towers, the moment capacity is reduced by implementing prestressed reinforcement during load combination two. Hence, the higher the amount of prestressed reinforcement, the lower the moment capacity.

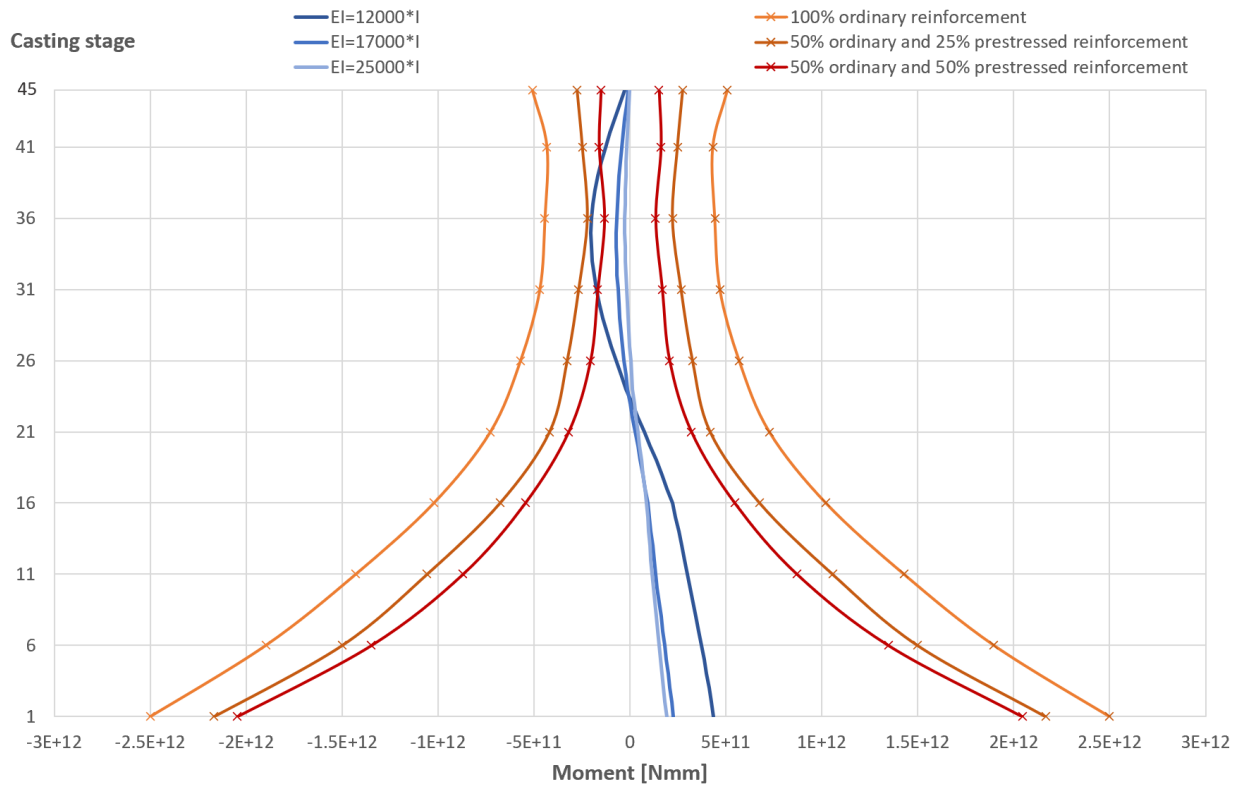


Figure 9.12: Moment capacity during load combination two using prestressed reinforcement

### 9.2.3 Bending in the transverse direction of the complete bridge

Equivalent to the sections above, the ordinary reinforcement is replaced with prestressed reinforcement in order to determine the effect. Similarly, as for the determination of the ordinary reinforcement, the "compressive" and "tensile" column will be considered separately. Both columns are analysed and presented in table 9.13 and 9.14, for the respectively "compressive" and "tensile" column. Notably, due to symmetric reinforcement, the capacity applies for both positive and negative side. However, only the negative side (most critical) is drawn in the diagram to enlighten the most relevant data.

As mentioned in section 8.2, the columns of the towers are imposed by large compressive axial forces. By replacing ordinary reinforcement with prestressed reinforcement, the axial force increases, causing failure before the cracking moment. Consequently, the moment capacity is decreased. Accordingly, adding more prestressed reinforcement reduces the capacity, illustrated by figure 9.13.

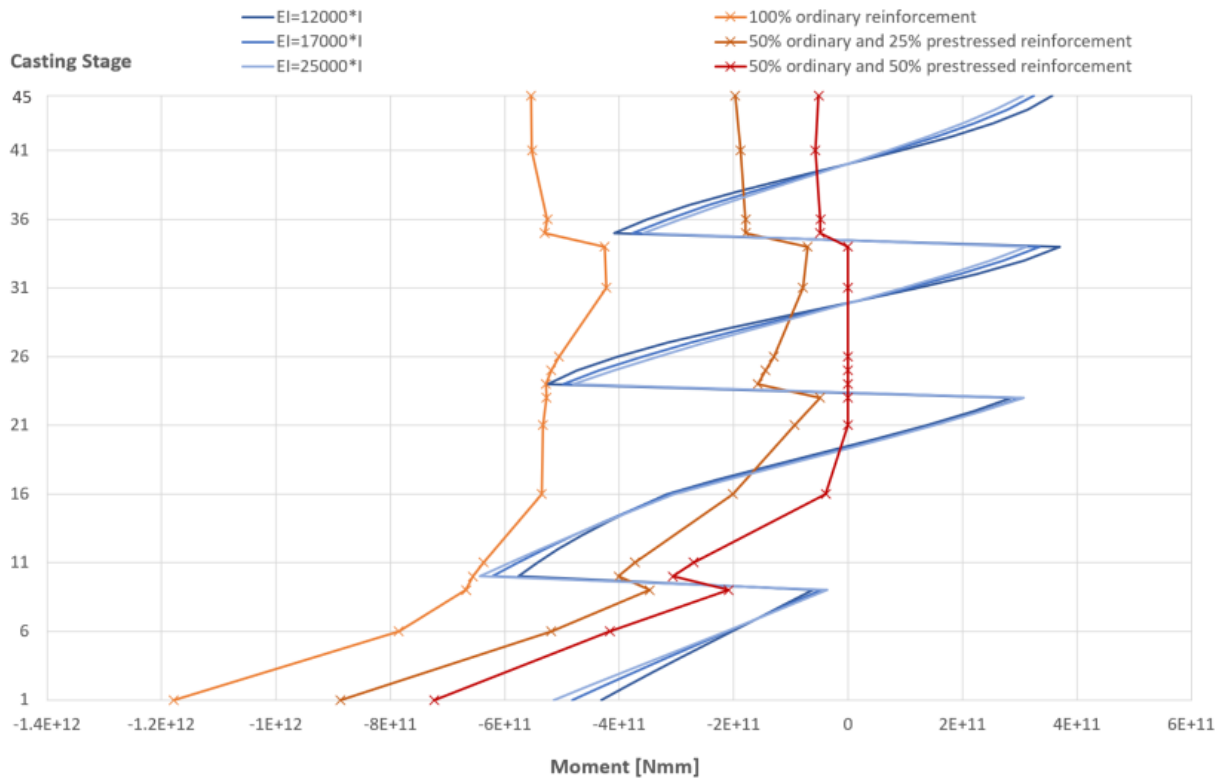


Figure 9.13: Effect of prestressed reinforcement on the "compressive" column during LC3

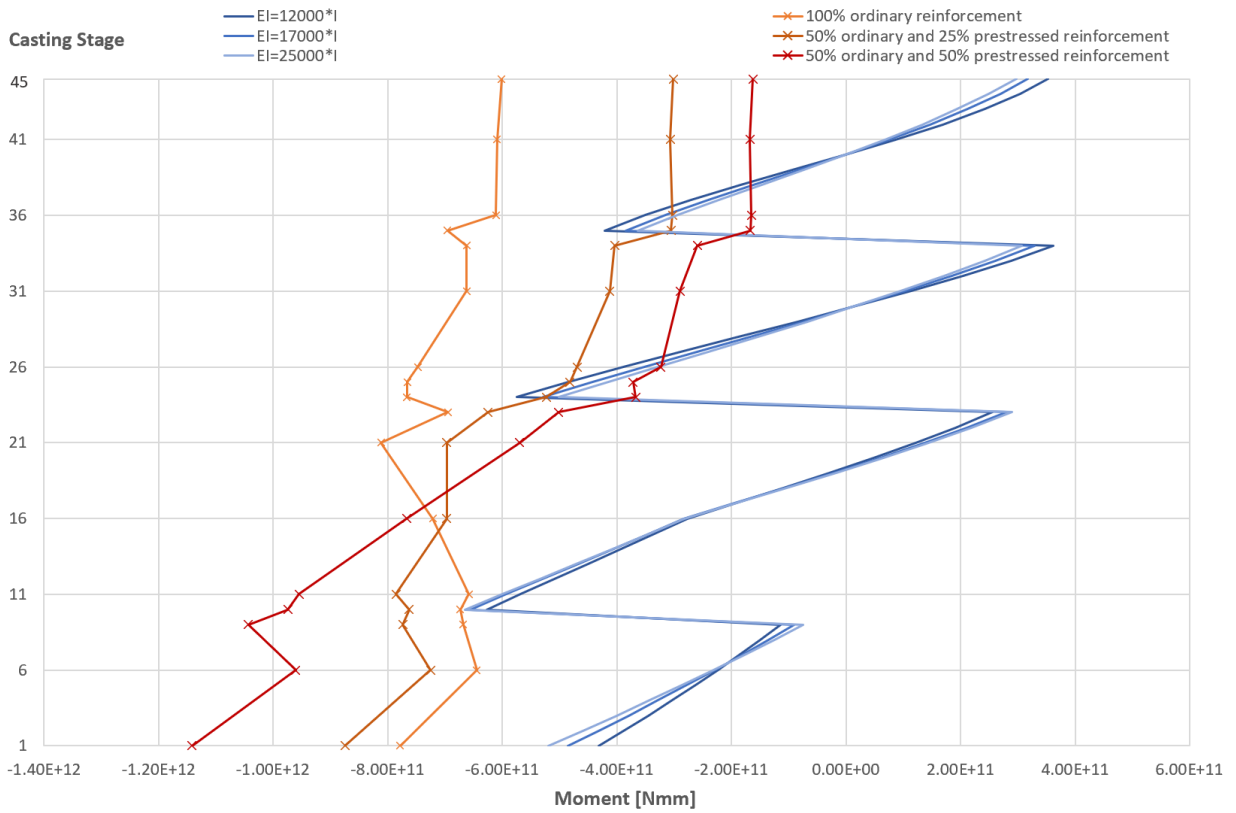


Figure 9.14: Effect of prestressed reinforcement on the "tensile" column during LC3

Compared to the "compressive" column, the effect of the prestressed reinforcement is more fortunate for the "tensile" column. In fact, between casting stage 1 and 15, replacing ordinary reinforcement with prestressed reinforcement is favourable. However, a necessary condition is that heavy wind could only blow in one direction. If the wind switch direction, the "tensile" and "compressive" column also change, which could lead to failure for casting stage 9-11. Furthermore, for casting stage 15(16) to 45, the axial force has increased, such that prestressed reinforcement is unfavourable. For these casting stages, the concrete would reach failure before the cracking moment, indicating reduced capacity.

### 9.3 Shear capacity

In addition to finding the moment capacity, the shear capacity is calculated. EC2.1-1 states that both tensile and compressive failure needs to be controlled according to section 6.2.2 and 6.2.3. First, the shear tensile capacity ( $V_{Rd,c}$ ) is calculated to examine whether shear reinforcement is necessary for the towers or not. The formula is given in equation 6.2.a and needs to be greater than the main shear tensile failure, calculated by equation 6.2.b.

If  $V_{Rd,c} > V_{Ed}$ , shear reinforcement is not necessary according to the calculations and the shear capacity is sufficient. Although the calculation shows that shear reinforcement can be excluded, section 9.2.2 in EC2.1-1 specifies that minimum shear reinforcement should be included. Following that, and the shear tensional capacity is sufficient, the shear compressive capacity should be calculated according to formula 6.5 in EC2.1-1. The formula investigates whether the concrete can withstand the shear forces that follows from the external load. If  $V_{Rd,max} > V_{Ed}$ , the capacity is sufficient and if not, the concrete area has to be increased. However, if  $V_{Rd,c} < V_{Ed}$ , shear reinforcement is necessary for the towers, and the dimensioning process is based on a truss model. The necessary shear reinforcement is calculated according to equation 6.8, and the compression capacity follows from equation 6.9 in EC2.1-1.

The shear capacity of the free-standing towers is calculated and presented in table 9.3. Both  $V_{Rd,c}$  and  $V_{Rd,max}$  is greater than  $V_{Ed}$ , hence the capacity is sufficient in regards to the reinforcement and the concrete. Consequently, minimum shear reinforcement is calculated according to equation NA.9.5N in EC2.1-1 and added to the flange. The maximum distance between the shear reinforcement ( $c/c$ ) is calculated by equation NA.9.6N. The result is listed in table 9.6, based on double-cut shear reinforcement stirrups.

Casting stage	$V_{Ed}$ [kN]	$V_{Rd,c}$ [kN]	$V_{Rd,max}$ [kN]
45	1 629	5 694	62 766
41	2 377	6 302	62 779
36	3 408	7 103	63 071
31	5 129	8 441	65 300
26	5 836	9 607	69 766
21	7 337	11 475	76 461
16	7 533	13 149	85 409
11	7 629	14 505	96 617
6	8 482	16 507	110 077
1	8 663	18 058	125 808

Table 9.3: Shear capacity LC1

Furthermore, the shear capacity is calculated for the complete bridge subject to load combination two. Alike the free-standing towers,  $V_{Rd,c}$  and  $V_{Rd,max}$  is larger than  $V_{Ed}$  and the result is shown in table 9.4. Hence the minimum shear reinforcement added to the flange is sufficient to withstand the shear forces from load combination two.

Casting stage	$V_{Ed}$ [kN]	$V_{Rd,c}$ [kN]	$V_{Rd,max}$ [kN]
45	1 384	15 179	64 748
41	1 090	15 113	64 762
36	417	15 114	65 054
31	-739	15 513	67 283
26	-1 368	16 471	71 749
21	-2 376	17 884	78 444
16	-2 541	19 873	87 392
11	-2 599	22 177	98 599
6	-3 160	24 711	112 059
1	-3 271	27 291	125 808

Table 9.4: Shear capacity LC2

The result of shear capacity control for the complete bridge subject to load combination three is presented in table 9.5. Both the "tensile" and the "compressive" column are included in the table. Similarly, as the moment capacity, it is chosen to investigate the shear capacity more thoroughly near the transverse beams. Hence, some additional casting stages are included in the analysis. The shear capacity is insufficient for all casting stages except from casting stage 6 and 9. Applicable to both the tensile and compressive column of the tower. For this reason, minimum reinforcement is used for casting-stage 6 and 9, and the necessary amount of shear reinforcement is calculated for the other casting stages. For the web, double-cut reinforcement stirrups form the basis for the design, and the result is listed in table 9.6.

Casting stage	$V_{Ed}$ T [kN]	$V_{Rd,c}$ T [kN]	$V_{Ed}$ C [kN]	$V_{Rd,c}$ C [kN]	$V_{Rd,max}$ [kN]
45	7 493	7 358	7 491	7 358	28 492
41	11 062	7 360	11 542	7 360	28 498
36	11 901	7 394	11 213	7 394	28 635
35	11 493	7 426	10 360	7 426	28 765
34	10 199	7 467	9 638	7 467	28 931
31	12 799	7 654	13 503	7 654	29 680
26	14 470	8 175	13 357	8 175	31 774
25	14 439	8 311	12 503	8 311	32 319
24	14 306	8 456	11 465	8 456	32 900
23	11 516	8 613	11 790	8 613	33 531
21	12 900	8 956	14 076	8 956	34 912
16	15 348	9 997	15 199	9 997	39 106
11	16 425	11 299	13 750	11 299	44 360
10	16 619	24 904	13 399	24 904	45 530
9	12 812	9 924	14 750	11 892	46 756
6	13 870	14 554	15 197	19 241	50 669
1	15 607	11 548	15 367	14 603	58 043

Table 9.5: Shear capacity LC3 "Tensile" and LC3 "Compressive"

	Flange Ø16	Web Ø20
Casting stage	c/c [mm]	c/c [mm]
45	230	220
41	230	140
36	230	140
35	230	140
34	230	160
31	230	130
26	230	130
25	230	130
24	230	130
23	230	160
21	230	140
16	230	150
11	230	160
10	230	360
9	230	180
6	230	360
1	230	220

Table 9.6: Shear reinforcement specification

## 9.4 Torsional capacity

Finally, the torsional capacity is calculated to investigate whether additional reinforcement has to be included. The calculations are found by assuming a massive cross-section. Similarly, as for the shear capacity, torsional capacity has to be controlled for both tensile and compression failure. The torsional capacity in tension ( $T_{Rd,c}$ ) is calculated according to equation 6.26 in EC2.1-1. If  $T_{Rd,c} > T_{Ed}$ , the capacity is sufficient and minimum reinforcement stirrups equal to the minimum shear reinforcement should be included. Because the towers are subject to both shear forces and torsional moments, a combined action is controlled according to equation 6.29. If the result obtained is smaller or equal to 1, the torsional compression capacity is sufficient; if not, the concrete area has to be increased.

Results of the calculations show that  $T_{Rd,c} > T_{Ed}$  for all load combinations. Consequently, minimum reinforcement stirrups need to be included. From the analysis of the shear capacity, the respectable reinforcement area is calculated, and the torsional capacity is therefore sufficient. The reinforcement amount is shown in table 9.6. Moreover, it was found that the combined action of shear forces and torsional moments are sufficient for all load combinations. The result is presented in table 9.7 for LC1 and LC2 and table 9.8 for both the "tensile" and "compressive" column of LC3.

	LC1	LC2		LC1	LC2
Casting stage	$T_{Ed}$ [kNm]	$T_{Ed}$ [kNm]	$T_{Rd,c}$ [kNm]	$\frac{T_{Ed}}{T_{Rd,max}} + \frac{V_{Ed}}{V_{Rd,max}} \leq 1.0$	
45	958	0.325	39 686	0.032	0.025
41	959	0.323	39 704	0.044	0.037
36	967	0.324	40 100	0.060	0.052
31	3 638	0.261	43 185	0.100	0.076
26	3 683	0.263	49 710	0.102	0.081
21	7 201	0.534	60 350	0.126	0.094
16	7 282	0.539	76 178	0.112	0.086
11	7 335	0.543	98 601	0.098	0.077
6	9 748	1.022	129 344	0.096	0.076
1	9 741	1.015	170 555	0.083	0.069

Table 9.7: Torsional capacity LC1 and LC2



	LC3 T	LC3 C		LC3 T	LC3 C
Casting stage	$T_{Ed}$ [kNm]	$T_{Ed}$ [kNm]	$T_{Rd,c}$ [kNm]	$\frac{T_{Ed}}{T_{Rd,max}} + \frac{V_{Ed}}{V_{Rd,max}} \leq 1.0$	
45	5 129	5 147	39 686	0.279	0.279
41	5 106	5 157	39 704	0.396	0.413
36	5 112	5 187	40 100	0.422	0.400
35	5 113	5 208	40 478	0.407	0.370
34	4 534	4 643	40 961	0.359	0.341
31	4 496	4 633	43 185	0.431	0.455
26	4 510	4 662	49 710	0.450	0.418
25	4 517	4 683	51 487	0.441	0.386
24	4 523	4 709	53 412	0.429	0.349
23	4 277	4 430	55 541	0.341	0.350
21	4 260	4 417	60 350	0.364	0.397
16	4 263	4 425	76 178	0.382	0.379
11	4 271	4 461	98 601	0.358	0.302
10	4 272	4 470	103 990	0.353	0.287
9	2 913	3 063	109 789	0.264	0.303
6	2 913	3 065	129 344	0.262	0.287
1	2 913	3 079	170 555	0.256	0.253

Table 9.8: Torsional capacity LC3 "Tensile" and LC3 "Compressive"

## 9.5 Transverse beams

Presented by the results in section 8.3, the transverse beams are imposed by large moments and shear forces throughout the analysis. The forces could be accounted for by adding reinforcement to the beams. Hence, a typical reinforcement design, in addition to size comparisons of the beams, is illustrated by figure 9.15. The concrete design is equal to the transverse beams used for Hardangerbrua. However, the reinforcement specifications are calculated based on the results from the Abaqus analysis.

Alike the towers, the lamellae program calculates the necessary reinforcement needed to obtain sufficient capacity. On the contrary to the heavily compressed tower columns, the axial forces in the beams are substantially smaller. Therefore, prestressed reinforcement is commonly used in the transverse beams to increase the axial force and capacity. Based on this, the transverse beams are only analysed with a combination of ordinary and prestressed reinforcement.

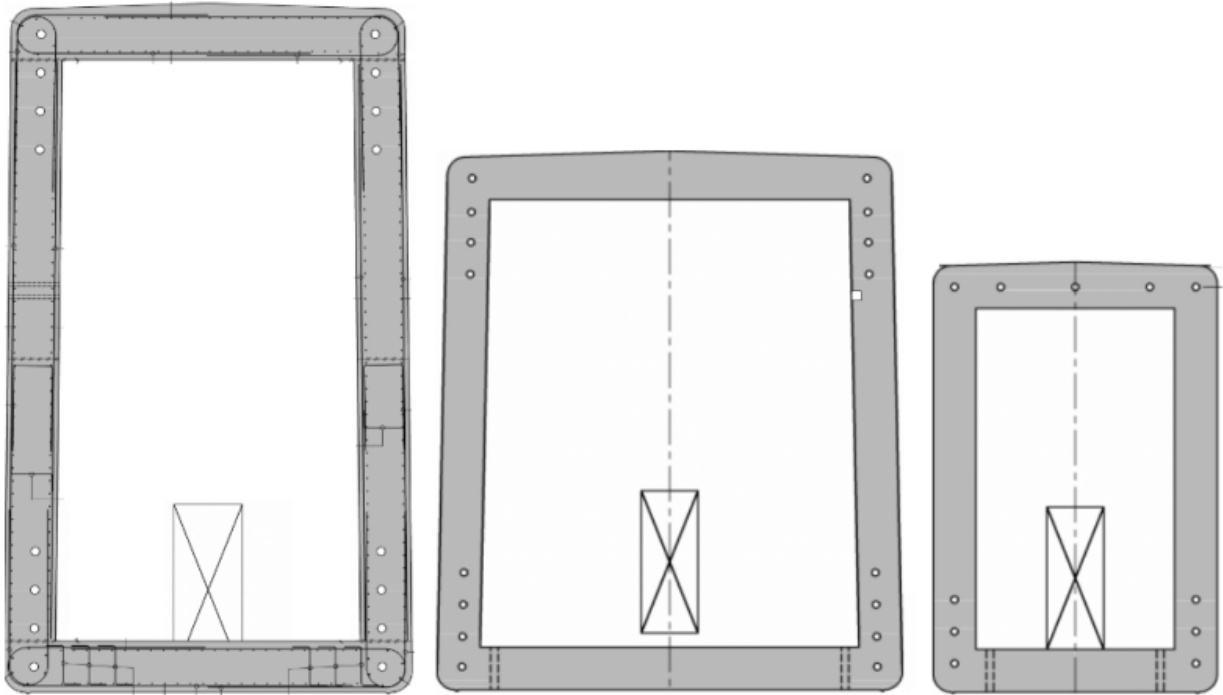


Figure 9.15: Placement of reinforcement and size comparison

In the longitudinal direction, the beams are imposed by bending moments and compressive axial forces. Based on this, the lamellae program could be used to calculate the necessary reinforcement. As previously stated, the axial forces are relatively small compared to the tower columns, making prestressed reinforcement favourable. The tendons are primarily positioned in the web to obtain sufficient anchorage to the towers, illustrated by the white circles in figure 9.15. In regards to bending about the x-axis, the reinforcement listed in table 9.12 provides a utilization ratio between 96% and 100%. However, it is possible to increase the number of bars, the diameter of bars or the dimensions of the beams to reduce the utilization ratio. Henceforth, bending about the z-axis doesn't require any reinforcement other than prestressed reinforcement. However, minimum reinforcement is added in accordance with equation NA.9.1N in EC2.

In regards to shear forces towards the strong axis, stirrups are added to obtain sufficient capacity. In general, the reinforcement requirements are calculated in accordance with section 6.2.2 and 6.2.3 in EC2.1-1. Accordingly, all four beams reach failure based on formula 6.2.a and 6.2.b in EC2.1-1, implying insignificant shear resistance capacity. Hence, the amount of shear reinforcement needs to be calculated. Based on the use of vertical shear reinforcement, the smaller value of equation 6.8 and 6.9 in EC2.1-1 decides the capacity, presented in table 9.9. For all four beams,  $\text{Ø}25$  double-cut stirrups are chosen, and the spacing in between each stirrup along the beam is presented in table 9.12. Individual reinforcement is calculated for all transverse beams. However, because the calculation process of shear reinforcement and torsion is equivalent for all the beams, only calculations covering the bottom transverse beam is presented in appendix G.

Transverse beam	$N_{Ed}$	$V_{Ed}$	$V_{Rd.C}$	$V_{Rd.s}$	$V_{Rd.max}$
Bottom	4.1 MN	50.4 MN	6.83 MN	50.4MN	210 MN
Lower middle	5.8 MN	84.1 MN	6.97 MN	84.1 MN	245 MN
Upper middle	1.8 MN	78.3 MN	7.09 MN	78.3 MN	245 MN
Top	8.9 MN	52.5 MN	5.58 MN	52.5 MN	165 MN

Table 9.9: Shear capacity (z-axis)

Only minimum reinforcement is required based on the shear forces towards the weaker axis of the transverse beams. All four beams have sufficient capacity in accordance with equation 6.2.a, 6.2.b and 6.5 in EC2.1-1. Accordingly, the minimum shear reinforcement is calculated by equation NA.9.5N in EC2.1-1 and presented in table 9.12.

Transverse beam	$N_{Ed}$	$V_{Ed}$	$V_{Rd.c}$	$V_{Rd.max}$
Bottom	1.4 MN	0.57 MN	4.8 MN	68.7 MN
Lower middle	0.74 MN	0.56 MN	3.84. MN	49.3 MN
Upper middle	0.97 MN	0.79 MN	3.9 MN	49.3 MN
Top	0.88 MN	0.80 MN	3.37 MN	42.2 MN

Table 9.10: Shear capacity (x-axis)

Lastly, the transverse beams are controlled for torsion in accordance with section 6.3.2 in EC2.1-1. A minimum longitudinal reinforcement area is calculated by equation 6.28 in EC2.1-1 and compared to the longitudinal reinforcement. Additionally, the beams are controlled for the combination of shear and torsion in accordance with equation 6.29 in EC2.1-1. Both requirements are fulfilled, implying no extra reinforcement needed.

Transverse beam	$T_{Ed}$	$T_{Rd.max}$	$\frac{T_{Ed}}{T_{Rd.max}} + \frac{V_{Ed}}{V_{Rd.max}} \leq 1.0$
Bottom	5.18 MNm	1.18 GNm	0.244
Lower middle	1.14 MNm	958 MNm	0.218
Upper middle	10.8 MNm	960 MNm	0.217
Top	7.7 MNm	544 MNm	0.320

Table 9.11: Torsional capacity

The dimensions and total amount of reinforcement in the transverse beams are summed up in table 9.12. In all cases, extra reinforcement could be added in order to reduce the utilization ratio, without exceeding the cover and distance requirements.

<b>Reinforcement specification for the transverse beams</b>				
Geometry	Bottom	Lower middle	Upper middle	Top
Height [mm]	7500	8600	8600	6000
Lower width [mm]	6567	4789	4789	4000
Upper width [mm]	6250	4600	4600	4000
Thickness [mm]	600	600	600	600
Area [ $m^2$ ]	15.25	14.51	14.51	10.56
Ordinary reinforcement	Bottom	Lower middle	Upper middle	Top
Each flange Ø25	250	230	250	220
Each web Ø20	78	66	66	56
Prestressed reinforcement	Bottom	Lower middle	Upper middle	Top
Number of tendons (each flange/web)	10	10	10	8
Shear reinforcement	Bottom	Lower middle	Upper middle	Top
Flange Ø25 c/c [mm]	110	80	80	90
Web Ø16 c/c [mm]	400	400	400	400

Table 9.12: Reinforcement specification

## 10 Discussion

In view of the approach, analysis and representation of the results, the following section addresses different aspects, choices and findings made throughout the project. Starting by considering the results from section 7.4 and section 9.2 in order to better understand the effects of prestressed reinforcement compared to ordinary reinforcement. Then, illuminating in which situations vertical prestressed reinforcement is favourable and in which situations it's not. Continuously, different sources of errors and their effects on the solution are discussed with the aim of distinguishing the validation of the results. Additionally, different choices made throughout the process are identified, argued and, alternatives debated.

### 10.1 Summary and comparison of the results

Based on the results from the exemplified column in section 7.4 and the bridge towers from section 9.2, the use of prestressed reinforcement has had a varying effect. In some cases, like the comparison in figure 7.33 and the bridge towers during load combination one, prestressing is favourable, improving the capacity substantially. In other cases, like the comparisons made in the M-N diagrams in section 7.4.1 and load combination three, prestressing affect the capacity negatively. For this reason, some key features need to be addressed to understand when and how vertical prestressed reinforcement is advantageous and when it's not.

Chronological starting by discussing the comparison of ordinary and prestressed reinforcement in the M-N diagram. The moment and axial force were calculated for five different strain conditions during the comparison of ordinary and prestressed reinforcement. Accordingly, different results were obtained, mostly unfavourable regarding the prestressing. The result from analysing the first strain condition represents a point in the M-N diagram. The point exemplifies a cross-section in compression with large axial forces and no moments. Compressive failure occurs while the concrete is still uncracked (stage I), illustrated by the vertical gap in figure 7.28. The third strain condition (balance point) describes a situation where the concrete at the upper edge has reached ultimate compressive strain while the reinforcement at the lower edge has reached the yield strain. The compressive force imposed by the prestressing is large compared to the compressive capacity of the cross-section, implying low capacity. Correspondingly, the last strain distributions are also affected by the over-dimensioned prestressed reinforcement. In fact, the compressive force contribution from the prestressing is superior to the compressive contribution of the concrete, causing tensile failure in the cross-section. The various results are highly correlated to the extensive symmetrical prestressed reinforcement compared to the concrete with low compressive strength (C30). By increasing the compressive strength and/or reducing the amount and layout of prestressing, favourable results could be obtained.

In contrast to the M-N diagrams, the comparisons made in the moment-curvature diagrams are more fortunate. First illustrated by the comparison of  $150 \text{ mm}^2$  ordinary and prestressed reinforcement in figure 7.31. In particular, there are two important features illustrated by the figure. Firstly, both reinforcement types cause compressive failure in the concrete after the yielding moment (stage III). Secondly, the moment capacity is increased by using prestressed reinforcement. Hence, the cross-section is responsive to additional compressive forces. By adding more reinforcement, the moment capacity increases, both for the ordinary and prestressed reinforcement. Correspondingly illustrated by the comparison of  $450 \text{ mm}^2$  reinforcement in figure 7.32. In this comparison, the failure of concrete has moved closer to the yielding moment for the prestressed reinforcement (between stage II and III). Additionally, the difference between first-order moment capacity of ordinary and prestressed reinforcement has increased, presented in table 7.4. In the last comparison, the characteristic strength is accounted for, illustrated by figure 7.33. In this example, the first-order moment capacity is larger for the prestressing than for the ordinary reinforcement. Mainly related to the cross-section, which is responsive to compressive forces.

There are four main reasons for the favourable results obtained by the moment-curvature diagrams compared to the results of the M-N diagrams. First, concrete with higher compressive strength is used. During the comparison in M-N diagram, a compressive strength of 30 MPa was used, compared to 45 MPa for the comparison in the moment-curvature diagram. A higher compressive strength is naturally more responsive to higher compressive forces, caused by either axial forces or prestressing. Secondly, the reinforcement amount is smaller than the amount used for the analyses in M-N diagrams, while the cross-section area is kept constant. By decreasing the amount of reinforcement, the compressive forces from the prestressing are also decreased. Thirdly, an external axial force of 450 kN is applied to the column. By implying the external force, the compressive contribution of the prestressing is less dominant, which is favourable for the symmetrically prestressed cross-section. In general, the effect is illustrated by the increased gradient of the lines in figure 7.27, implying increased second-order moments. In comparison, the gradient of the second-order moments for the M-N diagrams is naturally zero. In brief, the first three aspects are aimed towards the combined relation between the compressive strength of the cross-section and the compressive forces imposed by axial forces and prestressing. The increased capacity defines a cross-section responsive to additional compressive forces, fortunate for prestressing. In addition, the negative effect of using symmetrical prestressing is a factor, more thoroughly described in a later paragraph. Fourthly, the moment-curvature diagrams describe the cross-section capacity over multiple strain distributions. In comparison, the M-N diagram only accounts for strain-distributions based on yielding in steel and failure in the concrete. In general, by using moment-curvature diagrams, the optimal bending stiffness could be found, implying full utilisation of the cross-section. An equivalent optimized design is illustrated by the curve representing  $165 \text{ mm}^2$  prestressed reinforcement in figure 7.25.

The characteristic strength of prestressed reinforcement is around three times the capacity of ordinary reinforcement. Based on this, the capacity should increase by the factor of three by replacing ordinary with prestressed reinforcement. However, this is not the case, mainly related to the negative effects of symmetrical prestressed reinforcement. In general, the bending moment creates a strain distribution with tension at one side of the cross-section and compression at the other. Ordinary reinforcement affects the compressive side positively, increasing the capacity for axial forces and moments. However, due to the tension in the prestressed reinforcement on the compressive side, the force vector change direction. For this reason, the axial force and moment capacity is reduced. The effect is illustrated by the decreased moment capacity after yielding for the curve representing prestressing in figure 7.33 and figure 7.28. Accordingly, the negative effect is increased by using a large amount of prestressed reinforcement in relation to the compressive capacity of the cross-section.

In order to optimise the bending stiffness of a structure, the dimensioning moment from Abaqus needs to tangentially overlap the moment capacity curve obtained from the lamellae program. Best illustrated by the solution of  $165 \text{ mm}^2$  prestressed reinforcement in figure 7.25. The bending stiffness depends on the shape of the cross-section, the compressive strength of concrete, the axial force and the reinforcement. By changing one of the factors, better utilisation of the cross-section can be obtained. Optimisation could be favourable regarding material use and force distribution throughout the structure.

The main part of the thesis covers the effect of vertically prestressing the bridge towers. In comparison to the columns previously mentioned, the static system of the bridge is more complex. For this reason, the effect of ordinary and prestressed reinforcement depends on more factors. However, the outcome is comparatively similar. In this case, a concrete with higher compressive strength is used (C90), the cross-section is hollow, and the corresponding forces are greater.

During load combination one, the axial forces are small, but the bending moments are significant, illustrated by figure 8.7. For this reason, a combination of ordinary and prestressed reinforcement in the flange of towers are favourable, illustrated by figure 9.11. By increasing the amount of prestressing, a higher capacity is obtained, indicating that the cross-section is responsive to increased compressive forces. In detail, compressive failure occurs in the concrete equivalent to the yielding of reinforcement. Hence in the transition between stage II and III, indicating a high utilisation of the cross-section area. Accordingly, the first 16 casting stages have an utilisation ratio of 100 %. In regard to the rest of the tower, a minimum bending stiffness is needed due to second-order moments. If the bending stiffness of the upper casting stages is too small, larger second-order moments occur. For this reason, casting stage 17-45 need additional reinforcement, and therefore, can't obtain 100% utilisation with the current tower design. However, changing the shape and wall thickness makes it possible to obtain a higher utilisation ratio throughout the tower. Like the columns from the previous paragraph, the moment capacity is reduced due to the symmetrical reinforcement.

During load combination two the cables and the stiffening girder are attached to the towers. The self-weight of these components are transferred through the main cable to the top of the towers causing an increased axial force as shown in figure 8.4. Accordingly, adding prestressing to the concrete increases the compressive forces, causing compressive failure of the uncracked concrete (stage I). As a result, the capacity is reduced, illustrated by figure 9.12 and comparable to the purple lines in figure 7.25. Consequently, a higher amount of prestressed reinforcement will increase the compressive forces, which initiates failure at a lower moment, causing reduced moment capacity. Even though the capacity is reduced by the use of prestressed reinforcement, the capacity is still sufficient for all cases presented in the figure 9.12. Based on this, the relation between the advantage of prestressing the tower during load combination one and the negative effect of prestressing during load combination two decides if the application of prestressing in the flange is favourable.

The "compressive" column in load combination three is imposed by large compressive axial forces due to the self-weight of the bridge components. Due to the wind forces, extra compressive forces are transferred from the "tensile" column to the "compressive" column through the transverse beams. Based on the extensive axial force, the concrete initiates failure prior to the cracking of concrete (stage I) when prestressed reinforcement is included in the cross-section, presented by figure 9.13. In fact, the compressive capacity of concrete is surpassed for casting stage 21-34 if 50 % of the ordinary reinforcement is replaced with prestressing. On the other hand, some parts of the "tensile" column have favourable effects of prestressing. Due to smaller axial forces, adding prestressing increases the moment capacity in casting stage 1-15. For these casting stages, failure of concrete occurs after the cracking moment (stage II), illustrated by figure 9.14. Notably, if the wind changes direction, the "compressive" and "tensile" columns also change. Therefore, prestressing the web is not favourable for either column.

Another important effect that needs to be addressed is the combined effect of prestressed reinforcement in both the flange and the web. The three load combinations only account for one direction at the time and not the combined use of reinforcement in the flange and web. While ordinary reinforcement on one side has advantageous effects for the other side (based on the placement), the effect of prestressed reinforcement is more complex, highly dependent on the compressive capacity of the cross-section. By prestressing the flange, compressive forces are imposed to the cross-section. These forces need to be accounted for when calculating the web and vice-versa. By prestressing both sides, the cross-section is imposed by the combined compressive forces from the tendons. In brief, prestressing one side affect the bending stiffness and compressive capacity of the other side. Additionally, the effect on the moment capacity depends on the position of the tendons and is optimised by placing the cables at each corner, creating the largest moment arms. Based on this, the application of prestressing must be evaluated for all load combinations with the combined compressive force to conclude the effects. Therefore, by considering the positive effects of load combination one and the negative effects from load combination two and three, prestressing either the flange or web in the tower is not favourable.



In consideration of the environment, the  $CO_2$  emissions from prestressed reinforcement is 50% higher than for ordinary reinforcement. Hence, exchanging half of the ordinary reinforcement with prestressed reinforcement increases the  $CO_2$  emissions for the total design of the structure. By decreasing the prestressed reinforcement area by 50%, the  $CO_2$  emissions are equal to the ordinary reinforced cross-section. As a result, the cross-section using 50% ordinary and 25% prestressed reinforcement should obtain a higher or equal moment capacity in order to be favourable for the environment. For the free-standing towers, the moment capacity increases by the use of prestressing, hence profitable as shown in figure 9.11. However, the case is different for the complete model. The use of prestressed reinforcement decreases the capacity. For consideration of load combination two, the capacity is sufficient but decreased. For load combination three, the "compressive" column shows significantly unfavourable effects while the "tensile" column has some favourable results. The combined effect is negative regarding the  $CO_2$  emissions and the capacity.

Environmentally, customising the towers' shape according to the local geological and geographical conditions could save lots of material. Based on the results from the thesis, it is shown that a material-efficient rectangular cross-section with a ratio of two to one could be used. However, several other factors could also be optimised in order to improve the design environmentally. For instance; the overall shape of the tower, the height of the towers, wall thickness, width between each tower column, in addition to the angle of the towers, the material used and the number and design of the transverse beams. From the environmental perspective, concrete has the highest emissions of the three components, such that it is preferred to increase the amount of reinforcement instead of the concrete.

In summary, for prestressed reinforcement to be favourable in the towers, either the axial force must be decreased, the compressive strength of concrete increased, or the cross-section area enlarged. In addition, if the cross-section is responsive to compressive forces and the wind only blows in one direction, prestressing one side instead of symmetrically is fortunate. Environmentally, increasing the cross-section area is unfortunate due to concrete being the most adverse material regarding the  $CO_2$  emissions. Decreasing the axial force is also challenging when record-breaking bridges are built, pushing the limits beyond earlier designs. Regarding compressive strength, the development of concrete with increased compressive strength and environmental benefits is expected to evolve over the next years. Other, more creative solutions could also be applied. For instance, if the towers are built on a steep site, additional cables could be anchored in the mountainside above the tower to lift the towers upwards. Another solution could be to fill the towers with gasses lighter than air, like helium. A third alternative is to release the tension in the tendons after the main cables are attached. In general, retaining the positive effects of prestressing the free-standing towers without the over-sized compressive forces which occur for the complete bridge. If possible, the ducts could be grouted after releasing the tension, enabling the tendons to function as ordinary reinforcement throughout the lifetime of the bridge.

Furthermore, the use of vertical prestressed reinforcement could be applicable to other structures like tall chimneys or similar free-standing slim columns like highrise buildings or observation towers. Especially relevant in overcrowded cities with high area demands. Additionally, for thin-walled structures where the sufficient amount of ordinary reinforcement is exceeded regarding concrete cover and minimum distance between reinforcement bars, the prestressed reinforcement is beneficial. Henceforth, suppose the bridge is built across a valley, meaning the bottom part of each tower is extended, like the Millau Viaduct. In that case, prestressing could also be used favourably to obtain transverse stability.

## 10.2 Sources of errors

Based on the traffic demands, the stiffening girder used of Hardangerbrua could be applied to the bridge across Halsafjorden. Nevertheless, by increasing the total span from 1310 to 2050 meters and updating the static wind load, the stiffening girder should be customised by performing dynamic analysis. Based on the analysis, the width and weight might increase to obtain the specific dynamic requirements.

For the bridge to reach the desired length of 2050 meters, the scaling theory by Gimsing and Georgakis was used. The theory accounts for several factors, including the dead- and traffic load, to calculate the necessary quantity of the different materials. However, the theory doesn't include wind forces or the compressive strength of concrete. Because both the static wind load as well as the strength class for the concrete is changed, adjustments are made. Correspondingly, the wall thickness is reduced by 25 %, and the shape of the tower columns are changed. Notably, the changes are based on the findings of a prior master thesis [37].

Furthermore, the main cable of the bridge across Halsafjorden is of considerable size. Thus, the second moment of inertia of the cable has to be taken into account. As presented in section 3.3 there are two methods to find the correct value. Either by using 0.1%-1% of the second moment of inertia of an equivalent compact cross-section or analytically, based on formulas from the article "Bending stiffness of parallel wire cables including interfacial slips among wires" [30]. Thus, four different results are obtained. For the methods to be consistent, it would be assumed that the values for the second-order moments of inertia would be of the same magnitude. Instead, the values vary broadly. Even though the moment of inertia doesn't affect the relevant analysis of the towers, it might cause problems during other analysis types, such as dynamic analysis.

Section 1.7.2 ii) in the calculation report for Hardangerbrua [12] states that even though EC1.2 divides the carriageway into three notional lanes, only the number of existing lanes on the bridge could be loaded at the same time, thus two lanes. During the analysis, all three notional lanes are loaded simultaneously such that the total traffic load is increased in contrast to Hardangerbrua. However, this assumption is conservative, and the dimensions of the scaling theory include the traffic load based on three lanes. Therefore, some material could be saved by decreasing the loads.

The wind loads are calculated based on measurements executed by the Norwegian public roads administration. It is found that Halsafjorden is a generally calmer fjord than Hardangerfjorden, hence less wind load is expected to influence the structure. However, the anemometers have only measured the wind speed for 5-6 years, and for this reason, the magnitude of the wind loads could be uncertain.

In order to validate the applied wind forces, historical extreme weather data is found from Meteorologisk Institutt for the provinces of Trøndelag and Møre og Romsdal [42]. The maximal wind speed during the storms, along with the month and year, are plotted in figure 10.1. The wind speed is found by the use of the Beaufort scale from yr.no [43]. Based on this information, the frequency of storms in the area varies between one and five years. Despite this, the last extreme weather in the area was in 2016. Regarding the comparison of the measurements from the anemometers with the maximal wind speed during the historical storms, the result is plotted in the same figure. The light orange dots represent the wind speed along the bridge, while the orange dots represent the wind speed across the bridge. Both of the measurements are found from the Halsaneset anemometer at an altitude of 50.3 m. Even though there were storms in the area in 2015 and 2016, the figure shows that the storms didn't strike the anemometers. In addition, the overall values are found to be significantly lower than the ones obtained in the storms, approximately 10 m/s. Based on this, Halsafjorden might be shielded from the most extreme weather in the area. However, 5-6 years of wind data is unreliable such that more data is needed to determine the dimensioning wind speed correctly. Optimally, it is desirable to use wind data over a 50 year period.

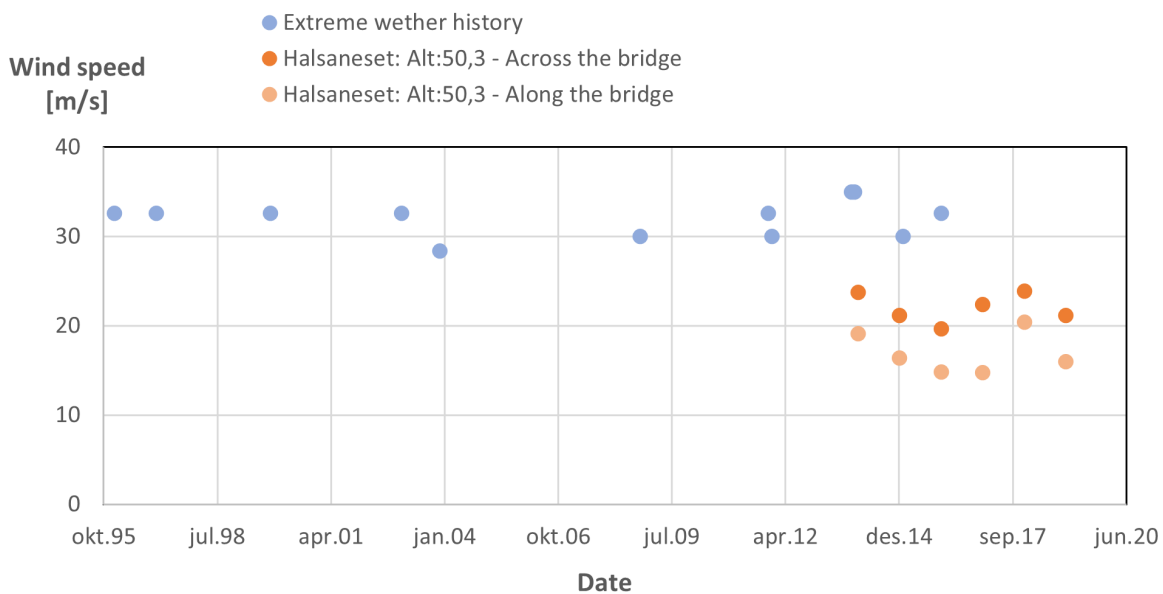


Figure 10.1: Extreme weather over the last years compared to results from the anemometers

During the wind speed calculations, certain assumptions were made to simplify the calculation process. Firstly, the wind in the transverse direction of the bridge could strike either from the sea or from inland. Similarly, for the longitudinal direction, the wind could strike from either Halså or Kanestråum. However, it is chosen to find the maximal annual wind speed, independent of the two directions, only dividing between the transverse and longitudinal direction of the total bridge. In order to validate the results, it is chosen to find the independent wind speed from the sea and inland for the transverse direction. All of the values are applicable for an altitude of 50.3 m and calculated using Gumbel distribution to obtain the wind speed with a return period of 50 years. Hence the result shows that from the sea, the 50-year wind speed is 28.17 m/s, it is 24.54 m/s from the inland, and combining these two directions result in a wind speed of 26.25 m/s. Accordingly, wind in different directions derives different wind speed at the bridge site. The combined value is a mean value of the two directions, and hence, the result is slightly inaccurate, and the directions should be accounted for to obtain the optimal design for the bridge. In addition, the two anemometers, Halsaneset and Aakvik, result in slightly different wind speeds, as previously mentioned. If the two towers were designed differently according to their wind speed, some material could be saved.

Regarding the wind acting on the stiffening girder and the main cable, the force coefficient for the different components has to be determined. In general, simplifications are made such that the same force coefficient used at Hardangerbrua is used on the bridge across Halsåfjorden. The force coefficient of the stiffening girder is determined based on wind tunnel trials, hence customised for the conditions of Hardangerbrua. For this reason, the force coefficient is most likely different for this bridge. In addition, the force coefficient for upstream and downstream wind is different because the stiffening girder is asymmetrical. Conservatively, the highest coefficient is used. In regards to the main cable, an equivalent force coefficient to Hardangerbrua is used. However, the coefficient depends on the cable's diameter such that, in reality, the force coefficient could be slightly different.

As earlier mentioned, the transverse beams used for Halsåfjorden are identical to the ones used for Hardangerbrua. The only difference made is by adding an extra middle beam. However, due to the scaling, the dimensions of the tower columns change, while the transverse beams are kept constant such that issues might occur. Firstly, the transverse beams have a wall thickness of 600 mm, while the wall thickness of the towers is 450 mm. Secondly, the width of the towers is increased, while the transverse beams are kept constant. For this reason, the beams are connected to the towers at the middle of each column, rather than towards the sides in contact with the walls, illustrated by 10.2. Based on this, particularly high local stresses could occur around the transitions, requiring extra attention. Optimally, the transverse beams are scaled equivalently to the towers, such that the transitions are kept. Notably, because the tower is modelled with beam elements connected by nodes, the problem is omitted. However, by scaling the transverse beams, each element provides updated geometrical properties that might change the force distribution throughout the static system.

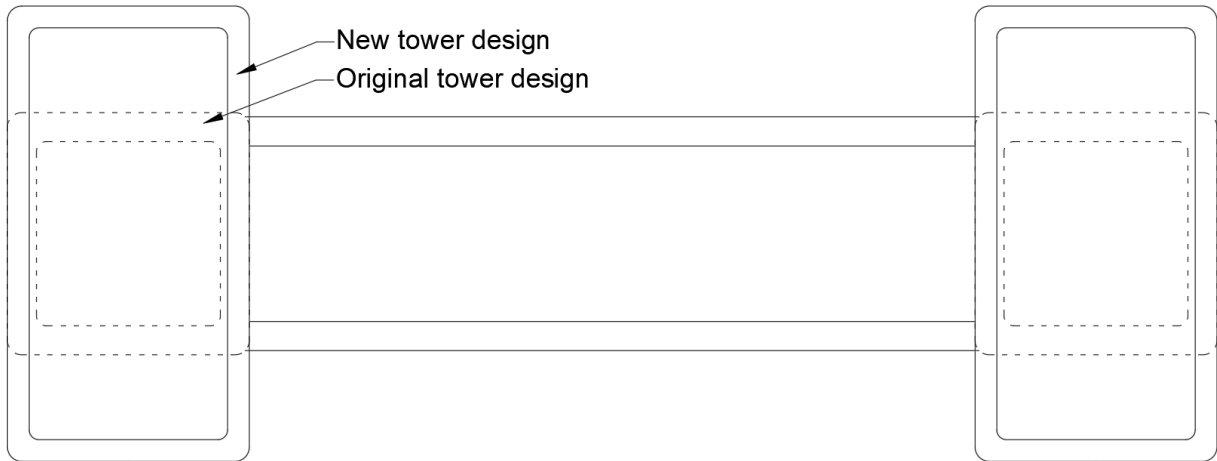


Figure 10.2: Connection between a transverse beam and the columns of the tower

In the global model of the complete bridge, boundary conditions, in addition to a T3D2H element, is used to connect the stiffening girder to the transverse beams. Based on this, only vertical forces are transferred in between the components. In reality, both horizontal and vertical forces are transferred by respectively a horizontal damper and the vertical pendulum bearings. Illustrated by figure 6.12 and 6.13. For this reason, additional shear forces could occur in the transverse beams, which needs to be accounted for during reinforcement design.

During the application of wind forces to the global model, a point load is added at the top of each tower column. The point load summarises all the transverse wind forces affecting the cables, vertical suspenders and stiffening girder during load combination three. In reality, some of the transverse forces are transferred from the stiffening girder to the towers directly. In general, increasing the force distribution at the bottom transverse beam and decreasing the force distribution at the top of the towers.

The analyses of the bridge in Abaqus is verified by a convergence analysis and by checking the global equilibrium. Both highly dependent on the functionality of the software. Although the modelling is performed to recreate reality, the structural system might correspond differently in reality. Therefore, measuring equipment could be used to independently measure the response of similar bridges imposed by different loads. The measured data could be scaled and compared to the corresponding motion from the model to improve the results' validity.

During the tower analyses, every fifth casting stage, in addition to the most critical ones, are analysed and controlled for capacity. Based on this, the total reinforcement specification needs to be calculated conservatively. Implying over-dimensioned reinforcement for the casting stages not prioritised for calculations. By analysing each casting stage, the reinforcement specifications could be customised for each stage. Based on this, material could be saved, and the margin of safety obtained for each casting stage. Furthermore, the torsional capacity of the towers is calculated based on a massive cross-section, while the cross-section used for the towers is hollow. Based on this, the capacity obtained from the calculations are extensive. However, the torsional forces is very small compared to the moments in the other directions, and therefore, the capacity is presumably sufficient based on the determined reinforcement.

## 11 Conclusion

The thesis aimed to investigate how vertical prestressed reinforcement affects the ULS capacity of large suspension bridge towers. Considering the record span crossing Halsafjorden, Hardangerbrua is used as a template, and the dimensions are scaled to fit the increased span of 2050 meters. In addition, the shape of each tower column is changed from quadratic to rectangular, the concrete compressive strength is increased from 45 to 90 MPa, and the wall thickness is decreased by 25%. Initially, the scaled bridge is analysed with ordinary reinforcement to establish a reference solution valid for construction. After that, 50% of the ordinary reinforcement is replaced with prestressed reinforcement, and the effects are evaluated. The analyses are based on three different load combinations, each illustrating critical phases of a suspension bridge life. Due to wind forces, the towers are reinforced symmetrically.

Initially, two models are created for the relevant analyses in Abaqus, one of the free-standing bridge tower and one of the complete bridge. The models are primarily created with the beam elements B31 and B32, in addition to some hybrid and truss elements. Before use, both models were verified by convergence analysis and by obtaining global equilibrium between the external forces and the reaction forces. Based on the results, it can be concluded that the models are functioning as desired and suitable for the relevant analyses.

The analyses in Abaqus takes into account geometrical non-linear effects such as second-order moments and linear material effects. Non-linear material effects such as cracking in concrete and yielding in the reinforcement, is not accounted for by Abaqus. Therefore, an excel program based on the lamellae method is used to calculate the necessary reinforcement to obtain sufficient ULS capacity for the bridge towers. The link between the Abaqus analysis and the excel lamellae program is by moment-curvature diagrams. The program is verified towards example 4.13 in "S.I.Sørensen" [40] and the M-N method for both ordinary and prestressed reinforcement. Based on the results, the excel lamellae program is calculating the correct values.

During load combination one, the towers are free-standing and imposed by self-weight and wind forces along the length of the bridge. By the use of ordinary reinforcement, the first 16 casting stages are utilised 100 %. Regarding the additional casting stages (17-45), additional reinforcement is added to verify the bending stiffness and account for the second-order moment. For this reason, casting stage 17-45 has a smaller utilisation ratio. In regards to shear and torsional capacity, only minimum reinforcement is required. Considering the transverse beams, ordinary and prestressed reinforcement is added in the longitudinal direction of the web to obtain a utilisation ratio of 100%. Only minimum reinforcement is required in regards to the flange, shear and torsional reinforcement for the beam. In all cases, it's possible to add additional reinforcement when considering concrete cover and minimum distance between the reinforcement bars. As a result, the towers could withstand forces imposed by load combination one by the use of ordinary reinforcement.

During load combination two, the complete bridge is imposed by wind forces along the length of the bridge, traffic load along the stiffening girder and self-weight of the following bridge components; towers, main cable, vertical suspenders and stiffening girder. In this case, the reinforcement calculated during load combination one is applied. Casting stage 26 is the highest utilised, with a 49 % utilisation ratio. In addition, the transverse beams have sufficient capacity. Based on this, it can be concluded that the towers could withstand load combination two by use of the same ordinary reinforcement as specified for load combination one.

During load combination three, the complete bridge is imposed by wind forces across the bridge and the self-weight of the same components as load combination two. In this case, the necessary reinforcement for the web is calculated. Based on the results, the highest utilised casting stage is stage number 10, which is utilised 98%. The casting stage is closely related to the joint between the bottom transverse beam and the columns of the tower. Furthermore, the bending stiffness is verified by adding additional reinforcement to casting stage 31-45. In regards to the transverse beams, 100% utilisation ratio is obtained by adding reinforcement to the flange. Moreover, shear- and torsional reinforcement is added to the web of the columns and to the flange of the transverse beams. In addition, minimum reinforcement is applied to the other components. Like load combination one, additional reinforcement could be added in all cases. Hence, it can be concluded that the towers could withstand load combination three by the use of ordinary reinforcement.

In order to evaluate the effect of vertical prestressing the towers subjected to load combination one, 50% of the ordinary reinforcement is replaced by prestressed reinforcement. The longitudinal reinforcement in the flange is replaced while the reinforcement in the web is disregarded. The amount is based on the necessary ordinary reinforcement referred to in the previous paragraphs. First, the ordinary reinforcement is replaced by the equivalent prestressed reinforcement area (50%) and then by half of the equivalent reinforcement area (25%). Based on the results, it can be concluded that prestressing increases the moment capacity. The capacity increases from the analysis of 25% prestressing and then additionally for 50% prestressing. Based on this, adding more prestressing increases the capacity further. Mainly because the cross-section is responsive to additional compressive forces. However, it can also be concluded that symmetrical reinforcement reduces the moment capacity.

The same procedure is conducted to investigate the effect of prestressing for load combination two. Based on the results, it can be concluded that the use of prestressed reinforcement decreases the moment capacity during load combination two. The more prestressed reinforcement, the lower the moment capacity. mainly because too large compressive forces impose the cross-section.



Equivalent to load combination one and two, 50% of the ordinary reinforcement is replaced by prestressed reinforcement. In this case, the longitudinal reinforcement in the web is replaced, and the reinforcement in the flange is negligible. Based on the results, it can be concluded that prestressing decreases the moment capacity during load combination three. The capacity decreases by adding additional prestressing. In fact, when 50% prestressed reinforcement is used, the compressive capacity of concrete is totally exceeded, indicating zero capacity for casting stage 21 to 34. For this reason, it's possible to conclude that adding more prestressing is unfavourable in regards to the moment capacity. Mainly because the cross-section is imposed to extensive compressive forces.

In summary, by evaluating the effect of prestressed reinforcement obtained by the three load combinations, vertically prestressing the towers is not recommended. However, it could be favourable in the towers if either the axial force is decreased, the compressive strength of concrete increased, the cross-section area enlarged. Another alternative is to release the tension in the tendons after the main cables are attached. In general, retaining the positive effects of prestressing the free-standing towers without the oversized compressive forces which occur for the complete bridge.

The use of vertical prestressed reinforcement could be applicable to other structures like tall chimneys or similar free-standing slim columns like highrise buildings or observation towers. This is especially relevant in overcrowded cities with high area demands. Additionally, for thin-walled structures where the space for a sufficient amount of reinforcement is exceeded regarding concrete cover and minimum distance between reinforcement bars, the prestressed reinforcement is beneficial.

## 12 Future work

Before the commencement of this master thesis, there were multiple suggestions for a problem formulation. Inspired by a previous master thesis [37], it was chosen to investigate whether prestressed reinforcement along the height of the towers is favourable for a suspension bridge with a span of 2050 m. The bridge is based on the design and calculations of Hardangerbrua with an increased span, height and strength class for the concrete. However, throughout the project, new problems are discovered and combined with earlier aspects, several problems are relevant to investigate in the future. The problems and aspects will be presented in this section.

The bridge towers of Hardangerbrua are almost squared, with three transverse beams and concrete with a compressive strength of 45 MPa. During the project, some changes were implemented to optimise the cross-section. Namely, increasing the compressive strength to 90 MPa, decreasing the wall thickness by 25%, changing the shape to rectangular and adding an extra transverse beam. However, regarding the bridge towers, there are numerous factors which needs further optimisation:

- The shape of the tower columns; squared, rectangle or something in between
- The inclined angle of the towers, narrowing the structure towards the height
- The distance between each tower column
- The wall thickness of the cross-section
- The bending stiffness of each casting stage such that the utilisation ratio is 100% for all casting stages
- The shape of the whole tower, for example, an A-shape or one circular column
- The number of transverse beams
- The relation between the stiffness of the towers and the transverse beams
- Horizontal versus diagonal transverse beams

Based on the analysis of the bridge towers with prestressed reinforcement, it's generally concluded that prestressing is favourable during construction, but not for the complete bridge due to extensive compressive forces imposed by the self-weight of the bridge components. However, modifications could be applied to increase the capacity. For prestressed reinforcement to be favourable in the towers, either the axial force must be decreased, the compressive strength of concrete increased, or the cross-section area enlarged. The modifications could be implemented by the following adjustments:

- The compressive strength of the concrete could be improved. NTNU is in the process of developing an environmental C100 concrete. For the future master thesis's it would be relevant to investigate whether this concrete could be favourable regarding the use of prestressed reinforcement.
- The cross-section could be increased or the shape changed. By increasing the moment of inertia of the critical sections, the capacity could be increasing without increasing the amount of concrete.
- Another solution could be to release the tension in the tendons after the main cable is attached, providing sufficient stability when free-standing and the negative effects on the complete bridge is removed. Fill the towers with light gasses, such as helium. Lift the towers towards the above laying mountainside (not possible at Halsafjorden).

In regards to the prestressed reinforcement, further examination could be conducted. Based on all the factors affecting the implementation of prestressing, a guide towards favourable and unfavourable use could be worked out, mapping how the different factors affect the capacity. Relevant factors to investigate further is:

- Effect of axial force
- Effect of cross-section area and bending stiffness
- Effect of concrete compressive strength
- Effect of ordinary reinforcement
- Effect of prestressed reinforcement
- Effect of motion of inertia of the cross-section
- Effect of combined use of ordinary and prestressed reinforcement
- Effect of combined prestressing the flange and web

Regarding the global static system, the solution for a suspension bridge across Halsafjorden is similar to Hardangerbrua. Even though this design was the best solution for Hardangerbrua, small changes in the design could be optimal for the bridge across Halsafjorden:

- The height of the towers
- The stiffness of the main cables
- The numbers of vertical suspenders
- The relationship between the height of the tower and the sag of the main cable
- The towers in a dynamic analysis
- The stiffening girder in a dynamic analysis

In addition to scaling theories, the book by Gimsing and Georgakis also provides theories regarding the optimisation of bridge parameters. For instance section 3.2.6 is relevant for the optimal tower height [24].

Simplifications are made in the thesis such that only the most dominating external forces are included. Hence, the self-weight as well as static wind- and traffic load. Additionally, short- and long-time losses affecting the tension of the tendons are taken into account. Other variable loads that could be included are:

- Thermal and seismic loads
- Accidental impacts
- Shrinkage, creep and relaxation in concrete
- Dynamic wind loads

Henceforth, the static wind load is considered in the thesis. However, a dynamic analysis is relevant for the towers and the other bridge components. Additionally, the anemometers continuously measure the wind data for the relevant bridge site, improving the database for future analysis.

As for the total analysis of the structure, the ultimate limit state is considered. However, it would be relevant to investigate smaller parts of the bridge for the serviceability limit state. This limit state is considering the comfort for the people, the functioning of the structure and the appearance after construction. By including some of the loads mentioned in the previous paragraph, other load combinations and local analysis could be relevant:

- Transverse wind at the free-standing towers; This could potentially lead to large transverse shear forces and moments in the towers columns and transverse beams
- Diagonally winds at the free-standing towers; This could produce large torsional forces.
- Local analysis of the joints between the transverse beams and the columns of the tower.
- Local analysis of the saddle connection joint
- Local analysis of the joint between the stiffening girder and the transverse beam
- Local analysis of the joint between the tower foundation

Finally, The Norwegian public roads administration has proposed four different solutions for the crossing of Halsafjorden [2]. As previously stated, a suspension bridge in one span is investigated. However, the other three solutions could be convenient for a master thesis:

- Suspension bridge in one span with a tower at Aakvikgrunnen,
- Suspension bridge in two spans supported on a tension leg platform
- Pontoon/floating bridge

## References

- [1] Vegvesen S. Ferjefri E39 [Internet]. Norway: Statens Vegvesen;. [Accessed: February 2021]. Available from: <https://www.vegvesen.no/vegprosjekter/ferjefriE39>.
- [2] Vegvesen S. Ett skritt nærmere valg av brukonsept for Halsafjorden og Sulafjorden [Internet]. Norway: Statens Vegvesen; 17.12.2020. [Accessed: 14.05. 2021]. Available from: <https://www.vegvesen.no/Europaveg/e39halsafjorden/nyhetsarkiv/ett-skritt-naermere-valg-av-brukonsept-for-halsafjorden-og-sulafjorden>.
- [3] Vegvesen S. Rv. 13 Hardangerbrua [Internet]. Norway: vegvesen.no;. [Accessed: 14.05. 2021]. Available from: <https://www.vegvesen.no/vegprosjekter/Hardangerbrua>.
- [4] Askeland T. Halsafjordkonferansen. Norway: Statens Vegvesen; 23. september 2020. [Accessed: February 2021]. Available from: <http://www.halsafjordsambandet.no/assets/Halsafjordkonferansen2020/Ferjefri-E39-prosjektet-Oversikt-ved-Tore-Askeland-Statens-vegvesen-Utbygging.pdf>.
- [5] Technology RT. World's longest suspension bridges [Internet]. Road Traffic Technology; 20.11.2020. [Accessed: February 2021]. Available from: <https://www.roadtraffic-technology.com/features/worlds-longest-suspension-bridges/>.
- [6] Kartverket. Norgeskart [Internet]. Norway: Kartverket; 2021. [Accessed: 12.02. 2021]. Available from: <https://www.norgeskart.no/#!?project=norgeskart&layers=1002&zoom=3&lat=7197864.00&lon=396722.00>.
- [7] no B. Broer i Norge [Internet]. Broer.no; 2021. [Accessed: February 2021]. Available from: <http://broer.no/liste/norge/lengde>.
- [8] Lin W, Yoda T. Bridge engineering: classifications, design loading, and analysis methods. 1. edition. Butterworth-Heinemann; 2017.
- [9] Eltvik L. Hengebruer. Norway: Aas-Jakobsen AS;. 22.
- [10] Seehusen J. Hardangerbrua blir første norske bru med støtdemper. Teknisk ukeblad bygg; 23.11.2012. [Accessed: February 2021]. Available from: <https://www.tu.no/artikler/hardangerbrua-blir-forste-norske-bru-med-stotdemper/236145>.
- [11] J Z. Spennarmering av oljeplattformer. Strandvegen 4, Stjørdal Norge: Equinor ASA; 2021. [Accessed: June 2021]. Available from: [www.equinor.com](http://www.equinor.com).
- [12] Vegvesen S. 12-2950 Hardangerbrua - beregninger, Kapittel 1: Grunnlag. Norway: Statens Vegvesen; 2008. Revisjon 5.
- [13] Vegvesen S. 12-2950 Hardangerbrua - Arbeidstegninger. Norway; 2007-2009.
- [14] Eurokoder [Internet];. [Accessed 17.02.2021]. Available from: <https://www.standard.no/fagomrader/bygg-anlegg-og-eiendom/eurokoder1/>.

- [15] Norge S. NS-EN 1990:2002+A1:2005+NA:2016, Eurocode: Basis of structural design, Norwegian Standard. Brussels: Standard Norge; 2002. [Accessed: February 2021].
- [16] Norge S. NS-EN 1991-1-1:2002+NA:2019, Eurocode 1: Actions on structures - Part 1-1: General actions - Densities, self-weight, imposed loads for building, Norwegian Standard. Brussels; 2002. [Accessed: February 2021]. Available from: <https://standard.no/>.
- [17] Norge S. NS-EN 1991-1-4:2005+NA:2009 Eurocode 1: Actions on structures - Part 1-4: General actions - Wind actions, Norwegian Standard. Brussels: Standard Norge; 2005. [Accessed: March 2021]. Available from: <https://standard.no/>.
- [18] Norge S. NS-EN 1991-2:2003+NA:2010, Eurocode1: Actions on structures - Part 2 - Traffic loads on bridges. Brussels; 2003. [Accessed: February 2021]. Available from: <https://standard.no/>.
- [19] NS-EN 1992-1-1:2004+A1:2014+NA:2018, Eurocode 2: Design of concrete structures - Part 1-1: General rules and rules for buildings, Norwegian Standard. Brussels: Standard Norge; 2004. [Accessed: February 2021]. Available from: <https://standard.no/>.
- [20] Vegdirektoratet. Håndbok N400 - Bruprosjektering. Norway: Statens Vegvesen; 2015. [Accessed: February 2021]. Available from: <https://www.vegvesen.no/fag/publikasjoner/handboker/om-handbokene/vegnormalene/n400>.
- [21] Johansen H. Beregningsveileder for etteroppspente betongbruer. Norway: Vegdirektoratet; 2017. [Accessed: February 2021]. Available from: <https://www.vegvesen.no/fag/publikasjoner/publikasjoner/statens+vegvesens+rappporter>.
- [22] Kanstad T, Døssland AL, et al. Publikasjon nr. 38, Fiberarmert betong i bærende konstruksjoner. Norway: Norsk Betongforening; Mars 2020. Available from: <https://betong.net/wp-content/uploads/NB-Publikasjon-nr.-6.pdf>.
- [23] NS 3576-3:2012, Ameringsstål - Mål og egenskaper - Del 3: Kamstål B500NC. Standard Norge; februar 2012. [Accessed: May 2021]. Available from: <https://standard.no/>.
- [24] Gimsing NJ, Georgakis CT. Cable supported bridges. 3. edition. John Wiley & Sons, Ltd.; 2012.
- [25] Zhang Y, Wang J, Ye G, Xu R. Bending stiffness of parallel wire cables including interfacial slips among wires. *Journal of Structural Engineering*. 2018;144(10):04018164.
- [26] Chen Z, Yu Y, Wang X, Wu X, Liu H. Experimental research on bending performance of structural cable. *Construction and Building Materials*. 2015;96:279–288.
- [27] Petersen . Modelling and dynamic analysis of long span suspension bridges. Norway: NTNU - Department of structural engineering; Fall 2020.
- [28] Samferdselsdepartementet. Forskrift for trafikklast på bruer, ferjekaier og andre bærende konstruksjoner i det offentlige vegnettet (forskrift for bruer m.m). Norway: Samferdselsdepartementet; 17.11.2017. [Accessed: Februar 2021]. Available from: <https://lovdata.no/>.

- [29] Vegvesen S. Maalinger [Internet]. Norway: Statens Vegvesen;. [Accessed 10.03.2021]. Available from: <https://www.vegvesen.no/Europaveg/e39halsafjorden/malinger>.
- [30] Hong H, Li S, Mara T. Performance of the generalized least-squares method for the Gumbel distribution and its application to annual maximum wind speeds. *Journal of Wind Engineering and Industrial Aerodynamics*. 2013;119:121–132.
- [31] Simiu E, Yeo D. *Wind Effects on Structures: Modern Structural Design for Wind*, 4th edition. Wiley Blackwell; 16.01.2019.
- [32] T R. Hardanger Bridge. flickr; Roth T.; April 2011. [Accessed: May 2021]. Available from: <https://www.flickr.com/photos/phantomfies/5725775840/in/photostream/>.
- [33] Abaqus S. Abaqus/CAE. Dassault Systems;. [Accessed: January 2021]. Available from: <https://www.3ds.com/products-services/simulia/products/abaqus/abaquscae/>.
- [34] Abaqus S. Abaqus Analysis User's Guide. Simulia Abaqus 6.14;. [Accessed: February 2021]. Available from: <http://130.149.89.49:2080/v6.14/books/usb/default.htm>.
- [35] Myhre M. Hardangerbrua. Vestfjordgaten 4, 1338 Sandvika: Norconsult; februar 2012. [Accessed: June 2021]. Available from: <https://www.norconsult.no/prosjekter/hardangerbrua/>.
- [36] Vegvesen S. Teknisk brosjyre. Norway: vegvesen.no; 16.05.217. [Accessed: March 2021]. Available from: [https://www.vegvesen.no/\\_attachment/113344/binary/206607?fast\\_title=Teknisk+brosjyre+Hardagerbrua%2C+bokm%C3%A51+%28pdf%29](https://www.vegvesen.no/_attachment/113344/binary/206607?fast_title=Teknisk+brosjyre+Hardagerbrua%2C+bokm%C3%A51+%28pdf%29).
- [37] Petter KS, Mats SS. Styrkebergening av brutårn: Løsning for rekordlang hengebru tilknyttet "Ferjebri E39". Trondheim: Norges teknisk-naturvitenskaplige universitet; 2020.
- [38] Reference MOV. Using the Solver VBA Functions. Microsoft; 2017. [Accessed: January 2021]. Available from: <https://docs.microsoft.com/en-us/office/vba/excel/concepts/functions/using-the-solver-vba-functions>.
- [39] Support M. Using the Solver VBA Functions. Microsoft; 2017. [Accessed: January 2021].
- [40] Sørensen SI. *Betongkonstruksjoner, beregning og dimensjonering etter Eurocode 2*, 2. utgave. Fagbokforlaget; 2013.
- [41] for konstruksjonsteknikk NI. *Stålkonstruksjoner - Profiler og formler*, 3. edition. Tapir akademisk forlag; 2003.
- [42] intitutt M. Norske ekstremvær får navn [Internet]. Norway: Meteorologisk intritutt; 31.06.2018, updated: 03.02.2021. [Accessed: 01.06.2021]. Available from: <https://www.met.no/vaer-og-klima/ekstremvaervarsler-og-andre-farevarsler/hva-er-et-ekstremvaervarsel/norske-ekstremvaer-far-navn>.
- [43] <https://www.yr.no/nb>. Vindpiler og Beaufortskalaen [Internet]. Norway: <https://www.yr.no/nb>; [Accessed: 01.06.2021]. Available from: <https://hjelp.yr.no/hc/no/articles/360002022134-Vindpiler-og-Beaufortskalaen>.

## A Calculations regarding scaling theory by Gimsing and Georgakis

### General parametres:

$$l_{m1310} := 1310 \text{ m}$$

$$l_{a1310} := 213.2 \text{ m}$$

$$k_{m1310} := 121 \text{ m}$$

$$h_{pl1310} := 180.5 \text{ m}$$

$$j_{m1310} := 2.05 \text{ m}$$

$$n_{1310} := 65$$

$$L_{smit1310} := 47 \text{ m}$$

$$A_{vs1310} := \pi \cdot (35 \text{ mm})^2 = 3848.5 \text{ mm}^2$$

$$A_{1310} := \pi \cdot (300 \text{ mm})^2 = 282743.3 \text{ mm}^2$$

$$\gamma_{cb} := 78.5 \frac{\text{kN}}{\text{m}^3}$$

$$f_{cbd} := 1570 \text{ MPa}$$

$$g_m := 8825 \cdot \frac{\text{kg}}{\text{m}} \cdot 9.81 \cdot \frac{\text{m}}{\text{s}^2} = 86.6 \frac{\text{kN}}{\text{m}}$$

$$p_m := 30.5 \frac{\text{kN}}{\text{m}}$$

$$k_a := 0$$

$$b_a := 0$$

$$\gamma_{pl} := 25 \frac{\text{kN}}{\text{m}^3}$$

$$f_{pld} := 0.85 \cdot 45 \frac{\text{MPa}}{1.5} \cdot 0.8 = 20.4 \text{ MPa}$$

$$l_{m2050} := 2050 \text{ m}$$

$$l_{a2050} := \frac{l_{m2050}}{l_{m1310}} \cdot l_{a1310} = 333.6 \text{ m}$$

$$k_{m2050} := \frac{l_{m2050}}{l_{m1310}} \cdot k_{m1310} = 189.4 \text{ m}$$

$$h_{pl2050} := k_{m2050} + 50 \text{ m} = 239.4 \text{ m}$$

$$j_{m2050} := \frac{l_{m2050}}{l_{m1310}} \cdot j_{m1310} = 3.2 \text{ m}$$

$$n_{2050} := 81 \text{ Amount vertical suspenders}$$

$$L_{smit2050} := 67.7 \text{ m Average length of vertical suspenders}$$

Area of original vertical suspenders

Area of original main cable

Density steel

Characteristic yield strength of cables,  $f_{yk}$

Dead weight - stiffening girder

Traffic load

Only different from 0 if there is sag in the side spans.

Density of material used in the pylons (Concrete)



## Scaling of the vertical suspenders:

$$Q_{hm1310} := \frac{\gamma_{cb}}{f_{cbd}} (g_m + p_m) \cdot \left( j_{m1310} + \frac{k_{m1310}}{3} \right) \cdot l_{m1310} = 325 \text{ kN}$$

$$Q_{hm2050} := \frac{\gamma_{cb}}{f_{cbd}} (g_m + p_m) \cdot \left( j_{m2050} + \frac{k_{m2050}}{3} \right) \cdot l_{m2050} = 795.9 \text{ kN}$$

$$f_{VS} := \frac{Q_{hm2050}}{Q_{hm1310}} = 2.4$$

$$f_{areaVS} := \frac{f_{VS} \cdot n_{1310} \cdot L_{snitt1310}}{n_{2050} \cdot L_{snitt2050}} = 1.4$$

Scaling factor, taking the amount and length of cables into account

$$A_{vs2050} := f_{areaVS} \cdot A_{vs1310} = 0.00525 \text{ m}^2$$

$$d_{vs2050} := 2 \cdot \sqrt{\frac{A_{vs2050}}{\pi}} = 81.8 \text{ mm}$$

New diameter of vertical suspenders

## Scaling of the main cable:

$$Q_{cm1310} := \frac{\gamma_{cb}}{f_{cbd}} (g_m + p_m) \cdot l_{m1310}^2 \cdot \frac{\sqrt{1 + 16 \left( \frac{k_{m1310}}{l_{m1310}} \right)^2}}{8 \cdot \frac{k_{m1310}}{l_{m1310}} - \frac{\gamma_{cb}}{f_{cbd}} \cdot l_{m1310} \cdot \sqrt{1 + 16 \left( \frac{k_{m1310}}{l_{m1310}} \right)^2}} \cdot \left( 1 + \frac{8}{3} \cdot \left( \frac{k_{m1310}}{l_{m1310}} \right)^2 \right) = 16369.4 \text{ kN}$$

$$Q_{cm2050} := \frac{\gamma_{cb}}{f_{cbd}} (g_m + p_m) \cdot l_{m2050}^2 \cdot \frac{\sqrt{1 + 16 \left( \frac{k_{m2050}}{l_{m2050}} \right)^2}}{8 \cdot \frac{k_{m2050}}{l_{m2050}} - \frac{\gamma_{cb}}{f_{cbd}} \cdot l_{m2050} \cdot \sqrt{1 + 16 \left( \frac{k_{m2050}}{l_{m2050}} \right)^2}} \cdot \left( 1 + \frac{8}{3} \cdot \left( \frac{k_{m2050}}{l_{m2050}} \right)^2 \right) = 42597.6 \text{ kN}$$

$$f_{cable} := \frac{\frac{Q_{cm2050}}{l_{m2050}}}{\frac{Q_{cm1310}}{l_{m1310}}} = 1.66$$

$$A_{2050} := A_{1310} \cdot f_{cable} = 0.4702 \text{ m}^2$$

$$d_{2050} := 2 \cdot \sqrt{\frac{A_{2050}}{\pi}} = 773.7 \text{ mm}$$

New main cable diameter

### Scaling of the towers:

$$Q_{pl1310} := \frac{(g_m + p_m) \cdot l_{m1310} + Q_{cm1310}}{8} \cdot \left( \frac{l_{m1310}}{l_{a1310}} + 4 \right) \left( \exp \left( \frac{\gamma_{pl}}{f_{pld}} \cdot h_{pl1310} \right) - 1 \right) = 53286.4 \text{ kN}$$

$$Q_{pl2050} := \frac{(g_m + p_m) \cdot l_{m2050} + Q_{cm2050}}{8} \cdot \left( \frac{l_{m2050}}{l_{a2050}} + 4 \right) \left( \exp \left( \frac{\gamma_{pl}}{f_{pld}} \cdot h_{pl2050} \right) - 1 \right) = 122152.7 \text{ kN}$$

$$f_A := \frac{\frac{Q_{pl2050}}{h_{pl2050}}}{\frac{Q_{pl1310}}{h_{pl1310}}} = 1.73 \quad \text{Scaling factor for area}$$

Casting stage	Hardangerbrua C45, t=600 mm		Halsafjorden C45, t=600mm		Halsafjorden C90, t=450mm	
	W [m]	L [m]	W [m]	L [m]	W [m]	L [m]
1	7051	8661	11.805	14.501	7.250	14.501
2	6939	8441	11.609	14.122	7.061	14.122
3	6830	8228	11.419	13.756	6.878	13.756
4	6723	8020	11.231	13.398	6.699	13.398
5	6618	7818	11.048	13.051	6.525	13.051
6	6517	7623	10.871	12.716	6.358	12.716
7	6417	7433	10.696	12.389	6.194	12.389
8	6321	7249	10.527	12.073	6.036	12.073
9	6266	7071	10.429	11.768	5.884	11.768
10	6134	6899	10.200	11.472	5.736	11.472
11	6045	6734	10.043	11.188	5.594	11.188
12	5958	6574	9.891	10.913	5.457	10.913
13	5874	6420	9.743	10.649	5.325	10.649
14	5792	6271	9.600	10.393	5.197	10.393
15	5713	6129	9.461	10.150	5.075	10.150
16	5636	5993	9.326	9.916	4.958	9.916
17	5562	5863	9.196	9.693	4.847	9.693
18	5490	5738	9.069	9.479	4.740	9.479
19	5421	5620	8.948	9.277	4.638	9.277
20	5355	5508	8.832	9.085	4.542	9.085
21	5290	5401	8.718	8.901	4.451	8.901
22	5229	5301	8.611	8.730	4.365	8.730
23	5170	5206	8.508	8.567	4.283	8.567
24	5113	5117	8.408	8.414	4.207	8.414
25	5059	5035	8.313	8.274	4.137	8.274
26	5007	4958	8.222	8.141	4.071	8.141
27	4958	4887	8.136	8.020	4.010	8.020
28	4911	4822	8.054	7.908	3.954	7.908
29	4867	4763	7.977	7.807	3.903	7.807
30	4826	4710	7.906	7.716	3.858	7.716
31	4786	4663	7.836	7.635	3.817	7.635
32	4750	4622	7.774	7.564	3.782	7.564
33	4716	4587	7.715	7.504	3.752	7.504
34	4684	4558	7.659	7.453	3.727	7.453
35	4655	4535	7.609	7.413	3.707	7.413
36	4628	4517	7.563	7.382	3.691	7.382
37	4604	4506	7.522	7.362	3.681	7.362
38	4583	4501	7.487	7.353	3.676	7.353
39	4564	4500	7.455	7.350	3.675	7.350
40	4547	4500	7.426	7.349	3.675	7.349
41	4533	4500	7.402	7.349	3.674	7.349
42	4521	4500	7.382	7.348	3.674	7.348
43	4512	4500	7.367	7.348	3.674	7.348
44	4506	4500	7.357	7.347	3.674	7.347
45	4502	4500	7.350	7.347	3.674	7.347

Halsafjorden C90				Thickness [m]: 0.450		
Casting stage	W [m]	L [m]	Area [m <sup>2</sup> ]	I <sub>y</sub> [m <sup>4</sup> ]	I <sub>x</sub> [m <sup>4</sup> ]	J [m <sup>4</sup> ]
1	7.250	14.501	18.766	510.853	170.306	394.065
2	7.061	14.122	18.255	470.455	156.631	362.513
3	6.878	13.756	17.760	433.435	144.111	333.620
4	6.699	13.398	17.277	399.218	132.550	306.932
5	6.525	13.051	16.808	367.764	121.932	282.418
6	6.358	12.716	16.356	339.020	112.240	260.033
7	6.194	12.389	15.915	312.496	103.304	239.392
8	6.036	12.073	15.488	288.174	95.120	220.480
9	5.884	11.768	15.077	265.979	87.659	203.236
10	5.736	11.472	14.677	245.466	80.770	187.311
11	5.594	11.188	14.294	226.895	74.541	172.907
12	5.457	10.913	13.923	209.809	68.816	159.665
13	5.325	10.649	13.566	194.199	63.592	147.578
14	5.197	10.393	13.221	179.856	58.797	136.482
15	5.075	10.150	12.892	166.864	54.459	126.440
16	4.958	9.916	12.577	155.023	50.510	117.297
17	4.847	9.693	12.276	144.245	46.920	108.981
18	4.740	9.479	11.987	134.365	43.633	101.365
19	4.638	9.277	11.714	125.464	40.675	94.511
20	4.542	9.085	11.454	117.390	37.994	88.298
21	4.451	8.901	11.207	110.006	35.546	82.622
22	4.365	8.730	10.975	103.393	33.356	77.543
23	4.283	8.567	10.755	97.361	31.361	72.915
24	4.207	8.414	10.549	91.927	29.565	68.748
25	4.137	8.274	10.359	87.102	27.972	65.052
26	4.071	8.141	10.181	82.727	26.529	61.704
27	4.010	8.020	10.017	78.825	25.244	58.719
28	3.954	7.908	9.866	75.359	24.103	56.071
29	3.903	7.807	9.729	72.302	23.098	53.736
30	3.858	7.716	9.606	69.626	22.219	51.694
31	3.817	7.635	9.497	67.304	21.456	49.923
32	3.782	7.564	9.401	65.320	20.805	48.410
33	3.752	7.504	9.320	63.654	20.259	47.141
34	3.727	7.453	9.252	62.290	19.812	46.102
35	3.707	7.413	9.198	61.217	19.461	45.286
36	3.691	7.382	9.155	60.382	19.187	44.649
37	3.681	7.362	9.129	59.865	19.018	44.256
38	3.676	7.353	9.116	59.619	18.937	44.069
39	3.675	7.350	9.113	59.551	18.915	44.017
40	3.675	7.349	9.112	59.530	18.908	44.001
41	3.674	7.349	9.111	59.512	18.902	43.988
42	3.674	7.348	9.110	59.497	18.897	43.976
43	3.674	7.348	9.109	59.485	18.894	43.967
44	3.674	7.347	9.109	59.478	18.891	43.962
45	3.674	7.347	9.109	59.473	18.890	43.958

Transverse beams					Wall thickness [m]: 0.600		
	Upper width [m]	Bottom width [m]	Height [m]	Area [m <sup>2</sup> ]	I <sub>x</sub> [m <sup>4</sup> ]	I <sub>z</sub> [m <sup>4</sup> ]	J [m <sup>4</sup> ]
Bottom	6.250	6.567	7.500	15.250	116.756	90.344	207.099
Lower middle	4.600	4.789	8.600	14.513	130.821	47.841	178.662
Upper middle	4.600	4.789	8.600	14.513	130.821	47.841	178.662
Top	4.000	4.000	6.000	10.560	46.195	23.219	69.414

## B Second moment of inertia of the main cables

07.06.21 13:14 C:\Users\Kristine\...\Cablestiffness.m 1 of 2

```

clear all
d_strand = 5.3; %[mm]
H_tot = 773; %[mm]
n_layers = 155;
h_layer = H_tot/n_layers;
n_slip = (n_layers-1)/2;
E = 200000; %[MPa]
sigma = 652; %[MPa]
L = 2095913; %[mm]
j = 1;
for i = 69:146
    n_cables(j) = i;
    A_layer(j) = pi * ((d_strand/2)^2)*n_cables(j);
    b_layer(j) = A_layer(j)/h_layer;
    I_layer(j) = 1/12 *b_layer(j) *h_layer^3;
    I_max(j) = 1/12*b_layer(j)*h_layer^3 +...
        (A_layer(j) *(((H_tot/2)-((2*(j-1)+1)*h_layer))^2));
    j = j+1;
end
EI_min = E*(2*sum(I_layer)-I_layer(end));
EI_max = E*(2*sum(I_max)-I_max(end));
k = (7*sigma)+50;
A_0 = 2*sum(A_layer)-A_layer(end);
F = sigma*A_0;
S(1) = A_layer(1)*((H_tot-h_layer)/2);
for i = 1:n_slip
    R(i) = ((k*((1/(E*A_layer(i)))+(1/(E*A_layer(i+1)))))+...
        (h_layer^2/((E*I_layer(i))+(E*I_layer(i+1))))))^1/2)*L;
    S(i+1) = S(i) + A_layer(i)*h_layer*(n_slip-i);
    eta(i) = (S(i)/S(1))-((S(i)/S(1))-1)*exp(-R(i));
end
eta_0 = 2*sum(eta);
alpha_2 = k*(((n_layers-1)*h_layer^2)/EI_min+(2/(E*A_layer(1)*eta_0))); %alpha^2
beta_2 = (2*k*EI_max)/(E*A_layer(1)*EI_min*eta_0); %beta^2
alpha_0 = (F/EI_max)^(1/2); %alpha0
lamda_1 = (0.5*(alpha_2 + F/EI_min)+0.5*((alpha_2+F/EI_min)^2-(4*beta_2*F/EI_max))^
(1/2))^1/2;
lamda_2 = (0.5*(alpha_2+F/EI_min)-0.5*((alpha_2+F/EI_min)^2-(4*beta_2*F/EI_max))^
(1/2))^1/2;
%Consentrated force
omega_max1_c = (1*L/4*F)+(((1*(F/EI_min)-lamda_2^2)/(2*F*lamda_1*(lamda_2^2-
lamda_1^2)))*tanh(lamda_1*L/2))...
    -(((1*(F/EI_min)-lamda_1^2)/(2*F*lamda_2*(lamda_2^2-lamda_1^2)))*tanh
(lamda_2*L/2));
omega_max2_c = (1*L/4*F)-(1*tanh(alpha_0*L/2)/(2*alpha_0*F));
%Evenly distributed force
omega_max1_q = -(1/F)*((EI_max*alpha_2)/(beta_2*F)-L^2/8)+(1*lamda_2^2)*
((EI_max*lamda_1^2)/(EI_min*beta_2))...
    -1)/(F*lamda_1^2*(lamda_1^2-lamda_2^2)*cosh(lamda_1*L/2)) - (1*lamda_1^2)*
((EI_max*lamda_2^2)/(EI_min*beta_2))...
    -1)/(F*lamda_2^2*(lamda_1^2-lamda_2^2)*cosh(lamda_2*L/2));
omega_max2_q = (1*L^2)/(8*F)+(1/(alpha_0^2*F))*(cosh(alpha_0*L/2)-sinh(alpha_0*L/2)
*tanh(alpha_0*L/2)-1));

```

```
delta_2_c = omega_max1_c/omega_max2_c;  
EI_cable_c = EI_max/delta_2_c;  
I_cable_c = EI_cable_c/E; %[mm^4]  
  
delta_2_q = omega_max1_q/omega_max2_q;  
EI_cable_q = EI_max/delta_2_q;  
I_cable_q = EI_cable_q/E; %[mm^4]
```

## C Wind loads

09.06.21 13:19 C:\Users\Kristi...\readHalsaneset\_lo.m 1 of 4

---

```
clear all
projectdir = 'C:\Users\Kristine\Documents\NTNU\Masteroppgave\Matlab\Halsaneset';
files = dir(fullfile(projectdir, '*nc'));
num_files = length(files);
filenames = fullfile (projectdir, {files.name});

for i = 1:num_files
    filename = filenames{i};
    time{i} = ncread(filename, 'time');
    w_speed{i} = ncread(filename, 'windspeed');
    w_dir{i} = ncread(filename, 'winddirection');
    alt{i} = ncread(filename, 'alt');
end

for i = 1:num_files
    for k = 1:length(w_speed{1,i})
        if w_speed{1,i}(1,k) < 0
            w_speed{1,i}(1,k) = 0;
        end
        if w_speed{1,i}(2,k) < 0
            w_speed{1,i}(2,k) = 0;
        end
        if w_speed{1,i}(3,k) < 0
            w_speed{1,i}(3,k) = 0;
        end
    end
end

for i = 1:num_files
    for k = 1:length(w_dir{1,i})
        if w_dir{1,i}(1,k) < 0
            w_dir{1,i}(1,k) = 0;
        end
        if w_dir{1,i}(2,k) < 0
            w_dir{1,i}(2,k) = 0;
        end
        if w_dir{1,i}(3,k) < 0
            w_dir{1,i}(3,k) = 0;
        end
    end
end

%ALTITUDE 1
j = 1;
for i = 1:length(time)
    for z = 1:length(w_speed{1,i}(1,:))
        k(i) = z;
        if (185 < w_dir{1,i}(1,z)) && (w_dir{1,i}(1,z) < 310)
            w_speed_lo1(j) = w_speed{1,i}(1,z);
        elseif (0 < w_dir{1,i}(1,z)) && (w_dir{1,i}(1,z) < 145)
            w_speed_lo1(j) = w_speed{1,i}(1,z);
        else
            w_speed_lo1(j) = 0;
        end
    end
end
```

```

        end
        j = j + 1;
    end
    z = 0;
end

w_speed_lo1_tot{1} = w_speed_lo1(1:k(1));
p = 1;
c2_lo1 = [k(1)];

for z = 2:1:length(time)
    c1_tv1(p) = [k(z-1)];
    c2_lo1(p+1) = [k(z)];
    s1 = sum(c1_tv1);
    s11 = s1 + 1;
    s2 = sum(c2_lo1);
    w_speed_lo1_tot{z} = w_speed_lo1(s11:s2);
    p = p + 1;
end

%ALTITUDE2

j = 1;
for i = 1:length(time)
    for z = 1:length(w_speed{1,i}(2,:))
        k(i) = z;
        if (185 < w_dir{1,i}(2,z)) && (w_dir{1,i}(2,z) < 310)
            w_speed_lo2(j) = w_speed{1,i}(2,z);
        elseif (0 < w_dir{1,i}(2,z)) && (w_dir{1,i}(2,z) < 145)
            w_speed_lo2(j) = w_speed{1,i}(2,z);
        else
            w_speed_lo2(j) = 0;
        end
        j = j + 1;
    end
    z = 0;
end

w_speed_lo2_tot{1} = w_speed_lo2(1:k(1));
p = 1;
c2_lo2 = [k(1)];

for z = 2:1:length(time)
    c1_tv2(p) = [k(z-1)];
    c2_lo2(p+1) = [k(z)];
    s1 = sum(c1_tv2);
    s11 = s1 + 1;
    s2 = sum(c2_lo2);
    w_speed_lo2_tot{z} = w_speed_lo2(s11:s2);
    p = p + 1;
end

%ALTITUDE 3

```



```

j = 1;
for i = 1:length(time)
    for z = 1:length(w_speed{1,i}(3,:))
        k(i) = z;
        if (185 < w_dir{1,i}(3,z)) && (w_dir{1,i}(3,z) < 310)
            w_speed_lo3(j) = w_speed{1,i}(3,z);
        elseif (0 < w_dir{1,i}(3,z)) && (w_dir{1,i}(3,z) < 145)
            w_speed_lo3(j) = w_speed{1,i}(3,z);
        else
            w_speed_lo3(j) = 0;
        end
        j = j + 1;
    end
    z = 0;
end

w_speed_lo3_tot{1} = w_speed_lo3(1:k(1));
p = 1;
c2_lo3 = [k(1)];

for z = 2:1:72
    c1_tv3(p) = [k(z-1)];
    c2_lo3(p+1) = [k(z)];
    s1 = sum(c1_tv3);
    s11 = s1 + 1;
    s2 = sum(c2_lo3);
    w_speed_lo3_tot{z} = w_speed_lo3(s11:s2);
    p = p + 1;
end

for s = 1:length(time)
    max_ws_lo1(s) = max(w_speed_lo1_tot{1,s}(1,:));
    max_ws_lo2(s) = max(w_speed_lo2_tot{1,s}(1,:));
    max_ws_lo3(s) = max(w_speed_lo3_tot{1,s}(1,:));
end

aar = [2014, 2015, 2016, 2017, 2018, 2019];
max_ws_aar11_lo = max(max_ws_lo1(1,1:12));
max_ws_aar21_lo = max(max_ws_lo1(1,13:24));
max_ws_aar31_lo = max(max_ws_lo1(1,25:36));
max_ws_aar41_lo = max(max_ws_lo1(1,37:48));
max_ws_aar51_lo = max(max_ws_lo1(1,49:60));
max_ws_aar61_lo = max(max_ws_lo1(1,61:72));
max_aar_ws_alt1_lo1 = [max_ws_aar11_lo, max_ws_aar21_lo, max_ws_aar31_lo,
max_ws_aar41_lo, max_ws_aar51_lo, max_ws_aar61_lo];

max_ws_aar12_lo = max(max_ws_lo2(1,1:12));
max_ws_aar22_lo = max(max_ws_lo2(1,13:24));
max_ws_aar32_lo = max(max_ws_lo2(1,25:36));
max_ws_aar42_lo = max(max_ws_lo2(1,37:48));
max_ws_aar52_lo = max(max_ws_lo2(1,49:60));
max_ws_aar62_lo = max(max_ws_lo2(1,61:72));
max_aar_ws_alt2_lo2 = [max_ws_aar12_lo, max_ws_aar22_lo, max_ws_aar32_lo,

```

```
max_ws_aar42_lo, max_ws_aar52_lo, max_ws_aar62_lo];

max_ws_aar13_lo = max(max_ws_lo3(1,1:12));
max_ws_aar23_lo = max(max_ws_lo3(1,13:24));
max_ws_aar33_lo = max(max_ws_lo3(1,25:36));
max_ws_aar43_lo = max(max_ws_lo3(1,37:48));
max_ws_aar53_lo = max(max_ws_lo3(1,49:60));
max_ws_aar63_lo = max(max_ws_lo3(1,61:72));
max_aar_ws_alt3_lo3 = [max_ws_aar13_lo, max_ws_aar23_lo, max_ws_aar33_lo,
max_ws_aar43_lo, max_ws_aar53_lo, max_ws_aar63_lo];

figure(1)
plot(aar, max_aar_ws_alt1_lo1);
hold on
plot(aar, max_aar_ws_alt2_lo2);
hold on
plot(aar, max_aar_ws_alt3_lo3);
title('Max wind speed in storm season during 6 years')
xlabel('Year')
ylabel('Windspeed [m/s]')
ylim([0,25])
xlim([2014,2019])
xticks(2014:1:2019)
```

## Wind - Halsafjorden

The wind speed affecting the towers are calculated for wind across and along the bridge. EC1.1-4 form the basis for the calculation.

$$v_{b.0.ac}(z) := \overline{\left( \frac{z}{1.631 \cdot 10^{-14}} \right)^{\left( \frac{1}{10.64} \right)}} \frac{m}{s} \quad v_{b.0.al}(z) := \overline{\left( \frac{z - 4.703}{1.485 \cdot 10^{-10}} \right)^{\left( \frac{1}{8.177} \right)}} \frac{m}{s}$$

$v_b := c_{dir} \cdot c_{season} \cdot c_{alt} \cdot c_{prob} \cdot v_{b.0}$  Basis wind velocity, characteristic 10 minutes mean wind velocity.  
Section NA.4.2(2), equation NA.4.1

$c_{dir} := 1$  The directional factor is taken into account when finding the extreme values from the wind data.

$c_{season} := 1$  The season factor: the extreme values for each storm season was found and the respectable values is therefore 1 and conservative.

$c_{alt} := 1$  The level factor, conservative determined to be 1, taken into account by the logartimic law.

$c_{prob} := 1$  Factor used to take accout of return periodes different than 50 years, hence equal to 1 for both construction phase and completion.

Section NA.4.2 states that the factores mentioned above can in general be desided as the value 1. This is a conservative assumption.

$$v_{b.ac}(z) := \overline{c_{dir} \cdot c_{season} \cdot c_{alt} \cdot c_{prob} \cdot v_{b.0.ac}(z)} \quad v_{b.al}(z) := \overline{c_{dir} \cdot c_{season} \cdot c_{alt} \cdot c_{prob} \cdot v_{b.0.al}(z)}$$

$v_m := c_r \cdot c_o \cdot v_b$  10 min mean wind velocity, section 4.3, equation 4.3

$z_0$  Roughnesslength, determined from table 4.1.

$$z_{0.ac} := 0.003 \text{ m} \quad z_{0.al} := 0.05 \text{ m} \quad z_{0.2} := 0.05 \text{ m}$$

$k_r$  Terrain factor dependent on the roughness length  $z_0$  equation 4.5

$$k_{r.ac} := 0.19 \cdot \left( \frac{z_{0.ac}}{z_{0.2}} \right)^{0.07} = 0.156 \quad k_{r.al} := 0.19 \cdot \left( \frac{z_{0.al}}{z_{0.2}} \right)^{0.07} = 0.19$$

$c_r$  Roughness factor, assuming wind at a height  $z > z_0$ , equation 4.4

$$c_{r.ac}(z) := \overrightarrow{k_{r.ac} \cdot \ln\left(\frac{z \cdot m}{z_{0.ac}}\right)} \quad c_{r.al}(z) := \overrightarrow{k_{r.al} \cdot \ln\left(\frac{z \cdot m}{z_{0.al}}\right)}$$

$c_0$  Orography factor, section 4.3.3, assuming  $c_0 := 1$

$$v_{m.ac}(z) := \overrightarrow{c_{r.ac}(z) \cdot v_{b.ac}(z)} \quad v_{m.al}(z) := \overrightarrow{c_{r.al}(z) \cdot v_{b.al}(z)}$$

$I_u(z)$  Turbulensintensity for the longitudinal component u, section 4.4.

$k_l := 1$  Turbulens factor

$$I_{u.ac}(z) := \frac{\overrightarrow{k_l}}{\ln\left(\frac{z \cdot m}{z_{0.ac}}\right)} \quad I_{u.al}(z) := \frac{\overrightarrow{k_l}}{\ln\left(\frac{z \cdot m}{z_{0.al}}\right)}$$

$k_p := 3.5$  Top factor, determined according to section NA.4.5.

Wind gust speed, determined according to section NA.4.4.

$$v_{p.ac}(z) := \overrightarrow{v_{m.ac}(z) \cdot \sqrt{1 + 2 \cdot k_p \cdot I_{u.ac}(z)}} \quad v_{p.al}(z) := \overrightarrow{v_{m.al}(z) \cdot \sqrt{1 + 2 \cdot k_p \cdot I_{u.al}(z)}}$$

$\rho := 1.25 \frac{kg}{m^3}$  Air density

Wind gust speed pressure, section NA.4.5, equation NA.4.8. Used to determine the static wind load action on the different bridge components.

$$q_{p.ac}(z) := \frac{1}{2} \cdot \rho \cdot \overrightarrow{v_{p.ac}(z)^2} \quad q_{p.al}(z) := \frac{1}{2} \cdot \rho \cdot \overrightarrow{v_{p.al}(z)^2}$$

## Windloads at the deck:

Determined based on formulas in "12-2950 Hardangerbrua beregninger"

$$F_D := C_D \cdot q \cdot H \cdot L \quad \text{Section 1.7.3 ii)}$$

$$H := 3.33 \text{ m} \quad \text{Same deck as for Hardangerbrua, this height includes everything attached to the deck (asphalt, railings, stiffeners etc. ).}$$

$$L_{Hf} := 2050 \text{ m}$$

$$C_{D.deck} := 0.854 \quad \text{Assuming upstream wind, conservative for both directions. The coefficient is increased by 6% to take into account the hangers and the attachment of these.}$$

$$F_{D.deck} := C_{D.deck} \cdot q_{p.ac}(43) \cdot H = 5.435 \frac{kN}{m}$$

$$F_{D.deck.tot} := F_{D.deck} \cdot L_{Hf} = 11.141 \text{ MN}$$

$$F_{D.deck.p} := F_{D.deck.tot} \cdot \frac{1}{2} \cdot \frac{1}{2} = 2.785 \text{ MN} \quad \text{Force at the top of each pylon for each cable}$$

## Windloads on the main cable:

Determined based on formulas in "12-2950 Hardangerbrua beregninger"

Assuming a mean height of 142 m.

$$F_{D.mainc} := C_{D.mainc} \cdot q \cdot \emptyset \cdot L \quad \text{Section 1.7.3 iii)}$$

$$\emptyset := 773 \text{ mm} + 0.02 \text{ m} = 0.793 \text{ m} \quad \text{Diameter of the cable including protection.}$$

$$L := 2095.913 \text{ m} \quad \text{Deformed state of the cable, due to gravitation and deck.}$$

$$C_{D.mainc} := 1 \quad \text{Assuming the same force coefficient as for Hardangerbrua. This is a conservative value that takes into account the hangers and the attachment of the hangers.}$$

$$F_{D.mainc} := C_{D.mainc} \cdot q_{p.ac}(142) \cdot \emptyset \cdot L = 4.795 \text{ MN} \quad \text{Force in each main cable.}$$

$$F_{D.mainc.p} := F_{D.mainc} \cdot \frac{1}{2} = 2.397 \text{ MN} \quad \text{Force in the top of each pylon for each cable.}$$

The wind on the hangers is included in the calculation of the wind loads at the deck and the main cable.

## Wind loads on the towers:

Determined based on formulas in "12-2950 Hardangerbrua beregninger"

$$F_D := C_D \cdot q \cdot L \cdot H \quad \text{Section 1.7.3 v)}$$

$C_D$  The force coefficients are calculated according to section 7.6 in EC1.1-4. A corner rounding of  $r = 0.25\text{m}$  is assumed, equal to Hardangerbrua.

$$C_{D.ac} := 2.025 \quad C_{D.al} := 1.4025$$

### Construction phase:

An additional 3m is added at the width and the length of the cross-section to account for the form work.

Wind acting on the construction elevator and the crane is calculated for each casting stage and summarized in the total static wind load at the structure.

$$W_{elevator} := 1.9 \frac{m^2}{m}$$

$$W_{crane} := 1.9 \frac{m^2}{m}$$

Wind acting on the crane top is calculated and added to the tower top as a concentrated force.

$$A_{crane} := 40 \text{ m}^2$$

$$F_{c.top} := q_{p.al}(255) \cdot A_{crane} \cdot \frac{1}{2} = 58.561 \text{ kN} \quad \text{Point load at each towertop}$$

$$F_{D.cons}(z) := \overrightarrow{C_{D.al} \cdot q_{p.al}(z) \cdot (W_{tower} + W_{crane})}$$

### Completion phase:

$$F_{D.comp.al}(z) := \overrightarrow{C_{D.al} \cdot q_{p.al}(z) \cdot W_{tower}}$$

$$F_{D.comp.ac}(z) := \overrightarrow{C_{D.ac} \cdot q_{p.ac}(z) \cdot L_{tower}}$$

### Windloads on the transverse beams:

Valid for both construction phase and after completion.

$$C_{D,planum} := 1.7425 \quad H_{planum} := 7.5 \text{ m}$$

$$C_{D,lowermid} := 2.0700 \quad H_{lowermid} := 8.6 \text{ m}$$

$$C_{D,uppermid} := 2.1420 \quad H_{uppermid} := 8.6 \text{ m}$$

$$C_{D,top} := 1.7475 \quad H_{top} := 6 \text{ m}$$

$$F_{D,planum} := C_{D,planum} \cdot q_{p.al}(36) \cdot H_{planum} = 15.5 \frac{\text{kN}}{\text{m}}$$

$$F_{D,lowermid} := C_{D,lowermid} \cdot q_{p.al}(108) \cdot H_{lowermid} = 35.667 \frac{\text{kN}}{\text{m}}$$

$$F_{D,uppermid} := C_{D,uppermid} \cdot q_{p.al}(174) \cdot H_{uppermid} = 45.672 \frac{\text{kN}}{\text{m}}$$

$$F_{D,top} := C_{D,top} \cdot q_{p.al}(237) \cdot H_{top} = 29.746 \frac{\text{kN}}{\text{m}}$$

### **Load combinations:**

Determined in accordance with EC0.

Load factors, found in table NA.A2.4.

$\gamma_{G.sup} := 1.35$  Permanent load if unfavorable

$\gamma_{G.inf} := 1.0$  Permanent load is favorable

$\xi := 0.89$

$\gamma_{Q.T} := 1.35$  Traffic load if unfavorable, 0 if favorable

$\gamma_{Q.W} := 1.60$  Wind load if unfavorbale, 0 if favorable

$\psi_{0.T} := 0.7$  Reduction factor traffic

$\psi_{0.W} := 0.7$  Reduction factor wind load

Equation 6.10a  $\gamma_{G.sup} \cdot G + \gamma_Q \cdot \psi_0 \cdot Q$

Equation 6.10b  $\xi \cdot \gamma_{G.sup} \cdot G + \gamma_Q \cdot Q$

### **Construction phase:**

- Wind load and self weight, second order effect makes the contribution from the self weight unfavorable

$$\begin{aligned} \text{Equation 6.10a} \quad & \gamma_{G.sup} \cdot G + \gamma_{Q.W} \cdot \psi_{0.W} \cdot W \\ & = 1.35 \cdot G + 1.60 \cdot 0.70 \cdot W \\ & = 1.35 \cdot G + 1.12 \cdot W \end{aligned}$$

$$\begin{aligned} \text{Equation 6.10b} \quad & \xi \cdot \gamma_{G.sup} \cdot G + \gamma_Q \cdot Q \\ & = 0.89 \cdot 1.35 \cdot G + 1.60 \cdot W \\ & = 1.2 \cdot G + 1.60 \cdot W \end{aligned}$$

### **Completion phase:**

- Wind load, self weight and traffic load. Two different load cases because the wind has different directions, along and across the bridge.



Wind along the bridge:

Combination 1: Traffic load as the dominating force and wind as remaining force

$$\begin{aligned}\text{Equation 6.10a} \quad & \gamma_{G.sup} \cdot G + \gamma_{Q.T} \cdot \psi_{0.T} \cdot T + \gamma_{Q.W} \cdot \psi_{0.W} \cdot W \\ & = 1.35 \cdot G + 1.35 \cdot 0.70 \cdot T + 1.60 \cdot 0.70 \cdot W \\ & = 1.35 \cdot G + 0.945 \cdot T + 1.12 \cdot W\end{aligned}$$

$$\begin{aligned}\text{Equation 6.10b} \quad & \xi \cdot \gamma_{G.sup} \cdot G + \gamma_{Q.T} \cdot T + \gamma_{Q.W} \cdot \psi_{0.W} \cdot W \\ & = 0.89 \cdot 1.35 \cdot G + 1.35 \cdot T + 1.60 \cdot 0.70 \cdot W \\ & = 1.2 \cdot G + 1.35 \cdot T + 1.12 \cdot W\end{aligned}$$

Combination 2: Wind load as the dominating force and traffic as other.  
According to NA.A2.1, when the wind is assumed to be the dominating force, the reduction factor for traffic is zero.

$$\psi_{0.T} := 0$$

$$\begin{aligned}\text{Equation 6.10a} \quad & \gamma_{G.sup} \cdot G + \gamma_{Q.W} \cdot \psi_{0.W} \cdot W + \gamma_{Q.T} \cdot \psi_{0.T} \cdot T \\ & = 1.35 \cdot G + 1.60 \cdot 0.70 \cdot W + 1.35 \cdot 0 \cdot T \\ & = 1.35 \cdot G + 1.12 \cdot W\end{aligned}$$

$$\begin{aligned}\text{Equation 6.10b} \quad & \xi \cdot \gamma_{G.sup} \cdot G + \gamma_{Q.W} \cdot W + \gamma_{Q.T} \cdot \psi_{0.T} \cdot T \\ & = 0.89 \cdot 1.35 \cdot G + 1.60 \cdot W + 1.35 \cdot 0 \cdot T \\ & = 1.2 \cdot G + 1.60 \cdot W\end{aligned}$$

Wind across:

- Wind is the dominating force this means that the traffic load is not included.

$$\begin{aligned}\text{Equation 6.10a} \quad & \gamma_{G.sup} \cdot G + \gamma_{Q.W} \cdot \psi_{0.W} \cdot W + \gamma_{Q.T} \cdot \psi_{0.T} \cdot T \\ & = 1.35 \cdot G + 1.60 \cdot 0.70 \cdot W + 1.35 \cdot 0 \cdot T \\ & = 1.35 \cdot G + 1.12 \cdot W\end{aligned}$$

$$\begin{aligned}\text{Equation 6.10b} \quad & \xi \cdot \gamma_{G.sup} \cdot G + \gamma_Q \cdot Q + \gamma_{Q.T} \cdot \psi_{0.T} \cdot T \\ & = 0.89 \cdot 1.35 \cdot G + 1.60 \cdot W + 1.35 \cdot 0 \cdot T \\ & = 1.2 \cdot G + 1.60 \cdot W\end{aligned}$$

## Load combinations - Wind Load:

### Load combination 1: Construction

$$F_{D.tower.cons}(z) := \overrightarrow{F_{D.cons}(z)} \cdot 1.60 \quad \text{Calculated by the use of excel and listed below.}$$

$$F_{D.planum} := C_{D.planum} \cdot q_{p.al}(36) \cdot H_{planum} \cdot 1.60 = 24.8 \frac{kN}{m}$$

$$F_{D.lowermid} := C_{D.lowermid} \cdot q_{p.al}(108) \cdot H_{lowermid} \cdot 1.60 = 57.067 \frac{kN}{m}$$

$$F_{D.uppermid} := C_{D.uppermid} \cdot q_{p.al}(174) \cdot H_{uppermid} \cdot 1.60 = 73.076 \frac{kN}{m}$$

$$F_{D.top} := C_{D.top} \cdot q_{p.al}(237) \cdot H_{top} \cdot 1.60 = 47.593 \frac{kN}{m}$$

### Load combination 2: Global model

$$F_{D.tower.al}(z) := \overrightarrow{F_{D.comp.al}(z)} \cdot 1.12 \quad \text{Calculated by the use of excel and listed below.}$$

$$F_{D.planum} := C_{D.planum} \cdot q_{p.al}(36) \cdot H_{planum} \cdot 1.12 = 17.36 \frac{kN}{m}$$

$$F_{D.lowermid} := C_{D.lowermid} \cdot q_{p.al}(108) \cdot H_{lowermid} \cdot 1.12 = 39.947 \frac{kN}{m}$$

$$F_{D.uppermid} := C_{D.uppermid} \cdot q_{p.al}(174) \cdot H_{uppermid} \cdot 1.12 = 51.153 \frac{kN}{m}$$

$$F_{D.top} := C_{D.top} \cdot q_{p.al}(237) \cdot H_{top} \cdot 1.12 = 33.315 \frac{kN}{m}$$

### Load combinaion 3: Global model

$$F_{D.tower.ac}(z) := \overrightarrow{F_{D.comp.ac}(z)} \cdot 1.60 \quad \text{Calculated by the use of excel and listed below.}$$

$$F_{D.tot.p} := (F_{D.mainc.p} \cdot 1.6) + (F_{D.deck.p} \cdot 1.6) = 8.292 \text{ MN}$$

Static wind load on the towers			
	Load combination 1	Load combination 2	Load combination 3
Casting stage	F_D.tower.cons [kN/m]	F_D.tower.al [kN/m]	F_D.tower.ac [kN/m]
1	8,668	5,069	36,024
2	8,668	5,069	45,963
3	11,494	6,692	52,180
4	13,476	7,811	56,556
5	15,011	8,662	59,803
6	16,251	9,334	62,257
7	17,276	9,877	64,136
8	18,140	10,322	65,582
9	18,871	10,686	66,668
10	19,502	10,990	67,497
11	20,043	11,240	68,093
12	20,513	11,447	68,510
13	20,919	11,616	68,768
14	21,278	11,756	68,918
15	21,594	11,872	68,973
16	22,195	12,143	69,692
17	22,725	12,371	70,235
18	23,199	12,569	70,661
19	23,627	12,740	70,985
20	24,013	12,886	71,218
21	24,370	13,018	71,407
22	24,698	13,134	71,540
23	25,006	13,240	71,648
24	25,302	13,342	71,758
25	25,583	13,437	71,853
26	25,857	13,529	71,958
27	26,128	13,622	72,082
28	26,398	13,718	72,234
29	26,671	13,817	72,424
30	26,948	13,923	72,656
31	27,234	14,036	72,939
32	27,529	14,158	73,279
33	27,837	14,291	73,681
34	28,159	14,436	74,152
35	28,493	14,590	74,679
36	28,850	14,762	75,301
37	29,226	14,950	76,006
38	29,614	15,147	76,763
39	30,000	15,343	77,522
40	30,379	15,537	78,266
41	30,752	15,727	78,997
42	31,119	15,915	79,714
43	31,480	16,099	80,420
44	31,835	16,281	81,113
45	32,185	16,460	81,796
Tower top	52,750	16,896	83,454

## D User guide for the lamellae program

```

Sub SolverElena()
'
' SolverElena2 Macro
'
'
Do
    Range("L5").Value = Range("L5").Value + 0.0002

    SolverReset
    SolverOk SetCell:="$K$48", MaxMinVal:=3, ValueOf:=-900000, ByChange:="$L$6", Engine:=1, EngineDesc:="GRG Nonlinear"
    SolverAdd CellRef:="$L$6", Relation:=1, FormulaText:="0.000001"
    SolverAdd CellRef:="$L$6", Relation:=3, FormulaText:="-0.0035"
    SolverOk SetCell:="$K$48", MaxMinVal:=3, ValueOf:=-900000, ByChange:="$L$6", Engine:=1, EngineDesc:="GRG Nonlinear"
    SolverSolve userFinish:=True

Dim lastRow As Long
lastRow = Sheets("Results Model 1").Range("F" & Rows.Count).End(xlUp).Row

With Sheets("Results Model 1")
    If .Cells(3, 6).Value = "" Then
        .Cells(3, 2).Value = Sheets("Multi-layer method").Range("L5").Value
        .Cells(3, 3).Value = Sheets("Multi-layer method").Range("L6").Value
        .Cells(3, 4).Value = Sheets("Multi-layer method").Range("L8").Value
        .Cells(3, 5).Value = Sheets("Multi-layer method").Range("L7").Value
        .Cells(3, 6).Value = Sheets("Multi-layer method").Range("L48").Value
        .Cells(3, 7).Value = Sheets("Multi-layer method").Range("K48").Value
    Else
        .Cells(lastRow + 1, 2).Value = Sheets("Multi-layer method").Range("L5").Value
        .Cells(lastRow + 1, 3).Value = Sheets("Multi-layer method").Range("L6").Value
        .Cells(lastRow + 1, 4).Value = Sheets("Multi-layer method").Range("L8").Value
        .Cells(lastRow + 1, 5).Value = Sheets("Multi-layer method").Range("L7").Value
        .Cells(lastRow + 1, 6).Value = Sheets("Multi-layer method").Range("L48").Value
        .Cells(lastRow + 1, 7).Value = Sheets("Multi-layer method").Range("K48").Value
    End If

End With

Loop Until Range("L5").Value >= 0.006

End Sub

```

Step size for the strain at the lower edge

Solver

Boundaries for the strain at the upper edge

Target value of the axial force

Print the results

Maximum strain at the lower edge

Figure D.1: Macro with internal solver

```
Sub ResetElena()  
'  
' ResetElena Macro  
'  
'  
    Sheets("Results Model 1").Select  
    Range("B3:G34").Select  
    Selection.ClearContents  
    Sheets("Multi-layer method").Select  
    Range("L5").Select  
    ActiveCell.FormulaR1C1 = "-0.0030"  
    Range("L6").Select  
    ActiveCell.FormulaR1C1 = ""  
End Sub
```

Initial strain at  
lower edge

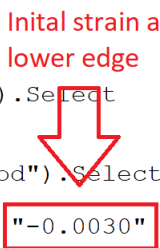


Figure D.2: Macro which reset the calculations

## E Calculations of a slim column

$$L := 12000 \text{ mm}$$

$$b := 300 \text{ mm}$$

$$h := 400 \text{ mm}$$

$$c' := 50 \text{ mm}$$

$$c := 50 \text{ mm}$$

$$h' := h - c' - c = 300 \text{ mm}$$

$$A_c := b \cdot h = 120000 \text{ mm}^2$$

$$f_{ck} := 45 \text{ MPa}$$

$$\gamma_c := 1.5 \quad \alpha_{cc} := 0.85$$

$$f_{cd} := \alpha_{cc} \cdot \frac{f_{ck}}{\gamma_c} = 25.5 \text{ MPa}$$

$$A'_p := 250 \text{ mm}^2$$

$$A_p := 250 \text{ mm}^2$$

$$A_{p\_tot} := A_p + A'_p = 500 \text{ mm}^2$$

$$f_{p0.1k} := 1550 \text{ MPa}$$

$$\gamma_s := 1.15$$

$$f_{pd} := \frac{f_{p0.1k}}{\gamma_s} = 1347.83 \text{ MPa}$$

$$N_{ed} := 900 \text{ kN}$$

$$i := \frac{h}{\sqrt{12}} = 115.47 \text{ mm}$$

Radius of gyration of a rectangle

$$i_s := \frac{h'}{2} = 150 \text{ mm}$$

Radius of gyration imposed by reinforcement

$$k_a := \left( \frac{i_s}{i} \right)^2 = 1.688$$

S. I. Sørensen, Eq. 6.7

$$\omega := \frac{f_{pd} \cdot A_{p\_tot}}{f_{cd} \cdot A_c} = 0.22$$

Mecanical reinforcement ratio, EC2, 5.8.3.1

$$n := \frac{N_{ed}}{f_{cd} \cdot A_c} = 0.294$$

Relative normal force, EC2, 5.8.3.1

$$\lambda := \frac{L}{i} = 103.923$$

Slenderness ratio, EC2, Eq 5.14

$$\lambda_{max} := 80 \cdot \sqrt{1 + 2 \cdot k_a \cdot \omega} = 105.627 \quad \lambda < \lambda_{max}$$

S. I. Sørensen, Eq. 6.15

$$\lambda_n := \lambda \cdot \sqrt{\frac{n}{1 + 2 \cdot k_a \cdot \omega}} = 42.686$$

S. I. Sørensen, Eq. 6.6

$$\lambda_{n\_max} := 45$$

$$\lambda_n < \lambda_{n\_max}$$

S. I. Sørensen, Eq. 6.14

## F Abaqus analysis of the transverse beam

### Abaqus analysis of bottom transverse beam

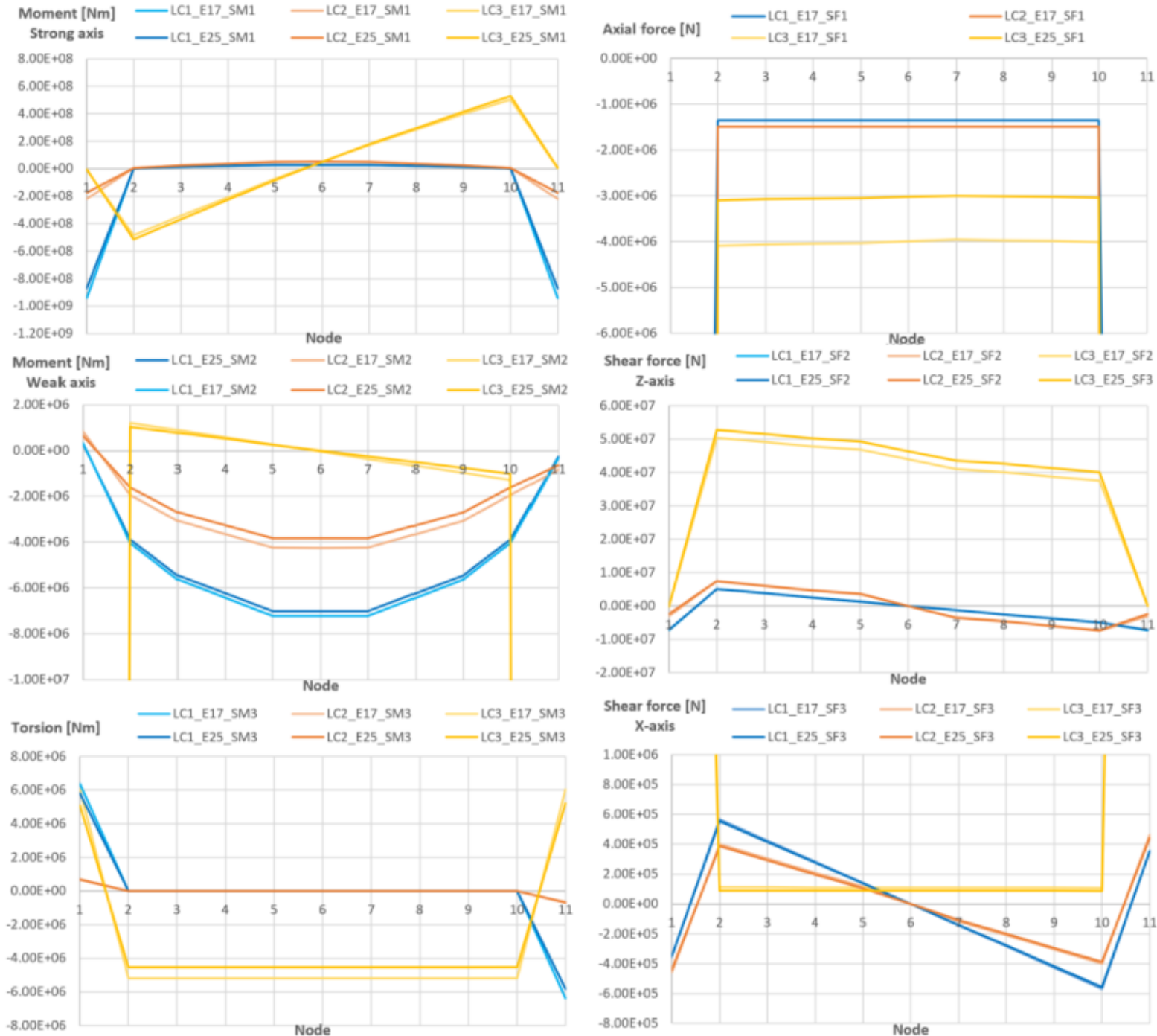


Figure F.1: Bottom transverse beam

# Abaqus analysis of lower middle transverse beam

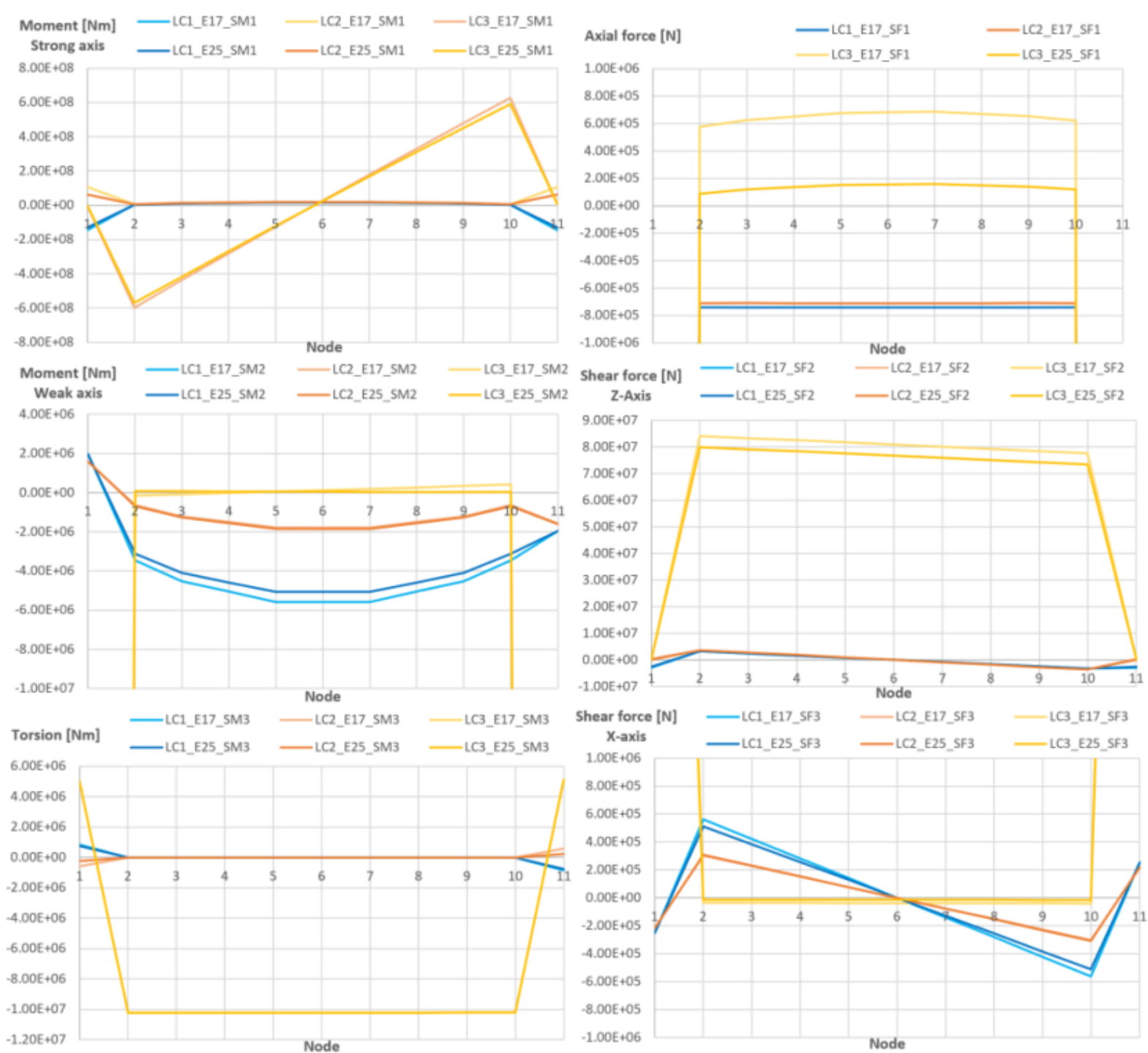


Figure F.2: Lower middle transverse beam



# Abaqus analysis of upper middle transverse beam

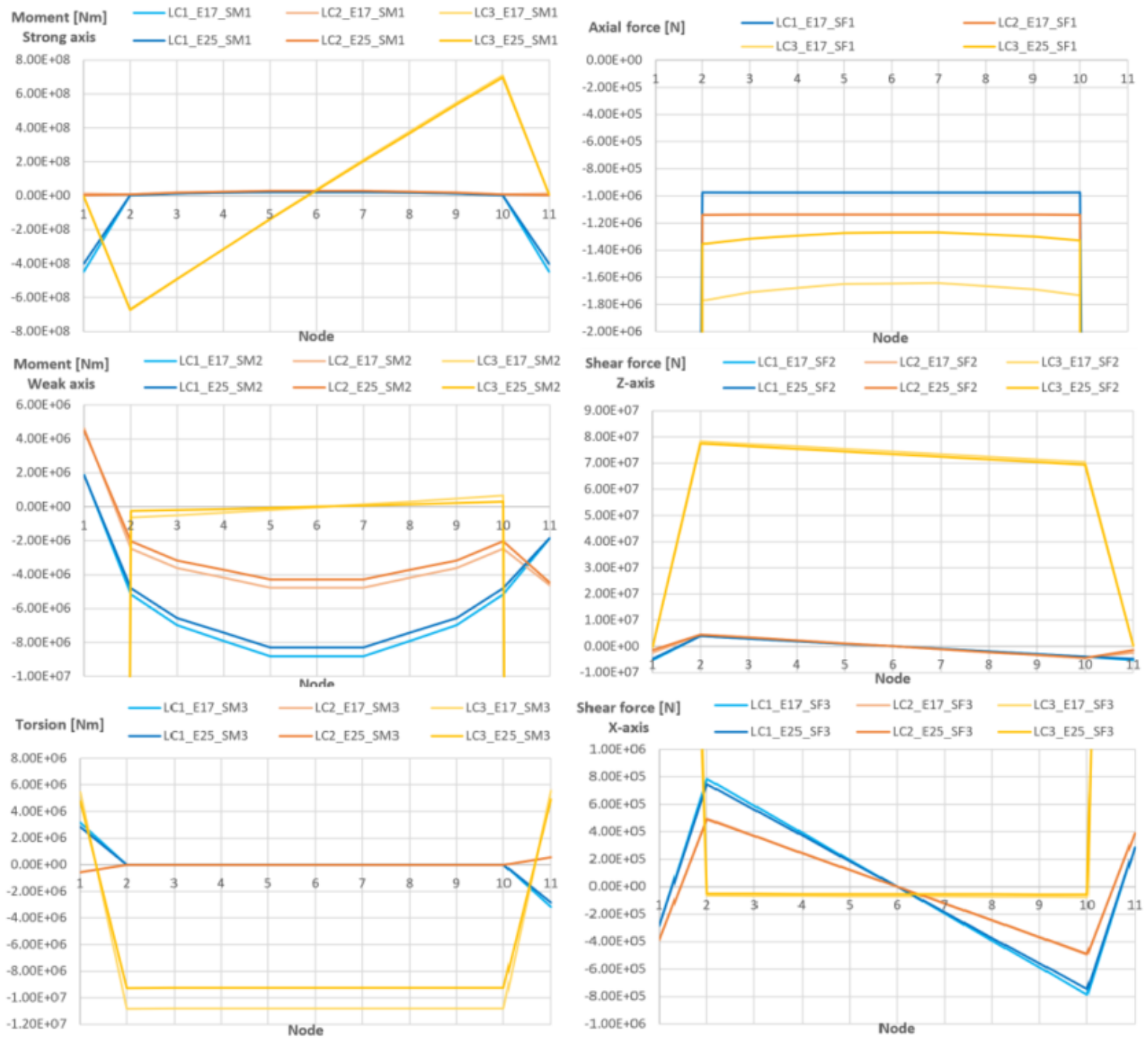


Figure F.3: Upper middle transverse beam

# Abaqus analysis of transverse top beam

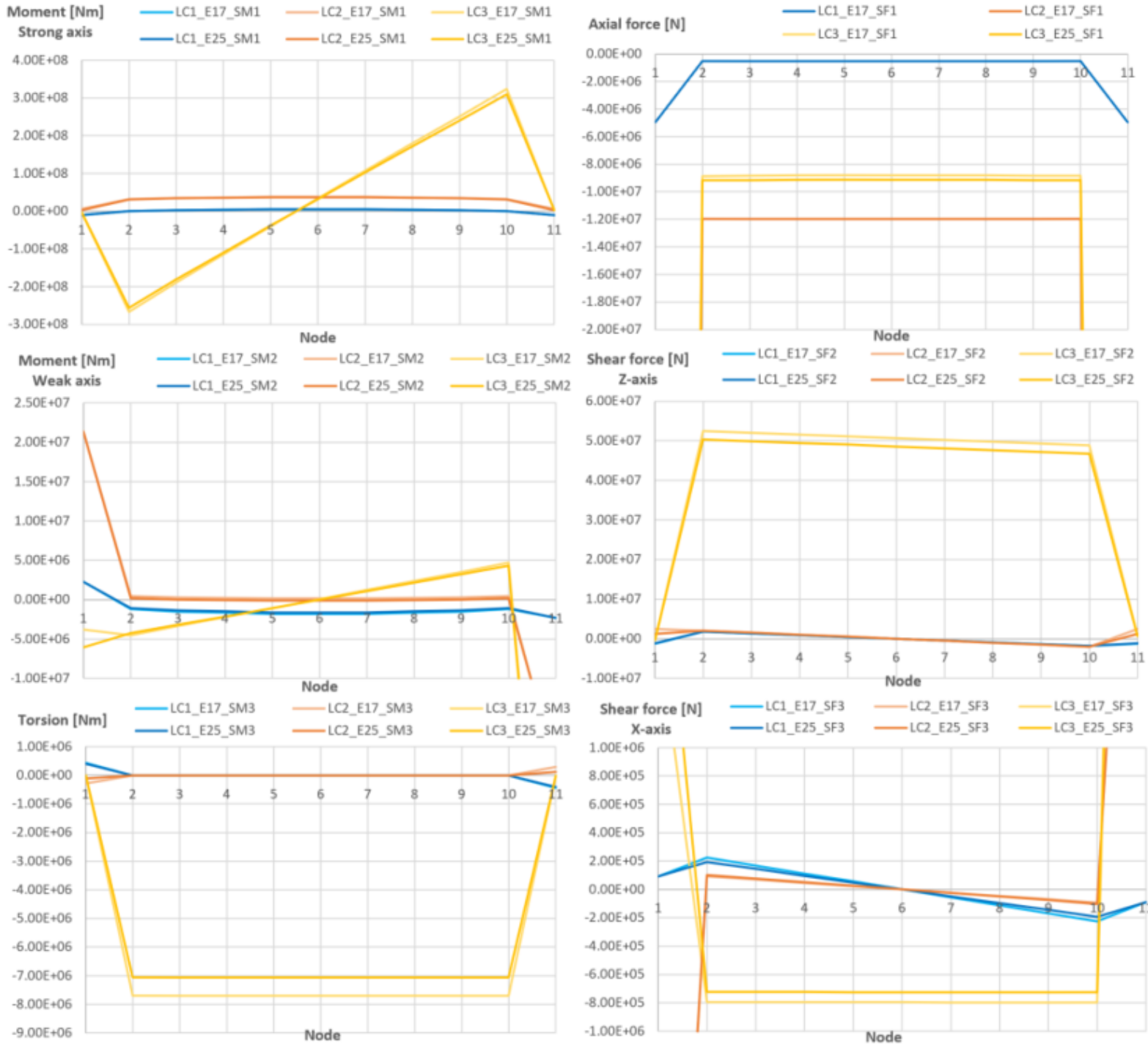


Figure F.4: Top transverse beam

## G Calculations of shear reinforcement for the bottom transverse beam

### Shear forces in Z-direction:

#### Geometry:

$$h := 7500 \text{ mm}$$

$$t := 600 \text{ mm}$$

$$b_w := 2 \cdot t = 1200 \text{ mm}$$

$$A_c := 15.25 \text{ m}^2$$

$$c_{nom} := 300 \text{ mm}$$

$$c_{p.nom} := 450 \text{ mm}$$

#### Material properties

$$\alpha_{cc} := 0.85$$

$$\gamma_c := 1.5$$

$$\gamma_s := 1.15$$

$$\gamma_p := 1.15$$

$$f_{ck} := 90 \text{ MPa}$$

$$f_{cd} := \alpha_{cc} \frac{f_{ck}}{\gamma_c} = 51 \text{ MPa}$$

$$f_{yk} := 500 \text{ MPa}$$

$$f_{yd} := \frac{f_{yk}}{\gamma_p} = 434.783 \text{ MPa}$$

$$F_p := 3869 \text{ kN}$$

#### Reinforcement:

$$A_{\phi 16} := (8 \text{ mm})^2 \cdot \pi = 201 \text{ mm}^2$$

$$A_{\phi 20} := (10 \text{ mm})^2 \cdot \pi = 314 \text{ mm}^2$$

$$A_{\phi 25} := (12.5 \text{ mm})^2 \cdot \pi = 491 \text{ mm}^2$$

$$A_{\phi 32} := (16 \text{ mm})^2 \cdot \pi = 804 \text{ mm}^2$$

#### General:

$$N_{Ed} := 4.1 \cdot 10^6 \text{ N}$$

Dimensioning axial force

$$V_{Ed} := 5.04 \cdot 10^7 \text{ N}$$

Dimensioning shear force

### **Shear tensile capacity:**

Checking whether the members require design shear reinforcement. Controlled according to 6.2.2 and NA.6.2.2. in EC2.1-1

$$\begin{aligned} A_s &:= 250 \cdot A_{\phi 25} = 122718.463 \text{ mm}^2 && \text{Ordinary reinforcement area in tension} \\ A_p &:= 2850 \text{ mm}^2 \cdot 10 = 28500 \text{ mm}^2 && \text{Prestressed reinforcement area on tensile side} \\ S_p &:= F_p \cdot 10 = 38690 \text{ kN} \\ S_d &:= A_s \cdot f_{yd} = 53355.853 \text{ kN} \\ d_p &:= h - c_{p.nom} = 7050 \text{ mm} \\ d_s &:= h - c_{nom} - 25 \text{ mm} - 32 \frac{\text{mm}}{2} = 7159 \text{ mm} \\ d_{mid} &:= \frac{d_p \cdot S_p + d_s \cdot S_d}{S_p + S_d} = 7113.184 \text{ mm} && \text{Effective height of the cross-section} \\ \rho_t &:= \frac{A_p + A_s}{b_w \cdot d_{mid}} = 0.018 && \rho_t \leq 0.02 \quad \text{Ok, according to 6.2.2(1), EC2.1-1} \\ k &:= 1 + \sqrt{\frac{200 \text{ mm}}{d_{mid}}} = 1.168 && k \leq 2.0 \quad \text{Ok, according to 6.2.2(1), EC2.1-1} \end{aligned}$$

$k_1$  is set equal to 0.15 for compression and to 0.3 for tension, according to NA.6.2.2(1) in EC2.1-1. Calculating compression in this case.

$$k_1 := 0.15$$

$k_2 := 0.18$  for concrete with maximum size of aggregate  $D$ , greater than or equal to 16 mm, according to NA.6.2.2(1), EC2.1-1.

$$k_2 := 0.18$$

$$C_{Rd.c} := \frac{k_2}{\gamma_c} = 0.12 \quad \text{NA.6.2.2(1) in EC2.1-1}$$

$$\sigma_{cp} := \frac{N_{Ed}}{A_c} = 0.269 \text{ MPa}$$

$$0.2 \cdot f_{cd} = 10.2 \text{ MPa} \quad \sigma_{cp} \leq 0.2 \cdot f_{cd} \quad \text{OK, according to 6.2.2 in EC2.1-1.}$$

Shear tensile capacity is calculated according to equation 6.2.a in EC2.1-1:

$$V_{Rd.c} := \left( \frac{N}{mm^2} \cdot C_{Rd.c} \cdot k \cdot \left( \frac{mm^2}{N} \cdot 100 \cdot \rho_l \cdot f_{ck} \right)^{\frac{1}{3}} + k_1 \cdot \sigma_{cp} \right) b_w \cdot d_{mid} = (6.83 \cdot 10^6) \text{ N}$$

### **Capacity of main tensile failure:**

Minimum shear force capacity ( $V_{min}$ ) is calculated according to NA.6.3N, EC2.1-1:

$$V_{min} := 0.035 \cdot k^{\frac{3}{2}} \cdot f_{ck}^{\frac{1}{2}} \cdot MPa^{\frac{1}{2}} = 0.419 \text{ MPa}$$

Capacity for main tensile failure is calculated according to equation 6.2.b in EC2.1-1:

$$V_{Rd.c.min} := (V_{min} + k_1 \cdot \sigma_{cp}) \cdot b_w \cdot d_{mid} = (3.92 \cdot 10^6) \text{ N}$$

Due to  $V_{Rd.c} > V_{Rd.c.min}$ ,  $V_{Rd.c}$  is used for design shear tensile capacity.

$$V_{Rd.c} < V_{Ed} \quad \text{Design shear reinforcement necessary}$$

### **Shear compressive capacity:**

The shear force  $V_{Ed}$  can't exceed the shear capacity in compression  $V_{Rd.max}$  according to 6.2.1(8) in EC2.1-1.

$\nu$  og  $V_{Rd.max}$  is calculated in accordance with equation 6.5 og 6.6N in EC2.1-1:

$$\nu := 0.6 \cdot \left( 1 - \frac{f_{ck}}{250 \text{ MPa}} \right) = 0.384$$

$$V_{Rd.max} := 0.5 \cdot b_w \cdot d_{mid} \cdot \nu \cdot f_{cd} = (8.358 \cdot 10^7) \text{ N}$$

$$V_{Rd.max} > V_{Ed}$$

### **Members requiring design shear reinforcement:**

Calculated in accordance with 6.2.3 in EC2.1-1:

For members with vertical shear reinforcement, the shear resistance,  $V_{Rd}$  is the smaller value of equation 6.8 and 6.9 in EC2.1-1:

**Tensile shear capacity, equation 6.8:**

$$z := h - 2 c_{nom} = 6900 \text{ mm} \quad \theta := 26.56 \quad \text{Assuming concrete compressive diagonal at } 26.56^\circ$$

$$f_{ywd} := f_{yd} = 434.783 \text{ MPa}$$

$$\theta_{rad} := \frac{\theta}{360} \cdot 2 \cdot \pi = 0.464$$

$$X := \frac{V_{Ed}}{f_{ywd} \cdot z \cdot \cot(\theta_{rad})} = 8.398 \frac{\text{mm}^2}{\text{mm}}$$

$$A_{sw} := 2 \cdot A_{\phi 25} = 981.748 \text{ mm}^2$$

Using double-cut stirrups

$$s := \frac{A_{sw}}{X} = 116.9 \text{ mm}$$

Minimum distance between stirrups

$$V_{Rd,s} := \frac{A_{sw}}{s} \cdot z \cdot f_{ywd} \cdot \cot(\theta_{rad}) = 50.4 \text{ MN}$$

**Compressive shear capacity, equation 6.9:**

$$v_1 := 0.9 - \frac{f_{ck}}{200 \text{ MPa}} = 0.45 \quad v_1 \geq 0.5 \quad v_1 := 0.5 \quad 6.10.bN \text{ in EC2.1-1}$$

$$\alpha_{cw} := 2.5 \cdot \left( 1 - \frac{\sigma_{cp}}{f_{cd}} \right) = 2.487 \quad 6.11.cN \text{ in EC2.1-1}$$

$$V_{Rd,max} := \alpha_{cw} \cdot z \cdot b_w \cdot v_1 \cdot \frac{f_{cd}}{\cot(\theta_{rad}) + \tan(\theta_{rad})} = (2.1 \cdot 10^8) \text{ N}$$

Due to  $V_{Rd,max} > V_{Ed}$ , the required shear reinforcement is  $\text{Ø}25\text{c}110$

### Shear forces in X-direction:

#### Geometry:

$$h := 6250 \text{ mm}$$

$$t := 600 \text{ mm}$$

$$b_w := 2 \cdot t = 1200 \text{ mm}$$

$$A_c := 15.52 \text{ m}^2$$

$$c_{nom} := 300 \text{ mm}$$

$$c_{p,nom} := 450 \text{ mm}$$

#### General:

$$N_{Ed} := 1.36 \cdot 10^6 \text{ N}$$

Dimensioning axial force

$$V_{Ed} := 5.67 \cdot 10^5 \text{ N}$$

Dimensioning shear force

### Shear tensile capacity:

Checking whether the members require design shear reinforcement. Controlled according to 6.2.2 and NA.6.2.2. in EC2.1-1.

$$A_s := 62 \cdot A_{\phi 25} + 78 \cdot A_{\phi 20} = 54938.602 \text{ mm}^2 \quad \text{Ordinary reinforcement area in tension}$$

$$A_p := 2850 \text{ mm}^2 \cdot 10 = 28500 \text{ mm}^2 \quad \text{Prestressed reinforcement area on tensile side}$$

$$S_p := F_p \cdot 8 = 30952 \text{ kN}$$

$$S_d := A_s \cdot f_{yd} = 23886.348 \text{ kN}$$

$$d_p := h - c_{p,nom} = 5800 \text{ mm}$$

$$d_s := h - c_{nom} - 25 \text{ mm} - 32 \frac{\text{mm}}{2} = 5909 \text{ mm}$$

$$d_{mid} := \frac{d_p \cdot S_p + d_s \cdot S_d}{S_p + S_d} = 5847.478 \text{ mm} \quad \text{Effective height of the cross section}$$

$$\rho_l := \frac{A_p + A_s}{b_w \cdot d_{mid}} = 0.012 \quad \rho_l \leq 0.02 \quad \text{Ok, according to 6.2.2(1), EC2.1-1}$$

$$k := 1 + \sqrt{\frac{200 \text{ mm}}{d_{mid}}} = 1.185 \quad k \leq 2.0 \quad \text{Ok, according to 6.2.2(1), EC2.1-1}$$

$k_1$  is set equal to 0.15 for compression and to 0.3 for tension, according to NA.6.2.2(1) in EC2.1-1. Calculating compression in this case.

$$k_1 := 0.15$$

$k_2 := 0.18$  for concrete with maximum size of aggregate  $D$ , greater than or equal to 16mm, according to NA.6.2.2(1), EC2.1-1.

$$k_2 := 0.18$$

$$C_{Rd.c} := \frac{k_2}{\gamma_c} = 0.12 \quad \text{NA.6.2.2(1)}$$

$$\sigma_{cp} := \frac{N_{Ed}}{A_c} = 0.088 \text{ MPa}$$

$$0.2 \cdot f_{cd} = 10.2 \text{ MPa} \quad \sigma_{cp} \leq 0.2 \cdot f_{cd} \quad \text{OK. According to 6.2.2 i EC2.1-1.}$$

Shear tensile capacity is calculated according to equation 6.2.a in EC2.1-1:

$$V_{Rd.c} := \left( \frac{N}{\text{mm}^2} \cdot C_{Rd.c} \cdot k \cdot \left( \frac{\text{mm}^2}{N} \cdot 100 \cdot \rho_l \cdot f_{ck} \right)^{\frac{1}{3}} + k_1 \cdot \sigma_{cp} \right) b_w \cdot d_{mid} = (4.829 \cdot 10^6) \text{ N}$$

### **Capacity of main tensile failure:**

Minimum shear force capacity ( $V_{min}$ ) is calculated according to NA.6.3N, EC2.1-1:

$$V_{min} := 0.035 \cdot k^{\frac{3}{2}} \cdot f_{ck}^{\frac{1}{2}} \cdot \text{MPa}^{\frac{1}{2}} = 0.428 \text{ MPa}$$

Capacity for main tensile failure is calculated according to equation 6.2.b in EC2.1-1:

$$V_{Rd.c.min} := (V_{min} + k_1 \cdot \sigma_{cp}) \cdot b_w \cdot d_{mid} = (3.098 \cdot 10^6) \text{ N}$$

Due to  $V_{Rd.c} > V_{Rd.c.min}$ ,  $V_{Rd.c}$  is used for design shear tensile capacity.

$$V_{Rd.c} > V_{Ed} \quad \text{Design shear reinforcement not necessary}$$



### **Shear compressive capacity:**

The shear force  $V_{Ed}$  can't exceed the shear capacity in compression  $V_{Rd,max}$  according to 6.2.1(8) in EC2.1-1.

$\nu$  and  $V_{Rd,max}$  is calculated in accordance with equation 6.5 og 6.6N in EC2.1-1:

$$\nu := 0.6 \cdot \left( 1 - \frac{f_{ck}}{250 \text{ MPa}} \right) = 0.384$$

$$V_{Rd,max,x} := 0.5 \cdot b_w \cdot d_{mid} \cdot \nu \cdot f_{cd} = (6.871 \cdot 10^7) \text{ N}$$

$$V_{Ed} := 5.04 \cdot 10^7 \text{ N}$$

$V_{Rd,max,x} > V_{Ed}$  Due to  $V_{Rd,c} > V_{Ed}$  and  $V_{Rd,max} > V_{Ed}$ , the members don't require design shear reinforcement. However, minimum shear reinforcement for beams is required according to NA.9.2.2(5), EC2.1-1.

### **Minimum shear reinforcement:**

Minimum shear reinforcement ratio ( $\rho_w$ ) is taking the form of stirrups/links. The area is calculated according to NA.9.5N, EC2.1-1.

$$\rho_w := \frac{(0.1 \cdot \sqrt{f_{ck} \cdot \text{MPa}})}{f_{yk}} = 0.0019$$

$$\alpha := \frac{\pi}{2}$$

$$X := \rho_w \cdot b_w \cdot \sin(\alpha) = 2.2768 \text{ mm}$$

$$A_{sw} := 2 \cdot A_{\phi 16} = 402.124 \text{ mm}^2$$

$$s := \frac{A_{sw}}{X} = 176.615 \text{ mm}$$

Angle between the shear reinforcement and beam is  $90^\circ$   
(vertical stirrups)

Using double-cut stirrups

Longitudinal spacing between the stirrups

**Required shear reinforcement: Ø16c400**

### **Torsion:**

The torsional capacity is calculated according to 6.3.2 in EC2.1-1:

$$h := 7.5 \text{ m} \quad b := 6.25 \text{ m} \quad t := 0.6 \text{ m} \quad \theta := \frac{\pi}{4}$$

$$A_k := \left(h - \frac{t}{2}\right) \cdot \left(b - \frac{t}{2}\right) = 42.84 \text{ m}^2$$

$$T_{Ed} := 5.18 \cdot 10^6 \text{ N} \cdot \text{m}$$

$$\tau_{ti} t_{ef,i} := \frac{T_{Ed}}{2 A_k} = (6.046 \cdot 10^4) \frac{\text{N}}{\text{m}} \quad 6.26 \text{ in EC2.1-1}$$

$$z_i := b - 2 \cdot c_{nom} = 5.65 \text{ m}$$

$$u_k := 2 \cdot \left(h - \frac{t}{2}\right) + 2 \cdot \left(b - \frac{t}{2}\right) = 26.3 \text{ m}$$

$$V_{Ed,i} := \tau_{ti} t_{ef,i} \cdot z_i = 341584.967 \text{ N} \quad 6.27 \text{ in EC2.1-1}$$

$$A_{s1} := \frac{T_{Ed} \cdot u_k \cdot \cot(\theta)}{2 \cdot A_k \cdot f_{yd}} = 3657.075 \text{ mm}^2 \quad 6.28 \text{ in EC2.1-1}$$

$$A_{cap} := A_{\phi 25} \cdot 250 \cdot 2 = 245436.926 \text{ mm}^2$$

Additionally prestressed reinforcement.

$$u := 2 \cdot h + 2 \cdot b = 27.5 \text{ m}$$

$$t_{ef,i} := \frac{A_c}{u} = 0.564 \text{ m}$$

The maximum resistance of a member subjected to torsion and shear:

$$T_{Rd,max} := 2 \cdot \nu \cdot \alpha_{cw} \cdot f_{cd} \cdot A_k \cdot t_{ef,i} \cdot \sin(\theta) \cdot \cos(\theta) = (1.177 \cdot 10^9) \text{ N} \cdot \text{m} \quad 6.30 \text{ in EC2.1-1}$$

$$C := \frac{T_{Ed}}{T_{Rd,max}} + \frac{V_{Ed}}{V_{Rd,max}} = 0.244 \quad C \leq 1.0 \quad 6.29 \text{ in EC2.1-1}$$

